The role of endocytic machinery during Vaccinia Virus egress and spread

Xenia Snetkov

University College London

and

Cancer Research UK London Research Institute

PhD Supervisor: Dr Michael Way

A thesis submitted for the degree of

Doctor of Philosophy

University College London

September 2015

Declaration

I, Xenia Snetkov, confirm that the work presented in this thesis is my own. Where information has been derived from other sources, I confirm that this has been indicated in the thesis.

Abstract

During its egress, Vaccinia virus induces a series of events at the plasma membrane of infected cells that ultimately enhance the spread of infection. Immediately following fusion with the plasma membrane, the virus recruits the endocytic adaptor protein, AP-2 and clathrin in an A36-dependent manner. Clathrin recruitment acts to cluster the viral integral membrane protein, A36 underneath the virion to generate a robust signalling platform that recruits the adapters Nck and Grb2 downstream of phosphorylated tyrosines 112/132 respectively. This subsequently results in the recruitment of the WIP:N-WASP complex, which stimulates Arp2/3 complex dependent actin polymerization to propel the virus along the plasma membrane and onto neighbouring uninfected cells. In addition, the virus also promotes Arp2/3 driven actin polymerization via recruitment and activation of the GTPase Cdc42, facilitating its interaction with N-WASP. The ability of the virus to activate Cdc42 is dependent on the RhoGEF Intersectin-1, which is also capable of interacting with AP-2. My studies have sought to investigate the molecular mechanism and role of AP-2 and clathrin recruitment during viral egress. I found that three highly conserved Asn-Pro-Phe (NPF) motifs at the C-terminus of A36 interact directly with the Eps15 Homology (EH) domains of intersectin-1 and Eps-15. A recombinant virus lacking all three NPF motifs (ΔNPF) is unable to recruit clathrin, AP-2 or intersectin-1. Besides changes in actin polymerization this virus also has defects in viral release and spread. NPF motifs are conserved endocytic interaction modules that a found in all eukaryotes, however A36 is the first viral protein containing functional NPF motifs to be identified to date.

Acknowledgements

Firstly, I would like to thank Michael for giving me the chance to work with such an outstanding group of people, and for all of the support over the last four years, now more than ever.

To all the Way lab members past and present, thank you. Ashley, you are a great scientist and have been an amazing mentor, even from the other side of the Atlantic. I hope I've done you proud. Charlotte and Sara from the minute I joined the lab your help, advice, and friendship was invaluable. Jasmine, I've always looked up to you as a scientist, you're a truly incredible researcher and friend, and I promise to take good care of your project. Joe, you were there at the very start, and the lab is certainly more sober and more polite without you. Luckily you left us Chiara, you're a joy to work with, you light up the lab and never fail to make me smile. Good luck for writing up. Theresa, thank you for your endless patience, for being a great friend, and for never turning down wine. The rest of the coconut girls, Caitlin, Flavia, and Julia it's been a joy to have you start in the lab, thank you all for your enthusiasm, encouragement and coffee throughout. Antonio and Dave, the lone Y-chromosomes, you deserve a medal of bravery on that fact alone. Thank you both for help with numerous virology and imaging questions, and your wit throughout.

Leo, I know you can't wait to read my thesis. Thank you for being there for every high and low. You have never once doubted me, and for that I couldn't be more grateful. Finally, I would like to thank my parents and my sister, Aglaya for unconditional support and belief in me throughout; I hope you enjoy another book for the shelf.
Я посвящаю эту диссертацию вам в знак признательности за все, что вы сделали для меня. С любовью, Ксения.

Table of Contents

Abstract **3**

Acknowledgements **4**

List of Figures **8**

List of Tables **10**

Abbreviations **11**

Chapter 1. Introduction **15**

1.1 Vaccinia Virus **15**

1.1.1 The Poxvirus family 15

1.1.2 Genome and Gene Expression 17

1.1.3 Viral entry 19

1.1.4 Viral Replication and Assembly 20

1.1.5 Viral Egress and Spread 25

1.2 The Actin Cytoskeleton and N-WASP in pathogen spread **29**

1.2.1 Actin polymerisation 29

1.2.2 The Arp2/3 Complex 30

1.2.3 N-WASP function and regulation 31

1.2.4 Vaccinia actin tail formation 35

1.2.5 Actin-based motility of pathogens 37

1.2.6 A Clathrin-dependent step 38

1.2.7 Subversion of endocytic machinery by pathogens 41

1.3 Clathrin Mediated Endocytosis **42**

1.3.1 Clathrin 42

1.3.2 Clathrin Adaptors 45

1.3.3 The Endocytic pathway 48

1.3.4 The role of actin during Clathrin-Mediated Endocytosis 50

1.4 Eps15 Homology family proteins **52**

1.4.1 Discovery and members 52

1.4.2 Epidermal growth factor receptor substrate 15 – Eps15 56

1.4.3 The Intersectin family 57

1.4.4 Interplay between intersectin-1 and actin 58

1.5 Aims of this thesis **60**

Chapter 2. Materials & Methods **61**

2.1 General buffers and culture media **61**

2.1.1 General Buffers 61

2.1.2 Cell Culture Media 61

2.1.3 Bacteriological Media 62

2.2 Cell Culture **63**

2.2.1 Culturing stocks 64

2.2.2 Freezing stocks 64

2.2.3 Transfection 64

2.3 Molecular Biology **66**

2.3.1 Expression vectors 66

2.3.2 Polymerase Chain Reaction 68

2.3.3 Overlap PCR....69
2.3.4 Sub-cloning....70
2.3.5 Bacterial transformation....70
2.3.6 Colony screening by PCR....70
2.3.7 Preparation of chemically competent bacteria....71
2.3.8 Plasmid DNA preparation....72
2.3.9 DNA sequencing....72
2.4 Vaccinia Virus....73
2.4.1 General buffers for virology....73
2.4.2 Sucrose Purification of vaccinia virus....74
2.4.3 Plaque Assay....74
2.4.4 Infection....75
2.4.5 EEV release assays....75
2.4.6 Single step growth curve....75
2.4.7 Drug treatments during infection....76
2.4.8 Amplification of vaccinia DNA....76
2.4.9 Recombinant viruses....77
2.4.10 Analytical PCR from plaque picks....78
2.5 Biochemistry....78
2.5.1 SDS-PAGE....79
2.5.2 Immunoblot Analysis....79
2.5.3 GST pull-down assay....80
2.5.4 GFP-Trap....81
2.5.5 Immunoprecipitation....82
2.5.6 Expression and purification of GST-EH domains....82
2.5.7 Peptide pull-down assays....83
2.5.8 Probing peptide arrays....84
2.6 Imaging....84
2.6.1 General reagents....84
2.6.2 Fixation....85
2.6.3 Immunofluorescence....85
2.6.4 Antibody staining of viral plaques....86
2.6.5 Microscopes....87
2.7 Statistical Analysis....87

Chapter 3. The C-terminus of A36 is essential for AP-2 binding....88
3.1 Introduction....88
3.2 Results....88
3.2.1 The C-terminus of A36 is essential for AP-2 binding....88
3.2.2 Three Asn-Pro-Phe (NPF) motifs mediate AP-2 binding....95
3.2.3 Intersectin-1 and Eps15 are recruited to vaccinia virus....98
3.2.4 The A36 NPF motifs directly bind intersectin-1 and Eps15....100
3.2.5 NPF motifs are conserved amongst the *Orthopoxviruses*....104
3.3 Summary....105

Chapter 4. Generation and characterisation of Vaccinia A36 ΔNPF 1-3 106
4.1 Introduction 106
4.2 Results 107
4.2.1 Intersectin-1 and Eps15 are essential to mediate AP-2 binding to A36 107
4.2.2 Loss of a single NPF motifs leads to longer actin tails 112
4.2.3 Generation of the recombinant A36 ΔNPF 1-3 virus 114
4.2.4 The A36 NPF motifs recruit intersectin-1 and Eps15 to Vaccinia virus 117
4.2.5 Yaba-like disease virus YL126 is unable to recruit intersectin-1 and Eps15 119
4.2.6 NPF motifs are required for robust actin tail formation 121
4.2.7 Recruitment of N-WASP, WIP, Grb2, and Nck is not NPF dependent 125
4.3 Summary 127

Chapter 5. The role of the A36 NPF motifs during Vaccinia virus spread 128
5.1 Introduction 128
5.2 Results 129
5.2.1 A36 NPF motifs promote viral spread 129
5.2.2 A36 NPF motifs promote viral release 133
5.2.3 The role of the A36 NPF motifs during vaccinia super-repulsion 135
5.2.4 A36 NPF motifs are required for Cdc42 recruitment 144
5.2.5 Distinguishing the duel roles of intersectin-1 146
5.2.6 Viral release mediated by the A36 NPF motifs is actin-dependent 152
5.3 Summary 155

Chapter 6. Discussion 156
6.1 The first characterised viral NPF motifs 156
6.2 Interactions and organisation of A36 160
6.3 Interplay between clathrin machinery and actin dynamics 162
6.3.1 Recruitment and activation of intersectin-1 162
6.3.2 Atypical EH domain containing proteins 165
6.4 The super-repulsion hypothesis 166
6.5 What governs viral release? 168
6.6 NPF motifs as a conserved pathogen signalling scaffold 172
6.7 Future Perspectives 173

References 175

List of Figures

Figure 1.1 Phylogenetic tree of the Poxvirus family....16
Figure 1.2 The vaccinia virus genome....18
Figure 1.3 The vaccinia replication cycle....22
Figure 1.4 Topology of IEV specific proteins....23
Figure 1.5 Mechanisms promoting vaccinia egress....26
Figure 1.6 The super-repulsion hypothesis....28
Figure 1.7 N-WASP regulation....34
Figure 1.8 The vaccinia actin-signalling network....36
Figure 1.9 Vaccinia IEV proteins and their potential adaptor binding motifs....39
Figure 1.10 Model of clathrin function during vaccinia virus egress....40
Figure 1.11 Domain and subunit organisation of clathrin and AP-2....44
Figure 1.12 Mammalian clathrin-mediated endocytosis....49
Figure 1.13 Domain and subunit organisation of Eps15 and intersectin-1....55
Figure 3.1 A far western approach used to identify AP-2 binding to A36....91
Figure 3.2 A36 WE and WD motifs do not mediate AP-2 binding....92
Figure 3.3 A36 residues 155-197 mediate AP-2 binding....94
Figure 3.4 Intersectin-1 and AP-2 bind A36 via NPF motifs....97
Figure 3.5 Co-localisation of EH domain proteins with extracellular virus particles....99
Figure 3.6 A36 NPF motifs directly bind EH domains of intersectin-1 and Eps15....103
Figure 3.7 The A36 NPF motifs are highly conserved among the *Orthopoviridae*....104
Figure 4.1 Intersectin-1 and Eps15 depletion leads to longer actin tails and the loss of AP-2 binding to A36....109
Figure 4.2 Intersectin-1 recruitment to CEV is independent of AP-2 and clathrin....110
Figure 4.3 Loss of AP-2 and intersectin-1 reduces the cell-to-cell spread of WR....111
Figure 4.4. Loss of individual A36 NPF motifs results in longer actin tails....113
Figure 4.5. Generation of recombinant A36 NPF mutant viruses....115
Figure 4.6. Loss of NPF motifs does not impact on A36 expression or virus replication....116
Figure 4.7. Three A36 NPF motifs are required to recruit clathrin, AP-2, intersectin-1, and Eps15 to CEV....118

Figure 4.8. YLDV YL126 is unable to recruit endocytic machinery.....120
Figure 4.9. Loss of the A36 NPF motifs leads to longer, faster moving actin tails.....123
Figure 4.10. Actin tail nucleation is facilitated by the A36 NPF motifs.....124
Figure 4.11 A36 ΔNPF 1-3 is able to recruit the core vaccinia actin-signalling network 126
Figure 5.1 The A36 NPF motifs promote viral spread.....131
Figure 5.2 The A36 ΔNPF 1-3 and YL126R viruses are deficient in viral spread 132
Figure 5.3 The A36 NPF 1-3 virus is deficient in EEV release.....134
Figure 5.4 Does A36 clustering enhance accelerated viral spread?.....135
Figure 5.5 Generation of A36 wild type and ΔNPF 1-3 under a late promoter 138
Figure 5.6. Characterisation of the $A36^{late}$ and the ΔNPF^{late} viruses.....139
Figure 5.7 The $A36^{late}$ and ΔNPF^{late} viruses are equally deficient in viral spread 140
Figure 5.8 Do A36 NPF motifs contribute to super-repulsion? 143
Figure 5.9 A36 NPF motifs are required to recruit Cdc42.....145
Figure 5.10 N-WASP cannot form a stable complex with A36 ΔNPF 1-3.....146
Figure 5.11 Loss of N-WASP-Cdc42 interaction mimics the loss of the A36 NPF motifs 150
Figure 5.12 ZCL278 treatment of GFP-N-WASP cell lines confirms the requirement of the NPF motifs for viral spread.....151
Figure 5.13 Loss of NPF motifs does not impact viral spread in the absence of actin polymerisation.....154
Figure 6.1 A36 contains two low complexity regions (LCRs), a NPxY motif, and a PDZ-binding motif.....157
Figure 6.2 Mechanisms of A36 self-organisation.....161
Figure 6.3 Updated model of the A36 vaccinia actin and clathrin signaling network..164
Figure 6.4 Models of actin-mediated vaccinia egress.....171
Figure 6.5 Yaba-like disease virus 150R reveals conserved NPF motifs 173

List of Tables

Table 1.1 Common endocytic motifs and their binding adaptor proteins.....47
Table 1.2 Binding specificity of EH domains.....53
Table 2.1 Cell lines and culture conditions.....63
Table 2.2 siRNA target sequences.....65
Table 2.3 Expression vectors.....66
Table 2.4. Primers used for mutagenesis.....69
Table 2.5. Recombinant viruses used in this thesis.....73
Table 2.6 List of inhibitors.....76
Table 2.7 Antibodies used for immunoblot analysis.....79
Table 2.8 Primary antibodies used for immunofluorescence.....86

Abbreviations

%	percent
A-domain	acidic domain
ADF	actin depolymerization factor
ADP	Adenosine 5'-diphsphate
ANTH	AP180 N-terminal homology domain
AP-2	Adaptor protein 2
Arp 2/3	actin related proteins 2 and 3
ATP	Adenosine 5'-triphsphate
B-domain	basic domain
BAR	Bin-amphiphysin-rvs domain
BDT	Big dye terminator
bp	base pairs
BSA	Bovine serum albumin
C-domain	central domain
C-terminus	carboxy terminus
C2	Membrane targeting
CA	central acidic region
CB	cytoskeleton buffer
CCV	Clathrin-coated vesicle
Cdc42	Cell division cycle 42
CEV	cell-associated enveloped virion
CHC	Clathrin heavy chain
CLC	Clathrin light chain
cm	centimetre
CME	Clathrin-mediated endocytosis
CRIB	Cdc42 and Rac interactive binding
CSTN	Calsyntenin
DAPI	4',6 diamidino-2-phenylindole
DH	Dbl homology
DMEM	Dulbecco's modified eagle medium
DMSO	Dimethyl sulfoxide
DNA	deoxyribonucleic acid
dNTP	deoxynucleoside 5'-triphosphate
DPF	Asp-Pro-Phe
E.coli	Escherichia coli
ECL	enhanced chemiluminescence
ECM	Extracellular matrix
EDTA	ethyl diamine N,N,N',N'-tetraacetic acid
EEV	extracellular enveloped virion
EGFR	Epidermal growth factor receptor
EGTA	Ethylene glycol tetraacetic acid
EH	Eps15 homology

EHD	EH domain containing
EM	Electron microscopy
ENTH	epsin N-terminal homology domain
EPEC	Enteropathogenic Escherichia coli
Eps15	Epidermal growth factor substrate 15
ER	endoplasmic reticulum
ExB5	Extracellular B5 stain
F-actin	filamentous actin
FCHo	F-BAR-containing Fer/Cip4 homology domain-only protein
FCS	foetal calf serum
FITC	fluorescin isothiocyanate
FRAP	fluorescence recovery after photo-bleaching
FSB	Final sample buffer
g	gram
G-actin	monomeric actin
GAG	Glycosaminoglycan
GBD	GTP-binding domain
GEF	Guanine nucleotide exchange factor
GFP	green fluorescent protein
Grb2	Growth factor receptor-bound protein 2
GST	Glutathione-S-transferase
GTP	Guanosine 5'-triphsphate
GTPase	Guanosine-5'-triphosphatase
Hip1R	Huntingtin interacting protein 1-related
hpi	hours post infection
hr	hour
HRP	horseradish peroxidase
HSC70	heat shock cognate 71 kDa protein
IEV	intracellular enveloped virion
IF	immunofluorescence
IMV	intracellular mature virion
IP	immunoprecipitation
ITSN	Intersectin
IV	immature virion
kb	kilobase
kDa	kiloDalton
KLC	Kinesin light chain
l	litre
LB	Luria Bertani
M	Molar
MEF	mouse embryo fibroblast
MEM	modified eagle medium
MES	2-(N-morpholino)-ethanesulphonic acid
mg	milligram

min	minute
ml	millilitre
mm	millimetre
mM	Millimolar
MOI	multiplicity of infection
ms	milliseconds
MT	Microtubule
MTOC	Microtubule organising centre
N-terminus	amino terminus
N-WASP	neural Wiskott Aldrich syndrome protein
Nck	Non-catalytic region of tyrosine kinase adaptor protein
ng	nanogram
nm	nanometer
NPF	Asparagine-Proline-Phenylalanine
NPF	nucleating promoting factor
ns	Not significant
NTP	nucleoside 5'-triphosphate
ºC	degrees Celsius
OD	optical density
Oligo	Oligonucleotide
ORF	Open reading frame
PAGE	Polyacrylamide gel electrophoresis
PBS	phosphate buffered saline
PCR	polymerase chain reaction
pE/L	early late promoter
Pen	penicillin
PFA	Paraformaldehyde
PFU	plaque forming units
PH	Pleckstrin homology
Pi	inorganic phosphate
PI(4,5)P2	Phosphatidylinositol 4,5-bisphosphate
PM	Plasma membrane
pmol	picomolar
PRD	Polyproline-rich domain
PT	paraformadlehyde with 0.1% Trition
PTB	Phospho-tyrosine binding domain
RFP	red fluorescent protein
Rho	Ras homolog gene family
RNAi	Ribonucleic acid interference
rpm	Revolutions per minute
RT	room temperature
RTK	receptor tyrosine kinase
SDS	sodium dodecyl sulphate
Sec	seconds

SEM	Standard error of the mean
SH	Src homology domain
siRNA	small interfering ribonucleic acid
Src	Sarcoma
Strep	streptomycin
t1/2	half time
TBE	Tris-borate-EDTA buffer
TD	Terminal domain
TGN	trans Golgi network
TM	Transmembrane
TMB	Tetramethylbenzidine
TS	Tris saline
V	volts
V-domain	Verprolin or WH2 domain
v/v	volume per volume
VSV-G	vesicular stomatitis virus –G pseudotyped
w/v	weight/volume
WASP	Wiskott-Aldrich-Syndrome protein
WBD	WASP binding domain
WCA	WASP homology 2, central and acidic region
WH	WASP homology domain
WIP	WASP interacting protein
WR	Western Reserve
WT	Wild-type
Y	Tyrosine
YFP	yellow fluorescent protein
YLDV	Yaba-like disease virus
Δ	delta
µl	microlitre
µM	microMolar
µm	micrometer
Φ	Bulky hydrophobic amino acid

Chapter 1. Introduction

1.1 Vaccinia Virus

1.1.1 The Poxvirus family

Vaccinia virus is the prototypical member of the poxvirus family and is best known for its role as a vaccine in the worldwide eradication of smallpox (Variola Virus) (WHO, 1972). Smallpox is estimated to have killed over 500 million people in the 20th century alone, and over a thousand years of combined luck and research have led to the development of vaccinia virus as the first live vaccine against smallpox. The first evidence of variolation to combat smallpox goes back to first century China (960-1280). Smallpox scabs were dried, powdered, and inhaled, in order to prevent smallpox infection (Oldstone, 1998). Much later, in the 18th century, Dr. Jenner observed that milkmaids, who often caught the non-lethal cowpox virus in their line of work, were unaffected during smallpox epidemics. In 1796 he performed the first modern vaccination with cowpox that successfully prevented subsequent smallpox infection (Jenner, 1798; Oldstone, 1998). By 1972, the closely related vaccinia virus was isolated and used as the vaccinating agent against smallpox. A successful worldwide vaccination effort coordinated by the World Health Organization, led to the last outbreak of naturally occurring smallpox to be recorded in Somalia in 1977 (Newmark, 1980; WHO, 1972).

The poxvirus family are subdivided into two distinct subfamilies: the *Entomopoxviridae* (insect specific) and the *Chordopoxviridae* (vertebrate specific). The *Chordopoxviridae* are further subdivided into ten genera, with vaccinia virus classified under the *Orthopoxviridae* (Figure 1.1). Ninety genes are conserved throughout the *Chordopoxviridae* subfamily, 49 of which are conserved among the entire poxvirus family, and are thought to represent the minimal poxvirus genome (Gubser et al., 2004; Upton et al., 2003). Poxviruses possess relatively wide cellular tropism within their respective host and are able to infect epithelial cells, fibroblasts, and hematopoietic cell types (McFadden, 2005).

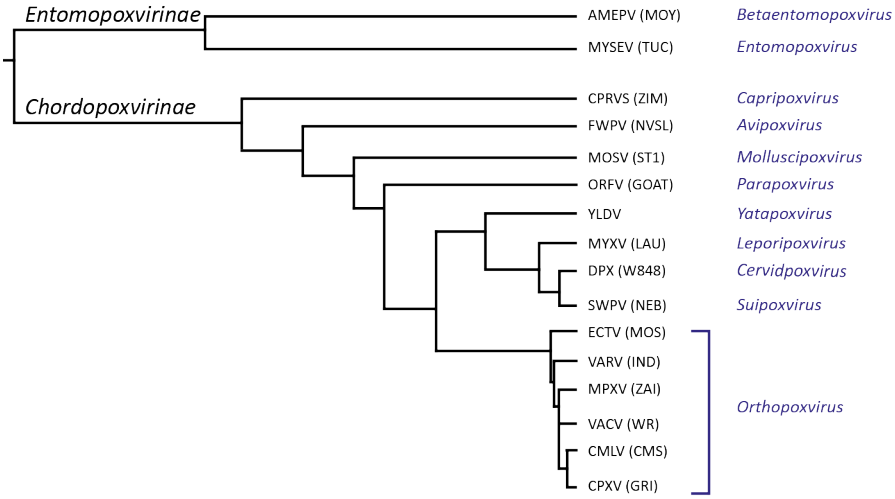

Figure 1.1 Phylogenetic tree of the Poxvirus family

Phylogeny based on sequence alignment of the poxvirus DNA polymerase sequence. Linkage tree based on Clustal Omega sequence alignment. A prototypic virus from each genus (labelled in blue) is shown (strain is given in parentheses).

Vaccinia, like all members of the poxvirus family, is a double stranded DNA virus that undergoes its entire replication cycle in the cytoplasm of the host cell, unlike other large DNA viruses such as herpes or adenovirus, which replicate in the host nucleus (Tolonen et al., 2001). Following the eradication of smallpox, the study of vaccinia virus and other members of the *Orthopoxviridae* has remained a key research tool in unravelling many host-cell mechanisms due to their complex manipulation of the host-cell machinery. Vaccinia is genetically tractable and easy to visualize, making it an ideal tool to study cellular processes. Vaccinia has been at the forefront of immunotherapy and viral oncolytics, in part due to the amenability of the viral genome to accept up to 25 kbp of foreign DNA, in addition to a long track record of safety as a vaccine (Albelda and Thorne, 2014; Thorne, 2008). Lastly, the study of vaccinia virulence remains high on the agenda amidst renewed concerns of the use of smallpox in biological warfare. Only two officially stored stocks of variola virus exist at WHO collaborating laboratories at the CDC (Georgia, USA) and VECTOR (Koltsovo, Russia) (Mayr, 2003). Debate continues as to whether these stocks should be destroyed to prevent future outbreaks or misuse, or whether they should continue to be stored for future research (Agwunobi, 2007; Hammond, 2007).

1.1.2 Genome and Gene Expression

The vaccinia virus genome consists of 195 kbp encoding around 260 proteins, including its own replication and transcription machinery (Boone and Moss, 1978; Goebel et al., 1990; Hruby et al., 1979; Moss, 1990; Paoletti and Grady, 1977). This allows the virus to undergo its entire replicative cycle in a perinuclear compartment in the cytoplasm of the host cell (Dahl and Kates, 1970; Pennington, 1974; Prescott et al., 1971; Roberts and Smith, 2008; Smith et al., 2002). The viral genome can be viewed as a self-complementary circular strand of DNA due to the presence of 12-kb inverted terminal repeats at the either end of its genome (Figure 1.2 A) (Baroudy and Moss, 1982; Goebel et al., 1990). Nomenclature of genes is derived from the distribution of 15 HindIII restriction sites throughout the genome. HindIII digestion results in 16 fragments designated A to P according to decreasing size (DeFilippes, 1982). Open reading frames within a HindIII fragment are numbered left to right, denoting the order based on the position of the first in-frame start codon. As both DNA strands are transcribed, genes are additionally denoted with a 'L' or 'R' indicating the direction of transcription (Figure 1.2 A) (Goebel et al., 1990).

Viral transcriptional promoters, found approximately 30 bp upstream of the initiating methionine, tightly control viral gene expression throughout infection (Condit and Niles, 2002). Viral genes are therefore additionally characterised by their expression kinetics during replication (Figure 1.2 B). The mRNA's encoding early, intermediate, or late genes can be detected respectively from 20, 100, and 140 minutes post infection in HeLa cells (Assarsson et al., 2008; Broyles, 2003; Joklik and Becker, 1964).

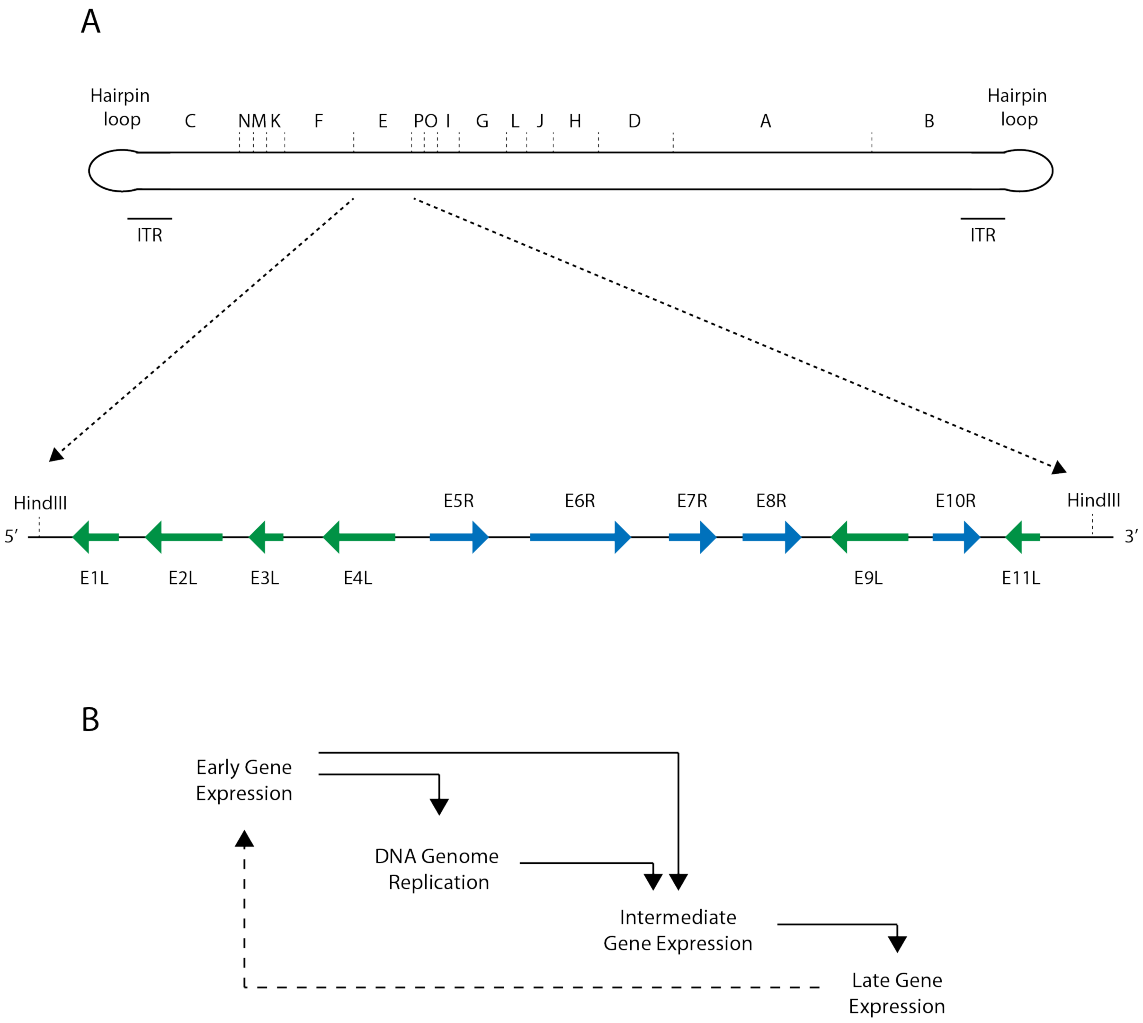

Figure 1.2 The vaccinia virus genome

A The vaccinia virus genome is a self-complementary circular strand of DNA containing a hairpin loop of 101 nucleotides at each terminus. The 12-kbp inverted terminal repeats (ITRs) are underlined. The 16 fragments that arise from HindIII digest are labeled 'A-P' (indicted by dashed lines). The 'E' HindIII fragment consists of 11 genes represented by green or blue arrows. The direction of the arrows indicates the direction of transcription (L or R). **B** The temporal gene expression cascade that occurs during the course of vaccinia infection.

1.1.3 Viral entry

Vaccinia virus particles are approximately 350 x 270 x 250 nm and were the first virus to be visualized by light microscopy due to their large size (Condit et al., 2006; Cyrklaff et al., 2005; Roos et al., 1996). Vaccinia belongs to a class of over 20 diverse viruses that actively trigger their internalization (Grove and Marsh, 2011; Mercer and Helenius, 2009). Two infectious forms of the virus exist, intracellular mature virions (IMVs) and extracellular enveloped virions (EEVs) that must both breach the plasma membrane in order to initiate infection (Figure 1.3 – 1) (Roberts and Smith, 2008). EEVs are wrapped in an additional host derived membrane compared to IMV, and therefore these virions contain no common surface proteins and are structurally and antigenically distinct from one another (Boulter and Appleyard, 1973). IMVs and EEVs therefore utilise distinct clathrin-independent mechanisms of entry (Mercer and Helenius, 2008; Schmidt et al., 2011; Schmidt and Mercer, 2012).

During IMV entry, several outer viral membrane proteins are able to bind a range of host glycosaminglycans (GAGs) at the plasma membrane. These include A27 and H3 to heparin sulphate, A26 to laminin, and D8 to chondroitin sulphate (Chiu et al., 2007; Chung et al., 1998; Hsiao et al., 1999; Lin et al., 2000). Although IMV particles can enter the cell via direct fusion of the viral and host membrane in a pH-independent manner, the primary entry route of IMV, is thought to be via the induction of endocytic and macropinocytic uptake (Mercer and Helenius, 2008; Mercer et al., 2010; Sandgren et al., 2010; Schmidt et al., 2011; Townsley et al., 2006). Upon contact with the plasma membrane large actin-dependent blebs are induced by phosphatidylserine in the viral membrane to facilitate uptake into the cell, in a manner mimicking the clearance of apoptotic bodies (Hoffmann et al., 2001; Mercer and Helenius, 2009; Mercer et al., 2010). Tyrosine kinases, protein kinase C (PKC), p21-activated kinase 1 (PAK), myosin and a host of other cellular triggers act in concert to mediate the large actin rearrangements required for macropinosome formation (Locker et al., 2000; Mercer and Helenius, 2008; Mercer et al., 2010). Following uptake, IMVs utilise a macromolecular viral entry fusion complex (EFC), which is activated upon acidification of macropinosomes. This facilitates fusion with the macropinosomal membrane and subsequent release the genomic viral core (Laliberte et al., 2011).

The entry of EEV is not yet entirely understood at a molecular level, due to the intrinsic instability of the additional host derived membrane. No EEV specific cellular attachment factors have been uncovered thus far, and it is a widely supported hypothesis that the EEV outer membrane is disrupted prior to fusion, thus revealing the IMV fusion machinery (Law et al., 2006; Schmidt et al., 2011; Senkevich et al., 2004). It addition it has now been established that EEV actively induce their macropinocytic uptake in a mechanism similar to that of IMVs (Laliberte and Moss, 2009; Mercer and Helenius, 2008; Sandgren et al., 2010; Schmidt et al., 2011). Like IMV, EEVs appear to require the acidification of the endosome in order to disrupt the outer EEV membrane, after which the viral core can be released via endosomal fusion in an IMV-like manner (Schmidt et al., 2011; Schmidt et al., 2013; Townsley and Moss, 2007).

The specific method of viral entry is likely to be strain dependent, with some vaccinia strains (e.g. IHD-W and MVA) shown to invade preferentially via direct membrane fusion (Chang et al., 2010; Mercer et al., 2010). Viral entry is also likely to be cell type specific, altogether resulting in multiple modes of entry (Mercer et al., 2010; Norbury, 2006).

1.1.4 Viral Replication and Assembly

Following entry into the host cell viral cores accumulate in the perinuclear region of the cell via an unknown microtubule-dependent mechanism and/or by vaccinia-induced cell contraction (Figure 1.3 – 2) (Carter et al., 2003; Schramm et al., 2006). Viral RNA polymerase and early transcription factors are pre-assembled on early viral promoters and initiate early viral gene expression immediately after core release (Yang and Moss, 2009). Early genes make up approximately half of the 260 genes encoded by vaccinia. Early genes are primarily responsible for encoding the viral DNA replication machinery, subverting the host immune system and preventing host cell apoptosis (Broyles, 2003; Postigo and Ferrer, 2009). There are fewer intermediate genes, which primarily function to regulate the expression of late genes (Assarsson et al., 2008). Late genes are largely required for the assembly of new virions including the production of structural proteins and those required for viral egress and spread (Rosel and Moss, 1985). These initial sites of early DNA replication can be detected and grow over time to form a large DNA-rich viral factory that is anchored at the microtubule-organising centre (Domi and

Beaud, 2000; Ploubidou et al., 2000; Schepis et al., 2006). The complex morphogenesis of vaccinia results in the production of distinct forms of the virus (Leite and Way, 2015; Roberts and Smith, 2008). The first discernible viral structures observed at the viral factory are crescent membranes (Dales and Mosbach, 1968; Hollinshead et al., 1999; Risco et al., 2002). Crescent-shaped lipid structures composed of a single lipid bilayer, which are thought to be derived from ER-Golgi compartments, grow to enclose newly synthesised viral cores to form the immature virion (IV) (Figure 1.3 – 3) (Husain et al., 2006; Rodriguez et al., 1985; Sodeik et al., 1993; Sodeik and Krijnse-Locker, 2002; Zhang and Moss, 1992). Proteolytic cleavage of several viral core and membrane proteins results in the maturation of IVs into the first infectious form of the virus, the intracellular mature virus (IMV) (Figure 1.3. – 4) (Condit et al., 1983). IMVs make up around 80% of infectious particles and form dense, brick shaped virions that are only released from the cell upon lysis (Dubochet et al., 1994; Roos et al., 1996; Roper et al., 1996).

A subset of IMVs is transported in a microtubule dependent manner away from the viral factory to the trans-Golgi network (TGN) or the endosomal network whereby they become wrapped in an additional membrane cisternae (Figure 1.3 – 5) (Earley et al., 2008; Payne and Kristenson, 1979; Sanderson et al., 2000; Schmelz et al., 1994; Tooze et al., 1993). The mechanisms defining how IMVs are sorted into those to be wrapped, and how IMVs are transported to the TGN are at present unknown. Prior to wrapping of IMVs, the TGN-derived membrane is preloaded with a number of viral proteins that are crucial for the wrapping process such as B5 and F13, that mediate wrapping via interactions with the IMV specific surface protein, A27 (Duncan and Smith, 1992; Husain et al., 2007; Rodriguez and Smith, 1990). The integral membrane proteins A33, A34, A36, A56, B5, K2, E2, F12, along with membrane-associated F13, are unique to the intracellular enveloped virus (IEV) membrane and play crucial roles during IEV transport and release (Figure 1.4). A36 and F12 are solely associated with the outer IEV membrane, and are therefore absent from EEV following release from the plasma membrane (van Eijl et al., 2002; van Eijl et al., 2000).

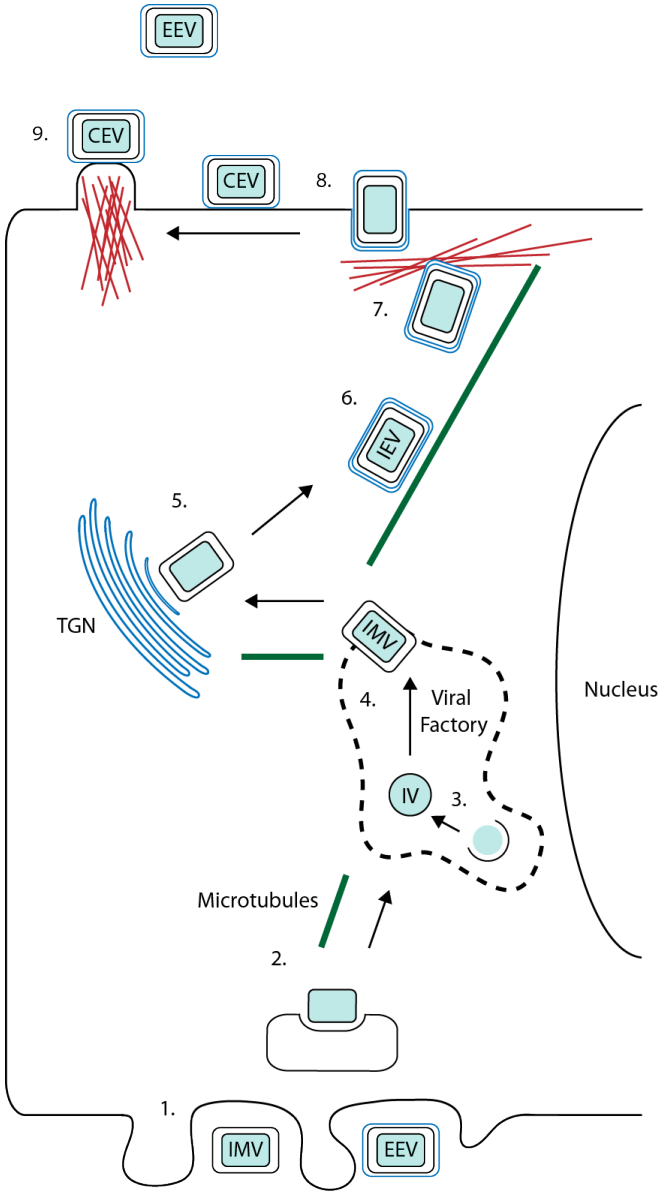

Figure 1.3 The vaccinia replication cycle

IV = immature virion, IMV = intracellular mature virion, IEV = intracellular enveloped virion, CEV = cell-associated enveloped virion, EEV = extracellular enveloped virion.

1. IMV and EEV attach to the cell, stimulate macropinocytosis, and breach the host membrane. **2.** The viral core is released into the cytosol following fusion of the outer viral membrane with endosomal membranes (Schmidt et al., 2011). Viral cores are transported in a microtubule dependent manner to the perinuclear region. **3.** Early transcription of mRNAs commences, crescents form, and immature virions (IV) are assembled. **4.** IVs are processed to form intracellular mature virions (IMVs). **5.** IMVs are transported to the TGN where they are wrapped by a double membrane cisternae. **6.** IEVs are transported to the cell periphery in a microtubule dependent manner by kinesin-1. **7.** IEVs breach the cortical actin beneath the plasma membrane with which they then fuse. **8.** Outside-in activation of Src/Abl family kinases stimulates the formation of the actin tails (shown in red) by CEVs on the plasma membrane. **9.** CEVs either directly infect a neighboring cell, or can be released into the extracellular space as EEV.

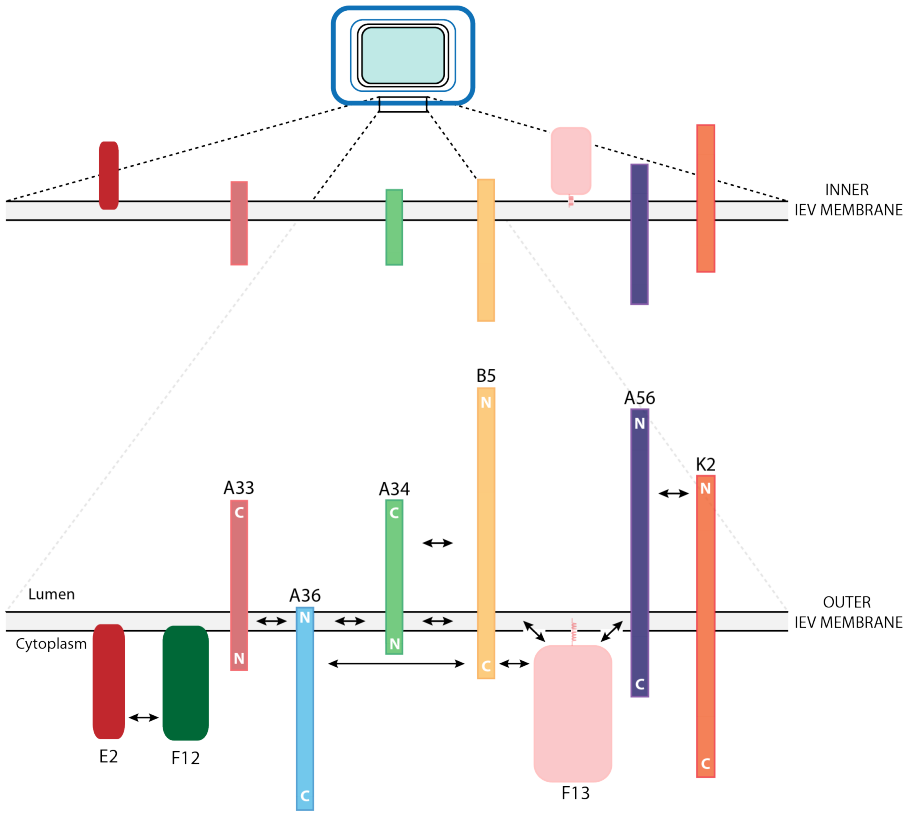

Figure 1.4 Topology of IEV specific proteins

Arrows indicate interactions between the IEV proteins. Domains are drawn to size aside from that of F13, which is a large membrane associated IEV protein, tethered to the membrane by a lipid anchor. The outer IEV membrane fuses with the host plasma membrane during EEV release (bottom). The EEV remain enveloped by the inner IEV-derived membrane lacking F12 and A36 (top).

Wrapped IMVs, termed intracellular enveloped virions (IEVs), are subsequently transported to the cell periphery in a microtubule-dependent manner by kinesin-1 (Figure 1.3 – 6) (Dodding et al., 2009; Geada et al., 2001; Moss and Ward, 2001; Rietdorf et al., 2001). Kinesin-1 is recruited to IEVs via binding of the kinesin-light chain (KLC) tetratricopeptide repeat (TPR) to IEV specific A36 (Rottger et al., 1999; van Eijl et al., 2000; Ward and Moss, 2004). Deletion of A36 leads to accumulation of IEV in the perinuclear region, and consequently reduces the cell-to-cell spread of vaccinia (Moss and Ward, 2001; Parkinson and Smith, 1994; Rietdorf et al., 2001; Wolffe et al., 1998). A combination of GST pull-down assays and yeast two hybrid

screens together revealed that A36 could directly bind kinesin-1 via two conserved tryptophan motifs in the cytoplasmic domain of A36 (Dodding et al., 2011; Dodding et al., 2009; Konecna et al., 2006; Morgan et al., 2010). The A36 WE and WD motifs are conserved kinesin-1 binding motifs that are found in mammalian Calsyntenin-1 and γ-BAR (also known as Gadkin) (Araki et al., 2007; Dodding et al., 2011; Schmidt et al., 2009). Mutation of both of these motifs significantly reduces the spread of IEV to the plasma membrane and also results in defective cell-to-cell spread of the virus, as is observed following infection with vaccinia lacking A36 expression entirely (ΔA36R) (Dodding et al., 2011; Wolffe et al., 1998).

In addition to A36, the IEV proteins F12 and E2 have been implicated in microtubule-transport of IEVs (Carpentier et al., 2015; Morgan et al., 2010; van Eijl et al., 2002). Deletion of either F12 (ΔF12L) or E2 (ΔE2L) also led to a reduction in cell-to-cell spread (Dodding et al., 2009; Johnston and Ward, 2009; Zhang et al., 2000). Like A36, F12 contains a potential kinesin-1 binding WD motif, however, in isolation F12 is unable to mediate binding to kinesin-1 (Carpentier et al., 2015; Morgan et al., 2010). F12 in complex with E2, however, is able to associate with kinesin-1 (KLC isoform 2) (Carpentier et al., 2015). Interestingly, overexpression of a F12 mutant lacking the WD motif during infection with ΔF12L is unable to rescue IEV spread or kinesin-1 recruitment, suggesting that the WD motifs are clearly important for the functional role of F12 (Morgan et al., 2010). Whether A36 and the F12/E2 complex function together to mediate IEV transport is yet to be elucidated (Dodding et al., 2009; Johnston and Ward, 2009). Live cell imaging and ultrastructural analysis following infection with ΔF12L, suggest that F12, rather than acting as an essential component of viral transport, is essential for the formation of IEVs (Dodding et al., 2009). Curiously, it has been shown that IMV of the IHD-W strain of vaccinia are able to reach the cell periphery of infected cells in an microtubule-independent manner, although little is known about how this process is mediated and whether this occurs in other viral strains (Schepis et al., 2006; Tsutsui, 1983; Tsutsui et al., 1983).

1.1.5 Viral Egress and Spread

Once IEV reach the cell periphery, the outermost IEV membrane fuses with the plasma membrane, resulting in the presentation of the cell-associated enveloped virion (CEV) on the cell surface (Figure 1.3 – 8) (Arakawa et al., 2007; Blasco and Moss, 1992; Cudmore et al., 1995). During this process of fusion, kinesin-1 dissociates, and the largely cytoplasmic A36 localizes to the base of the virion (Figure 1.4) (Newsome et al., 2004; van Eijl et al., 2000). A36 is subsequently phosphorylated in a Src/Abl family kinase-dependent manner, initiating a complex signalling cascade which results in the recruitment of Arp2/3 and the assembly of actin structures, termed actin tails (Figure 1.3 – 9) (Blasco and Moss, 1992; Cudmore et al., 1995; Frischknecht et al., 1999a; Moreau et al., 2000; Newsome et al., 2004; Scaplehorn et al., 2002; Stokes, 1976; Zhang et al., 2000).

CEVs are propelled on the plasma membrane via these actin protrusions and mediate the direct cell-to-cell spread of vaccinia (Wolffe et al., 1998). While a proportion of CEVs (approximately 15-20 % in the case of vaccinia WR strain) are released as EEV, the majority of virions are retained as CEV on the surface of infected cells. CEV are largely responsible for the formation of viral plaques (Blasco and Moss, 1992). Vaccinia is able to spread directly via cell-to-cell contacts in distinct processes that are both dependent and independent on the formation of actin tails beneath the CEV. This may suggest that mechanisms of direct cell-to-cell spread via CEV are highly context dependent.

Actin polymerisation beneath CEV has been postulated to directly aid egress of the virus from the host membrane (Horsington et al., 2013). The driving force generated by actin polymerisation is thought to disrupt crucial luminal interactions of the IEV proteins that span the CEV membrane and the plasma membrane, and thus disrupt association with the cell itself, facilitating the release of EEV (Figure 1.5) (Horsington et al., 2013). The viral proteins B5, A33 and A34 all contain signification luminal domains thought to mediate adhesion with one another and therefore to the host plasma membrane (Figure 1.4) (Duncan and Smith, 1992; Isaacs et al., 1992; Roper et al., 1996). In support of this, a C terminal deletion in A33, and point mutations in B5

(P189S) and A34 (K151E) that disrupt luminal interactions, all led to an increase in EEV release (Blasco et al., 1993; Katz et al., 2003; Katz et al., 2002).

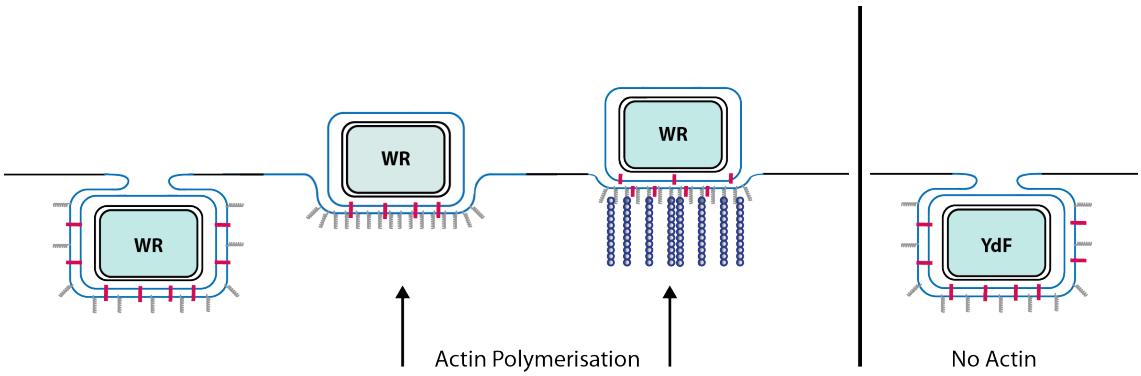

Figure 1.5 Mechanisms promoting vaccinia egress

A proposed mechanism in which actin polymerisation beneath the CEV clusters IEV proteins beneath the virion and provides the driving force to disrupt luminal interactions of the IEV proteins tethering the CEV to the plasma membrane. A virus that cannot induce actin tails, A36 YdF, was shown by EM to be trapped in invaginated pits in the membrane, tethered by multiple luminal interactions of the IEV proteins shown in Figure 1.4 (indicated by pink lines above). (Horsington et al., 2013).

Despite only representing a fraction of infectious virions, the spread of vaccinia through tissue is predominantly mediated by EEV (Payne, 1980). EEV are resistant to neutralizing antibodies and the immune complement, providing a huge biological advantage over IMV mediated spread in vivo (Law et al., 2002; Law and Smith, 2001; Smith et al., 2002; Vanderplasschen et al., 1998). Extracellular enveloped virions (EEVs) are formed once the CEVs are released from the plasma membrane, and are able to infect adjacent cells in addition to facilitating the long-range spread of infection via the release of free EEVs into the blood stream of an infected organism (Payne, 1980; Roberts and Smith, 2008).

More recently, however, it has been found that released EEVs may also play a role in long-range actin tail mediated spread of infection in order to enhance viral spread (Condit, 2010; Doceul et al., 2012; Doceul et al., 2010). The kinetics of viral spread

through a monolayer of cells were found to be four-fold faster than expected given the temporal dynamics of the viral replication cycle (Figure 1.3). Reinfection of infected cells is inhibited by the presence of A56-K2 dimers at the plasma membrane following infection (Turner and Moyer, 2008; Wagenaar and Moss, 2009). The A56-K2 complex engages with the entry fusion complex (EFC) on incoming viral particles to prevent reinfection (Wagenaar and Moss, 2007; Wagenaar et al., 2008). The transmission of vaccinia through a monolayer can, however, be enhanced by the presence of the IEV proteins A36 and A33 at the plasma membrane of recently infected cells (Doceul et al., 2010). A36 and A33 are expressed early following infection and are crucial for the formation of actin tails. Prior to the production of infectious particles from recently infected cells (Figure 1.6 A), released EEV can arrive at the plasma membrane, and although inhibited from reinfection, can utilise A36 and A33 at the membrane (Figure 1.6 B) to propel the EEV along the cell surface, until an uninfected cell is reached (Figure 1.6 C) (Doceul et al., 2012; Doceul et al., 2010). This model of rapid transmission of EEV would ensure that infected cells are able to promote viral spread even prior to the production of infectious particles. These 'secondary' actin tails induced by A36 and A33 upon contact with EEVs therefore enhances the rate of viral spread through a monolayer (Condit, 2010; Doceul et al., 2012; Doceul et al., 2010).

Lastly, in addition to direct viral spread mediated by the dissemination of CEV and EEV, vaccinia infection may also be enhanced via viral-induced cell motility. Following infection, the expression of early viral genes appear to be responsible for dramatic cellular morphological changes that lead to cellular contraction, re-spreading, migration, and cytopathic effect (CPE) (Bablanian et al., 1978; Sanderson and Smith, 1998; Schepis et al., 2006; Schramm et al., 2006). The precise mechanism and requirement of viral-induced cell motility remains to be elucidated at this point, however the induction of cell migration upon infection enhances the ability of vaccinia to come into contact with uninfected cells and therefore disseminate rapidly through cells and tissues.

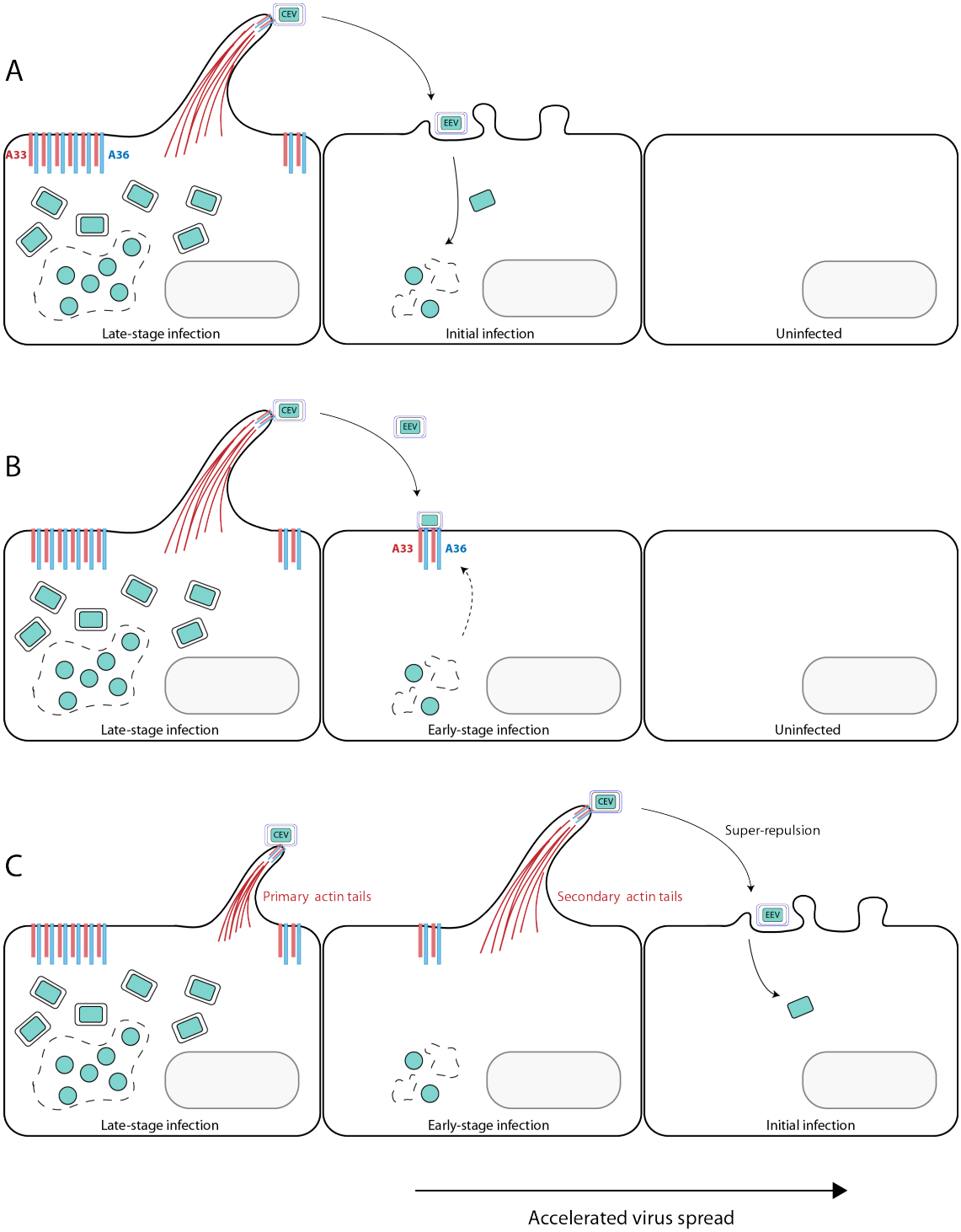

Figure 1.6 The super-repulsion hypothesis

A Infection is initiated on a neighbouring cell mediated by CEV or EEV particles released after 6-8 hours of infection. **B** EEVs arrive on an adjacent recently infected cell that is undergoing the early stages of viral infection. A36 and A33 are expressed early following infection and are therefore present on the plasma membrane. **C** The presence of A36 and A33 is sufficient to induce a secondary actin tail beneath the EEV and propel the EEV even further in order to infect distal, uninfected cells (Doceul et al., 2010). Adapted from Pickup, 2010.

1.2 The Actin Cytoskeleton and N-WASP in pathogen spread

1.2.1 Actin polymerisation

During infection, vaccinia virus hijacks the actin cytoskeleton to facilitate both macropinosomal entry and actin tail mediated egress and spread (Doceul et al., 2010; Horsington et al., 2013; Mercer and Helenius, 2009). Actin is highly conserved throughout evolution and is one of the most abundant proteins in eukaryotic cells (Erickson, 2007; Firat-Karalar and Welch, 2011). Therefore, it comes as no surprise that a number of pathogens utilise actin-dependent processes to facilitate entry or spread.

The ability of actin to self-polymerise plays an essential role in a large number of cellular structures and processes that are fundamental to cell function. At a cellular level polymerisation of actin at the leading edge drives cell migration as well as the formation of lamellipodia and filopodia protrusions (Panner and Honig, 1967; Ridley, 2011; Woodrum et al., 1975). Furthermore, at a subcellular level actin plays a key role to facilitate and regulate membrane trafficking and endocytic events (Anitei and Hoflack, 2012; Mooren et al., 2012). Actin is able to cycle from monomeric 42 kDa globular G-actin, to filamentous F-actin. F-actin has polarised ends, comprising a pointed and a barbed end, derived from the appearance of actin filaments in electron micrographs (Huxley, 1963; Woodrum et al., 1975). The initial assembly of three G-actin monomers forms a stable ‘seed’ which nucleate filament growth (Gilbert and Frieden, 1983; Nishida and Sakai, 1983). Following this nucleation phase, rapid filament elongation can proceed. During elongation G-actin can be added to both ends of the filament, however, more rapid polymerization occurs at the barbed end (Goley and Welch, 2006; Pollard and Borisy, 2003; Woodrum et al., 1975).

Despite high cellular concentration of actin, *in vitro* the establishment of trimeric G-actin nuclei is extremely thermodynamically unfavorable, with the dissociation equilibrium constant in the Molar range (Pollard and Cooper, 1986; Pollard and Weeds, 1984). Several cellular actin nucleators, have evolved to overcome this kinetically unfavorable process (Campellone and Welch, 2010). The Arp2/3 complex was the first

actin nucleator to be discovered, and plays a vital role during vaccinia induced actin polymerization.

1.2.2 The Arp2/3 Complex

The Arp2/3 complex is composed of seven highly evolutionarily conserved subunits forming a large 220 kDa complex (Goley and Welch, 2006; Machesky et al., 1994). The Arp2/3 core consists of Arp2 and Arp3 (actin-related proteins 2 and 3) that associate with the additional Arp subunits C1-C5 (Goley and Welch, 2006; Pollard, 2007). Highly conserved from yeast to man, the Arp2/3 complex is crucial for nucleation of new actin filaments, and cross-linking of actin filaments into the characteristic 70 degree, Y-branches first observed in electron micrographs (Blanchoin and Pollard, 2002; Mullins et al., 1998). The core Arp2 and Arp3 subunits have 47% and 40% identity to actin respectively and are brought into close proximity in the active state of the complex, mimicking dimeric actin (Kelleher et al., 1995; Robinson et al., 2001). This overcomes the kinetic barrier preventing spontaneous actin nucleation and provides a template from which filament elongation can proceed. Activated Arp2/3 can bind to the side of a pre-existing mother filament, thus promoting the nucleation of a nascent daughter filament (Amann and Pollard, 2001; Blanchoin et al., 2000; Mullins et al., 1998). The ability of the Arp2/3 complex to induce networks of branched actin filaments provides a key driving force in formation of lammellipodia, invadopodia, and pathogen induced actin structures (Bailly et al., 2001; Welch and Way, 2013; Yamaguchi et al., 2005).

In order to bring the Arp2 and Arp3 subunits into close proximity to promote Arp2/3 activation *in vivo*, several key regulators have been identified (Bonder et al., 1983; Pollard and Borisy, 2003; Wang, 1985). *In vitro* reconstitution of the actin-based motility of the bacterium *Listeria monocytogenes* identified a bacterial protein, ActA that was able to promote the actin nucleating ability of Arp2/3 and stimulate bacterial motility (Loisel et al., 1999; Welch et al., 1997; Welch et al., 1998; Welch and Way, 2013). Several cellular proteins that perform the analogous function *in vivo* have now been uncovered. These are known as nucleation-promoting factors or NPFs (Campellone and Welch, 2010; Le Clainche and Carlier, 2008).

The NPFs are subdivided into two distinct classes. Class I NPFs make up the largest group of NPFs and are characterised by the presence of a conserved C-terminal WCA domain (WASP-homology2-Central-Acidic) that bind G-actin and the Arp2/3 complex. *In vitro*, this domain is sufficient to mediate activation of Arp2/3 (Goley and Welch, 2006). Class II NPFs lack the G-actin binding WH2 domain, and instead contain a F-actin binding domain (FAB) that has been shown to be essential for Arp2/3 activation (Goode et al., 2001; Uruno et al., 2001; Weaver et al., 2001). The binding of NPFs to Arp2/3, acts to enhance Arp2/3 activity in a temporal and spatial manner (Ma et al., 1998; Mullins et al., 1998; Rohatgi et al., 1999; Welch et al., 1998). A number of NPFs have been identified including WASP (Winter et al., 1999; Yarar et al., 1999), N-WASP (Rohatgi et al., 1999), ActA (Welch et al., 1998), WAVE (Machesky et al., 1999), yeast Abp1p (Duncan et al., 2001), and yeast Pan1p (Duncan et al., 2001) to name a few. The diversity of the NPF family of proteins reflects the wide variety of actin dependent processes that they mediate, including pathogen spread (Welch and Way, 2013). Vaccinia hijacks both Arp2/3 and its well-characterized nucleation-promoting factor, N-WASP to induce the formation of actin tails (Cudmore et al., 1995; Moreau et al., 2000).

1.2.3 N-WASP function and regulation

The Class I NPF, N-WASP is expressed in most cell types and is highly conserved amongst eukaryotes (Miki et al., 1996; Snapper et al., 2001). N-WASP plays a vital role in multiple host cell processes such as phagocytosis, endocytosis, the formation of invadopodia and filopodia, as well as pathogen induced actin polymerisation (Dart et al., 2012; Miki et al., 1998; Qualmann et al., 2000; Snapper et al., 2001; Yamaguchi et al., 2005). N-WASP is composed of a N-terminal WH1 (WASP homology 1) domain, followed by a basic region (B), GTPase binding domain (GBD), a proline-rich domain (PRD), and C-terminal WCA domain crucial for the activation of Arp2/3 (Figure 1.7). The WCA domain consists of a WH2 region (W), and a central region (C) and a terminal acidic region (A). The CA region directly interacts with multiple subunits in the Arp2/3 complex (Rodal et al., 2005; Weaver et al., 2002; Zalevsky et al., 2001). Multiple structural studies supports the role of CA binding in order to induce a large conformational change to bring the Arp2 and Arp3 subunits into close proximity, thus activating the Arp2/3 complex (Chereau et al., 2005; Marchand et al., 2001; Panchal et

al., 2003). The WH2 domain recruits G-actin, delivering actin to the Arp2/3 complex, together mimicking the G-actin trimer 'seed' required to nucleate filament growth.

N-WASP is itself tightly regulated in order to facilitate the correct spatial and temporal activation of Arp2/3 mediated actin polymerisation (Miki et al., 1996; Snapper et al., 2001). N-WASP together with WIP (WASP-interacting protein) and the SH3 containing proteins Nck and Grb2 cooperate to mediate Arp2/3-dependent vaccinia induced actin polymerisation (Figure 1.8) (Moreau et al., 2000; Zettl and Way, 2002). N-WASP exists in an autoinhibited conformation and requires activation to facilitate binding of Arp2/3 and actin (Kim et al., 2000; Miki et al., 1998; Prehoda et al., 2000; Rohatgi et al., 2000).

In its inactive conformation the N-WASP GTP-binding domain (GBD) is bound to its WCA domain, preventing Arp2/3 recruitment (Kim et al., 2000; Miki et al., 1998; Rohatgi et al., 2000). One of the first characterised activators of N-WASP was the Rho-family GTPase, Cdc42 (Miki et al., 1998). Rho GTPases are small 20-25 kDa proteins that act as molecular switches due to their ability to cycle from a GTP-bound active state to a GDP-bound inactive state (Hall, 2012). Guanine nucleotide exchange factors (GEFs), GTPase activation proteins (GAPs) and guanine-nucleotide-dissociation inhibitors (GDIs) regulate the conversion between these two states. The majority of Rho-family GTPases, including Cdc42 are post-translationally modified at their C-terminus by the addition of an isoprenoid lipid, which plays an essential role in their localisation to cellular membranes (Boulter and Garcia-Mata, 2012). In order to activate N-WASP, active (GTP-bound) Cdc42 binds the N-WASP GBD (Kim et al., 2000). The GBD cannot interact with both Cdc42 and the WCA domain, therefore binding of Cdc42 to the GDB induces a large conformation change that releases autoinhibition of N-WASP and frees the WCA domain, allowing it to engage with the Arp2/3 complex (Figure 1.7 A, B) (Kim et al., 2000; Miki et al., 1998; Torres and Rosen, 2006).

In addition, the proline-rich domain (PRD) that links the GBD and the WCA domain can interact with several SH3-domain containing N-WASP binding partners. These include Nck, Grb2, Toca-1, Abi1, syndapin and Abp1 (Carlier et al., 2000; Ho et al., 2004; Innocenti et al., 2005; Kessels and Qualmann, 2004; Rohatgi et al., 2001).

Although interactions of the SH3 domains with the PRD do not directly disrupt GBD-WCA autoinhibition, they help to promote and maintain the formation of the active 'open' state of N-WASP. Nck and Grb2 have both been shown to synergize with PI(4,5)P_2 and Cdc42 respectively to enhance activation of N-WASP (Carlier et al., 2000; Rohatgi et al., 2001). The combination of Cdc42-mediated activation and binding of the SH3-containing proteins together maintains N-WASP in its open conformation and promotes Arp2/3-dependent actin polymerization (Figure 1.7 A).

Oligomerization of N-WASP has been identified as a key mechanism in the regulation of N-WASP function (Padrick et al., 2008; Padrick et al., 2011). The Arp2/3 complex contains two WCA binding sites, and it has been show that dimerization of two N-WASP WCA domains enhances the ability of the Arp2/3 complex to polymerise actin 100-200 fold (Figure 1.7 B) (Higgs and Pollard, 2000; Padrick et al., 2011; Ti and Pollard, 2011). Supporting this, antibody-mediated clustering of Nck, led to the induction of N-WASP and Arp2/3 dependent actin comets from which the relative ratios of Arp2/3 and N-WASP were able to be determined (Ditlev et al., 2012). This reported a 2:1 ratio of N-WASP to Arp2/3, consistent with the earlier observations that two WCA domains are required to interact with each Arp2/3 complex (Figure 1.7 C).

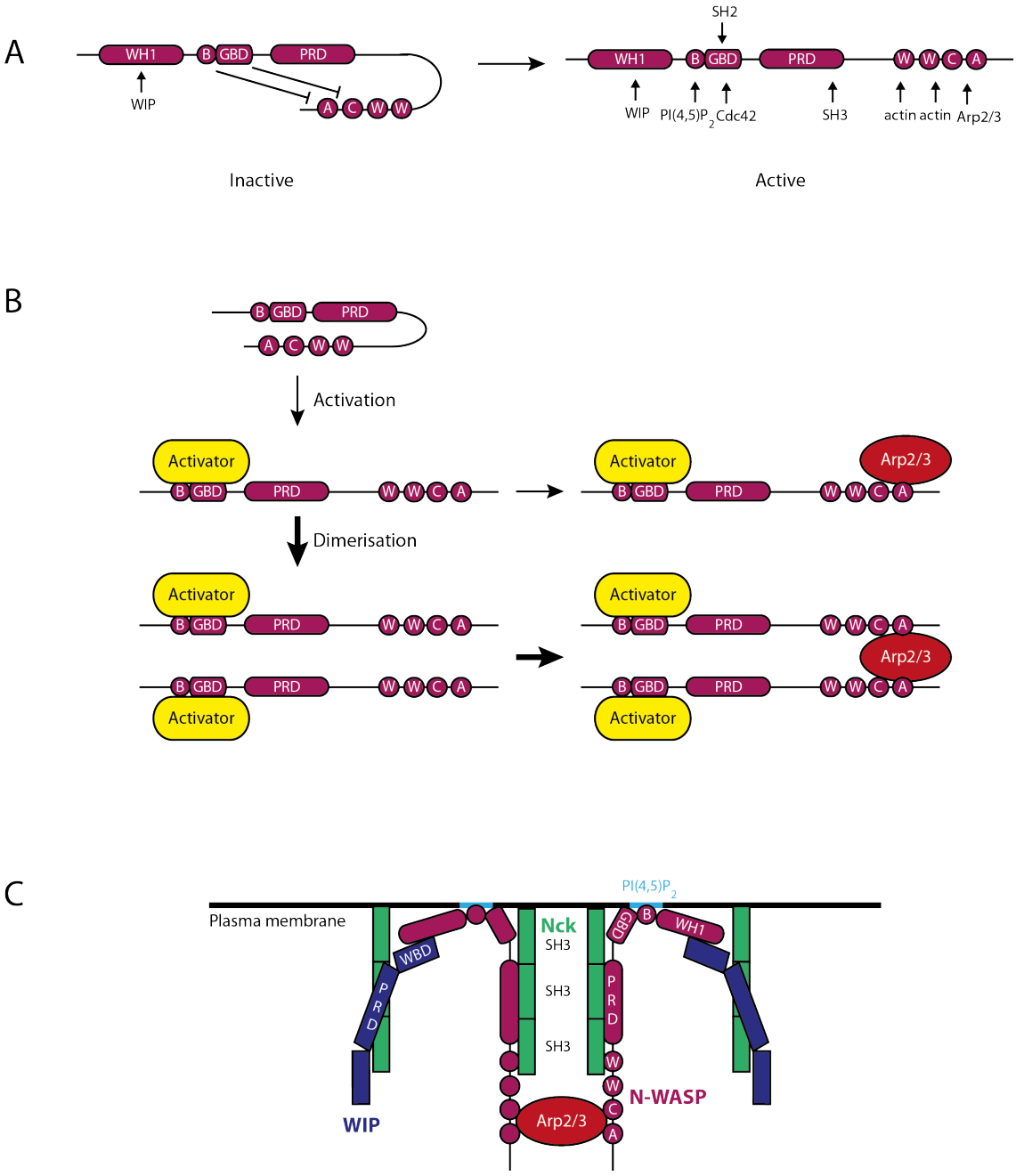

Figure 1.7 N-WASP regulation

A N-WASP is autoinhibited via intramolecular interactions between the GBD and the WCA domains (left). Active conformation and binding sites of N-WASP interacting proteins (right) (Campellone and Welch, 2010). **B** The activation of N-WASP. Activator binding releases the WCA domain, and promotes binding of the Arp2/3 complex. Dimerisation results in higher affinity binding of the WCA domain to Arp2/3 (adapted from Padrick et al., 2008). **C** Antibody-mediated clustering of the SH3 domains of Nck proposed a ratio of two N-WASP molecules to one Arp2/3 complex, consistent with the presence of two WCA binding sites in Arp2/3 (adapted from Ditlev et al., 2012).

1.2.4 Vaccinia actin tail formation

The hijacking of the actin polymerisation machinery by pathogens has led to numerous insights about the regulation of actin polymerisation *in vivo* (Welch and Way, 2013). In a mechanism that is conserved among the poxviruses, vaccinia virus assembles actin structures to facilitate egress and mediate cell-to-cell spread (Dodding and Way, 2009).

During vaccinia egress, following fusion of the virus with the plasma membrane, the outer IEV membrane is incorporated into the plasma membrane. The virus induces outside-in signalling to locally activate Src and Abl family kinases in a process dependent on B5 (Frischknecht et al., 1999b; Newsome et al., 2004; Newsome et al., 2006). Activated Src phosphorylates A36 at tyrosine 112 and 132, in a manner mimicking receptor tyrosine kinase signalling. Phosphotyrosines 112 and 132 can recruit the SH3-adaptor proteins, Nck and Grb2 respectively (Frischknecht et al., 1999a; Newsome et al., 2004; Scaplehorn et al., 2002). Nck directly interacts with WIP in order to recruit the WIP:N-WASP complex (Figure 1.8) (Donnelly et al., 2013; Weisswange et al., 2009). This results in the local activation of the Arp2/3 complex beneath the CEV, and the induction of actin tails (Frischknecht et al., 1999b; Moreau et al., 2000). The N-WASP PRD also interacts with Grb2 downstream of phosphotyrosine 132 (Donnelly et al., 2013; Frischknecht et al., 1999b; Moreau et al., 2000; Snapper et al., 2001; Zettl and Way, 2002). Grb2 although not essential for actin tail formation, functions as a secondary adaptor (Scaplehorn et al., 2002; Weisswange et al., 2009). FRAP experiments revealed that Grb2, Nck, and WIP all exhibit rapid rates of exchange beneath the virus, 3.5 times faster than N-WASP turnover (Weisswange et al., 2009). Loss of Grb2 led to even higher turnover of Nck and WIP, suggesting that the primary role of Grb2 is to stabilise the vaccinia actin-signalling complex (Weisswange et al., 2009).

In addition, Cdc42 has been found to regulate the activity of N-WASP to stimulate Arp2/3 dependent actin tails (Humphries et al., 2014). Expression of a N-WASP mutant (N-WASP H208D) that is unable to bind Cdc42, leads to a decrease in the ability of the virus to nucleate actin tails, and inhibition of viral spread (Humphries et al., 2014; Miki et al., 1998). Cdc42 acts cooperatively with Nck and Grb2 to stabilise N-WASP beneath

the virus. Furthermore, the RhoGEF intersectin-1 is recruited to the virus prior to actin tail formation via an unknown mechanism, and thought to locally activate Cdc42 upon its binding to N-WASP (Figure 1.8) (Humphries and Way, 2013; Hussain et al., 2001). Mediated by multiple interactions with WIP, Nck, Grb2, and Cdc42, N-WASP can stably recruit actin and the Arp2/3 complex, facilitating actin polymerisation beneath the CEV, thus enhancing viral spread (Frischknecht et al., 1999a; Snapper et al., 2001; Weisswange et al., 2009).

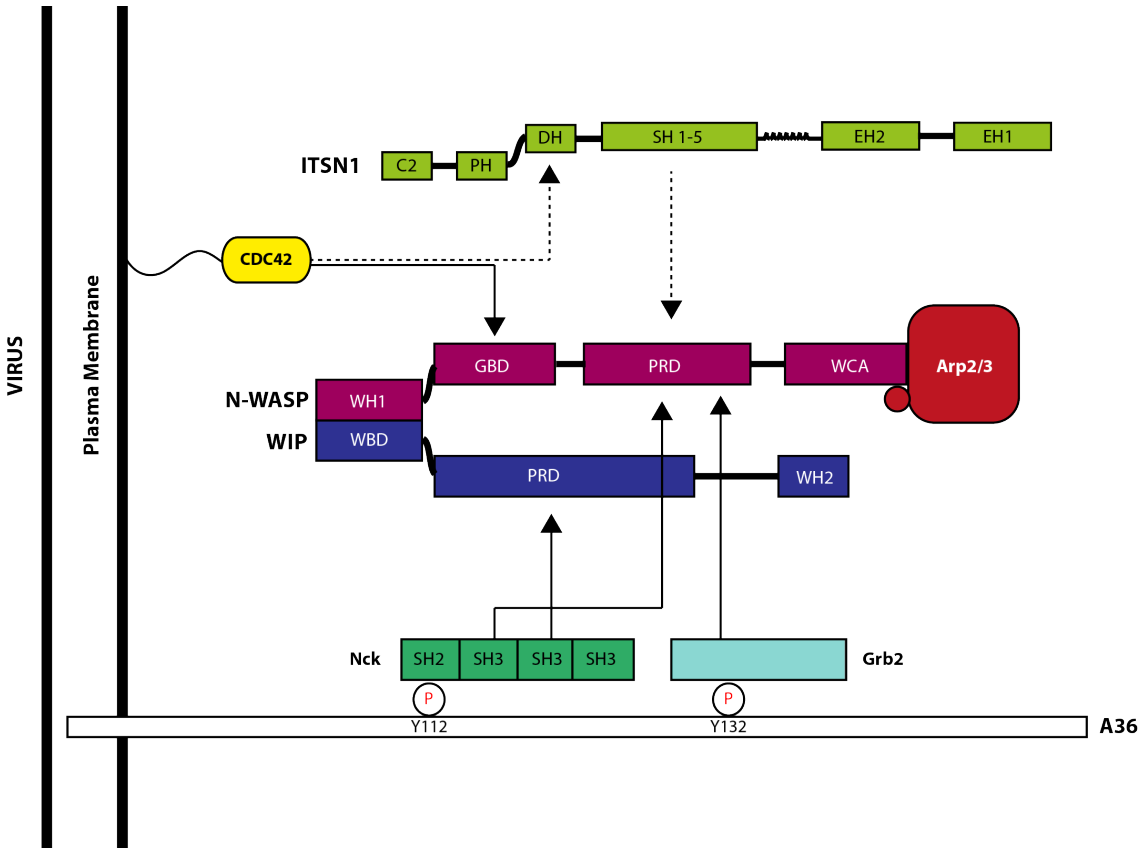

Figure 1.8 The vaccinia actin-signalling network

The actin-signaling network mediated by phosphorylation of A36 Y112 and Y132. Bold lines indicate experimentally confirmed interactions between components of the vaccinia-signaling complex. Dashed lines indicate interactions between components of this actin signaling complex determined in another systems, which may also occur in the case of viral induction of actin tails. Domains are annotated: SH2 (Src homology 2), SH3 (Src homology 3), WBD (WASP binding domain), PRD (Polyproline-rich domain), WH1 (WASP homology 1), GBD (GTPase binding domain) and WCA (WH2, central and acidic region), EH (Eps15-homology domain), DH (Dbl-homology domain), PH (Pleckstrin-homology domain), C2 (Membrane targeting motif).

1.2.5 Actin-based motility of pathogens

A number of bacterial pathogens also utilise the host actin polymerisation machinery to promote infection such as EPEC, *Listeria,* and *Shigella,* (Bernardini et al., 1989; Heinzen et al., 1993; Tilney and Portnoy, 1989). Both enteropathogenic *Escherichia coli* (EPEC) and vaccinia virus recruit N-WASP and Arp2/3 in mechanism analogous to tyrosine phosphorylation dependent signalling {Frischknecht, 1999 #79}{Frischknecht, 2001 #156}{Welch, 2013 #768}. Upon contact of EPEC with the host cell, a type III secretion system inserts the bacterial effector protein Tir (translocated intimin receptor) into the host plasma membrane (Kenny et al., 1997). Tir is tyrosine phosphorylated by Src, resulting in Nck recruitment mediated by phosphotyrosine 474 (Kenny, 1999; Phillips et al., 2004; Swimm et al., 2004). Nck binding mediates the recruitment of N-WASP and Arp2/3, stimulating the polymerisation of actin beneath the bacterium (Gruenheid et al., 2001). This forms highly dynamic actin pedestals that promote efficient bacterium colonization (Kenny et al., 1997).

Shigella flexneri and *Listeria monocytogenes* both induce actin-rich structures that propel them through the cytoplasm. The *Shigella* protein IcsA is the sole mediator of actin-based motility during infection, and acts to both recruit and activate N-WASP beneath the bacterium (Bernardini et al., 1989; Egile et al., 1999; Goldberg and Theriot, 1995; Kocks et al., 1995; Moreau et al., 2000). *Listeria* ActA, was the first NPF to be identified and like both A36 and IcsA is the sole component of *Listeria* required to mediate actin polymerisation (Cameron et al., 1999; Domann et al., 1992; Kocks et al., 1992; Smith et al., 1995; Welch et al., 1998). ActA is a class I NPF that mimics the N-WASP WCA domain and is able to directly recruit and activate the Arp2/3 complex (Egile et al., 1999; Tilney and Portnoy, 1989; Welch et al., 1997; Welch et al., 1998).

The host actin polymerisation machinery is not alone in being hijacked by pathogens in order to enhance the spread of infection. The endocytic clathrin machinery forms another system of highly conserved proteins that are manipulated during pathogen entry and spread.

1.2.6 A Clathrin-dependent step

Clathrin is most commonly associated with endocytosis at the plasma membrane, however during vaccinia infection, it instead appears to facilitate the formation of actin tails during viral egress (Humphries et al., 2012). Following the fusion of the viral particle with the plasma membrane, clathrin and its adaptor, AP-2, are recruited. Live cell imaging showed that AP-2 and clathrin are transiently recruited following the loss of kinesin-1, and dissociate upon actin tail formation. Super-resolution imaging also revealed that AP-2 plays a role to cluster A36 and N-WASP beneath the CEV (Figure 1.10) (Humphries et al., 2012). In this regard, clathrin machinery appears to mimic the early stages of endocytosis, which begins by selective sequestration of cargo. While the actin-signalling network can function in the absence of clathrin, the loss of clathrin-mediated A36 and N-WASP polarisation leads to a less robust actin-signalling platform and delayed actin tail nucleation (Humphries et al., 2012). Once formed, actin tails are significantly longer and fewer in number. It is hypothesised that the clustering of A36 and N-WASP facilitates the oligomerization of N-WASP, which is known to enhance the activation of the Arp2/3 complex (Figure 1.7). Precisely how AP-2 and clathrin recruitment results in this altered actin tail behaviour is yet to be elucidated. To similar effect, *in vitro* motility assays have demonstrated that the density of N-WASP or its WCA domain determines Arp2/3-dependent bead or vesicle motility (Bernheim-Groswasser et al., 2002; Delatour et al., 2008; Wiesner et al., 2003). Once an actin tail is formed, the viral particle is propelled away from the AP-2 and clathrin-rich membrane, and AP-2 and clathrin dissociate.

The cytoplasmic domain of A36 (residues 24-221) was shown to associate with AP-2. Earlier studies identified that the IEV protein, F13, is also able to associate with AP-2 (Husain and Moss, 2003). Several potential adaptor-binding motifs exist within the IEV proteins that may be responsible for AP-2 or clathrin recruitment (Figure 1.9). The molecular basis of AP-2 and clathrin recruitment could therefore involve a combination of weak interactions mediated by multiple IEV proteins. It has been shown that actin nucleation itself promotes the polarization of A36 beneath the virus and disrupts luminal interactions of IEV proteins that tether the virus to the plasma membrane (Figure 1.5) (Horsington et al., 2013). Clathrin-mediated clustering of A36 beneath the

virion may therefore aid EEV release by contributing to the disruption of IEV tethering to the plasma membrane.

Figure 1.9 Vaccinia IEV proteins and their potential adaptor binding motifs

The amino acid sequences of the IEV specific proteins, A36, F13, B5, A33 and A34. The predicted transmembrane domains are highlighted in green. Sequences exposed within the cytoplasm are in black and those that are outside of the cell following the fusion of IEV with the plasma membrane are in grey. Potential clathrin adaptor binding sites are indicated in red.

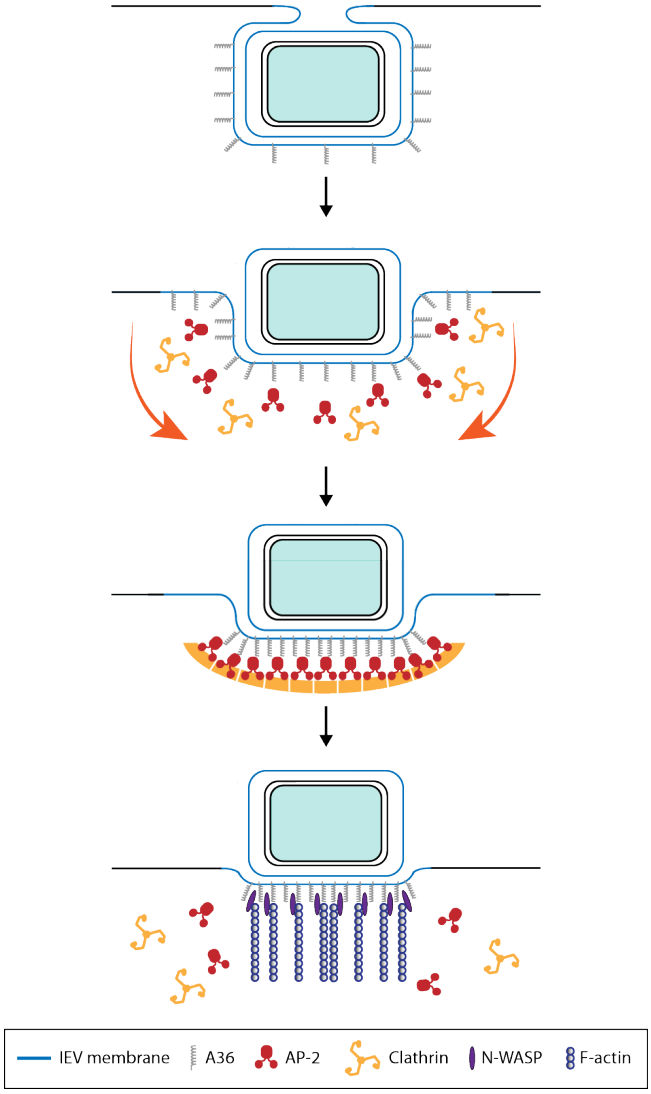

Figure 1.10 Model of clathrin function during vaccinia virus egress

During IEV egress the outer viral membrane (blue) fuses directly with the plasma membrane and viral IEV proteins, including A36, become incorporated. In this model proposed by Humphries et al 2012, AP-2 together with clathrin cluster A36 beneath the virus particle. This creates a stable protein platform to which N-WASP and other components of the actin-signaling network can be recruited.

1.2.7 Subversion of endocytic machinery by pathogens

The plasma membrane barrier is the first obstacle pathogens face during infection of a host cell. To facilitate internalisation, a number of endocytic pathways are hijacked to overcome the plasma membrane, among them, macropinocytosis and phagocytosis (Cossart and Sansonetti, 2004; Gruenberg, 2009; Marsh and Helenius, 2006; Mercer et al., 2010; Pelkmans and Helenius, 2003; Schelhaas, 2010). Typically clathrin-coated vesicles range in size from 30 nm – 150 nm, however in many instances clathrin facilitates the uptake of far larger objects. This was first demonstrated to be the case during internalisation of vesicular stomach virus (VSV). VSV, which is 200 nm in diameter, is able to enter cells in a clathrin-dependent manner, hijacking the actin cytoskeleton in order to breach the host cell membrane (Cureton et al., 2009; Cureton et al., 2010; Johannsdottir et al., 2009).

Retroviruses despite the small complement of proteins they encode, have also found unique ways to hijack the endocytic machinery during entry and budding from the host. It has been shown the HIV-1 Gag protein recruits clathrin adaptors, AP-2 and AP-1 in order to promote trafficking of viral proteins and budding at the membrane (Batonick et al., 2005; Camus et al., 2007). The HIV-1 glycoprotein (gp41) plays a crucial role in facilitating fusion between viral and target cell membranes upon viral entry. Following contact with a target cell, the gp41 N-terminus is inserted into the host plasma membrane. Work has uncovered that the HIV-1 gp41 core specifically binds the Asn-Pro-Phe (NPF) repeats in the early endocytic protein, epsin (Huang et al., 2006; Huang et al., 2008) A peptide mimicking the epsin NPF motifs (470-499) causes a block in HIV-1 entry (Huang et al., 2008). Furthermore, the overexpression of dominant negative Eps15 which is recruited downstream of epsin also results in a 95% decrease in viral entry, suggesting that the entire early endocytic pathway is required for HIV-1 uptake (Nakashima et al., 1999).

Clathrin is also recruited to EPEC induced actin pedestals described in 1.2.5. EPEC induced pedestal formation is an AP-2 independent process, and instead the endocytic adaptor protein Dab2 along with the early endocytic proteins, epsin and Eps15 are responsible for clathrin recruitment (Lin et al., 2011; Maurer and Cooper, 2006). The

role of clathrin at the EPEC pedestal is yet to be fully elucidated, however it has been shown that the phosphorylation of clathrin heavy chain is triggered upon infection, which leads to the formation of a robust signalling platform and subsequent actin polymerization (Bonazzi et al., 2011).

1.3 Clathrin Mediated Endocytosis

Clathrin was first isolated by Barbara Pearse in 1976, and has been intimately linked to the process of vesicle trafficking, endocytosis, and recycling (Pearse, 1976). The first observations of what were later found to be clathrin-coated pits were reported during the study of yolk-protein uptake in mosquito oocytes in 1964 (Roth and Porter, 1964). This revealed coated baskets of triskelia at the plasma membrane around 30 nm in length. The observation of coated pits, vesicles, and fused granules led to an initial description of pinching, uncoating, and fusion that we now understand as characterising classical clathrin-mediated endocytosis (McMahon and Boucrot, 2011; Roth and Porter, 1964). More recently newly emerging roles of clathrin have become more apparent. Clathrin has crucial functions in the regulation of signal transduction, neuronal development, cell division, and of course during pathogenesis (Cossart and Veiga, 2008; Cureton et al., 2009; Veiga and Cossart, 2005; Warner et al., 2006). Several viral and bacterial pathogens described thus far, have been shown to hijack the clathrin machinery at the plasma membrane in order to force entry into the host cell (Cossart and Veiga, 2008; Cureton et al., 2009; Gruenberg, 2009; Marsh and Helenius, 2006; Mercer et al., 2010; Pizarro-Cerda et al., 2010; Veiga and Cossart, 2005). In the case of vaccinia, clathrin appears to have a unique role to support actin dynamics and enhance viral spread (Figure 1.10) (Humphries et al., 2012; Humphries and Way, 2013).

1.3.1 Clathrin

It is the unique structure of clathrin observed by electron microscopy (EM) in 1976 that led to the discovery of its role in the formation of vesicles at the plasma membrane. The characteristic triskelia organisation of clathrin, results from the trimerisation of three identical clathrin heavy chains (CHC - 180 kDa) via the central ‘hub’ (Kirchhausen et al., 1987; Liu et al., 1995). Each heavy chain associates with one clathrin light chain

(CLC – 33-36 kDa) via the CHC proximal leg domain (Figure 1.11 A) (Kirchhausen and Harrison, 1981; Ungewickell and Branton, 1981). Self-assembly of clathrin triskelia forms the polyhedral lattice structure first observed by EM (Roth and Porter, 1964). It is this unique self-assembly property of clathrin that mediates its function at the plasma membrane. Like actin, the CHC is conserved in all eukaryotes (Wakeham et al., 2005). Regulation of clathrin lattice formation and assembly is mediated by a combination of clathrin light chain binding, adaptor binding, phosphorylation and the isoform diversity of the clathrin itself (Brodsky, 2012; Delom and Fessart, 2011; Di Pietro et al., 2010; Reider and Wendland, 2011; Wang et al., 2013; Ybe et al., 1998). The clathrin heavy and light chains are encoded by two genes; CHC17/CHC22 and CLCa/CLCb respectively (Jackson et al., 1987; Kirchhausen et al., 1987). CHC17 is ubiquitously expressed in all tissues (Brodsky, 2012). In contrast CHC22, despite 85% sequence homology to CHC17, appears to have a more specialised role, and is most highly expressed in muscle tissue (Vassilopoulos et al., 2009). CHC22 can associate with the adaptors AP-1 and AP-3 but not AP-2, however is able to rescue CHC17 function in CHC17 depleted cells, suggesting a degree of redundancy between the heavy chain isoforms (Hood and Royle, 2009; Liu et al., 2001; Vassilopoulos et al., 2009). While both CLC isoforms associate with CHC17, neither can bind CHC22, again alluding to the more distinct role of CHC22 (Liu et al., 1995).

The hub of the CHC is composed of a central trimerization domain, proximal leg extension, and knee joint, followed by the distal leg domain (Figure 1.11 A) (Smith and Pearse, 1999). A flexible linker region connects the hub to the ankle region altogether terminating in the N-terminal domain (TD). The CLC contains three key tryptophan residues that mediate binding to the CHC (Ybe et al., 1998). The rearrangement of the N-terminus of the CLC in relation to the heavy chain facilitates a bent knee conformation, compatible with the formation of the clathrin lattice (Wilbur et al., 2010). In addition to CLC, other clathrin binding proteins are able to bind the TD region in order to induce clathrin assembly (Drake et al., 2000; Miele et al., 2004; ter Haar et al., 1998).

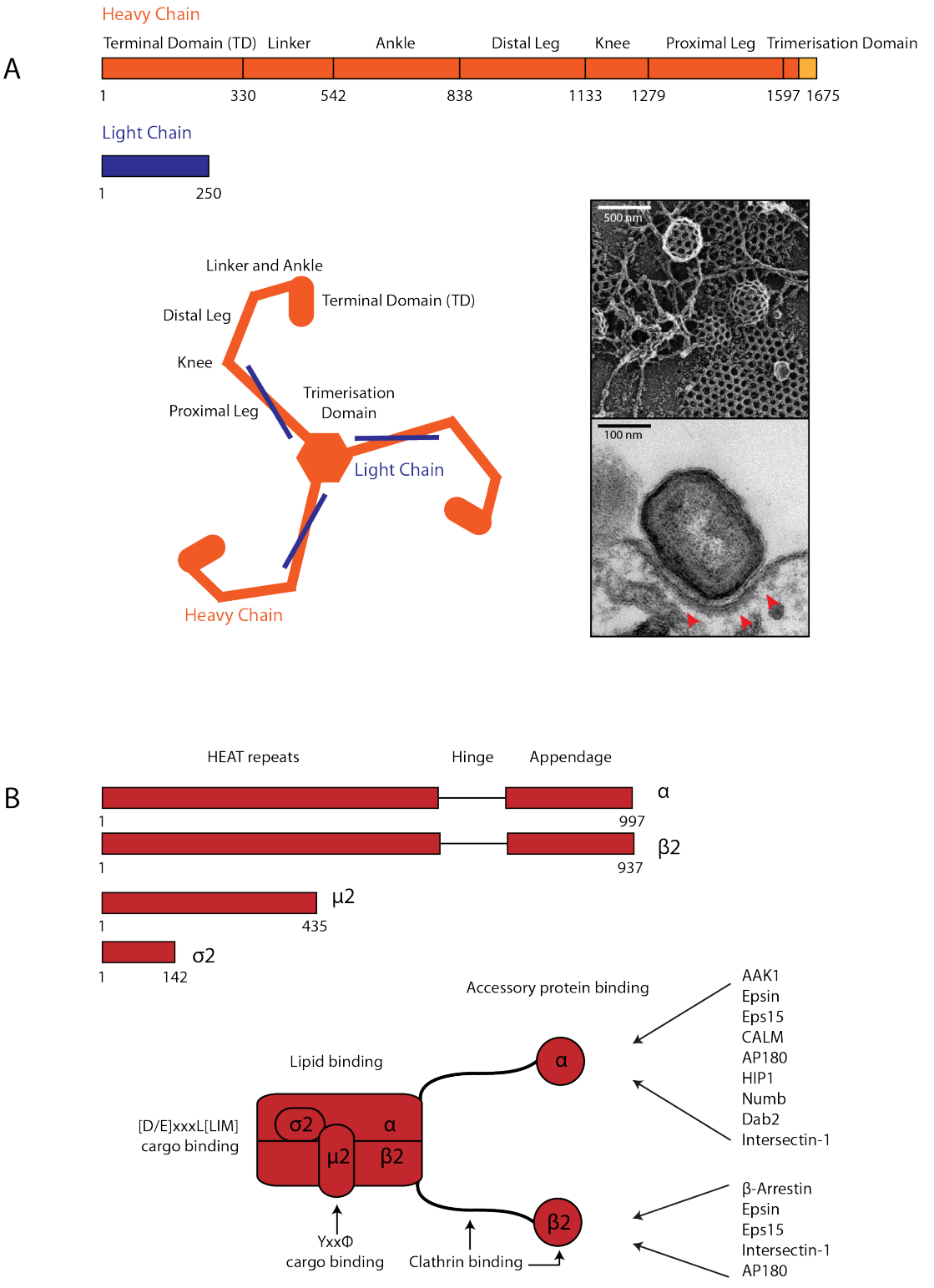

Figure 1.11 Domain and subunit organisation of clathrin and AP-2

A The domain organisation of clathrin light and heavy chains and their organisation in the triskelia. Top panel - Inset depicts quick-freeze deep-etch images of clathrin-coated vesicles budding from the plasma membrane (with thanks to John Heuser) Bottom panel - vaccinia recruiting clathrin during viral egress. **B** AP-2 is composed of four subunits. Common accessory proteins that bind the appendages are shown to the right. Adapted from (Kirchhausen et al., 2014; Ohno, 2006).

1.3.2 Clathrin Adaptors

The term adaptor was first coined in 1981, as it was clear that there must be a family of proteins to link clathrin, which itself lacks membrane binding activity, to its designated cargo (Dannhauser and Ungewickell, 2012; Kirchhausen, 1999; Pearse and Bretscher, 1981; Robinson, 2004). Currently over 20 endocytic accessory proteins have been described (excluding splice variants) (Owen et al., 2004). Although diverse in function, clathrin adaptors share many common characteristics. Firstly, most adaptors contain modular cargo-binding domains (Kalthoff et al., 2002; Merrifield and Kaksonen, 2014; Traub, 2009). Secondly, the clathrin adaptors also contain short, highly conserved linear motifs often followed by largely unstructured linker regions that mediate binding to the N-terminal domain (TD) in the large CHC (Figure 1.11 B).

The 'AP' family of clathrin adaptors were first identified following the observation that clathrin in isolation could only form cages in physiological conditions upon the addition of cytosolic extract (Keen et al., 1979; Pearse and Bretscher, 1981). These assembly polypeptide (AP) complexes consist of four subunits: two large ~ 100 kDa subunits (β and α/δ/γ/ε), a medium ~ 50 kDa subunit (μ), and a small 17 kDa subunit (σ) (Ahle et al., 1988; Keen et al., 1987; Matsui et al., 1990). The large subunits are themselves split into three domains that together with the μ and σ subunit make up the adaptor core (Figure 1.11 B). The large subunits α/δ/γ/ε and β consist of N-terminal HEAT repeats, followed by a flexible hinge region linking to the C-terminal appendage. The large β subunit is responsible for direct interaction with clathrin via the highly conserved clathrin box motif, LΦxΦ[D/E] (where Φ represents a bulky hydrophobic residue), with the β appendage providing an additional site of clathrin binding (Dell'Angelica et al., 1998; Gallusser and Kirchhausen, 1993; ter Haar et al., 2000). The appendages can also function to mediate binding to a host of accessory factors required to mediate specificity and function to the adaptor proteins *in vivo* (Figure 1.11 B).

Vertebrate genomes encode five adaptors: AP-1 – AP-5 (Hirst et al., 2013; Kirchhausen, 1999; Robinson and Bonifacino, 2001). AP-1 and AP-3 function during intracellular clathrin-dependent events between endosomes and the TGN (Klumperman et al., 1993; Meyer et al., 2000; Peden et al., 2002). AP-4 and AP-5 are the most recently

characterised adaptor proteins and have been linked to neuronal specific endosomal trafficking (Dell'Angelica et al., 1998; Hirst et al., 2011; Hirst et al., 2013). AP-2 mediates protein sorting and endocytic events specific to the plasma membrane and is responsible for clathrin recruitment to vaccinia prior to actin tail formation (Ahle et al., 1988; Humphries et al., 2012; Kirchhausen et al., 1997; Robinson, 1987).

AP-2, described in 1984, is one of the best-characterised clathrin adaptors and is conserved amongst all eukaryotes. After clathrin, AP-2 is the most abundant protein found in the vesicle (Brodsky et al., 2001; Pearse and Robinson, 1984). Loss of AP-2 in mice results in embryonic lethality, highlighting its essential role in cellular homeostasis (Mitsunari et al., 2005; Zizioli et al., 1999). Interestingly, in *Saccharomyces cerevisiae,* AP-2 depletion does not affect clathrin function to the same extent, and is not lethal (Carroll et al., 2009; Huang et al., 1999; Yeung et al., 1995). AP-2 is specific to the plasma membrane and is able to bind both $PI(4,5)P_2$ and cargo destined for internalisation. The large subunits (α and β2) mediate targeting to the plasma membrane and clathrin recruitment, while the μ2 subunit specifically interacts with common cargo internalisation motifs (Ohno et al., 1995; Owen and Evans, 1998). The majority of AP-2, however, exists in the cytoplasm in a locked, inactive state (Collins et al., 2002; Jackson et al., 2010; Rapoport et al., 1997). In this locked state, cargo binding sites are buried and AP-2 must undergo a large conformation change mediated by $PI(4,5)P_2$ binding to reveal cargo binding motifs (Jackson et al., 2010). Phosphorylation of the μ2 subunit of AP-2 enhances the affinity of AP-2 to $PI(4,5)P_2$ and thus facilitates cargo recruitment (Fingerhut et al., 2001; Honing et al., 2005; Ricotta et al., 2002).

The role of AP-2 is well characterised; however, the essential requirement for AP-2 during clathrin-mediated endocytosis remains a subject of fierce debate. Several studies were able to show that clathrin-mediated internalisation could still occur following AP-2 depletion (Hinrichsen et al., 2003; Keyel et al., 2006; Lakadamyali et al., 2006; Maurer and Cooper, 2006; Motley et al., 2003). This suggests that additional accessory proteins may be required to mediate binding between the plasma membrane, cargo, and clathrin. Several endocytic proteins with the right properties exist and may act alone or in complex with AP-2 to recruit clathrin in a cargo-specific manner. Epsin1/2, ARH,

NUMB, Dab2 and β-arrestin have all been proposed to function in this regard (Maurer and Cooper, 2006; Traub and Bonifacino, 2013). Even so, AP-2 depletion results in a ~12-fold reduction in the formation of clathrin-coated pits, and it has been suggested that incomplete RNAi mediated depletion of AP-2 is responsible for the detection of clathrin dependent endocytic events in the aforementioned studies (Kelly et al., 2014). By and large it has been accepted that AP-2 is the dominant adaptor required for initiation of clathrin-coated pits (Cocucci et al., 2012).

Protein-protein interactions facilitating endocytic events are low affinity and commonly mediated by highly conserved short linear motifs. The most well characterised AP-2 binding motifs consist of tyrosine (YxxΦ) and dileucine ([D/E}xxxL[L/I/M]) motifs which designate cargo for AP-2 mediated internalisation (Doray et al., 2007; Kelly et al., 2008; Owen et al., 2004). Via multiple low affinity interactions with sorting signals, AP-2 coordinates high avidity endocytic structures that are highly transient in their nature. Other cofactors implicated as cargo-specific adaptor proteins, acting either in conjunction or independently of the role of AP-2, also utilise short conserved linear stretches to recognise cargo (Table 1.1).

Motif:	**Adaptor:**	**Corresponding cargo protein:**
YxxΦ	AP-2 (μ2)	Tranferrin receptor
[DE]xxxL[LI]	AP-2 (α-σ2)	CD4 / LIMP4 / Nef
[FY]xNPx[YF]	DAB2 (PTB domain)	LDL receptor / LRP1/2
	NUMB	
	ARH	
II	AP-2	K+ channel Kir2.3
Phosphate group	β-arrestin1	GPCRs
	β-arrestin2	
Acidic cluster	AP-2 (putative)	Furin / CD-M6PR
Ubiquitin	Epsin (UIM)	EGFR / MHC class 1
	Eps15 (UIM)	

Table 1.1 Common endocytic motifs and their binding adaptor proteins

Motifs denoted according to PROSITE annotation. Φ denotes a bulky hydrophobic residue (L, M, I, F, V), x - any amino acid. When known the subunit mediating binding is given in parenthesis. Adapted from (Traub, 2009).

1.3.3 The Endocytic pathway

The mechanism of clathrin-mediated endocytosis at the plasma membrane is well established and requires the recruitment of several adaptors and cofactors at distinct temporal stages (McMahon and Boucrot, 2011). During endocytosis, nucleation, cargo selection, coat assembly, scission, and uncoating of the vesicle all occur in a highly coordinated manner (Engqvist-Goldstein and Drubin, 2003; Geli and Riezman, 1998; McMahon and Boucrot, 2011; Sorkin, 2004; Toret and Drubin, 2006). $PI(4,5)P_2$ is essential for the initiation of the endocytic clathrin-coated pit, and also plays a key role in the regulation of pit size and stability (Antonescu et al., 2011).

Recent single molecule imaging was able to reveal that the simultaneous recruitment of two AP-2 complexes with one clathrin triskelion is responsible and essential for the initiation of clathrin-coated pits (Figure 1.12 A) (Cocucci et al., 2012). The RIM complex is subsequently recruited following initiation of the clathrin-coated pit. This complex comprises of the F-BAR domain containing protein, FCHo1/2 which binds to $PI(4,5)P_2$-rich sites of the plasma membrane, along with epsin, Eps15 and intersectin-1 (Henne et al., 2010; Reider et al., 2009; Stimpson et al., 2009). Together this complex specifically localises to the edge of the growing pit and plays a crucial role to enhance membrane curvature, thus promoting vesicle formation (Henne et al., 2010; Reider et al., 2009; Saffarian et al., 2009; Tebar et al., 1996). These accessory proteins form multiple low affinity interactions with one another and AP-2, and the depletion of any one of these components results in defective vesicle formation (Loerke et al., 2009; Mettlen et al., 2009).

Upon recruitment to $PI(4,5)P_2$ at the plasma membrane AP-2 autoinhibition is released, to reveal dileucine and tyrosine cargo binding sites (Collins et al., 2002; Jackson et al., 2010; Page and Robinson, 1995). Polymerization of the clathrin triskelia acts to facilitate the maturation of the growing pit by promoting curvature of the membrane (Hinrichsen et al., 2003). Finally, membrane scission of the nascent vesicle from the plasma membrane occurs via the GTPase dynamin. Dynamin oligomerises into tetramers that form tubules of approximately 26 dynamin molecules around the neck of the vesicle (Baba et al., 1995; Grassart et al., 2014; Hinshaw, 2000; Kosaka and Ikeda,

1983). Once the mature vesicle buds off from the plasma membrane, uncoating of clathrin is initiated in an HSC70 and auxillin dependent manner (Massol et al., 2006; Taylor et al., 2011). Auxillin is recruited after budding and localizes to the hub of the clathrin triskelia via binding to the terminal domains and ankle region (Fotin et al., 2004; Scheele et al., 2001). HSC70 is then recruited by auxillin, allowing internalization and sorting of the vesicle to proceed (Schlossman et al., 1984; Ungewickell et al., 1995).

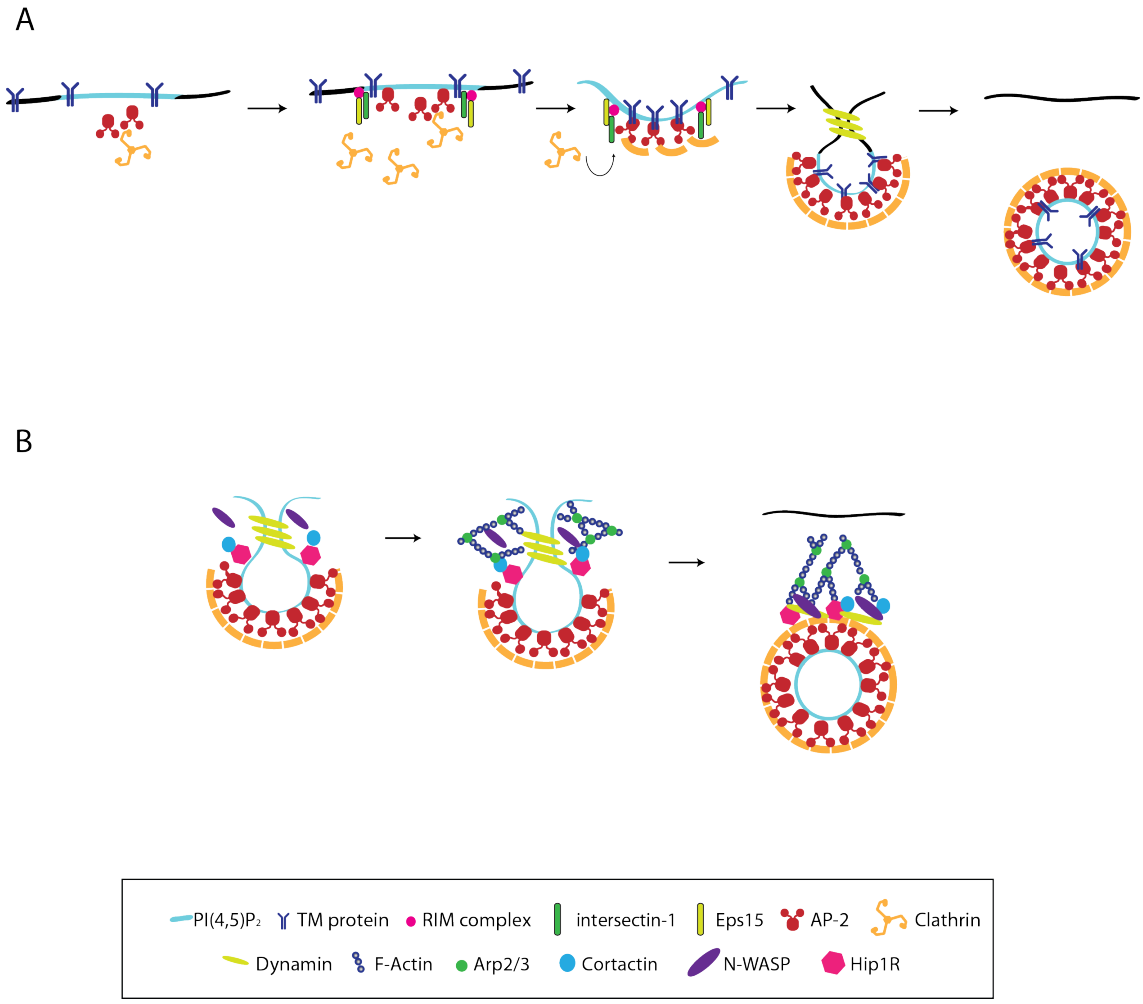

Figure 1.12 Mammalian clathrin-mediated endocytosis

A The progression of protein internalisation during clathrin-mediated endocytosis. The site of nucleation is defined by the coordinated arrival of two AP-2 molecules and one clathrin triskelia. Vesicle progression and cargo incorporation is then reliant on the recruitment of additional accessory proteins, prior to vesicle maturation and scission from the plasma membrane by dynamin. **B** Proteins that coordinate actin polymerization during clathrin-mediated endocytosis. Adapted from Humphries, 2012.

1.3.4 The role of actin during Clathrin-Mediated Endocytosis

Actin polymerisation and endocytic events are two complex and highly regulated processes; moreover the role of actin is intimately coupled with the process of endocytosis in several instances (Engqvist-Goldstein and Drubin, 2003; Merrifield, 2004; Yarar et al., 2005). Genetic studies in yeast were the first to uncover a link between actin polymerisation and endocytosis whereby disruption of genes required for either process, was shown to inhibit the other (Ayscough, 2000; Engqvist-Goldstein et al., 2004; Kaksonen et al., 2006; Wendland et al., 1998). This relationship, however, is not so clear in mammalian cells. Chemical inhibition of actin polymerisation with latrunculin A revealed that actin plays a supporting rather than essential role in endocytic events in mammalian cells (Fujimoto et al., 2000; Gottlieb et al., 1993; Lamaze et al., 1997). In contrast, more recent evidence from electron microscopy and live cell imaging has revealed a crucial role for actin polymerisation during vesicle pinching off from the plasma membrane, and the subsequent internalisation of cargo (Boulant et al., 2011; Taunton, 2001).

Analogous to the role of vaccinia-induced actin tails, actin polymerisation has been detected on vesicles and macropinosomes propelling them into the cytoplasm from their site of generation at the plasma membrane (Figure 1.12 B) (Frischknecht et al., 1999b; Kaksonen et al., 2000; Merrifield et al., 1999; Yarar et al., 2005). Like many actin dependent processes, endosomal motility is thought to require the presence of both Arp2/3 and N-WASP (Merrifield, 2004; Merrifield et al., 2002). Overexpression of WASP/N-WASP inhibits endosome motility, and the efficiency of endocytic events is significantly reduced in WASP null lymphocytes (Benesch et al., 2005; Rozelle et al., 2000; Zhang et al., 1999). N-WASP can bind several endocytic proteins, such as intersectin-1 and endophilin A, however the precise mechanism of N-WASP recruitment during endocytosis remains elusive (Hussain et al., 2001; McGavin et al., 2001; Otsuki et al., 2003).

Aside from the well-characterised role of dynamin in vesicle neck scission, dynamin may provide a key link between the actin and clathrin machinery during vesicle transport (Danino and Hinshaw, 2001; Lee and De Camilli, 2002; Orth et al., 2002).

Overexpression of dynamin mutants inhibits both the formation of actin stress fibres and actin-dependent vesicle motility (Lee and De Camilli, 2002; McNiven et al., 2000; Orth et al., 2002). Dynamin can interact indirectly with N-WASP (via intersectin-1 and endophilin A), but can also directly bind the class II NPF, cortactin and profilin, a key regulator of actin dynamics (Le Clainche et al., 2007; McNiven et al., 2000; Merrifield, 2004; Qualmann and Kelly, 2000; Roos and Kelly, 1998).

Mammalian adaptors Hip1 and Hip1R also act to mediate the actin and clathrin networks. Found at the site of clathrin-coated pits, Hip1R is able to directly bind actin, clathrin and the plasma membrane (Brett et al., 2006; Engqvist-Goldstein et al., 1999; Engqvist-Goldstein et al., 2001; Hyun et al., 2004; Legendre-Guillemin et al., 2005; McCann and Craig, 1997; Wilbur et al., 2008). Abolishing the interaction between Hip1R and clathrin, or depletion of Hip1R, results in actin accumulation at the site of vesicle formation, leading to the suggestion that the Hip1R-clathrin interaction is crucial for regulation of actin dynamics during endocytic events (Boettner et al., 2011). A key component of the early endocytic RIM complex, epsin has also been reported to play a role to mediate Hip1R function during endocytosis (Messa et al., 2014). Mouse knockout cell lines lacking all three isoforms of epsin could still make clathrin coats pits, however these vesicles were unable to mature and failed to internalize (Messa et al., 2014). Interestingly, Hip1R is no longer recruited at these clathrin-rich sites in cells lacking epsin, which once again results in aberrant actin accumulation at these sites (Engqvist-Goldstein et al., 2004; Messa et al., 2014).

This link between the clathrin and actin machinery also appears to play a crucial role in the formation of non-classical clathrin structures. Recent studies have linked the roles of clathrin and actin during the formation and maintenance of long-lived clathrin structures at the plasma membrane, termed clathrin plaques (Saffarian et al., 2009). These clathrin plaques form a flat extended lattice on the plasma membrane and are enriched at the adherent surface of cells. These plaques appear to be composed of a unique hexagonal array of clathrin that is dependent on the presence of actin (Saffarian et al., 2009). These structures are rich in both Hip1R and epsin, which are localised throughout these flat lattices, unlike their distinct localisation at the nascent vesicle edge during canonical

clathrin-mediated endocytosis (Boulant et al., 2011). The extent to which actin is required during endocytic events is still under a degree of discussion, with evidence pointing to a greater requirement for actin under conditions of stress, such as high turgor pressure, high membrane tension, or the presence of large cargo (Aghamohammadzadeh and Ayscough, 2009; Batchelder and Yarar, 2010; Boulant et al., 2011; Cureton et al., 2010; Liu et al., 2009).

1.4 Eps15 Homology family proteins

1.4.1 Discovery and members

The RhoGEF intersectin-1 is recruited to vaccinia during its egress where it is thought to locally activate Cdc42. In addition intersectin-1 is a component of the cellular endocytic machinery and contains conserved EH domains described in more detail below.

The Eps15 Homology (EH) domains were as their name suggests, originally identified as a conserved domain present in three copies in the N-terminus of Epidermal growth factor receptor substrate 15 (Eps15) (Fazioli et al., 1993). The EH domains are around 100 residues in length, and are highly conserved from yeast to man (Fazioli et al., 1993; Wong et al., 1994; Wong et al., 1995). The EH domains of a number of proteins have been structurally determined, and are characterised by the presence of two EF-hand domains linked by an anti-parallel beta-sheet (de Beer et al., 1998). While EF-hand motifs are usually calcium binding, not all EH domains contain the required residues to facilitate the interaction with calcium (Enmon et al., 2000; Heizmann and Hunziker, 1991; Lewit-Bentley and Rety, 2000; Strynadka and James, 1989). Since their initial discovery by DiFiore and colleges in 1991, the SMART database currently lists 35 human proteins containing 60 EH domains in total. In mammals the EH domain proteins can be grouped into five distinct families: Eps15, intersectin, Reps, synergin, and EH domain containing proteins 1-4 (EHD 1-4). EH domain containing proteins are typically associated with endocytic events at the plasma membrane as well as trafficking of endosomes to the TGN (Chen et al., 1998; Fernandez-Chacon et al., 2000).

To date, the best characterised EH domain containing proteins are mammalian Eps15, intersectin-1, and their yeast homologues, End3p and Pan1p, all which have been implicated in early endocytic events (Benedetti et al., 1994; Wendland et al., 1998).

A number of approaches have been used to determine EH domain-binding targets, and thus far, three classes of highly conserved motifs have been identified. The majority of EH domains bind class 1 peptides, containing the NPF motif (Asn-Pro-Phe) (Paoluzi et al., 1998; Salcini et al., 1997). Class II peptides contain WW (Trp-Trp), FW (Phe-Trp), or SWG (Ser-Trp-Gly) that mediate recruitment to the third EH domain of Eps15, and first EH domain of yeast YBL47c. The first EH domain of yeast End3p was also shown to bind a third class of peptides, containing a H(S/T)F (His-Ser/Thr-Phe) motif (Salcini et al., 1997) (Table 1.2)

Name	EH domain	Binding Specificity
Eps15	EH1	NPF
	EH2	NPF
	EH3	FW
Eps15R	EH1	NPF(R)
	EH2	NPR
	EH3	NPF(R)
ITSN1	EH1	NPF
	EH2	(S)xNPF
ITSN2*	*EH1*	*NPF*
	EH2	*NPF*
YBL047Cp	EH1	(S)FW(R)
	EH2	NPF / WW
	EH3	NPF(R)
End3p	EH1	HTF
Pan1p	EH2	(S)xNPF

Table 1.2 Binding specificity of EH domains

Experimentally determined binding specificity of the best studied EH domain containing proteins. * - The ITSN2 EH domains lack comprehensive experimental evidence determining specific binding to NPF motifs, however this is presumed due to its similarity to ITSN1, and the ITSN2 binding partners identified thus far. (Kay et al., 2004; Paoluzi et al., 1998; Yamabhai et al., 1998).

Structural determination of EH domain-NPF binding reveals that NPF-containing peptides bind a hydrophobic pocket in the EH domain mediated by highly conserved leucine and tryptophan residues (Figure 1.13 B) (Enmon et al., 2000; Paoluzi et al., 1998; Rumpf et al., 2008; Salcini et al., 1997). Mutation of these key residues abolishes binding to NPF containing peptides (Rumpf et al., 2008). It has been noted that around 50% of NPF containing ligands contain a conserved serine or threonine (S/T) at positions -1, and -2, suggesting that there is potential for additional regulation of EH domain binding via phosphorylation (Paoluzi et al., 1998). Confirmed NPF-containing ligands include epsin, stonin2, Numb, CALM, synaptojanin, and Hrb (Chen et al., 1998; Doria et al., 1999; Haffner et al., 2000; Legendre-Guillemin et al., 2005; Morgan et al., 2003; Smith et al., 2004).

EH domain binding proteins were found to have no conserved sequence similarity aside from the presence of the NPF motif repeats (Salcini et al., 1997). These proteins typically contain multiple, equally spaced NPF motifs that mediate weak binding to EH domains in the range of 10^3-10^4 M^{-1} (de Beer et al., 1998; Paoluzi et al., 1998; Yamauchi et al., 2004). How EH domains determine binding specificity between multiple NPF motifs is still unclear. Interestingly, the crystal structure of the second EH domain of Eps15 (EH2) bound to stonin2 revealed a unique mechanism to enhance binding affinity. Eps15-EH2 was able to bind stonin2 via interactions with both of its NPF motifs (Figure 1.13 C) (Rumpf et al., 2008). Multiple contacts resulted in a binding affinity in the order of 10^6 M^{-1}, far higher than typically observed (Rumpf et al., 2008). All other EH domain structures determined thus far have only been shown to bind single NPF motifs, however the Eps15 EH2-stonin2 model may be indicative of the ability of EH domains to coordinate multiple NPF containing ligands *in vivo*.

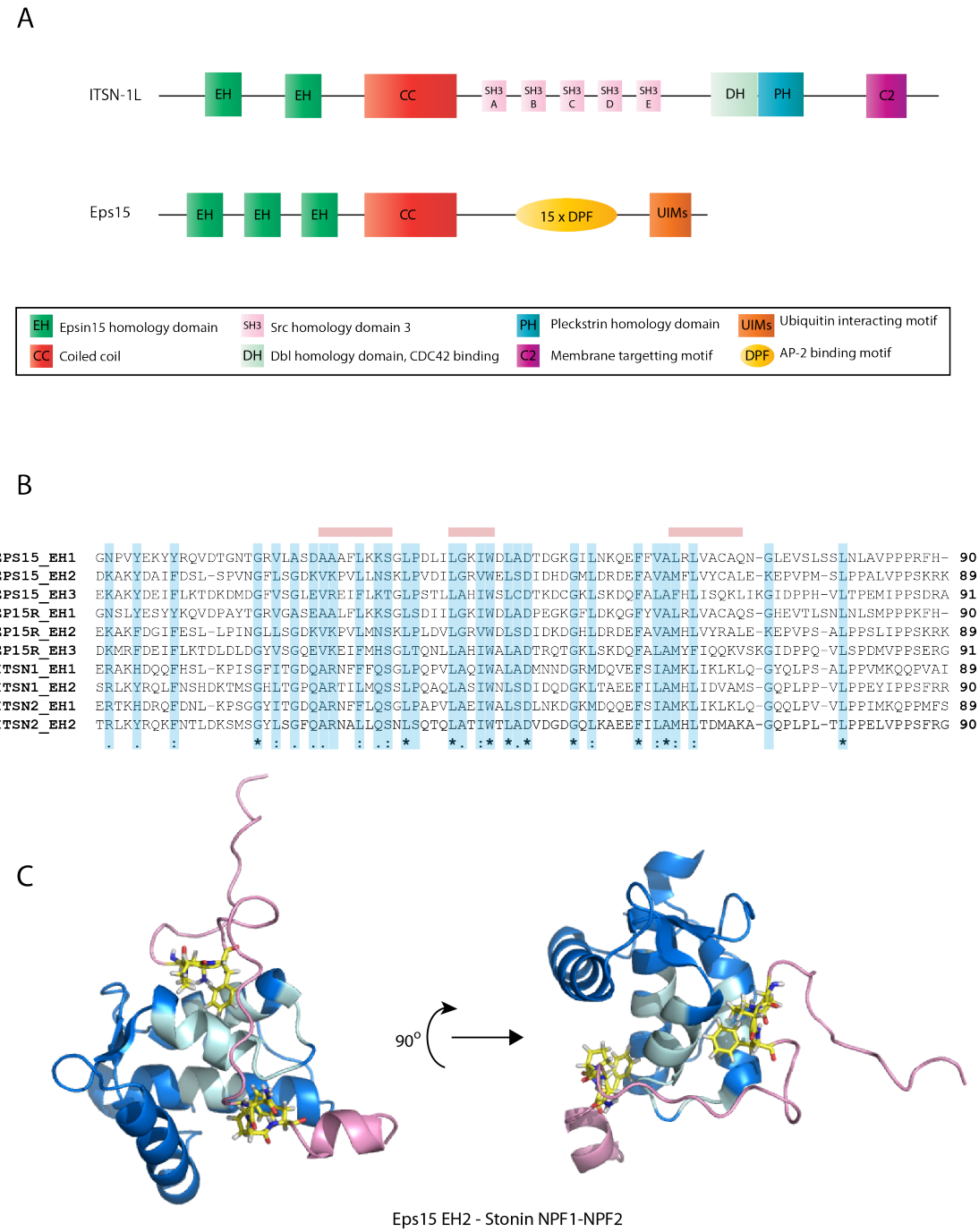

Figure 1.13 Domain and subunit organisation of Eps15 and intersectin-1

A Domain organisation of Eps15 and intersectin-1. **B** Sequence alignment of the three EH domains of Eps15/R with the two EH domains found in intersectin-1/2. Sequence similarity is highlighted in blue and residues required to mediate NPF recruitment are shown above the sequence in pink. **C** NMR solution structure of the Eps15 EH2 domain (blue) in complex with a peptide containing two NPF motifs found in Stonin2 (pink). PDB=2JXC. One EH domain is sufficient to mediate binding to both NPF motifs simultaneously. Cyan patches annotate NPF binding residues. The NPF motif is highlighted in yellow. (Rumpf et al., 2008)

1.4.2 Epidermal growth factor receptor substrate 15 – Eps15

Eps15 was originally identified on the basis of its rapid phosphorylation on tyrosine 850 by EGFR upon ligand binding (Fazioli et al., 1993). While Eps15 had been found to be a key regulatory component of clathrin mediated endocytic machinery, it is becoming more apparent that the EH domain family of proteins plays a more diverse role during intracellular signalling and regulation of the actin cytoskeleton.

Eps15 is composed of a globular head region containing three N-terminal EH domains, a central coiled-coil stalk domain and 15 Asp-Pro-Phe (DPF) repeats. These DPF repeats mediate direct binding to the α-appendage of AP-2 (Benmerah et al., 1996; Iannolo et al., 1997). The central coiled-coil region is thought to mediate both homo- and hetero-oligomerisation with other EH domain proteins such as Eps15R and the intersectin family (Figure 1.13 A) (Coda et al., 1998; Sengar et al., 1999). Ultrastructural studies using EM have confirmed that Eps15 can form homo-dimers in parallel and homo-tetramers in antiparallel, via the central coiled-coil region (Cupers et al., 1997). Gel filtration experiments have also revealed that Eps15 within the cell is primarily contained in large macromolecular complexes, primarily in complex with AP-2 (Tebar et al., 1997; Tebar et al., 1996). As a component of the RIM complex, Eps15 is known to play an essential role during the early initiation of endocytosis (Carbone et al., 1997; Suzuki et al., 2012). Eps15 specifically localises to the rim of the growing coated pit, unlike AP-2 that is found on the vesicle at all stages of endocytosis (Figure 1.12 A)(Ehrlich et al., 2004; Saffarian et al., 2009; Tebar et al., 1996). *In vitro* analysis reveals that Eps15 binding to AP-2 is disrupted upon the recruitment of clathrin to AP-2, suggesting that Eps15 is mutually exclusive to clathrin polymerisation (Cupers et al., 1998).

Eps15R (Eps15-related protein) has 63% identity and only differs in 33 positions to Eps15 and was identified largely due to its high sequence similarity with Eps15 (Paoluzi et al., 1998). Eps15R is found in complex with Eps15 at the rim of the growing pit (Coda et al., 1998). However, it also has distinct localisation to that of Eps15. Whereas Eps15 contains a C-terminal nuclear export signal within the last 25 C terminal residues, due to the absence of this domain in Eps15R, it is able to maintain

nuclear localisation (Offenhauser et al., 2000; Poupon et al., 2002). In addition, Eps15R lacks tyrosine 850, which is present in Eps15 and phosphorylated specifically upon EGRF internalisation, once again suggesting these proteins may have unique roles (Confalonieri et al., 2000). Aside from their distinct cellular localisations, the binding specificity of the Eps15 family EH domains also differs. While the third Eps15 EH domain (EH3) preferentially binds FW containing peptides, the EH3 domain of Eps15R has significantly higher binding specificity to NPF motifs with an arginine residue at the +1 position (NPFR) (Table 1.2) (Paoluzi et al., 1998).

1.4.3 The Intersectin family

Intersectin is encoded by two mammalian isoforms, Intersectin-1 and Intersectin-2 (also known as Ese-1/Ese-2 in mice) (Sengar et al., 1999; Yamabhai et al., 1998). Intersectin-1 was originally identified during a cDNA screen in *Xenopus Laevis* with an SH3 peptide ligand (Yamabhai et al., 1998). Like Eps15, Intersectin-1 contains two N-terminal EH domains and a central coiled-coil region required to mediate oligomerisation (Wong et al., 2012; Yamabhai et al., 1998). The C-terminus differs vastly from that of Eps15, and contains five C-terminal SH3 domains (Yamabhai et al., 1998). In addition, the long splice variant contains DH, PH, and C2 domains (Fig 1.13 A) (Guipponi et al., 1998; Hussain et al., 1999; Sengar et al., 1999). Like Eps15, the function of intersectin-1 is intimately coupled to endocytic events, where it is thought to acts as a scaffold to maintain the specific localisation of endocytic proteins (Koh et al., 2004; Marie et al., 2004; Wong et al., 2012).

Intersectin-1 co-localises with clathrin during endocytosis and is constitutively associated to Eps15 and Eps15R via their coiled-coil domains (Hussain et al., 1999; Sengar et al., 1999; Yamabhai et al., 1998). Yeast 2-hybrid screens have also found that intersectin-1 can interact with itself and intersectin-2, suggesting that like Eps15, intersectin-1 may homo- and heteroligmerize *in vivo* (Wong et al., 2012). Together with Eps15, intersectin-1 associates with FCHo1/2 during early nucleation and initiation of clathrin-coated pits (Henne et al., 2010). As is typical of many early endocytic proteins described thus far, overexpression of intersectin-1 has also been shown to block endocytosis (Sengar et al., 1999).

In fact, intersectin-1 may play a more direct role during endocytosis than previously appreciated. The linker region between SH3A-SH3B has been shown to directly associate with both the α- and β- appendages of AP-2 (Pechstein et al., 2010). This stretch of intersectin-1 does not contain consensus AP-2 binding motifs. It does, however, contain two aromatic patches consisting of the **W**AD**F** and **W**Dx**W** motifs that are sufficient to facilitate AP-2 recruitment (Pechstein et al., 2010). These motifs are capable of binding both α- and β- appendages, although *in vitro* intersectin-1 preferentially binds β- (490 nM) over α- (5 μM) appendages of AP-2 (Pechstein et al., 2010). These tryptophan motifs are also found within the intersectin-2 SH3A-SH3B linker region, suggesting that both isoforms are equally capable of direct AP-2 binding (Pechstein et al., 2010).

Screening of potential binding partners of the intersectin-1 EH domains reveals that both EH1 and EH2 typically bind class I NPF motifs, with EH1 in general mediating higher affinity binding that EH2 (Wong et al., 2012; Yamabhai et al., 1998). In addition, it was found that the binding affinity to C-terminal NPF motifs (e.g. NPF-COOH) is 200 times higher than that of internal NPF motifs. This suggests that the tertiary structure of NPF plays a crucial role in influencing specificity and affinity of intersectin-1 EH domain binding, which may be a common feature among other EH domain containing proteins (Yamabhai et al., 1998).

1.4.4 Interplay between intersectin-1 and actin

Eps15 and intersectin-1 are the two best studied EH domain containing proteins and share several similar features. Both have the ability to bind one another, epsin, NPF motifs and AP-2 directly. The ability of Eps15 and intersectin-1 to form homo- and hetero-oligomers, and the multiple protein-protein interaction domains they contain, suggests that they act as a molecular scaffolds during endocytic events at the plasma membrane (Hussain et al., 1999; Okamoto et al., 1999; Roos and Kelly, 1998; Sengar et al., 1999; Yamabhai et al., 1998). Although the regulation of the EH domain containing proteins is yet to be fully elucidated, clear evidence points towards a functional interaction between Eps15 and intersectin-1. Intersectin-1 affects the localisation of Eps15, mirroring observations from their yeast homologues, End3p and Pan1p, in which

End3p mediates the localisation of Pan1p (Benedetti et al., 1994; Raths et al., 1993; Tang et al., 1997; Toshima et al., 2007; Wendland et al., 1998). In addition earlier studies determined a role for the End3p/Pan1p complex for the correct localization of endocytic components and the correct formation of the actin cytoskeleton in yeast. (Benedetti et al., 1994; Suzuki et al., 2012; Tang et al., 1997).

Intersectin-1, unlike Eps15, contains five SH3 domains, a Dbl homology (DH) domain, and a Pleckstrin homology (PH) domain (Figure 1.13 A). Intersectin-1 recruits GDP-bound Cdc42 via the DH-PH domains, which is thought to facilitate intersectin-1 binding to N-WASP. The interaction of intersectin-1 and N-WASP is direct and mediated by the intersectin-1 SH3 domains (Hussain et al., 2001; Zamanian and Kelly, 2003). Binding of N-WASP to intersectin-1 also stimulates its GEF activity towards GDP-bound Cdc42, which is then exchanged to GTP-Cdc42. In turn, GTP-bound Cdc42 can then directly bind N-WASP, activating its ability to bind Arp2/3. This feed-forward loop appears conserved between isoforms, as similarly intersectin-2 is able to interact with both N-WASP and activate Cdc42 in the context of T-cell antigen receptor endocytosis (McGavin et al., 2001). Analysis of rat brain extracts have shown that intersectin-1, N-WASP, and actin are all components of purified clathrin-coated vesicles (Hussain et al., 2001). Interestingly, the intersectin-1 N-WASP signalling pathway does not appear to be exclusive to endocytic events and is also activated during both exocytosis and phagocytosis (Gasman et al., 2004; Humphries et al., 2014).

More recently a link between intersectin-1 and the N-WASP binding protein, WIP, has been uncovered (Anton et al., 2007; Gryaznova et al., 2015; Martinez-Quiles et al., 2001; Moreau et al., 2000). WIP is a component of a multitude of actin-based structures, directly recruiting N-WASP to podosomes, invadopodia, and vaccinia-induced actin tails (Donnelly et al., 2013; Garcia et al., 2012; Garcia et al., 2014; Martinez-Quiles et al., 2001; Moreau et al., 2000; Yamaguchi et al., 2005). The SH3 domains A, C and E of both intersectin-1 and intersectin-2 have been shown to directly mediate binding to WIP *in vitro*, enabling the formation of an intersectin:WIP:N-WASP complex (Gryaznova et al., 2015; Wong et al., 2012). In addition to the localisation of intersectin-1 to clathrin-coated pits, intersectin-1 has also been shown to localise *in vivo*

to invadopodia in a WIP dependent manner (Gryaznova et al., 2015). Taken together, it appears that intersectin-1 acts as a crucial link between the endocytic and actin machinery during a number of cellular events.

1.5 Aims of this thesis

Decades of research have elegantly dissected how vaccinia and other viruses cleverly hijack host machinery to facilitate their spread. Determining exactly how viruses use and regulate host machinery during their egress promises to provide novel insights into mechanisms of host cell and pathogen biology. In spite of initial characterisation of the roles of AP-2 and clathrin during vaccinia infection, we still lack an understanding of how they are recruited to the virus. My studies were aimed at understanding the molecular basis for the recruitment of AP-2 to vaccinia during viral egress. In addition, I aimed to further investigate the interplay between endocytic machinery and actin dependent processes, which can cooperate together in cellular host processes and during pathogen spread (Humphries and Way, 2013).

Chapter 2. Materials & Methods

2.1 General buffers and culture media

The in house Cell Services facility at London Research Institute provided general buffers and culture media, with details listed below. Specific reagents will be described in the relevant section.

2.1.1 General Buffers

Phosphate Buffered Saline A (PBSA)

8.00 g	NaCl
0.25 g	KCl
1.43 g	Na_2HPO_4
0.25 g	KH_2PO_4

Reagents were dissolved in distilled water, and pH adjusted to 7.2, to a total volume of 1 L. Solutions were autoclaved prior to use.

2.1.2 Cell Culture Media

Trypsin Solution: 0.25% in Tris Saline

Tris Saline (TS)

8.00 g	NaCl
2.00 ml	19% (w/v) KCl solution
0.10 g	$Na_2H_2PO_4$
1.00 g	D-Glucose
3.00 g	Trizma Base
1.50 ml	1% (w/v) Phenol red solution
0.06 g	Penicillin
0.10 g	Streptomycin

Versene Solution

8.00 g	NaCl
0.20 g	KCl
1.15 g	Na_2HPO_4
0.20 g	KH_2PO_4
0.20 g	EDTA
1.50 ml	1% (w/v) Phenol red solution

0.05% Trypsin working stock

0.25% trypsin was diluted 1:5 in versene and filter sterilised through a 0.22 μm filter prior to use.

Minimal Essential Medium (MEM)

9.68 g	MEM powder
3.70 g	$NaHCO_3$

The reagents above were dissolved in 10 L of distilled water and pH adjusted to 7.0. MEM solution was sterilised through a 0.22 μm filter and stored at 4ºC until use.

2.1.3 Bacteriological Media

Luria-Bertani (LB) Medium

10 g	Bacto-tryptone
5 g	Bacto-yeast extract
10 g	NaCl

LB Agar

15 g of Bacto-agar was dissolved in 1 L of LB medium and autoclaved prior to use.

2.2 Cell Culture

All cell lines used in this thesis along with their culture conditions are listed in Table 2.1.

Table 2.1 Cell lines and culture conditions

Cell Line	Species	Medium	Source
HeLa	Human	MEM, 10% FCS[3], Pen/Strep[4], 2 mM Glutamine	Dr Sally Cudmore (EMBL)
HeLa LifeAct-Cherry	Human	MEM, 10% FCS[3], Pen/Strep[4], 2 mM Glutamine, 1 µg/ml puromycin	Dr Charlotte Durkin (LRI)
HeLa GFP-N-WASP	Human	MEM, 10% FCS[3], Pen/Strep[4], 2 mM Glutamine	Dr Ina Weisswange (LRI)
BS-C-1	Monkey	DMEM[1], 10% FCS[3], Pen/Strep[4], 2 mM Glutamine	ATCC
A549	Human	MEM, 10% FCS[3], Pen/Strep[4], 2 mM Glutamine	ATCC
N-WASP -/- MEFs	Mouse	DMEM[2], 10% FCS[3], Pen/Strep[4], 2 mM Glutamine	Dr Scott Snapper (MGH)
N-WASP -/- GFP-N-WASP (WT & H208D)	Mouse	DMEM[2], 10% FCS[3], Pen/Strep[4], 2 mM Glutamine, 1 µg/ml puromycin	Dr Ashley Humphries (LRI)

[1] Dulbecco's Modified Eagle Medium 1000 mg/l glucose (Sigma D-6046)

[2] Dulbecco's Modified Eagle Medium 4500 mg/l glucose (Sigma D-6429)

[3] Fetal Calf Serum (PAA laboratories A15-101)

[4] Penicillin G sodium/streptomycin sulphate 100x stock (Invitrogen 1540-122)

2.2.1 Culturing stocks

Cells were cultured at 37ºC in 5% CO_2 and maintained at a confluency of ~70% by passage every 2-3 days. To passage cells, media was removed and cells were washed once with PBSA and 2 ml of 0.05% trypsin was added to cells per 10 cm dish. After brief incubation at 37ºC, detached cells were resuspended in complete media and passaged to the desired confluency. When required, cells were counted using the Scepter 2.0 Cell Counter (Merke Millipore).

2.2.2 Freezing stocks

To generate cell stocks for storage in liquid nitrogen, 70% confluent cells were trypsinised as above and collected by centrifugation at 100 g for 5 minutes. Cells were resuspended in 1 ml FCS with 10% DMSO per 10 cm dish, aliquoted, and transferred to -80ºC prior to long term storage in liquid nitrogen. To recover frozen stocks, aliquots stored in liquid nitrogen were rapidly thawed and resuspended in warm complete MEM (10% FCS) into a 10 cm dish. Following cell adhesion, media was refreshed to remove storage DMSO.

2.2.3 Transfection

Effectene

Effectene (Qiagen) was used in all transfection assays, unless otherwise stated. Cells were plated to 70% confluency the day prior to transfection. In a 6 well dish, 400 ng of DNA was diluted in 100 µl EC buffer. 3.2 µl of enhancer was then added and the solution was vortexed and incubated for 5 mins at room temperature. Next 5 µl of effectene was added and the mixture vortexed and incubated for an additional 10 mins at room temperature. The transfection mix was added dropwise directly to cells in fresh MEM. In a 10 cm plate the following volumes were used; 2 µg DNA, 300 µl EC buffer, 16 µl Enhancer and 30 µl effectene. The protocol was followed as above.

HiPerFect

HiPerFect (Qiagen) was used for RNAi transfection of HeLa cells, using the following standard fast-forward protocol. For a 6 well dish, 2 µl siRNA (20 µM) was diluted in 100 µl MEM, with the addition of 12 µl HiPerFect. The mixture was vortexed and incubated at room temperature for 5 mins. This transfection mix was added to 2 ml of freshly seeded HeLa cells ($0.5x10^5$ per ml). Media was refreshed after 24 hrs, and cells were analysed 48 hrs post transfection. In a 10 cm plate the following volumes were used; 8 µg siRNA, 300 µl MEM, and 40 µl Hiperfect added to 5 x 10^5 freshly seeded HeLa cells. The protocol was followed as above.

Lipofectamine 2000

Lipofectamine 2000 transfection reagent (Qiagen) was used for the transfection of vaccinia targeting vectors during the generation of recombinant viruses. Cells were plated to 80% confluency the day prior to transfection in a 10 cm plate. Prior to transfection cells were infected with ΔA36R at an MOI=0.1. 10 µl of Lipofectamine 2000 was diluted in 250 µl Opti-MEM (Invitrogen 31985), while 4 µg DNA was diluted in 250 µl Opti-MEM. After a 5 minute incubation, DNA and Lipofectamine solution were mixed and incubated at room temperature for a further 20 mins. At 1 hpi the Lipofectamine transfection mix was added dropwise to cells. After 24 hpi cells were harvested for the generation of recombinants.

Table 2.2 siRNA target sequences

Gene	Target sequence	Source
Intersectin-1	GAUAUCAGAUGUCGAUUGA GGCCAUAACUGUAGAGGAA	Dharmacon D-008365-03 and 04
Intersectin-2	AAACUCAGCUGGCUACUAU	Sigma Aldrich
Eps15	ATGCTGTAGGTTGAACCATTA	Sigma Aldrich
Eps15R	GCACTTGGATCGAGATGAG	Sigma Aldrich
AP-2 alpha subunit AP-2 mu2 subunit	AGAGCAUGUGCACGCUGGC GCGAGAGGGUAUCAAGUAU	Motley et al., 2003 Dharmacon J-004233-06
CHC	GAAAGAAUCUGUAGAGAAA UGACAAAGGUGGAUAAAUU	Dharmacon D-004001-01 and 03

2.3 Molecular Biology

10 x DNA Loading Buffer

0.25% (w/v)	Bromophenol Blue
30% (v/v)	Glycerol

Diluted in 5 x TBE

5 x TBE

445 mM	Tris Base
445 mM	Boric Acid
10 mM	EDTA

Made up to a final volume of 1 L with distilled water

2.3.1 Expression vectors

Four different expression vectors were used in this thesis. The pE/L vector contains a synthetic vaccinia early/late promoter and was used to drive expression during the course of infection in mammalian cells (Chakrabarti et al., 1997). The pMW172 vector contains a leaky T7 promoter and was used to for bacterial expression of recombinant proteins (Way et al., 1990). Both of these vectors contained a GFP or GST tag at the N-terminus of the protein of interest. The pBlueScript SKII vector and the pJS4 vector were used for the expression of targeting constructs during the generation of viral recombinants (Chakrabarti et al., 1997). Constructs used throughout this thesis are listed in Table 2.3.

Table 2.3 Expression vectors

Vector	Figure	Generated by
pEL-GFP-stop	3.2, 3.3, 3.4, 4.1, 5.13, 6.2	Rietdörf et al., 2001
pEL-GFP-A36 24-211	3.2, 3.3, 3.4, 4.1, 5.13, 6.2	I. Weisswange
pEL-GFP-A36 WE/AA	3.2	Dodding et al., 2009
pEL-GFP-A36 WD/AA	3.2	Dodding et al., 2009
pEL-GFP-A36 WEWD/AAAA	3.2	Dodding et al., 2009
pEL-GST-stop	3.3	Rietdörf et al., 2001

pEL-GST-A36 24-221	3.3, 6.2	I. Weisswange
pEL-GST-A36 (24-118, 24-155, 24-169, 24-186, 24-197, 24-210)	3.3	I. Weisswange
pEL-GST-A36 (35-221, 55-221, 82-221, 118-221, 155-221, 186-221, 197-221)	3.3	X. Snetkov
pEL-GST-A36 120-155	6.2	I. Weisswange
pEL-GFP-A36 (24-197, 24-186, 155-221, 186-221)	3.3	X. Snetkov
pEL-GFP-A36 (88-155, 88-141, 88-133, 120-155, 120-141, 120-133, 24-120, 35-120, 55-120, 88-120)	6.2	X. Snetkov
pEL-GFP-A36 24-221 ΔNPF1, ΔNPF2, ΔNPF3, ΔNPF1-3	3.4	X. Snetkov
pEL-GFP-Intersectin-1L	3.4	A. Humphries
pEL-GFP-Intersectin-1L ΔEH	3.4	X. Snetkov
pMW172-GST-Intersectin-1L-EH1-2	3.6	X. Snetkov
pMW172-GST-Eps15-EH1-3	3.6	X Snetkov
pMW172-GST-Intersectin-1L-EH1	3.6	X. Snetkov
pMW172-GST-Intersectin-1L-EH2	3.6	X. Snetkov
BS SKII-LA-A36R-RA Targeting vector	4.4, 4.5	X. Snetkov
BS SKII-LA-A36R ΔNPF1-RA Targeting vector	4.4, 4.5	X. Snetkov
BS SKII-LA-A36R ΔNPF2-RA Targeting vector	4.4, 4.5	X. Snetkov
BS SKII-LA-A36R ΔNPF3-RA Targeting vector	4.4, 4.5	X. Snetkov
BS SKII-LA-A36R ΔNPF1-3-RA Targeting vector	4.5	X. Snetkov
BS SKII –LA-RFP-A3-RA Targeting vector	4.5	S. Schleich
BS SKII-LA-A36R-YdF-ΔNPF1-3-RA Targeting vector	5.13	X. Snetkov
pEL-GFP-Nck	4.11	Frischknecht et al., 1999

pEL-GFP-Grb2	4.11	N. Scaplehorn
pEL-GFP-WIP	4.11	M. Zettl
pEL-GFP-N-WASP	4.11, 5.9, 5.10	Frischknecht et al., 1999
pEL-GFP-N-WASP H208D	5.7, 5.10	Moreau et al., 2000
pEL-GFP-A36-YdF	5.13	Frischknecht et al., 1999
JS4-4b-A36R Targeting vector	5.5	X. Snetkov
JS4-4b-A36R ΔNPF1-3 Targeting vector	5.5	X. Snetkov
pEL-GST-Cdc42	5.10	J. Cordiero
pEL-GFP-Cdc42	5.9	Moreau et al., 2000

2.3.2 Polymerase Chain Reaction

PCR was used to amplify plasmid DNA and to insert suitable restriction sites for sub-cloning. A typical 100 µl PCR reaction contained 100 ng of template DNA, 1 µM of forward and reverse primer, 1 x Phusion HF buffer, 1 µM dNTP mix (0.25 µM of each nucleotide), and 2 units of Phusion High Fidelity DNA polymerase (NEB). PCR reactions were performed using an Applied Biosystems GeneAmp PCR machine under the following conditions:

1. 95°C 1 minute

2. 95°C 15 seconds
   55°C 30 seconds
   72°C 30 seconds / kb of product length 25 cycles

3. 72°C 10 minutes

The PCR reaction was resolved on a 1% agarose gel (made in 1 x TBE) containing 1:10,000 SYBR safe DNA gel stain (Invitrogen). The PCR product was visualised at 470 nm using a Safe Imager (Invitrogen). The desired PCR product was cut from the gel and purified using the Qiagen QIAquick gel extraction kit. The PCR product was eluted 35 µl of distilled water to be used for subsequent subcloning.

2.3.3 Overlap PCR

This method was used to generate A36 ΔNPF mutants used throughout this thesis. Two sets of internal primers were designed containing the necessary mutations. Mutations were designed in the center of the complementary sequence, flanked by 20 bp of complementary sequence on either side (Table 2.4). Two initial PCR reactions were carried out to amplify the segments of the gene containing the point mutations. These PCR products were gel purified and final PCR reaction was carried out using a 1:1 mixture of these products as a template. Forward and reverse primers containing the N and C-terminal restriction sites were used in the final PCR reaction and the resulting product was cloned into the desired vector.

For each reaction the following PCR mix was prepared containing: 100 ng DNA, 10 pmol of each primer, 1x Phusion HF buffer, 1 μM dNTP mix (0.25 μM of each nucleotide) and 2 units of Phusion High Fidelity DNA polymerase (NEB) in 100 μl total volume. The PCR reaction was carried out under the following conditions:

1.	95°C	5 minute	
2.	95°C	30 seconds	
	55°C	30 seconds	
	72°C	1 minutes	25 cycles
3.	72°C	7 minutes	

Table 2.4. Primers used for mutagenesis

Construct	Primer sequence
A36 ΔNPF1 For	GAATCCTAACTATTCATCCGCCGCCGCCGTAAATTATAATAAAAC
Rev	GTTTTATTATAATTTACGGCGGCGGCGGATGAATAGTTAGGATTC
A36 ΔNPF2 For	GTATTTGTAGCAAGTCAGCCGCCGCCATTACAGAACTCAAC
Rev	GTTGAGTTCTGTAATGGCGGCGGCTGACTTGCTACAAATAC
A36 ΔNPF3 For	CAATAAATTTAGTGAGAATGCCGCCGCCAGACGAGCACATAGC
Rev	GCTATGTGCTCGTCTGGCGGCGGCATTCTCACTAAATTTATTG

2.3.4 Sub-cloning

Insert and vector DNA was digested in a 20 µl reaction volume containing 10U of restriction enzyme (NEB) and the corresponding NEB buffer. The digestion mix was incubated at 37°C for 2 hrs. The digestion reaction was resolved on a 1% (w/v) agarose gel and the desired products purified using the Qiagen QIAquick gel extraction kit and eluted in 35 µl of distilled water as described above. Ligation reaction were performed at a 3:1 insert to vector ratio. Ligation reactions contained 1 x T4 ligase buffer and 200U T4 ligase (NEB) and were incubated for 1 hr at room temperature. The ligation reactions were subsequently transformed into chemically competent XL-10 *E.coli* cells.

2.3.5 Bacterial transformation

To transform competent bacteria, 50 ng of plasmid DNA (or total ligation reaction) was incubated with 25 µl of chemically competent XL-10 cells on ice for 15 min. Bacteria and DNA were heat shocked at 42°C for 45 seconds and placed on ice for a further 5 min. 100 µl of LB was added to the transformation mix, and incubated shaking at 37°C for 30 min. The bacterial culture was spread on LB-agar plates containing the appropriate antibiotics and incubated at 37°C overnight.

2.3.6 Colony screening by PCR

To identify XL-10 colonies containing the insert of interest, colony screening by PCR was performed following the transformation of cloning ligation reactions. Bacterial colonies were picked and transferred into a 25µl PCR reaction composed of: 1x PCR buffer, 1.5 mM MgCl2, 0.5 µM of each primer, 1 mM dNTP mix (0.25 mM each nucleotide) and 5 U/µl Taq DNA Polymerase (Invitrogen). The PCR reaction was carried out under the following conditions:

1.	95°C	10 minute	
2.	95°C	30 seconds	
	55°C	30 seconds	
	72°C	1 minutes	30 cycles
3.	72°C	10 minutes	

2.3.7 Preparation of chemically competent bacteria

To prepare chemically competent XL-10 cells a 5 ml starter culture was incubated at 37°C overnight. 500 ml of LB media was inoculated with 2 ml of starter culture and incubated at 37°C until the bacteria reached the exponential growth phase at an OD_{600} = 0.5. The bacterial culture was then incubated on ice for 30 min, prior to centrifugation at 2500 rpm for 12 min. The bacterial pellet was resuspended in RF1 buffer, and incubated on ice for 15 min and centrifuged at 2500 rpm for 10 min. The pellet was placed on ice and resuspended in 7 ml of RF2 buffer. Resuspended cells were snap frozen in liquid nitrogen, aliquoted and stored at -80°C.

RF1 Buffer

12 g	Rubidium chloride
9 g	Manganese chloride
2.94 g	Potassium acetate
150 g	Glycerol

The reagents above were dissolved in 900 ml distilled water, and pH adjusted to 5.8 to a final volume of 1 L. RF1 was filtered through a 0.45 μm filter and stored at 4°C.

RF2 Buffer

2.09 g	MOPS
1.2 g	Rubidium chloride
11 g	Calcium chloride
150 g	Glycerol

The reagents above were dissolved in 900 ml distilled water, and pH adjusted to 6.8 to a final volume of 1 L. RF2 was filtered through a 0.45 μm filter and stored at 4°C.

2.3.8 Plasmid DNA preparation

XL-10 cultures from a single bacterial colony were grown in LB containing the appropriate antibiotic (typically 100 μg/ml ampicillin) shaking overnight at 37°C. Plasmid DNA was purified from XL-10 overnight cultures using Qiagen Miniprep kit according to manufacturers instructions.

2.3.9 DNA sequencing

To confirm the correct sequence of newly generated constructs, primers were designed flanking the region interest. The sequencing PCR reaction contained: 200 ng of plasmid DNA, 3.2 pmol primer, and 8 μl BDTv3.1 reaction mix (Big Dye Terminator Cycle sequencing kit), and the following cycling conditions were carried out:

1.	95°C	1 minute	
2.	95°C	10 seconds	
	55°C	5 seconds	
	60°C	4 minutes	25 cycles
3.	12°C	∞	

The PCR product was then purified using DyeEx columns (Qiagen) and vacuum dried. Sequencing was performed by the LRI equipment park facility.

2.4 Vaccinia Virus

Throughout this thesis the wild-type vaccinia strain used is the Western Reserve strain (WR). Recombinant viruses are listed in Table 2.5.

Table 2.5. Recombinant viruses used in this thesis

Virus	Source
ΔA36R	Geoffrey Smith (Parkinson and Smith, 1994)
A36 WEWD-AAAA	Dr Mark Dodding (LRI)
A36 YdF	Anna Holmström (Rietdörf et al., 2001)
A36 1-155 stop	Dr Ina Weisswange (LRI)
ΔA36R YLDV-126L	Dr Mark Dodding (LRI)
A36 ΔNPF1	X.Snetkov
A36 ΔNPF2	X.Snetkov
A36 ΔNPF3	X.Snetkov
A36 ΔNPF 1-3	X.Snetkov
$A36^{late}$	X.Snetkov
A36 $\Delta NPF1\text{-}3^{late}$	X.Snetkov
A36 YdF-ΔNPF	X.Snetkov

2.4.1 General buffers for virology

Tris buffer

10mM	Tris-HCl pH 9
2mM	MgCl2

Made up in distilled water and filter sterilised using a 0.22μm filter.

Sucrose cushion: 35% sucrose (w/v) in Tris buffer

Crystal violet

0.1%	Crystal violet (w/v)
20%	Ethanol

Viral lysis buffer

10mM	Tris-HCl pH 9
10mM	KCl
3mM	$Mg(CH_3COO)_2$

Made up in distilled water and filter sterilised using a 0.22 μm filter.

2.4.2 Sucrose Purification of vaccinia virus

HeLa cells were grown in 15 cm^2 culture dishes to a confluency of 90%. Cells were infected with vaccinia virus at a multiplicity of infection (MOI) = 0.1 for 48-72 hours until all cells displayed clear cytopathic effect (CPE). Media was removed and cells were harvested in 7 ml of PBSA. Infected cells were centrifuged for 7 minutes at 1,700rpm and were washed once in PBSA. The infected cell pellet was re-suspended in 7mls of Tris Buffer and cells sheared by 20 strokes of a 7ml Dounce homogenizer (Wheaton). The resulting solution was centrifuged at 1,700rpm for 7 minutes, to remove nuclei and cell debris, and the viral supernatant was stored at -20ºC. Viral supernatant was thawed at roomed temperature and was carefully layered onto an 8 ml 35% sucrose cushion in Beckman SV40 ultracentrifuge tubes, and made to a total volume of 30 ml with Tris buffer. The viral supernatant was centrifuged at 24,000 rpm for 30 mins in a Beckman Optima L-100 XP ultracentrifuge. The viral pellet was re-suspended in Tris buffer and stored in 100μl aliquots at -80°C.

2.4.3 Plaque Assay

Plaque assays were used in the generation of recombinant viruses, to determine the titer of viral stocks, to assess cell-to-cell spread, and to quantify EEV release. BS-C-1 cells were plated at 2 x 10^5 in 6 well dishes, forming a confluent monolayer after 24 hours. Viral preparations were sonicated and serially diluted 1:10 in 1ml of serum free MEM. The culture media was removed from the BS-C-1 cells and replaced with 10^{-5}, 10^{-6} and 10^{-7} dilutions of virus. After 1 hour of viral adsorbsion, serum free MEM was removed and replaced with a semi-solid overlay of 1 x MEM, 2% FCS and 1.5% carboxy-methyl cellulose. After 48 hours, the overlay was removed, cells were washed thoroughly with PBSA and fixed with 2% paraformaldehyde (PFA) in PBSA for 1 hour. Plaques were visualized with crystal violet staining for 30 mins. The plaque forming unit per ml

(PFU/ml) was determined by counting the number of cell cleared viral plaques per dilution, where plaques are both discernible and isolated.
Plaque assays performed in N-WASP null cell lines were performed as above.

2.4.4 Infection

The multiplicity of infection (MOI) was calculated from the PFU of the viral stock and the number of cells per experiment. A MOI of 2 was used to infect cells for immunofluorescence and live-cell imaging. Prior to infection, viral aliquots were sonicated in a water bath for 30 seconds. Cells were washed and the appropriate volume of virus was added to cells in serum free MEM. 1 hour post infection serum free MEM was removed and was replaced for complete MEM. Cells were incubated at 37°C and fixed or imaged 8 hours post infection.

2.4.5 EEV release assays

To quantify EEV release, BS-C-1 cells were seeded at a density of a 1 x 10^5 in a 12 well dish, forming a confluent monolayer after 24 hrs. Cells were infected in triplicate at an MOI = 0.1 in all experiments. At 1 hour post infection, serum free MEM was removed and cells were washed twice with fresh serum free MEM. Complete media was added to cells and infection was allowed to proceed at 37°C. After 16 hours of infection, complete MEM was carefully harvested and the viral titer was immediately determined by plaque assay on pre-plated confluent BS-C-1 dishes as in 2.5.3. BS-C-1 cells were infected in duplicate with 10^{-1} or 10^{-2} dilutions of viral media, and EEV release quantified in PFU/ml.

2.4.6 Single step growth curve

Single step growth curves were carried out to determine replication dynamics of newly generated recombinant viruses. BS-C-1 cells in a 6 well dish were infected in duplicate at an MOI = 10. The inoculum was removed 1 hour post infection and cells washed twice with complete MEM. At 0, 4, 8, 12, and 24 hpi, the supernatant was removed and infected cells were collected. To collect the cell associated virus fractions, 2 ml of fresh complete MEM was added to cells and cells were thoroughly scraped into the media. Cell associated virus fractions were freeze/thawed three times in liquid nitrogen/37°C

incubator. Samples were sonicated and each time point was titrated by plaque assay as in 2.5.3. Each time point was titrated in triplicate.

2.4.7 Drug treatments during infection

HeLa cells and N-WASP MEF cell lines were treated with inhibitors at the indicated time prior to infection and maintain throughout infection, at the following concentrations:

Table 2.6 List of inhibitors

Compound	Concentration	Incubation time	Source
AraC	50 µM	1 hr prior to infection	
ZCL128	50 µM	1 hr prior to infection	Tocris (Friesland et al., 2013)

2.4.8 Amplification of vaccinia DNA

Touch-down PCR

Touch down PCR was used to amplify DNA from vaccinia genomic DNA from an aliquot of sucrose-purified WR virus. Approximately 1µl of vaccinia genomic DNA was added to a standard PCR mix (2.4.2) and the following PCR reaction was performed:

1.	95°C	1 minute		
2.	95°C	20 seconds		
	65°C	20 seconds	- 1°C / cycle	
	72°C	1 minute		10 cycles
3.	95°C	20 seconds		
	55°C	20 seconds		25 cycles
	72°C	1 minute		
4.	72°C	10 minutes		

2.4.9 Recombinant viruses

During this thesis two approaches were used to generate recombinant viruses. The first approach used was the insertion of the A36R gene containing ΔNPF mutations into the WR-ΔA36R locus via homologous recombination. The second approach was the introduction of the 4b-A36R / 4b-A36R-ΔNPF gene into the thymidine kinase (TK) locus of the WR-ΔA36R genome. This virus was used to study the role of early A36R expression during actin tail formation. Targeting vectors were cloned into pBlueScript / pJS4 vectors (Table 2.3). In both cases, the A36R gene was flanked on either side by 300bp of genomic DNA, homologous to the left and right regions flanking the targeting locus of the virus (Figure 4.5, 5.5).

To generate recombinants, HeLa cells were infected with ΔA36R at a MOI of 0.1. At 2 hpi cells were transfected with the 4 μg of targeting vector using Lipofectamine 2000 (Qiagen), according to the manufacturer's protocol (2.3.3). 24 hours post infection/transfection, media was removed and cells were scraped into 500 μl of viral lysis buffer. The infected cell lysate was freeze/thawed three times in liquid nitrogen/37°C incubator. Confluent monolayers of BS-C-1 cells in 6 well dishes were infected with 1:10 serial dilutions of the infected cell lysate in serum free MEM, and overlaid with carboxy-methyl cellulose (2.5.3). After 24 hours, plaques were identified in BS-C-1 monolayers on a widefield microscope using phase contrast to search for isolated cell clearance. To obtain recombinants, cells were stained with a neutral red to reveal plaques. A36R-recombinants resulted in a rescue of plaque size compared to those induced by ΔA36R. This allowed the selection of the virus of interest based on size. Plaques were transferred with a p1000 pipette tip into 250 μl viral lysis buffer, and freeze/thawed as before. For subsequent rounds of plaque purification 50 μl of the picked plaque solution was used to infect BS-C-1 monolayers as before. Recombinant virus purity was confirmed by analytical PCR using primers pairs that amplified the target locus and distinguished between parental and recombinant virus, by size of the PCR product (2.5.10). Positive plaques were than used to infect confluent monolayers of BS-C-1 cells for a repeated round of plaque assays. Following four rounds of purification two positive plaques were amplified in 15 cm dishes of HeLa cells and sucrose purified to obtain a pure viral stock (2.5.2).

2.4.10 Analytical PCR from plaque picks

In order to assess correct insertion during viral homologous recombination plaques selected during the generation of recombinant viruses were re-suspended in 250 µl Tris buffer and freeze/thawed three times. A digestion mix containing 16 µl of viral suspension, 2 µl of 10µg/ml Proteinase K (Fluka), and 3 µl of 10x Taq PCR buffer (Invitrogen), made up to a 25 µl volume was incubated for 20 minutes at 56°C followed by 10 minutes at 85°C. The mixture was then supplemented with 1mM dNTPs, 0.5 µM of each primer, 1.5mM $MgCl_2$ and 5 U/µl Taq DNA Polymerase (Invitrogen). The PCR reaction was performed as using the following conditions and the reaction product analysed on a 1% agarose gel as before.

1.	95°C	5 minute	
2.	95°C	20 seconds	
	50°C	30 seconds	
	72°C	2 minute	30 cycles
4.	72°C	10 minutes	

2.5 Biochemistry

2 x Final sample buffer (FSB)

125mM	Tris HCl pH6.8
4%	SDS
20%	Glycerol
10%	B-mercaptoethanol
+	Bromophenol blue

2.5.1 SDS-PAGE

To determine A36 expression during infection or to assess the efficiency of siRNA knockdown, cells were lysed directly into 2 x FSB and samples boiled for 10 minutes at 95ºC. Samples were loaded onto 4-12% Bis-Tris or 8% Tris-acetate NuPAGE pre cast gels (Invitrogen), and resolved for 1 hour at 175 V. SeeBluePlus2 protein standards (Invitrogen) were used as reference.

2.5.2 Immunoblot Analysis

Proteins resolved by SDS-PAGE were transferred onto nitrocellulose membranes using the iBlot semi-dry transfer system (Invitrogen) at 23V for 7 minutes or 20V for 10 minutes for large proteins. Membranes were incubated in blocking buffer (5% Milk in PBS-T (Phospho-buffered saline + 0.1% Tween20) for 30 minutes prior to overnight incubation with primary antibody in blocking buffer at 4ºC (Table 2.7). Membranes were washed three times with PBS-T, and then incubated with HRP-conjugated secondary antibody (Jackson ImmunoResearch) diluted 1:5000 in blocking buffer for 30 minutes at room temperature. Membranes were washed three times with PBS-T, and incubated with ECL reagent (Amersham Biosciences) for 5 minutes. The membrane was exposed on Hyperfilm-ECL (Amersham Biosciences). Immunoblots were developed using an IGP compact automated developer (IPG limited).

Table 2.7 Antibodies used for immunoblot analysis

Primary Antibody	Species	Dilution	Source
GST	Rabbit	1:2500	Sigma
GFP (3E12)	Mouse	1:2500	CRUK
AP-2 – alpha Adaptin (M11)	Mouse	1:1000	Thermo Scientific
Intersectin-1	Mouse	1:1000	BD Biosciences
Intersectin-2	Rabbit	1:1000	Peter McPherson (McGill)
Eps15	Rabbit	1:1000	BD Biosciences
Eps15R	Mouse	1:1000	Abcam
A36	Rabbit	1:2500	Dr S.Cudmore (Way Lab)
Vincullin	Mouse	1:1000	Cell Signalling
Grb2	Mouse	1:1000	Cell Signalling

Secondary Antibody	Species	Dilution	Source
HRP-Rabbit	Goat	1:5000	Jackson Immunoresearch
HRP-Mouse	Goat	1:5000	Jackson Immunoresearch
HRP-Rat	Goat	1:5000	Jackson Immunoresearch

2.5.3 GST pull-down assay

HeLa cells at 80% confluency in 10 cm dishes were infected with vaccinia virus (typically ΔA36R) in serum free MEM. 1 hour post infection the media was changed, and the relevant pE/L-GST-tagged constructs were transfected into cells using Effectene (2.3.1). 16 hours post infection/transfection, media was removed and the cells were washed 1 x with PBSA on ice. PBSA was subsequently removed and 300 µl of GST lysis buffer added. Cells were scraped into the lysis buffer, transferred to an eppendorf, and rotated at 4°C for 10 mins. Cell lysates were clarified at 13,000 rpm at 4°C for 5 mins and the supernatant retained. 30 µl of the lysate was retained as an input sample, to which 30 µl of FSB was added. 20 µl of pre-washed glutathione sepharose beads (Amersham biosciences) were added to cell lysates and the mixture rotated for 2 hrs at 4°C. Glutathione beads were then washed 3x with ice-cold wash buffer, and finally resuspended in 30 µl of FSB. Glutathione beads and input samples were boiled at 95°C for 10 mins and samples resolved by SDS-PAGE (2.6.1).

GST Lysis buffer

50 mM	Tris.HCl, pH7.5
150 mM	NaCl
0.5 mM	EDTA
0.5%	NP-40
0.5%	Triton-X
1 x	Protease Inhibitor

GST Wash buffer

50 mM	Tris.HCl, pH7.5
150 mM	NaCl
0.5 mM	EDTA
1 x	Protease Inhibitor

2.5.4 GFP-Trap

HeLa cells at 80% confluency in 10 cm dishes were infected with vaccinia virus (typically ΔA36R) in serum free MEM. 1 hour post infection the media was changed, and the relevant pE/L-GFP-tagged constructs were transfected into cells using Effectene (2.3.1). 16 hours post infection/transfection, media was removed and the cells were washed 1 x with PBSA on ice. PBSA was subsequently removed and 300 µl of GFP lysis buffer added. Cells were scraped into the lysis buffer, transferred to an eppendorf, and rotated at 4°C for 10 mins. Cell lysates were clarified at 13,000 rpm at 4°C for 5 mins and the supernatant retained. Lysates were diluted with the addition of 500 µl of wash buffer. 30µl of the diluted lysate was retained as an input sample, to which 30 µl of FSB was added. 20 µl of pre-washed GFP-Trap beads (Chromotek) were added to cell lysates and the mixture rotated for 2 hrs at 4°C. GFP-Trap beads were then washed 3 x with ice-cold wash buffer, and finally resuspended in 30 µl of FSB. GFP-Trap beads and input samples were boiled at 95°C for 10 mins and samples resolved by SDS-PAGE (2.6.1).

GFP-Trap Lysis buffer

10 mM	Tris.HCl, pH7.5
150 mM	NaCl
0.5 mM	EDTA
0.5%	NP-40
1 x	Protease Inhibitor

GFP-Trap Wash buffer

10 mM	Tris.HCl, pH7.5
150 mM	NaCl
0.5 mM	EDTA
1 x	Protease Inhibitor

2.5.5 Immunoprecipitation

Intersectin-1 immunoprecipitation was carried out using the ESE-1 antibody (BD Biosciences). For each condition a 10 cm dish of HeLa cells was infected with ΔA36R and transfected with GFP-A36 (2.3.1). At 16 hpi cells were lysed in 1 ml of GFP-Trap lysis buffer, and centrifuged for 10 mins at 13,000rpm. Clarified cell lysates were incubated with 30 µl prewashed Protein-G resin (Pierce) for 1 hr at 4°C. Resin was pelleted at 2000 rpm and cell lysates were transferred to a fresh tube. 30 µl of lysate was retained as input fraction. 5 µg of ESE-1 antibody was added to lysates and incubated rotating at 4°C overnight. 30 µl of prewashed Protein-G resin was added to cell lysates and incubated with each sample for 1 hr at 4°C. Resin was pelleted at 2000 rpm and washed 3 x with GFP-Trap wash buffer. Resin was boiled for 10 mins in FSB and analyzed by SDS-PAGE and immunoblot (2.6.1, 2.6.2).

2.5.6 Expression and purification of GST-EH domains

GST Binding buffer

50 mM	Tris-HCl pH 7.5
250 mM	NaCl
2 mM	DDT
2 mM	$CaCl_2$
1 x	Protease Inhibitor

GST Elution buffer

GST Binding buffer + 10 mM glutathione

2.5.6.1 Leaky Protein Expression

BL21 (DE3) Rosetta *E.coli* were transformed with pMW172-GST-intersectin-1 EH1-2 or pMW172-GST-Eps15 EH1-3. A single colony was used to inoculate a 5ml starter culture (LB-ampicillin). This was grown for 5 hrs at 37°C with vigorous shaking. 1 ml of starter culture was used to inoculate a 1 L culture (LB-ampicillin), and this was grown overnight shaking at 30°C. Bacteria was harvested at 5000 rpm for 15 minutes at 4°C and the resulting bacterial pellet snap frozen in liquid nitrogen. The bacterial pellet was thawed on ice and resuspended in 10 ml of GST binding buffer with the addition of 10 µl DNase. The bacterial total lysate was lysed by sonication. Lysates were clarified at 10,000 rpm for 30 mins at 4°C. GST-tagged recombinants were subsequently purified from the resulting bacterial soluble fraction.

2.5.6.2 Purification of GST-EH domains

GST sepharose resin (GE Amershem) was pre-equilibrated with 3 x washes with GST binding buffer. GST resin was added to the bacterial soluble fraction and incubated for 3 hours rotating at 4°C. Following binding, the unbound fraction was removed and GST resin was washed with 3 x GST buffer. GST-EH domains were eluted in 2 ml fractions of GST elution buffer overnight at 4°C. Protein purity in wash fractions and elution fractions was assessed by SDS-PAGE analysis and coomassie staining (2.6.1). Protein concentrations were measured by spectrophotometry (absorbance at 280 nm) using a NanoDrop spectrophotometer (Thermo Scientific).

2.5.7 Peptide pull-down assays

The $A36^{158-197}$ peptides used in Figure 3.6 were obtained from the peptide synthesis facility and synthesised with an N-terminal Biotin tag. Streptavidin beads (M-280 Dynabeads – ThermoFisher Scientific) were washed 4 x with PBSA. Peptides in PBSA were coupled to beads for 30 minutes, rotating at room temperature. 20 mg of peptide was used per pull-down. Uncoupled peptide was removed by 3 x washes with PBSA. Peptide loaded Streptavidin beads were resuspended in 500 µl of GST binding buffer and 5 µg of purified GST-EH domains was added per pull-down. Streptavidin coupled peptides were incubated with recombinant protein for 3 hours rotating at 4°C. Unbound

recombinant protein was removed and Stretavidin beads were subsequently washed 4 x in GST binding buffer. Beads were resuspended in 30 µl of FSB and boiled for 10mins. Binding of recombinant protein to Streptavidin coupled beads was assessed by SDS-PAGE (2.6.1). Gels were stained with coomasie to visualise bound protein.

2.5.8 Probing peptide arrays

The A36 peptide arrays used in Figure 3.2 were generated by the peptide synthesis laboratory at Cancer Research UK. Arrays comprised of 15-mer peptides that were synthesised and spotting onto a nitrocellulose membrane. Adjacent peptides were shifted by 1 amino acid each time. To carry out far western analysis, dried peptide arrays were pre-rinsed in 100% ethanol and subsequently washed 3 times in PBSA for 10 minutes each time. The array was blocked with blocking buffer (5% milk in PBS-T) for 1 hour. Peptide arrays were probed with cell lysates treated with AllStar or AP-2 siRNA for 48 hours prior to incubation. Total protein concentration of lysates was equalized prior to incubation with peptide arrays. Peptide arrays and cell lysates were incubated for 2 hours at 4°C. Peptide arrays were then washed thoroughly 4 x 10 min with blocking buffer and incubated with mouse anti-AP-2 antibody (1:5000) for 1 hour at room temperature. Primary antibody was removed and arrays were incubated and peptide arrays washed thoroughly 3 x 10 min with blocking buffer, followed by incubation with goat anti-mouse HRP conjugated secondary antibody (1:10000) for 45 mins. This was followed by 4 x 10 min washes with PBS-T and 1 x 10 min wash with PBS-T + 500 mM NaCl to reduce non-specific binding. Peptide arrays were developed using ECL as described in 2.6.2.

2.6 Imaging

2.6.1 General reagents

1 x Cytoskeletal buffer (CB)

10 mM	MES, pH 6.1
150 mM	NaCl
5 mM	EGTA
5 mM	MgCl2
5 mM	Glucose

Blocking buffer

1%	BSA
2%	FCS

These reagents were dissolved in 1x CB, filtered through a 0.45 μm filter and stored in aliquots at -20°C.

Mowoil

2.4 g	Mowoil
6 g	Glycerol
12 ml	200 mM Tris.HCl, pH 8.5

Mowoil and glycerol were added to 6 ml of distilled water. The mixture was then incubated stirring at room temperature, before the addition of Tris.HCl. This solution was then stirred for 10 mins at 60°C, and subsequently centrifugated at 5000 rpm for 5 mins. Mowoil was stored in aliquots at -20°C.

10% and 4% paraformaldehyde (PFA)

10% stocks of PFA were made by dilution of 50 g of PFA in 500 ml of warm PBSA. The solution gently stirred and 1 M NaOH tablets were added until PFA had dissolved. After cooling at room temperature, the pH was adjusted to 7.5, and the solution filtered through a 0.45 μm filter and stored in aliquots at -20°C. 10% aliquots were thawed and freshly diluted to 4% with PBSA prior to use.

2.6.2 Fixation

For PFA fixation, cells were incubated with 4% PFA in PBSA for 15 mins and subsequently washed 1 x with PBSA.

2.6.3 Immunofluorescence

Coverslips were incubated with blocking buffer for 10 mins, prior to incubation with antibody. For extracellular virus labelling, the B5 antibody was added prior to permeabilisation of cells. In all other cases, cells were permeabilised for 45 seconds with 0.1% Triton-X in PBSA. Coverslips were washed 3 x with PBSA. Cells were

incubated with primary antibody in blocking buffer for 1 hr, before washing 3 x with PBSA. Secondary antibodies diluted 1:500 in blocking buffer were then added for 30 mins. F-actin was stained using Phalloidin, which was diluted 1:1000 in blocking buffer, and was added at the same time as secondary antibody. Secondary antibodies were removed and cells incubated with DAPI (300 nM in PBS) for 2 mins. Cells were finally washed 3 x with PBSA, 1 x with distilled water, and mounted using Mowoil on microscopy slides.

Table 2.8 Primary antibodies used for immunofluorescence

Antibody	Species	Dilution	Source
B5	Rat	1:1000	Gerhardt Hiller
CHC	Rabbit	1:500	Abcam
AP-2 alpha Adaptin	Mouse	1:500	Abcam
Intersectin-1	Mouse	1:500	BD Biosciences
Intersectin-2	Rabbit	1:500	Peter McPherson (McGill)
Eps15	Rabbit	1:500	BD Biosciences
Eps15R	Rabbit	1:500	Abcam
A36	Rabbit	1:250	Dr S.Cudmore (Way Lab)
Phalloidin		1:1000	Molecular probes

2.6.4 Antibody staining of viral plaques

Plaques in A549 and N-WASP cell lines were additionally visualized using the B5 antibody. After fixation of infected 6 well dishes, cells were permeabilised for 2 mins with 0.1% Triton-X in PBSA. Cells were washed 3 x with PBSA and incubated with B5 antibody in blocking buffer at a dilution of 1:1000 for 1 hour with gentle rocking, before washing 3 x with PBSA. Cells were next incubated with anti-rat HRP conjugated secondary antibody diluted 1:1000 in blocking buffer for 45 mins with gentle rocking. Cells were washed 3 x with PBSA and 0.5 ml of TMB peroxidase substrate (Sigma) was then added to each well, and left to develop for 5-15 mins with gentle rocking. Once plaques were visible, the substrate was removed, cells were washed with distilled water, and the plate left to dry.

2.6.5 Microscopes

Zeiss Axioplan Upright

For imaging of fixed samples, a Zeiss Axioplan2 microscope equipped with a Photometrics Cool Snap HQ cooled CCD camera, external Prior Scientific filter wheels (DAPI; FITC; Texas Red; Cy5) and a 63x / 1.4 Plan Achromat objective was used. The system was purchased from Zeiss and Universal Imaging Corporation Limited and was controlled with MetaMorph 6.3r7 software. Images were analysed using the MetaMorph software and were processed with the Adobe software package.

Zeiss Inverted

To view and select plaques during generation of recombinant viruses a Zeiss Axiovert 200 equipped with a Photometrics Cool Snap HQcooled CCD camera, a Photometrics Cascade II camera, external Prior Scientific filter wheels (GFP, RFP) and a 10x/0.25 Ph1 objective was used. The system was purchased from Zeiss and Universal Imaging Corporation Ltd. The system was controlled by the MetaMorph 6.3r7 software.

Spinning-disk confocal

Live-cell imaging of actin tails was carried out on a Zeiss Axio Observer microscope equipped with a Plan Achromat 63x / 1.4 Ph3 M27 oil lens, an Evolve 512 camera and a Yokagawa CSUX spinning disk. The system was purchased from 3i Intelligent Imaging Innovations and was controlled by Slidebook 5.0. Movies were analysed using either the Slidebook or MetaMorph software.

2.7 Statistical Analysis

Data in all graphs are presented as the standard error of the mean, unless otherwise stated. Prism 5.0 (GraphPad) was used to perform standard statistical analysis of data sets. A Student's T-test was performed to compare two data sets. To compare multiple data sets a One Way Anova analysis was performed, followed by a Tukey Multiple Comparison to compare all pairs of samples. A p value of <0.05, <0.01 and <0.001 is represented as *, ** and ***, respectively. A P value > 0.05 was not considered statistically significant, and in this event the data was labelled, n.s., for not significant.

Chapter 3. The C-terminus of A36 is essential for AP-2 binding

3.1 Introduction

During vaccinia virus egress, the plasma membrane adaptor AP-2 and clathrin are recruited to cell-associated enveloped virions (CEV) following their fusion with the plasma membrane. The role that AP-2 and clathrin play during egress is yet to be fully elucidated. Thus far it has been shown that AP-2 and clathrin act to polarise A36 beneath the virus (Humphries et al., 2012). This results in a clustered A36 signalling platform that stabilises N-WASP recruitment, to promote efficient Arp2/3 dependent actin polymerisation beneath the virion. The molecular mechanism governing AP-2 and clathrin recruitment to vaccinia, however, is still unknown. Earlier work from live cell imaging and indirect biochemical assays has shown that AP-2 is able to associate with A36 (Humphries et al., 2012). The observation that a C-terminal truncation of A36 resulted in a similar long actin tail phenotype as cells depleted of AP-2 led to investigation of the requirement of the A36 C-terminus during AP-2 and clathrin recruitment.

3.2 Results

3.2.1 The C-terminus of A36 is essential for AP-2 binding

Vaccinia A36 is a 221-residue integral membrane protein, which is predicted to be largely disordered, and almost entirely cytoplasmic in orientation (Rottger et al., 1999; van Eijl et al., 2000). Alongside pull-down data indicating that A36 can associate with AP-2, A36 may contain several potential AP-2 binding motifs mimicking the canonical YxxΦ, DExxxL[L/I], or DxF motifs (Figure 3.1 A) (Humphries et al., 2012; Kelly and Owen, 2011; Pond et al., 1995). This suggests that A36 may either directly recruit AP-2 or conversely may require the presence of additional host factors to mediate clathrin recruitment. Other IEV proteins, such as F13 and B5, also containing potential adaptor binding motifs and may act in complex with A36 to mediate adaptor binding.

AP-2 and clathrin depletion both lead to an increase in actin tail length, a similar phenotype observed during infection with a recombinant virus expressing A36 truncated from residue 155 onwards (Humphries et al., 2012; Weisswange, 2008). To address the mechanism governing AP-2 recruitment, the initial characterisation of the role of A36 was carried out.

As a preliminary screen to identify AP-2 binding motifs present in A36, I utilised a far western approach. This method has been highly successful in the past to identify short interaction motifs following incubation with recombinant target proteins (Chen et al., 2014; Donnelly et al., 2013; Postigo et al., 2006). In addition, far western peptide arrays have been utilised to identify novel AP-1 binding motifs (Maritzen et al., 2010). AP-2 is a large tetrameric complex composed of four subunits, thus purification and reconstitution is a challenge. In addition, it was unknown whether the association of A36 and AP-2 is direct or indirect, therefore as an initial approach, a far western screen of overlapping A36 peptides was probed with endogenous AP-2 complexes from HeLa cell extracts.

An overlapping peptide array composed of 15-mer peptides spanning the sequence of A36, and shifted one residue per spot, was synthesised on a nitrocellulose membrane (schematic shown in Figure 3.1 B). This A36 peptide array was probed with cell lysates from HeLa cells that were treated with AP-2 or AllStar control (CTRL) siRNA in order to identify specific AP-2 binding sites (Figure 3.1 C). Successful AP-2 knock down was confirmed by immunoblot analysis prior to incubation with the membrane (Figure 3.2 A). Finally, peptide arrays were subjected to immunoblot analysis using an anti-AP-2 antibody. Two peptide spots were positive for AP-2 association and were absent from the A36 peptide array when cells were treated with AP-2 siRNA (Figure 3.2 A). These peptides corresponded to WEDHCSAMEQNNDVD and LIWDNESNVMAPSTE respectively. Interestingly these peptides contain the kinesin-1 binding WE and WD motifs (underlined) (Figure 3.2 B) (Dodding et al., 2011). Although not classical adaptor binding motifs, there have been reports of tryptophan-based motifs required to mediate both kinesin-1 recruitment and adaptor binding (Maritzen et al., 2010; Schmidt et al., 2009). Gadkin (also termed γ-BAR), is a key regulator of endosomal vesicle

recycling, and uses the WENDF motif as a novel link between the binding of the clathrin adaptor AP-1 and recruitment of kinesin-1 (Maritzen et al., 2010; Schmidt et al., 2009). Immunofluorescence imaging of fixed HeLa cells infected with vaccinia WR (wild type Western Reserve strain) has shown that AP-2 only localizes to CEV after fusion with plasma membrane and is not present on particles positive for kinesin-1, suggesting that binding is mutually exclusive (Humphries et al., 2012). The mechanism for the dissociation of kinesin-1 from A36 is unknown, and it may be the case that the displacement of kinesin-1 is the direct result of competitive AP-2 recruitment.

To examine the requirement of the A36 WE and WD motifs for AP-2 binding, a GFP-Trap pull-down assay was carried out. HeLa cells were infected with the WR-ΔA36R virus, in which the A36 coding region is deleted. Cells were then transiently transfected to express the cytoplasmic domain of A36 (residues 24-221), as well as the WE/AA, WD/AA, and WEWD/AAAA A36 mutants in which the respective tryptophan kinesin binding motifs are substituted with alanine residues. While GFP-A36$^{24-221}$ was able to associate with AP-2 as previously reported, abrogating either of the WE/WD motifs alone or in combination did not affect the association of AP-2 to A36$^{24-221}$ (Figure 3.2 C).

Previous work has shown that RNAi depletion of AP-2 during WR infection results in the production of significantly longer actin tails compared to control RNAi treatment (Humphries et al., 2012). As another assay to address whether or not the WE/WD motifs of A36 were required for AP-2 recruitment, the length of virus induced actin tails were measured following infection with WR or a virus expressing the full length A36 WEWD/AAAA mutant under the endogenous A36 promotor. If the WE/WD motifs of A36 were required to mediate AP-2 recruitment it would be expected that abolishing these motifs would phenocopy AP-2 depletion and result in an increase in actin tail length. WR and the A36 WEWD/AAAA virus both, however, induced actin tails that were on average the same length (2.20 ± 0.03 μm and 2.14 ± 0.03 μm respectively) (Figure 3.2 D). Taken together these results suggest that the A36 WE/WD motifs do not play a functional role in the recruitment of AP-2 to the virus at the plasma membrane. Binding of the A36 peptides containing the WE/WD motifs to AP-2 may be an artifact

of high peptide density spotted on the far western array and/or the hydrophobic properties of tryptophan inducing non-specific binding to AP-2 and/or an intermediate binding partner. In addition, peptides adjacent to the WE and WD positive peptide spots identified, differ by one residue and therefore also contain these motifs, yet were unable to mediate AP-2 binding. Density and accessibility of A36 motifs required for AP-2 binding on the CEV or affinity purified on GFP-Trap beads is likely to differ from peptides spotted on a far western array, and therefore may be more indicative of *in vivo* AP-2 and clathrin recruitment during vaccinia egress.

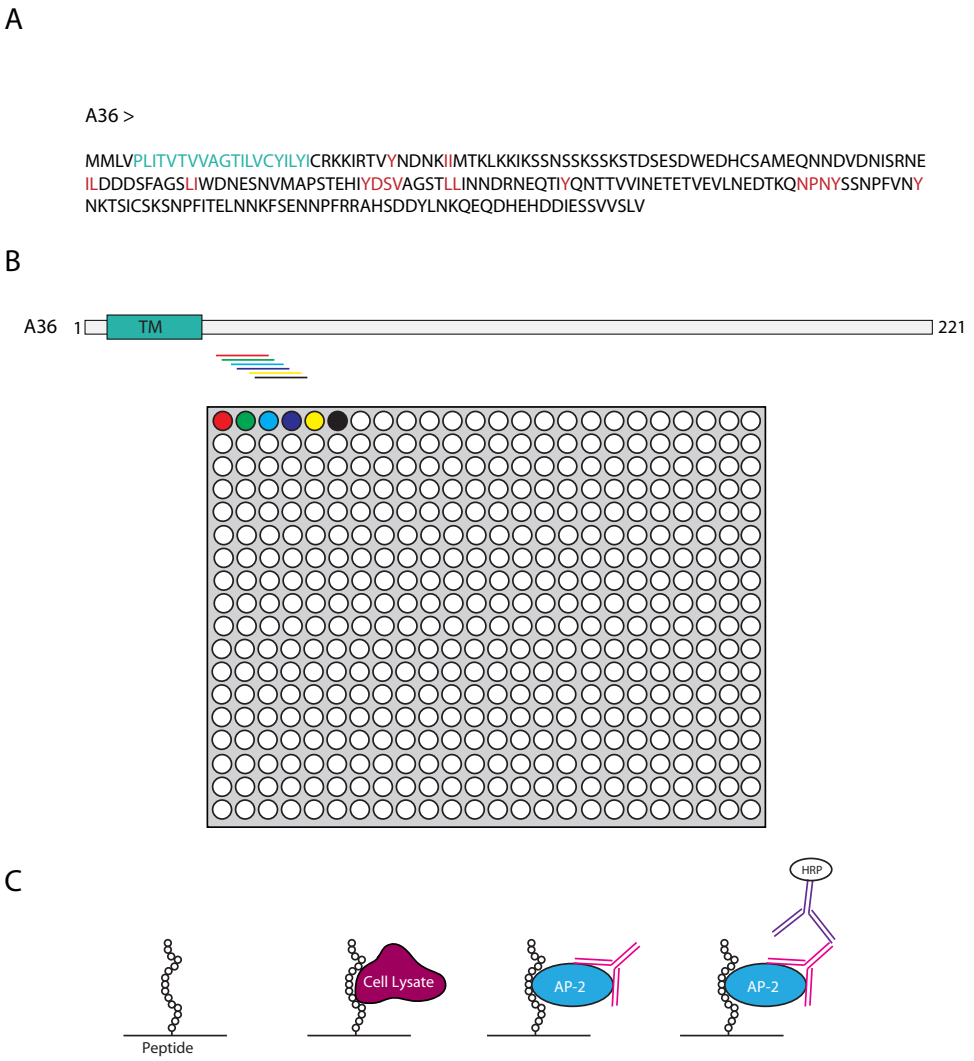

Figure 3.1 A far western approach used to identify AP-2 binding to A36

A Sequence of full-length vaccinia A36. The transmembrane domain is shown in green. Potential adapter binding sites are shown in red. **B** Overlapping peptides corresponding to the full-length sequence of A36 were spotted onto a nitrocellulose membrane. Peptides were 15 amino acids in length and adjacent peptides shifted by 1 amino acid. **C** Peptide arrays were incubated with HeLa cell lysates and probed for AP-2 binding with an anti-AP-2 antibody (pink) followed by detection with a HRP-conjugated secondary antibody (purple).

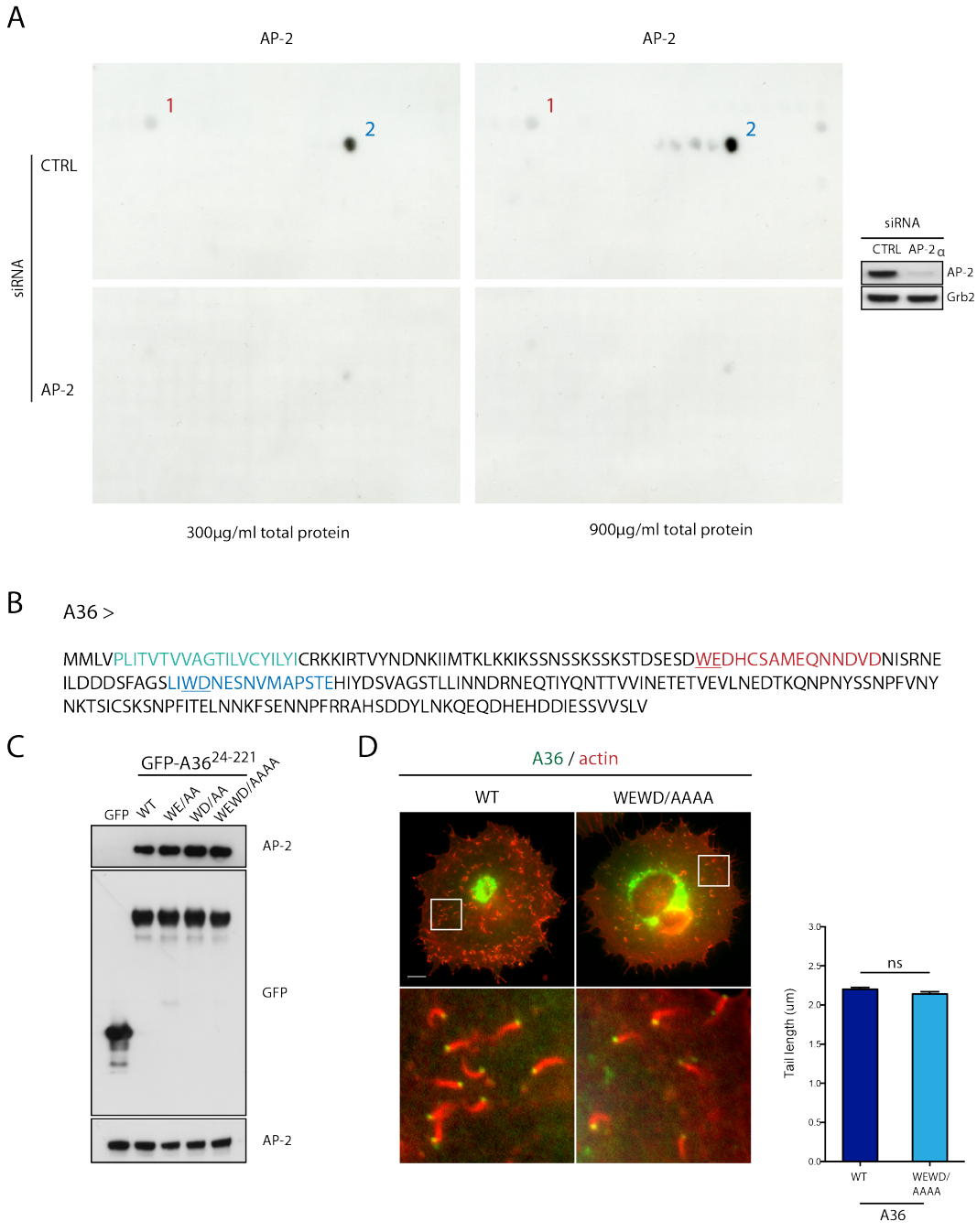

Figure 3.2 A36 WE and WD motifs do not mediate AP-2 binding

A Two distinct peptide spots were positive for AP-2 binding. Depletion of the α-adaptin subunit of AP-2 was confirmed by immunoblot analysis. Grb2 was used as a cellular loading control. **B** Vaccinia A36 sequence. The two positive peptide spots contain the WE (1) and WD (2) kinesin-binding motifs of A36 (highlighted in red and blue respectively). Transmembrane domain is shown in green **C** Immunoblot following GFP-Trap pull-down assays determined that alanine substitution of the A36 WE and WD motifs individually or together, did not affect AP-2 binding to GFP-A36$^{24-221}$. **D** Representative immunofluorescence images showing actin tails (red) induced by the A36 WEWD/AAAA virus additionally (green) remained the same as those induced by wild type A36 (green) 10 hours post infection (hpi). Quantification of actin tail length from N=300 tails over 3 independent experiments. ns indicates a p value > 0.05.

In order to determine which region of A36 was therefore required to mediate AP-2 binding, a series of C-terminally truncated constructs were generated by PCR from the largely disordered cytoplasmic domain of A36 ($A36^{24-221}$) (Figure 3.3 A). A GST-alone control, GST-$A36^{24-221}$, and a panel of GST-A36 C-terminal deletions were expressed under the exogenous viral pE/L promoter in ΔA36R infected HeLa cells. A glutathione pull-down assay was subsequently carried out on infected cell lysates to investigate the association of A36 with endogenous AP-2. Curiously, the GST-A36 construct that lacked the last 35 C-terminal residues ($A36^{24-186}$) was unable to associate with AP-2 (Figure 3.3 B). Conversely longer A36 constructs, $A36^{24-197}$, $A36^{24-210}$ and full length cytoplasmic $A36^{24-221}$ could all bind AP-2 from cell lysates (Figure 3.3 B).

To determine the boundaries required to mediate AP-2 binding, N-terminal truncations of cytoplasmic A36 were generated and expressed in the same manner as described above. In this case, residues 155-221 ($A36^{155-221}$) were sufficient for AP-2 binding (Figure 3.3 C). AP-2 binding was abolished entirely from shorter constructs, $A36^{186-221}$ and $A36^{197-221}$ (Figure 3.3 C). Taken together this suggests that A36 residues 155-197 are important for binding of AP-2. To confirm, pull-down assays were repeated using an alternative affinity tag. A36 deletion constructs were fused to GFP. GFP-alone, GFP-$A36^{24-197}$, -$A36^{24-186}$, -$A36^{155-221}$, and -$A36^{186-221}$ were transiently expressed in ΔA36R infected HeLa cells (Figure 3.3 D). In agreement with previous experiments, GFP-Trap pull-downs confirm that residues 186-197 and 155-186 were required for AP-2 binding, altogether suggesting that A36 residues 155-197 are required to mediate AP-2 binding to the virus during egress.

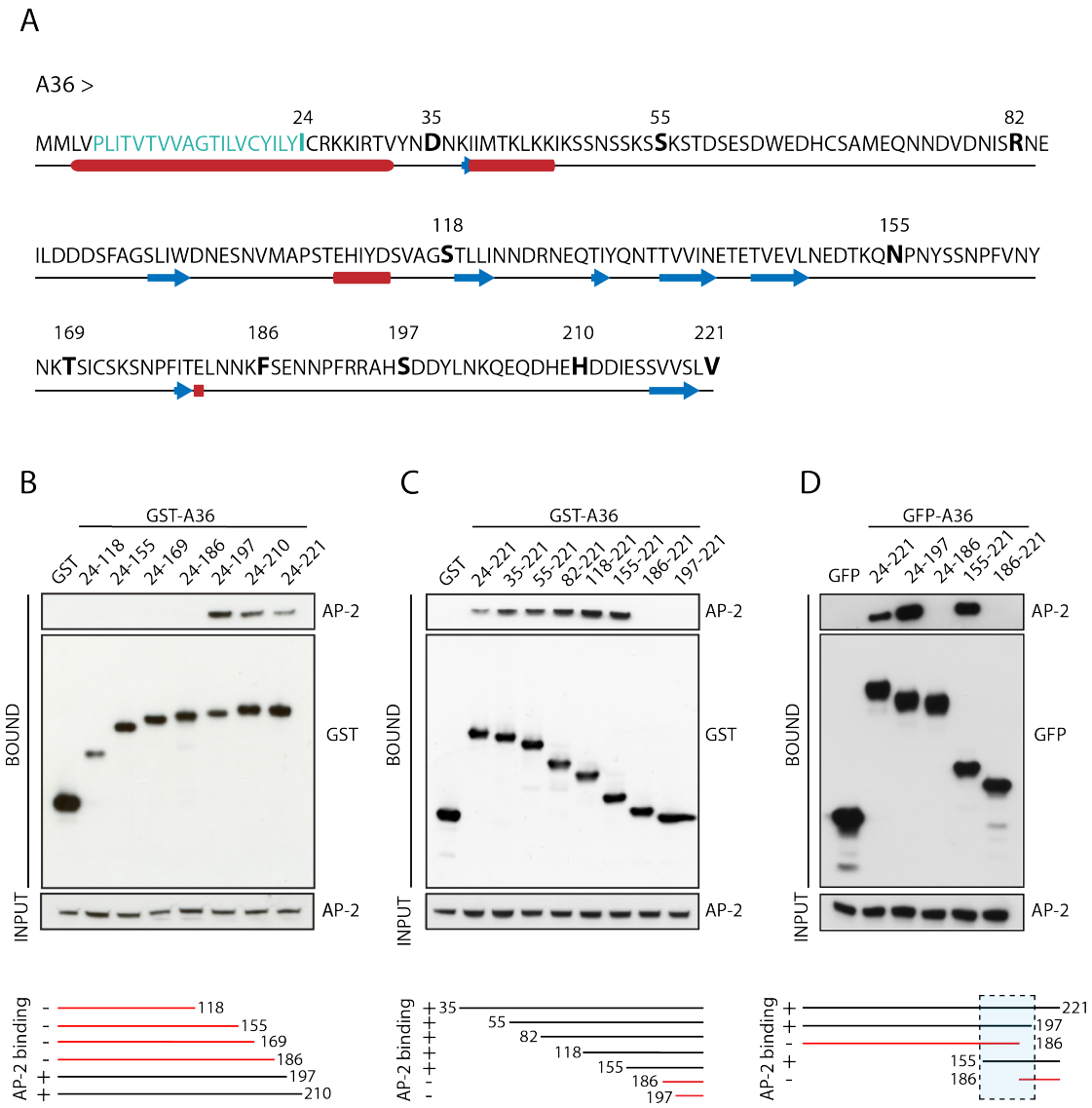

Figure 3.3 A36 residues 155-197 mediate AP-2 binding

A Secondary structure of A36 showing alpha helices (red) and beta sheets (blue arrows) predicted using the JPred server (Drozdetskiy et al., 2015). The cytoplasmic domain of A36 is largely composed of disordered coiled regions. Highlighted in bold are the residues at which C-terminal and N-terminal truncations were designed. Transmembrane domain is shown in green. **B** GST pull-down assays were carried out from HeLa cell lysates transfected with C-terminally truncated GST-A36. Immunoblot analysis shows that AP-2 binding requires residues 186-197 of A36. A36 schematic below illustrating constructs which can mediate AP-2 binding (black) or are unable to bind AP-2 (red). **C** Immunoblot analysis from GST-pull-downs on N-terminally truncated GST-A36 constructs. A36, residues 155-197, are required to mediate AP-2 binding from cell lysates. Schematic of A36 binding below as in B. **D** Immunoblot analysis confirms AP-2 binding shown in B and C. GFP-Trap pull-downs from GFP-A36 transfected cell lysates. Dashed box depicts the region of A36 (155-197) required to mediate AP-2 binding.

3.2.2 Three Asn-Pro-Phe (NPF) motifs mediate AP-2 binding

Closer examination of A36 residues 155-197, does not reveal the presence of a typical AP-2 binding motif, however, it does contain three highly conserved endocytic motifs. A36 155-197 contains three Asn-Pro-Phe (NPF) residues at positions 161-3, 176-8, and 190-2 (Figure 3.4 A). NPF motifs are commonly found in early endocytic adaptor proteins including epsin, synaptojanin, stonin, and AP180 (Chen et al., 1998; Haffner et al., 2000; Martina et al., 2001; McMahon, 1999). The vaccinia A36 NPF motifs are the first viral NPF motifs to be identified to date. During clathrin-mediated endocytosis NPF motifs directly bind Epsin-15 homology (EH) domain containing proteins at the plasma membrane facilitating the recruitment of AP-2 and clathrin. To date the best characterised EH domain containing proteins are intersectin-1 and Eps15. Intersectin-1 and Eps15 are modular proteins that contain two and three EH domains respectively, and are therefore attractive candidates for direct binding to the A36 NPF motifs (Figure 3.4 B). In addition, earlier work has shown that intersectin-1 is recruited to CEV at the plasma membrane during egress, where it is thought to activate Cdc42 via its intrinsic GEF activity to mediate the interaction between Cdc42 and N-WASP beneath the virus (Humphries et al., 2014).

To confirm whether the three A36 NPF motifs are indeed required to mediate binding to AP-2, NPF mutants were generated in the cytoplasmic domain of A36. Individual motifs (ΔNPF1, ΔNPF2, and ΔNPF3) and all three NPF motifs together (ΔNPF 1-3) were substituted with a tri-alanine (AAA) sequence to ascertain the role and contribution of each NPF motif to AP-2 binding. The GFP-tagged A36 NPF mutants were expressed under the viral pE/L promoter during the course of ΔA36R infection in HeLa cells. Alanine substitution of the individual NPF motifs was sufficient to abolish the interaction between the A36 cytoplasmic domain and AP-2 (Figure 3.4 C). Mirroring the A36:AP-2 interaction, mutation of any one of the three NPF motifs is also sufficient to abolish binding of A36 to intersectin-1 and Eps15 (Figure 3.4 C). This suggests that an intermediate EH domain containing protein is responsible for adaptor binding, as the NPF motifs are crucial requirement for A36 mediated binding of AP-2.

To confirm the requirement of the A36 NPF motifs, HeLa cells infected with the ΔA36R virus were transiently transfected with GFP-A36 or the GFP-A36 ΔNPF mutants. Endogenous intersectin-1 was immunoprecipitated from cell lysates and the interaction with GFP-A36 and endogenous AP-2 was investigated by immunoblot analysis. In agreement with previous results, intersectin-1 was able to associate with wild type GFP-A36 but was unable to associate with any of the A36 ΔNPF mutants (Figure 3.4 D). As expected, intersectin-1 is able to co-immunoprecipitate AP-2 from cell lysates in all cases (Figure 3.4 D).

To determine whether the A36 and intersectin-1 interaction was mediated by the intersectin-1 EH domains as would be predicted, a GFP-tagged intersectin-1 (ITSN1) construct was generated by PCR that lacks both N-terminal EH domains (residues 1-311) (GFP-ITSN1-ΔEH). GFP-ITSN1, GFP-ITSN1-ΔEH, and GST-A36$^{24-221}$ were expressed in HeLa cells under the pE/L promoter during infection with the ΔA36R virus. GFP-Trap pull-downs from cell lysates showed that GFP-ITSN1 ΔEH was unable to pull-down wild type GST-A36$^{24-221}$ (Figure 3.4 E). Wild type GFP-ITSN1 could still interact with GST-A36$^{24-221}$ as previously observed (Figure 3.4 E). Taken altogether this confirms that the interaction between A36 and intersectin-1 requires all three A36 NPF motifs and is mediated by the intersectin-1 EH domains. The specific requirement of the EH domains of Eps15 remains to be elucidated. Intersectin-1 and Eps15 are thought to act in complex and are known to oligomerise via their respective coiled-coil domains (Wong et al., 2012). As A36 binding from cell lysates is abolished upon the loss of the EH domains of intersectin-1, this may suggest that endogenous Eps15 is either unable, or not essential to mediate A36 binding in the absence of intersectin-1.

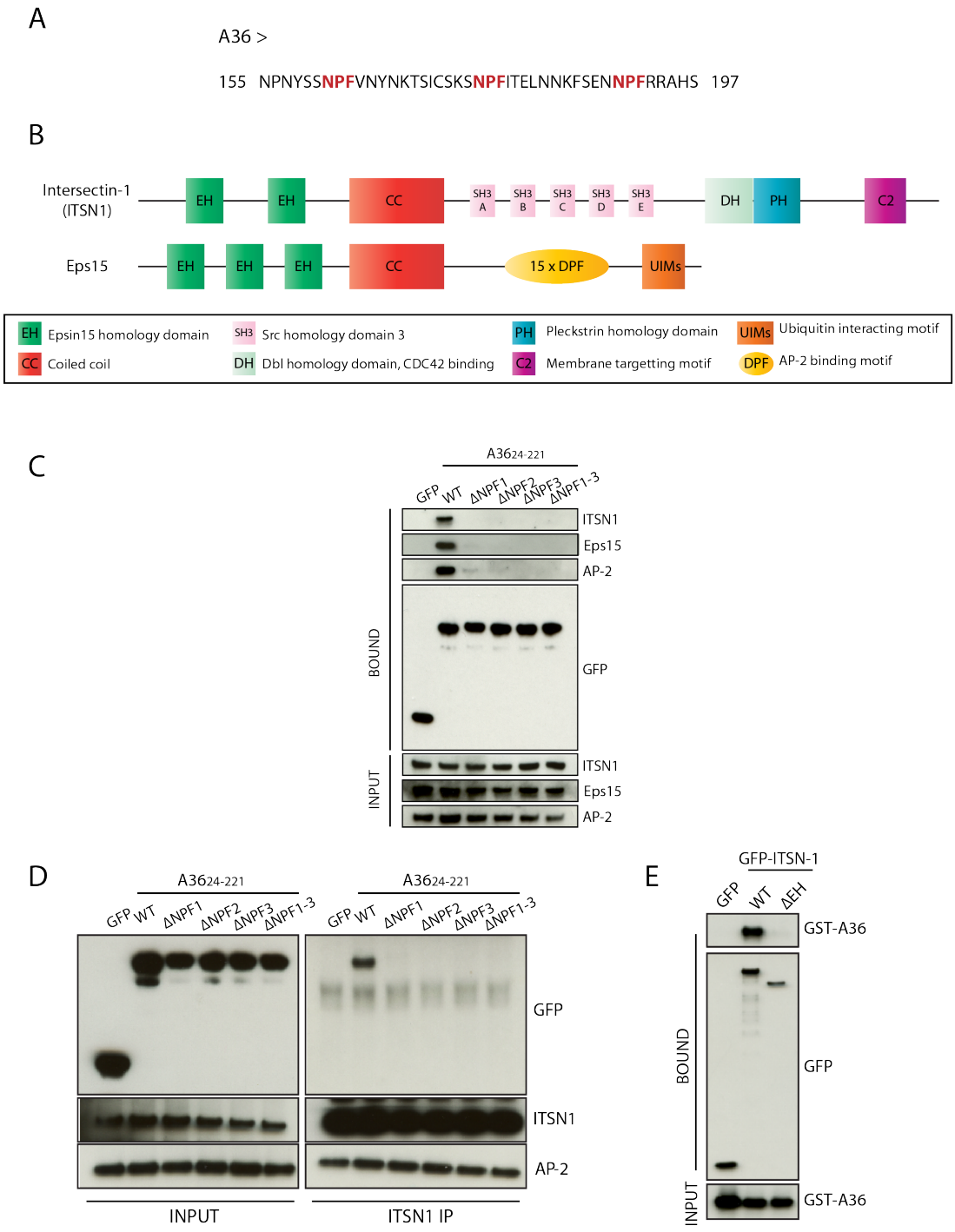

Figure 3.4 Intersectin-1 and AP-2 bind A36 via NPF motifs

A Vaccinia A36 contains three Asn-Pro-Phe (NPF) motifs (in red) within residues 155-197. **B** The domain architecture of intersectin-1 and Eps15, which contain two and three N-terminal EH domains respectively (green). **C** Immunoblot of GFP-Trap pull-down assays reveals that wild type GFP-A36$^{24-221}$ can pull-down AP-2, intersectin-1, and Eps15. A36 ΔNPF mutants are unable to mediate binding to AP-2, intersectin-1, and Eps15. **D** Immunoprecipitation (IP) of endogenous intersectin-1 can pull-down wild type GFP-A36$^{24-221}$ but not the A36 ΔNPF mutants. In all cases intersectin-1 co-IPs with AP-2. **E** Immunoblot of GFP-Trap pull-downs on GFP-ITSN1 wild type alongside ITSN1 lacking the N-terminal EH domains within residues 1-311 (GFP-ITSN1 ΔEH). Wild type GFP-ITSN1 but not GFP-ITSN1 ΔEH can bind GST-A36$^{24-221}$.

3.2.3 Intersectin-1 and Eps15 are recruited to vaccinia virus

Intersectin-1 and Eps15 form a group of several EH domain proteins linked to AP-2 recruitment during early endocytic events at the plasma membrane (Carbone et al., 1997; Cupers et al., 1998; Henne et al., 2010; Koh et al., 2004; Marie et al., 2004; Tebar et al., 1996; Yamabhai et al., 1998). Intersectin-1 and Eps15 both have homologous isoforms, intersectin-2 and Eps15R (Guipponi et al., 1998; Wong et al., 1995). Full-length intersectin-1 and intersectin-2 have 61.2% identity, and Eps15 and Eps15R have 50% sequence identity. There is a high degree of sequence conservation within the N-terminal EH domains of both families of proteins. The EH domains of Eps15/15R (EH 1-3) are 59.7% identical and the EH domains of intersectin-1/2 (EH 1-2) are 50.9% identical. Intersectin-2 and Eps15R are much less studied but are thought to play overlapping roles to their counterparts during endocytic events (Carbone et al., 1997; Coda et al., 1998; McGavin et al., 2001; Pucharcos et al., 2000).

In order to determine whether this family of endocytic proteins were recruited to the virus during egress, WR infected HeLa cells were fixed at 8 hours post infection (hpi) and immunofluorescence imaging was carried out. Immunofluorescence analysis revealed that endogenous intersectin-1, intersectin-2, Eps15, and Eps15R all co-localise to CEV particles at the plasma membrane (Figure 3.5 A). AP-2 and clathrin are mutually exclusive to vaccinia-induced actin tails (Humphries et al., 2012). Intersectin-1 however, has been shown to remain on the virus following the formation of the actin tail (Humphries et al., 2014). I next sought to determine whether this was also the case for intersectin-2, Eps15, and Eps15R. Like intersectin-1, all three EH domain proteins associate with virions inducing actin tails, in agreement with previous observations (Figure 3.5 B) (Humphries et al., 2014). Unlike AP-2 and clathrin, actin polymerisation is not sufficient for the dissociation of EH domain proteins from CEV during egress. Furthermore, intersectin-1 and Eps15 co-localise with one another on a subset of viral particles, suggesting that they may work in complex with one another (Figure 3.5 C). This is in keeping with previous observations in the literature that suggest that intersectin-1 and Eps15 have similar and/or complementary roles during endocytosis (Sengar et al., 1999).

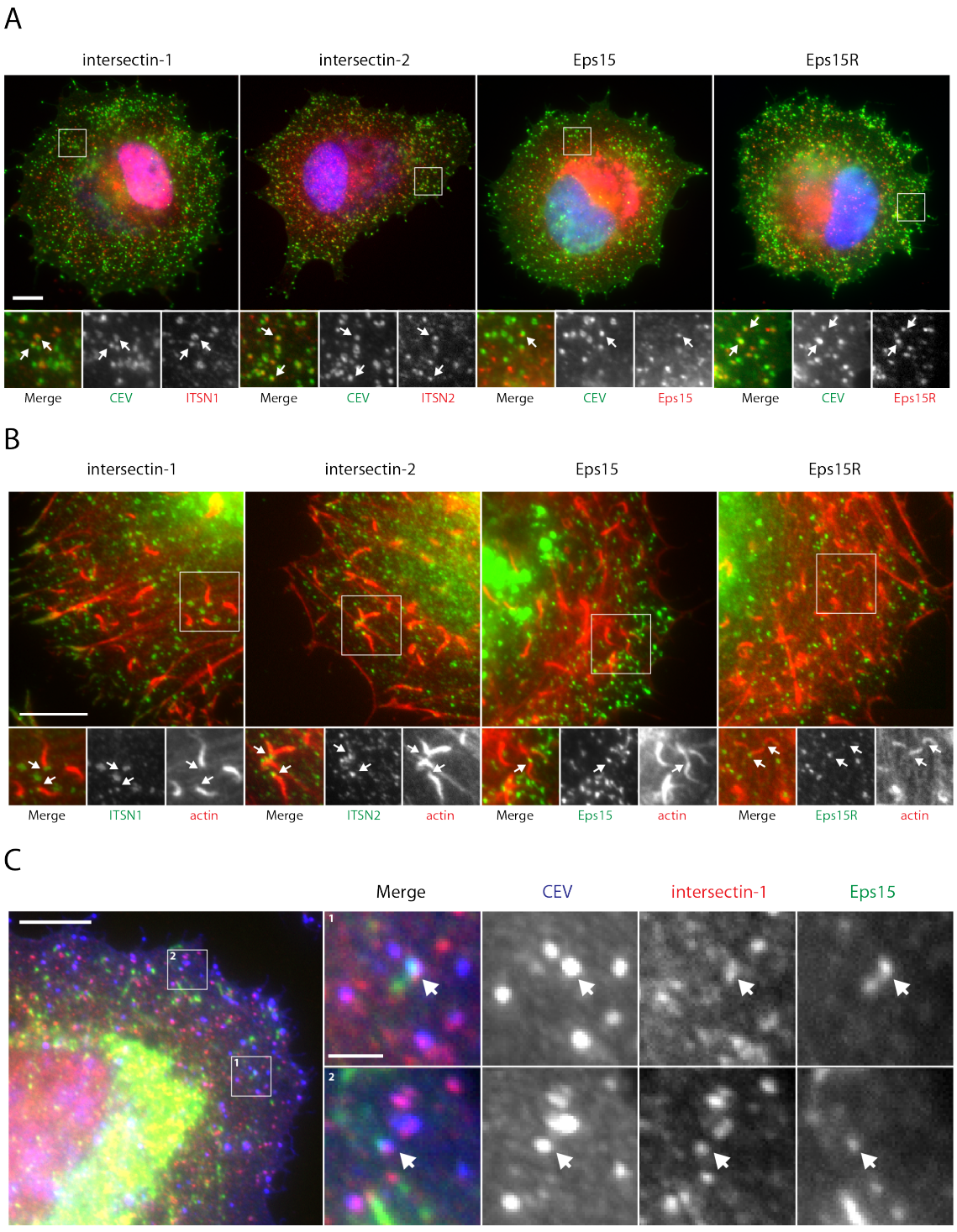

Figure 3.5 Co-localisation of EH domain proteins with extracellular virus particles

A Immunofluorescence staining shows that endogenous intersectin-1, intersectin-2, Eps15, and Eps15R can all be recruited to CEV. CEV were visualized by staining with anti-B5 prior to permeabilization. Scale bar = 10 µm. **B** All four EH domain proteins can be found on viruses inducing actin tails. Actin was detected with phalloidin staining. Scale bar = 10 µm. **C** Intersectin-1 and Eps15 can co-localise to a subset of CEV particles. Scale bar = 2 µm. White arrows indicate co-localisation.

3.2.4 The A36 NPF motifs directly bind intersectin-1 and Eps15

As both intersectin-1 and Eps15 localise to CEV particles at the plasma membrane, I next sought to determine whether intersectin-1 or Eps15 could bind directly to the A36 NPF motifs. To screen for direct binding, the GST-tagged EH domains of intersectin-1 and Eps15 were expressed in BL21 DE3 (Rosetta) *E.coli* cells (Figure 3.6 A). Recombinant GST-EH domains were subsequently affinity purified from *E.coli* soluble fractions via a glutathione resin. Due to the highly disordered nature of A36, previous attempts to express and purify recombinant A36, have resulted in low protein yields and significant degradation, therefore a peptide approach was taken. N-terminal biotinylated peptides of the NPF containing A36 residues 158-197 ($A36^{158-197}$) were synthesised in house. Wild type $A36^{158-197}$ containing all three NPF motifs intact was generated in addition to a panel of $A36^{158-197}$ peptides containing one (Δ1, Δ2, Δ3), two (Δ1+2, Δ1+3, Δ2+3), or all three (Δ1-3) NPF motifs substituted to a tri-alanine motif (Figure 3.6 B).

The $A36^{158-197}$ wild type, Δ1-3, and a scrambled peptide control (Scr) were bound to Streptavidin beads. Peptide loaded Streptavidin beads and an unloaded beads control (CTRL) were incubated with equimolar amounts of purified GST-intersectin-1 EH1-2 or GST-Eps15 EH1-3 (input). Both GST-intersectin-1 EH1-2 and GST-Eps15 EH1-3 could specifically bind $A36^{158-197}$ (Figure 3.6 C). This interaction was abolished entirely upon alanine substitution of all three NPF motifs (Δ1-3) (Figure 3.6 C). Neither GST-intersectin-1 EH1-2 nor GST-Eps15 EH1-3 could bind the $A36^{158-197}$ scrambled control (Scr) or unloaded Streptavidin beads (CTRL) (Figure 3.6 C).

In order to determine whether both of the intersectin-1 EH domains are required to mediate A36 binding, GST-tagged intersectin-1 EH1 and EH2 were expressed and purified from BL21 DE3 (Rosetta) *E.coli* cells. GST-intersectin-1-EH1 and GST-intersectin-1-EH2 were incubated with Streptavidin beads loaded with $A36^{158-197}$ wild type (WT), Δ1-3, and scrambled (Scr) peptides as above. GST-intersectin-1-EH1 and GST-intersectin-1-EH2 could both bind $A36^{158-197}$ wild type. Once again, there was no binding observed to the unloaded beads (CTRL), Δ1-3, or scrambled (Scr) peptides (Figure 3.6 D). This suggests that *in vitro*, both EH domains of intersectin-1 can mediate binding to the $A36^{158-197}$ NPF motifs, although intersectin-1 EH2 appears to

have higher binding affinity than EH1, in contrast to observed measurements in literature, in which the reverse has been observed (Yamabhai et al., 1998). Whether this is the case *in vivo*, and whether all three Eps15 EH domains can mediate binding to $A36^{158-197}$ *in vitro* or *in vivo* remains to be elucidated.

Next the contribution of the individual A36 NPF motifs to EH domain binding was determined. Purified GST-intersectin-1 EH1-2 or GST-Eps15 EH1-3 (input) were incubated with $A36^{158-197}$ peptide loaded Streptavidin beads and an unloaded beads control (CTRL) as previously described. GST-intersectin-1 EH1-2 and GST-Eps15 EH1-3, both had similar binding profiles to the panel of $A36^{158-197}$ peptides (Figure 3.6 E). Based on coomassie staining alone, $A36^{158-197}$ binding to GST-Eps15 EH1-3 appeared to be higher affinity than to GST-intersectin-1 EH1-2 (Figure 3.6 E). $A36^{158-197}$ binding to GST-intersectin-1 EH1-2 and GST-Eps15 EH1-3 was greatly reduced in the absence of NPF3 (Δ3) (Figure 3.6 E). Consistent with this the presence of NPF3 alone (Δ1+2) but not NPF1 (Δ2+3) was sufficient to mediate direct binding of both GST-intersectin-1 EH1-2 and GST-Eps15 EH1-3 (Figure 3.6 E). The presence of NPF2 alone (Δ1+3) was able to mediate weak binding to both GST-intersectin-1 EH1-2 and GST-Eps15 EH1-3 (Figure 3.6 E). Binding of GST-intersectin-1 EH1-2 and GST-Eps15 EH1-3 to $A36^{158-197}$ Δ1-3 was entirely abolished in agreement with earlier observations (Figure 3.6 C). These *in vitro* binding assays have determined that A36 NPF3 is the most essential motif for both GST-intersectin-1 EH1-2 and GST-Eps15 EH1-3 binding, with an additional contribution by NPF2. The A36 NPF1 motif alone does not appear to contribute to binding of either the intersectin-1 or Eps15 EH domains *in vitro*.

In order to investigate whether endogenous intersectin-1 and Eps15 also require A36 NPF3 to mediate binding, a HeLa cell extract was passed over the Streptavidin coupled $A36^{158-197}$ peptides. In addition to intersectin-1 and Eps15, the binding of intersectin-2, Eps15R, and AP-2 to $A36^{158-197}$ peptides was determined. Immunoblot analysis of endogenous intersectin-1/2, Eps15/15R, and AP-2 binding to the $A36^{158-197}$ peptides mirrored direct binding to some extent (Figure 3.6 E, F). Intersectin-1, intersectin-2 and Eps15R all exhibited identical binding profiles to the panel of $A36^{158-197}$ peptides. In addition, their binding was identical to that of recombinant GST-intersectin1 EH1-2 and

GST-Eps15 EH1-3 (Figure 3.6 E). The loss of A36 NPF3 in $A36^{158-197}$ (peptides Δ3, Δ1+3, Δ2+3 and Δ1-3) significantly reduced binding in all cases. A36 NPF1 alone was unable to mediate binding of endogenous intersectin-1, intersectin-2 and Eps15R, while NPF2 was able to mediate extremely weak association (Figure 3.6 E).

Unlike the other EH domain proteins, endogenous Eps15 was able to bind the $A36^{158-197}$ peptide in the absence of the third NPF motif (Δ3). This is in contrast to *in vitro* binding observed with recombinant GST-Eps15 EH1-3 (Figure 3.6 E, F). Endogenous AP-2 mirrors Eps15 binding, and is also able to associate with $A36^{158-197}$ lacking the NPF3 (Δ3) motif (Figure 3.6 F). Neither Eps15 nor AP-2 can bind $A36^{158-197}$ peptides containing NPF1 alone (Δ2+3), confirming once again that A36 NPF1 does not play a role in binding to EH domain-containing proteins, or AP-2 (Figure 3.6 F). Conversely, NPF2 alone (Δ1+3) is sufficient to bind Eps15 and AP-2 in contrast to intersectin-1, intersectin-2 and Eps15R (Figure 3.6 F). While the *in vitro* binding of intersectin-1 EH1-2 and endogenous intersectin-1 are identical, this is not the case with Eps15 EH1-3. Endogenous Eps15 retains the ability to associate with A36 in the absence of NPF3, unlike recombinant GST-Eps15 EH1-3. This may allude to an additional host protein required to mediate binding to A36 in cell extracts, or may be due to avidity effects of Eps15 oligomerization *in vivo* leading to enhanced binding. GST-Eps15 EH1-3 lacks the coiled-coil region required for oligomerization and therefore may exhibit distinct binding properties than endogenous Eps15 *in vivo*. These *in vitro* binding experiments determine that A36 NPF1 does not appear to mediate binding to intersectin-1/2, Eps15/15R or AP-2. A36 NPF2 alone is sufficient to bind Eps15 and AP-2, while A36 NPF3 is crucial for binding of intersectin-1/2 and Eps15R.

As observed following far western on a peptide array of A36, peptide binding does not entirely mimic that observed during GFP-Trap assays (Figure 3.4 C). The loss of any one of the A36 NPF motifs in GFP-$A36^{24-221}$ was sufficient to abolish binding of endogenous AP-2, intersectin-1 and Eps15. This may be indicative of an essential requirement of all three NPF motifs *in vivo*.

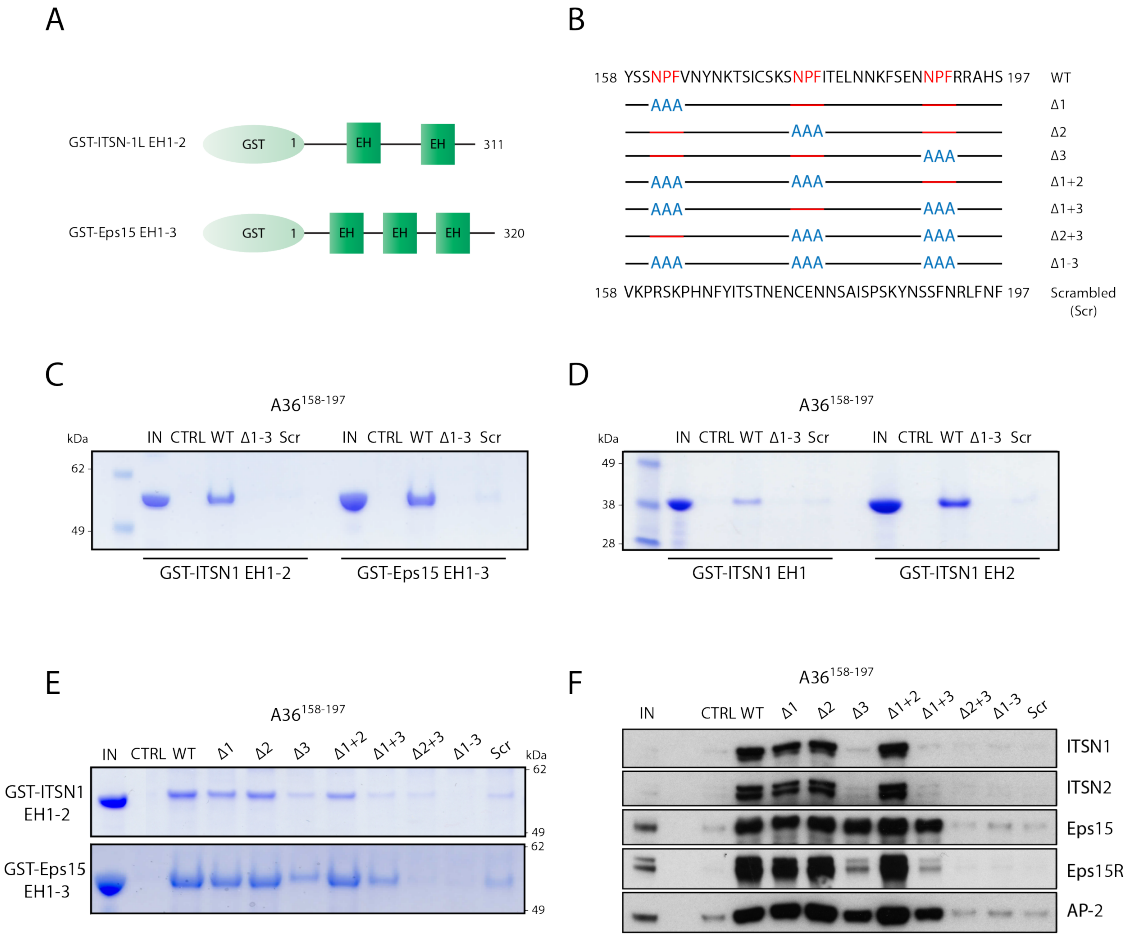

Figure 3.6 A36 NPF motifs directly bind EH domains of intersectin-1 and Eps15

A GST-ITSN1 EH1-2 and GST-Eps15 EH1-3 purified constructs that were used in peptide pull-down assays. **B** N-terminally biotinylated peptides of A36$^{158\text{-}197}$ were synthesised containing single, two, and all three NPF motifs substituted to a tri-alanine motif (AAA). A scrambled A36$^{158\text{-}197}$ peptide was generated to control for non-specific binding (Scr). **C** GST-EH domains were incubated with A36$^{158\text{-}197}$ loaded Streptavidin beads (IN = input protein levels). GST-ITSN1 EH1-2 and GST-Eps15 EH1-3 can directly bind wild type A36$^{158\text{-}197}$ (WT) but not Δ1-3, Scr, or unloaded Streptavidin beads (CTRL). **D** GST-ITSN1 EH1 and GST-ITSN1 EH2 were incubated with A36$^{158\text{-}197}$ loaded Streptavidin beads (WT, 1-3, Scr) and unloaded Streptavidin beads (CTRL). Both are able to bind wild type A36$^{158\text{-}197}$ but not Δ1-3. **E** Direct peptide pull-downs on the entire panel of A36$^{158\text{-}197}$ NPF-AAA peptides incubated with GST-ITSN1 EH1-2 and GST-Eps15 EH1-3. **F** Indirect peptide pull-downs on a panel of A36$^{158\text{-}197}$ NPF-AAA peptides incubated with HeLa cell lysates and probed for binding of endogenous intersectin-1, intersectin-2, Eps15, Eps15R and AP-2.

3.2.5 NPF motifs are conserved amongst the *Orthopoxviruses*

There are numerous examples of mechanisms by which viruses hijack host cell processes in order to enhance viral spread, and clearly the endocytic machinery is no exception (Humphries and Way, 2013). Several viruses subvert endocytic machinery for their entry, however, at this time functional NPF motifs have never been identified in a viral protein (Cossart and Veiga, 2008; Gruenberg, 2009; Marsh and Helenius, 2006; Mercer et al., 2010). In order to understand the extent of conservation of the NPF motifs among the poxvirus family, BLAST analysis was performed on vaccinia A36. A36 is highly conserved amongst the *Orthopoxvirus* genus, and has a vital role in microtubule-based and actin mediated viral spread (Parkinson and Smith, 1994; Rottger et al., 1999; Ward and Moss, 2001; Wolffe et al., 1998). The homologues of vaccinia A36 in variola virus, camelpox virus, monkeypox virus, rabbitpox virus, cowpox virus, and taterapox virus all contain three NPF motifs (Figure 3.7). Ectromelia virus, a natural pathogen of mice expresses a A36 homologue with 97% sequence identity to vaccinia A36, although it is truncated from residue 161 onwards, and therefore lacks all NPF motifs (Figure 3.7) (Esteban and Buller, 2005; Lynn et al., 2012). A previously characterised functional orthologue of A36 in yaba-like disease virus, is encoded by the 126R gene, also lacks the presence of NPF motifs. The conservation of the A36 NPF motifs amongst the *Orthopoxviridae* is a strong indicator of a selective evolutionary advantage of the NPF motifs during infection.

```
                                161-3           176-8          190-2
VACV    146 EVLNEDTKQNPNYSSNPFVNYNKTSICSKSNPFITELNNKFSENNPFRRAHSDD----YLNKQEQDHEHDDIESSVVSLV 221
VARV    145 EVLNEDTKQNPSYSSNPFVNYNKTSICSKSNPFITELNNKFSENNPFRRAHSDD----YLNKQ----EHDDIESSVVSLV 216
CMLV    146 EVLNEDTKQNHSYSSNPFVNYNKTSICSKSNPFITELNNKFSENNPFRRAHSDD----YLNNQEQE--HDDIESSVMSYH 219
MKPV    138 EILNEDTKQIPSYSSNPFVNYNKTSICSKSNPFIAELNNKFSDNNPFRRAHSDD----YLNKQ-QDHEHDDIESSVVSLV 212
RPXV    146 EVLNEDTKQNPNYSSNPFVNYNKTSICSKSNPFITELNNKFSENNPFRRAHSDD----YLNKQEQDHEHDDIESSVVSLV 221
COWPX   146 EVLNEDTKQNPSYSSNPFVNYNKTSICSKSNPFITELNNKFSENNPFRRAHSDD----YLNKQEQDHEHDDIESSVVSLV 221
TATV    145 EVLNEDTKQNPSYSSNPFVNYNKTSICSKSNPFITELNNKFSENNPFRRAHSDD----YLNKQEQ--EHDDIESSVVSLV 218
YLDV    148 DNVENITYDLPQDS----IIYDLDGKSDVAVYDIPESEDNVYENNICLESCFDDVKYNSPLNNFNKNYYSYNTNDFVSNV 223
ECTV    144 EVLNEDTKQNPNFHPILS------------------------------------------------------------ 161
```

Figure 3.7 The A36 NPF motifs are highly conserved among the *Orthopoviridae*

Clustal Omega sequence alignment of the C-termini of the following *Orthopoxvirus* A36 orthologues (Uniprot Entry in parenthesis). VACV – Vaccinia virus (P68619), VARV – Variola virus (Q0N502), CMLX – Camelpox virus (Q912R6), MKPV – Monkeypox virus (Q5IXM7), RPXV – Rabbitpox virus (Q6RZE7), COXPX – Cowpox virus (G0XSQ1), TATV – Taterapox virus (Q0NP51), YLDV – Yaba-like disease virus (Q9DHI7), ECTV – Ectromelia virus (Q912M8). Three conserved NPF motifs are highlighted in red.

3.3 Summary

Work presented in this chapter has identified vaccinia A36 as the first known viral protein containing functional EH domain binding Asn-Pro-Phe (NPF) motifs. NPF motifs are conserved from yeast to man and are abundant in early endocytic proteins (Chen et al., 1998; Fernandez-Chacon et al., 2000; Haffner et al., 1997; Martina et al., 2001; Salcini et al., 1997). These motifs act as scaffolds for the recruitment of additional endocytic components such as intersectin-1, Eps15 and AP-2 during endocytosis. A36 can directly recruit intersectin-1 and Eps15 via the NPF motifs *in vitro*, and is essential for binding of AP-2. *In vitro* A36 NPF3 is essential for the recruitment of intersectin-1/2 and Eps15R, with additional contribution mediated by NPF2. A36 NPF1 alone, in contrast, is unable to mediate binding of intersectin-1/2, Eps15/R, or AP-2. During infection CEV can recruit the EH domain-containing proteins intersectin-1, intersectin-2, Eps15, and Eps15R. Furthermore, intersectin-1, intersectin-2, Eps15, and Eps15R can remain associated with viral particles following the initiation of actin polymerisation. This differs from prior observations of AP-2 and clathrin, which are left behind at the plasma membrane upon the formation of actin tails. Moreover, the NPF motifs are a conserved feature of the *Orthopoxviridae,* and may represent a common mechanism required during viral egress. Subsequent characterisation of the A36 NPF motifs *in vivo*, will shed light on the functional role that they play during the course of infection.

Chapter 4. Generation and characterisation of Vaccinia A36 ΔNPF 1-3

4.1 Introduction

The previous chapter identified the molecular basis for the interaction of the endocytic components, intersectin-1 and Eps15 with vaccinia A36. Intersectin-1 and Eps15 have both been shown to directly bind AP-2 (Benmerah et al., 1996; Benmerah et al., 1995; Iannolo et al., 1997; Pechstein et al., 2010). Intersectin-1 and Eps15 are both recruited to the virus during infection and actin tail formation, suggesting that they act to mediate the recruitment of AP-2 to CEV via association with A36. In order to test the functional importance of intersectin-1 and Eps15 two approaches were carried out. Initially RNAi experiments were utilised to determine the effect of intersectin-1 and Eps15 depletion on AP-2 binding, actin tail formation, and cell-to-cell spread. Downregulation of endocytic adaptors by RNAi is often difficult to achieve due to functional redundancy among the components of clathrin-coated pits, including the EH domain containing proteins and their interactors. As demonstrated in the previous chapter, several EH domain-containing proteins can be recruited via the vaccinia A36 NPF motifs, suggesting that they may act together in complex. Furthermore, complete RNAi mediated depletion of endocytic proteins may not be achieved, therefore an additional approach was utilised.

A panel of recombinant A36 NPF mutant viruses were generated and characterised in order to closely examine the role of the A36 NPF motifs during viral infection. Recombinant viruses are a key tool to study the interplay between host and viral biology (Dodding and Way, 2009). Recombinant viruses are advantageous over RNAi depletion in several respects. They can be investigated over long time periods, with great reproducibility, and with no host off-target effects. Several vaccinia recombinants are not viable due to early defects in viral replication, however this is not the case in vaccinia lacking A36 (ΔA36R). ΔA36R is not lethal and is able to progress through the early viral life cycle. Creating a virus lacking the A36 NPF motifs aims to abolish A36-

dependent binding of intersectin-1/2 and Eps15/15R in addition to as-of-yet unknown EH domain containing proteins that may be recruited by A36.

4.2 Results

4.2.1 Intersectin-1 and Eps15 are essential to mediate AP-2 binding to A36

Vaccinia-induced actin tails in AP-2 depleted cells exhibited increased tail length and increased rate of motility (Humphries et al., 2012). FRAP analysis also revealed that N-WASP recruited to CEV in AP-2 depleted cells had a significantly faster turnover rate, consistent with the increased rate of actin-based motility of the virus upon the loss of AP-2 (Humphries et al., 2012; Weisswange et al., 2009). As an initial approach to determine whether intersectin-1 or Eps15 act in the same pathway as AP-2, RNAi depletion of intersectin-1 and Eps15 and a combined knock down of intersectin-1/2 and Eps15/15R (EH pool) was carried out in HeLa cells stably expressing LifeAct-Cherry, a reporter for filamentous actin. Actin tail length was subsequently measured 8 hours post infection (Figure 4.1 A). AllStar (CTRL) and AP-2 siRNA were used as negative and positive controls respectively.

The extent of RNAi depletion was determined by immunoblot analysis (Figure 4.1 B). To note, depletion of Eps15 also led to the decreased expression of intersectin-1, complicating the ability to analyse the role of Eps15 independent to that of intersectin-1. Nevertheless, depletion of intersectin-1, Eps15 and the EH pool during WR infection resulted in a significant increase in actin tail length compared to control treated cells (Figure 4.1 A, B). This increase in actin tail length phenocopies that observed following AP-2 depletion as previously observed (Figure 4.1 A, B) (Humphries et al., 2012). RNAi depletion of intersectin-1 also resulted in an increase in the velocity of actin tails to the same extent as that observed in AP-2 depleted cells (Figure 4.1 C). Loss of Eps15 however, had a small albeit not significant increase in tail speed (Figure 4.1 C). Taken together, this suggests that intersectin-1/Eps15 act in the same vaccinia-signalling pathway as AP-2. Depletion of the EH pool also resulted in an increase in actin tail speed compared to control treated cells, however, curiously to a lesser extent than observed following depletion of AP-2 and intersectin-1 alone.

In order to determine whether intersectin-1 or Eps15 mediate the binding of AP-2 to A36 in isolation of one another or as a complex, GFP-Trap pull-down experiments were performed on lysates from RNAi treated HeLa cells. Cells were treated with AllStar control (CTRL), AP-2, Eps15, and intersectin-1 siRNA for 48 hours prior to infection with the ΔA36R virus. Infected, RNAi treated cells were subsequently transfected with either GFP alone or GFP-A36$^{24-221}$. In agreement with the earlier observation that the depletion of Eps15 also affected intersectin-1 levels, in this case the reverse was also true, with the depletion of intersectin-1 resulting in a decrease in Eps15 and vice versa (Figure 4.1 B, D). As previously determined, intersectin-1, Eps15 and AP-2, could all interact with GFP-A36$^{24-221}$ in cells treated with AllStar (CTRL) RNAi (Figure 3.4, 4.1 D). Depletion of AP-2 did not impact on binding of either Eps15 or intersectin-1 to GFP-A36$^{24-221}$ (Figure 4.1 D). In contrast, the RNAi mediated loss of either Eps15 or intersectin-1 entirely abolished AP-2 binding to GFP-A36$^{24-221}$ (Figure 4.1 D). Interestingly, while the depletion of intersectin-1 also abolished Eps15 recruitment to GFP-A36$^{24-221}$, following treatment with Eps15 siRNA, residual intersectin-1 could still associate with GFP-A36$^{24-221}$.

This data may suggest a speculative model whereby intersectin-1 is responsible to mediate the recruitment of Eps15 to A36, and that intersectin-1 and Eps15 function in complex to mediate AP-2 recruitment. In order to confirm that intersectin-1 is upstream of AP-2 and clathrin recruitment during infection, RNAi treated cells were fixed 8 hours post infection and stained for extracellular virus and intersectin-1. The co-localisation of intersectin-1 to CEV was manually quantified in an unbiased manner following immunofluorescence imaging (Figure 4.2 A). Compared to AllStar (CTRL), RNAi depletion of AP-2 or clathrin did not affect the percentage of CEV that co-localised with intersectin-1 (Figure 4.2 B). Depletion of intersectin-1 decreased detected intersectin-1 to background levels and thus significantly reduced co-localisation to CEV. This confirms that intersectin-1 plays a role upstream of AP-2 and clathrin to facilitate their recruitment to the virus during egress.

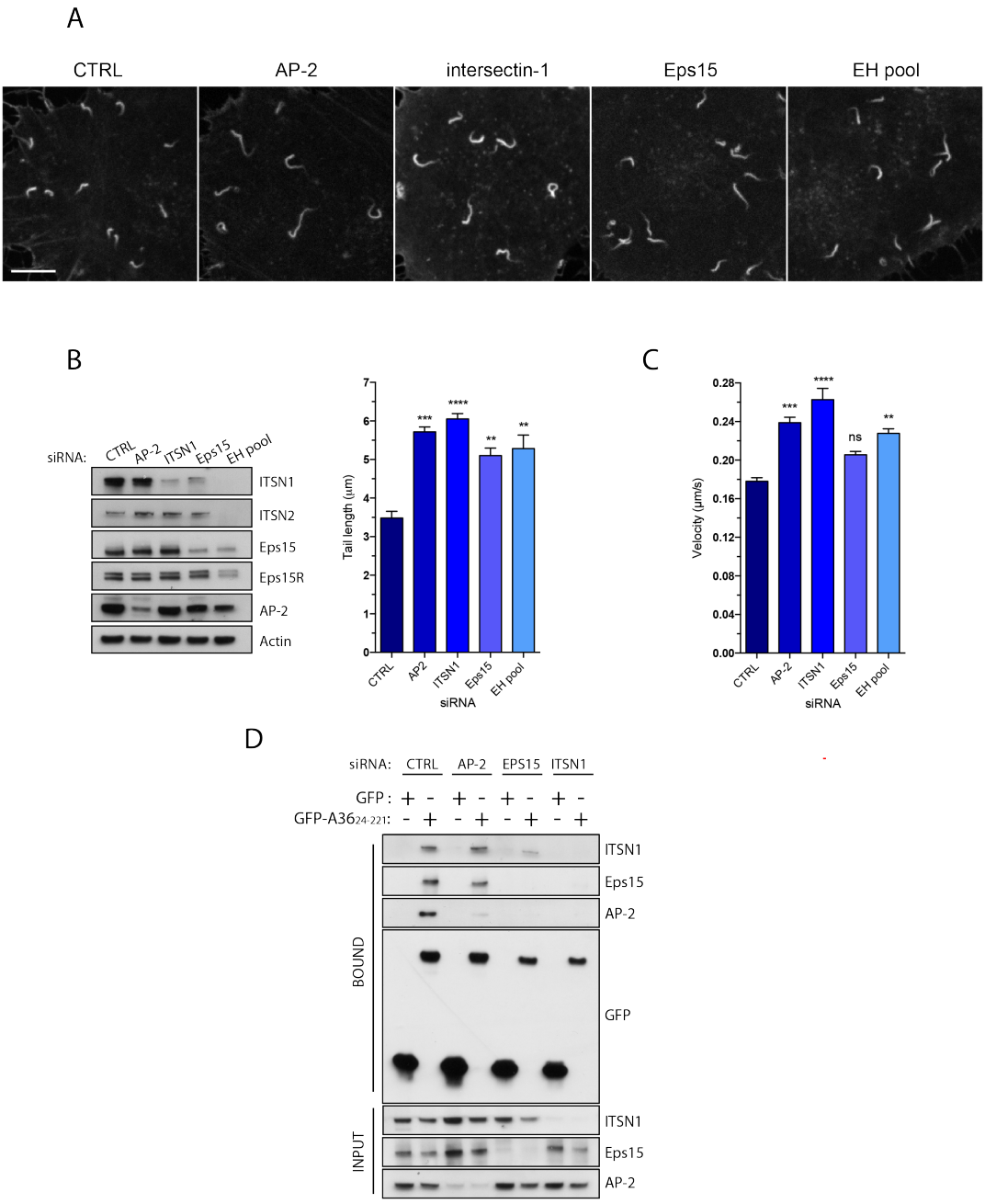

Figure 4.1 Intersectin-1 and Eps15 depletion leads to longer actin tails and the loss of AP-2 binding to A36

A Representative images of vaccinia-induced actin tails following RNAi depletion in HeLa-Lifeact Cherry cells. Scale bar = 5 µm. **B** RNAi depletion of AP-2, ITSN1, Eps15, and a pool of ITSN1/2, and Eps15/15R (EH pool) in HeLa-Lifeact Cherry cells results in the formation of longer actin tails compared to AllStar (CTRL). N = 300 tails per condition **C** AP-2, ITSN1 and the EH pool also results in faster moving actin tails. N = 75 tails per condition **D** GFP-Trap pull-downs on GFP or GFP-A36$^{24-221}$ from lysates of HeLa cells depleted of AllStar (CTRL), AP-2, Eps15, and ITSN1. Depletion of AP-2 does not affect binding of ITSN1 and Eps15 to A36. Conversely depletion of Eps15 and ITSN1 abolishes AP-2 recruitment. Error bars represent SEM from 3 independent experiments. A p value of <0.0001 is indicated by ****, <0.001 is indicated by ***, <0.01 is indicated by **. ns indicates a p value > 0.05.

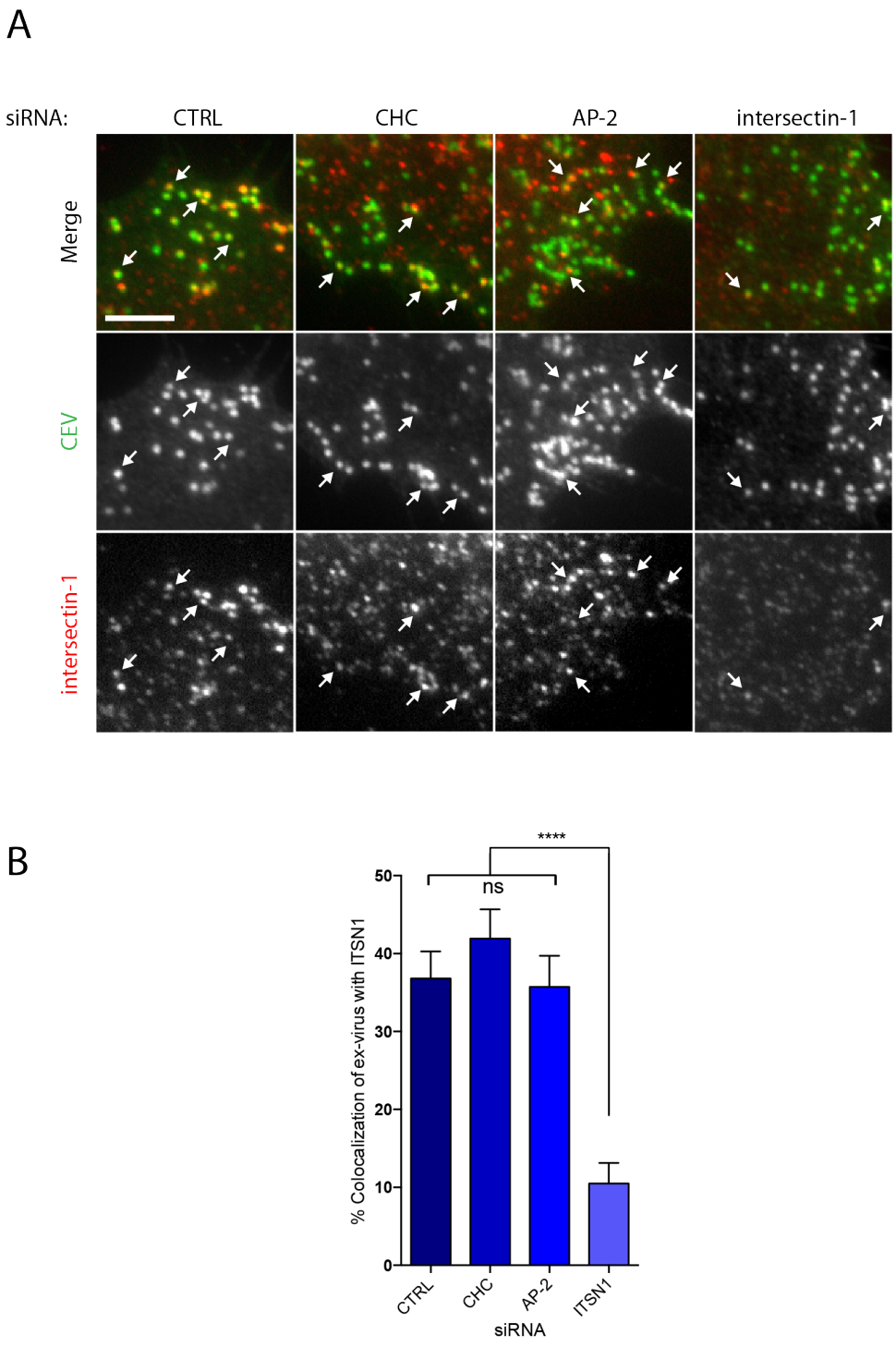

Figure 4.2 Intersectin-1 recruitment to CEV is independent of AP-2 and clathrin

A Representative immunofluorescence images of CEV following RNAi depletion in N-WASP -/- cells. Scale bar = 5 µm. **B** Depletion of clathrin (CHC) and AP-2 do not effect localisation of intersectin-1 on CEV (bottom panel). Intersectin-1 depletion is not absolute and there remains residual recruitment to CEV. Error bars represent SEM from N=300 particles counted in 3 independent experiments. A p value of <0.0001 is indicated by ****, <0.001 is indicated by ***, <0.01 is indicated by **. ns indicates a p value > 0.05.

The loss of AP-2 has also been shown to result in the reduction of cell-to-cell spread of vaccinia through a confluent cell monolayer (Humphries et al., 2012). To investigate the role of intersectin-1 during viral spread, the ability of WR to spread through confluent monolayers of RNAi treated A549 cells was determined. This experiment was performed under a semi-solid overlay of carboxy-methyl cellulose to restrict spread solely to that mediated by direct cell-cell transmission. A single plaque is therefore derived from a single infected cell. A549 cells were transfected with siRNA for 48 hours prior to infection with WR. At 48 hours post infection cells were fixed, permeabilized and stained for the viral IEV protein B5 in order to visualize viral plaques. As expected the virus was unable to spread efficiently in the absence of AP-2 (Figure 4.3) (Humphries et al., 2012). In addition, intersectin-1 depletion resulted in an equal defect in viral spread as that of AP-2, leading to a 40% reduction in viral plaque size compared to AllStar (CTRL) treated cells (Figure 4.3). This data further supports that intersectin-1 acts upstream of AP-2, and that intersectin-1 is key to enhance viral spread.

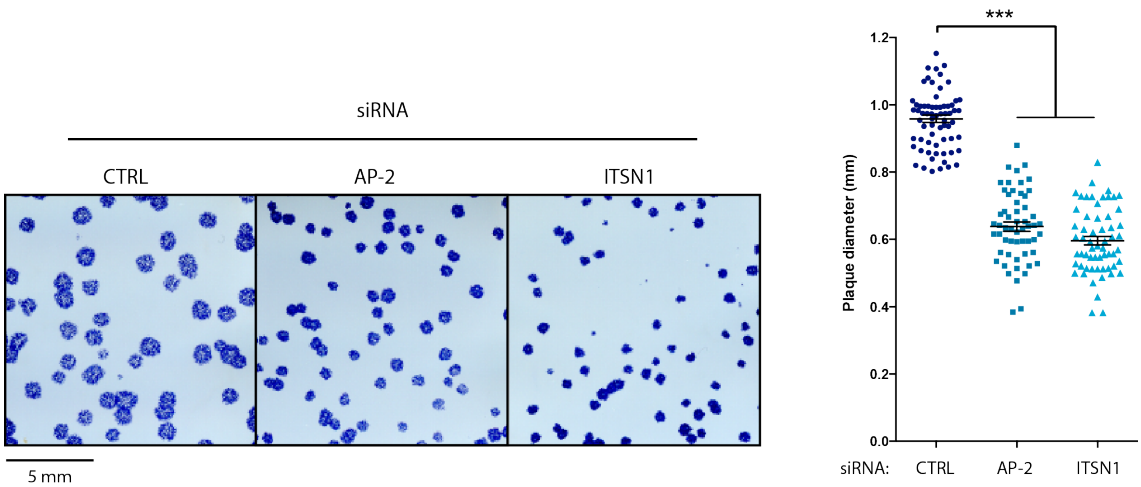

Figure 4.3 Loss of AP-2 and intersectin-1 reduces the cell-to-cell spread of WR

Depletion of AP-2 and intersectin-1 (ITSN1) in a confluent monolayer of A549 cells leads to the formation of smaller plaques following infection with WR than in AllStar control (CTRL) treated cells. Cells were permeabilized, and plaques were stained with anti-B5 and visualised with TMB peroxidase. Error bars represent SEM from N=100 plaques measured from 3 independent experiments. A p value of <0.001 is indicated by ***.

4.2.2 Loss of a single NPF motifs leads to longer actin tails

The length of actin tails was used as a functional read out to determine whether NPF motifs affect actin tail morphology to the same extent as the loss of AP-2 and clathrin. Prior to the generation of recombinant viruses, to initially assess the role of the NPF motifs on actin tails formation, the individual NPF motifs in full length A36 were substituted to alanines. Individual A36 ΔNPF constructs were transiently transfected in ΔA36R infected HeLa cells. After 8 hours of infection and transfection cells were fixed and stained for immunofluorescence imaging. Compared to expression of wild type A36, all three single NPF mutants (ΔNPF1, ΔNPF2, ΔNPF3) induced the formation of long actin tails (Figure 4.4). Expression of wild type A36 induced actin tails with a mean length of 3.1 ± 0.8 μm. The length of vaccinia-induced actin tails upon expression of A36 ΔNPF1, 2, or 3 was significantly longer, ranging between 5.16 ± 1.1 – 5.5 ± 1.4 μm (Figure 4.4).

Although transient transfection of the A36 ΔNPF mutants may lead to artefacts as a result of overexpression, this data provides initial evidence for a role of the A36 NPF motifs to regulate actin dynamics during actin tail formation. In contrast to *in vitro* peptide pull-down assays in Chapter 3, this data also suggests that the loss of a single A36 NPF motif is sufficient to result in changes in actin tail length to the same extent as depletion of intersectin-1 and AP-2, which also result in a long tail phenotype (Figure 4.1 A). This suggests that during infection all three NPF motifs play a functional role in the recruitment of EH domain containing proteins and AP-2 to some extent, in agreement with GFP-Trap assays (Figure 3.4 C)

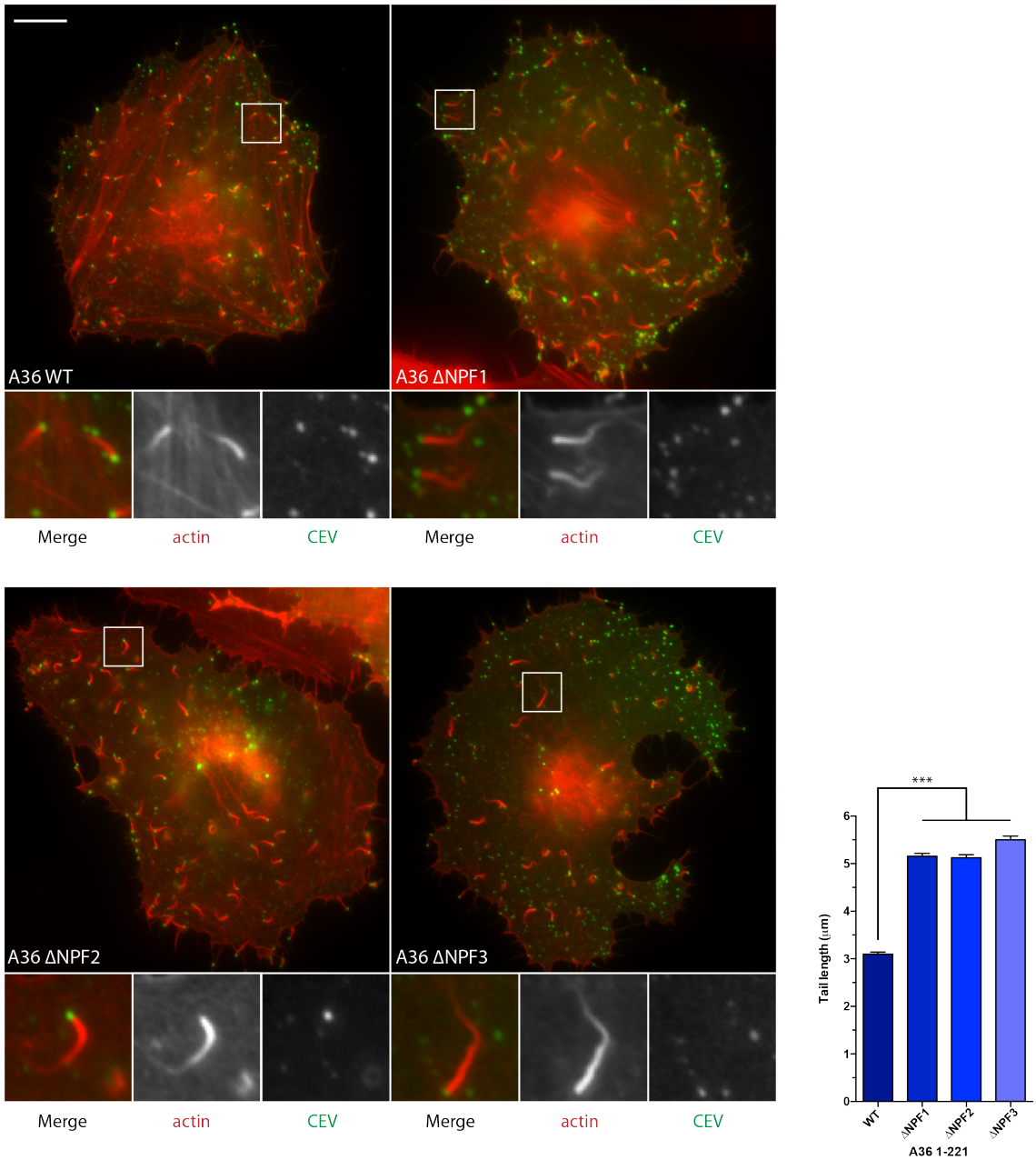

Figure 4.4. Loss of individual A36 NPF motifs results in longer actin tails

A Representative immunofluorescence images from HeLa cells infected with ΔA36R and transfected with A36 wild type and ΔNPF mutants (residues 1-221). Cells were fixed at 8 hpi and stained for extracellular virus (B5) and actin (phalloidin). Scale bar = 10 μm. **B** Quantification of actin tail length following infection with ΔA36R and transfection of WT and A36 ΔNPF mutants. A total of 400 actin tails per virus from 20 infected cells over three independent experiments were measured using ImageJ. Error bars represent SEM. A p value of <0.001 is represented by ***.

4.2.3 Generation of the recombinant A36 ΔNPF 1-3 virus

Next to determine the role of the NPF motifs during infection, a recombinant A36 virus lacking the NPF motifs was generated. The ΔA36R virus contains an internal deletion in the A36R gene, and is therefore truncated to a non-functional gene product (Parkinson and Smith, 1994). Taking advantage of this, a functional A36R gene containing the desired NPF mutations was incorporated into the vaccinia ΔA36R genome via homologous recombination of the regions flanking the A36R locus. The A36R gene was amplified from vaccinia WR genomic DNA by PCR using primers 300bp upstream and downstream of the A36R locus (Figure 4.5 A). Using a two-step mutagenesis approach, individual A36 NPF to AAA (ΔNPF1, 2, and 3) substitution mutants were generated and confirmed by sequencing. Sequential rounds of mutagenesis were carried out in order to generate the A36 triple NPF to AAA construct (hereon referred to as A36 ΔNPF1-3).

Given the requirement of A36 for both microtubule-based transport to the cell periphery and actin tail formation, infection with the ΔA36R virus results in significantly defective viral spread and therefore leads to the formation of small viral plaques in a confluent monolayer of BS-C-1 cells compared to WR (Figure 4.5 B) (Parkinson and Smith, 1994; Ward and Moss, 2001; Wolffe et al., 1998). The A36 ΔNPF mutants generated still contain the kinesin-1 binding WE/WD motifs and tyrosine 112 and 132, therefore are able to traffic to the plasma membrane and induce actins tails, as observed following transient transfection (Figure 4.4). Taking advantage of the ΔA36R rescue with A36, positive recombinants were identified by screening for an increase in plaque size above that of ΔA36R. A36 ΔNPF plaques were purified through four rounds of plaque selection in order to prevent cross contamination by ΔA36R. Recombinants were additionally screened for correct insertion and expression of A36 at every round by both PCR and immunoblot analysis (Figure 4.5 C). During previous characterisation of A36 phosphorylation during infection, a recombinant virus expressing a truncated A36 protein was generated (Weisswange, 2008). This recombinant expressed A36 truncated from residue 155 onwards (A36 1-155). The C-terminal deletion did not affect levels of tyrosine phosphorylation of A36, however this virus also lacks all three NPF motifs.

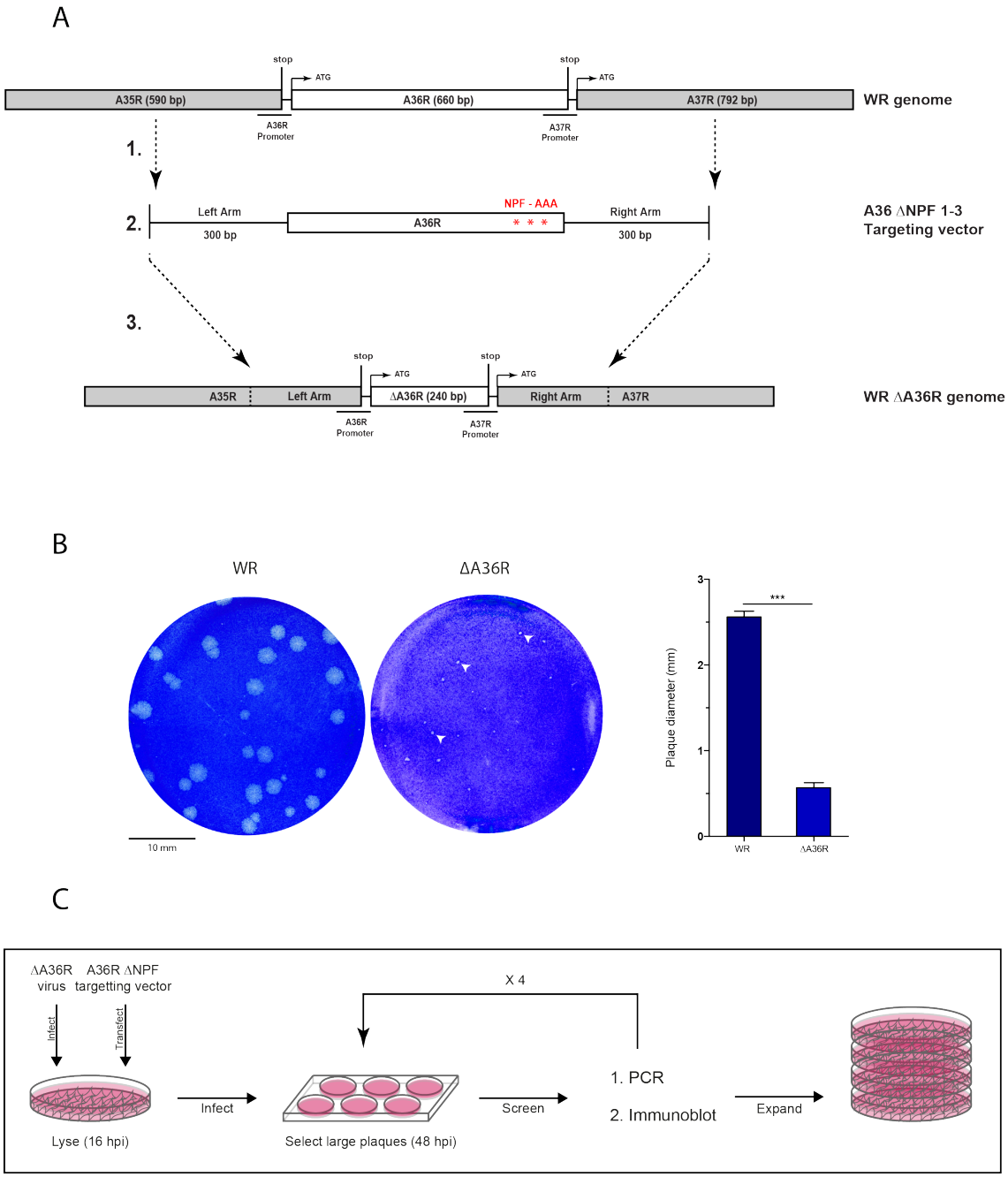

Figure 4.5. Generation of recombinant A36 NPF mutant viruses

A Targeting strategy for the generation of the A36 ΔNPF mutant viruses. 1. PCR of the A36 targeting vector from viral genomic DNA. 2. Subsequent mutagenesis of the NPF motifs to alanines (AAA). 3. Incorporation into the ΔA36R genome. **B** Plaque size 48 hours post infection of BS-C-1 cells with WR verses ΔA36R. White arrows indicate ΔA36R plaques. Quantification of WR and ΔNPF plaque diameter from N=100 plaques. Error bars represent SEM. A p value of <0.001 is represented by ***. **C** Representation of the generation and purification of the A36 ΔNPF viruses following initial homologous recombination.

To confirm that the loss of NPF motifs did not impact on the temporal dynamics of A36 expression or its stability during infection A36 expression was analysed during the course of infection. HeLa cell lysates were collected at 1 hour intervals following infection with each recombinant A36 virus and A36 expression determined by immunoblot analysis. In all cases A36 was expressed both early and late during infection, commencing at 1-2 hours post infection (Figure 4.6 A). Protein levels were comparable to those observed during WR infection and there was no obvious protein degradation, suggesting that the loss of the NPF motifs does not impact on the stability of A36. A36 is not required for viral replication or entry, however in order to rule out a possible early-stage defect of the A36 ΔNPF mutants, single-step growth curves were carried out. Single-step growth analysis is used to study a single replication cycle during viral infection. BS-C-1 cells were infected with high multiplicity of infection (MOI = 10) of each virus in order to synchronise infection of all cells. Infected cells were harvested at 0, 4, 8, 12, and 24 hours post infection (hpi), and viral titres determined by plaque assay on confluent BS-C-1 monolayers. At 24 hpi there was no significant change in total virus produced with the ΔNPF mutant viruses or vaccinia expressing truncated A36 1-155 compared to WR (Figure 4.6 B).

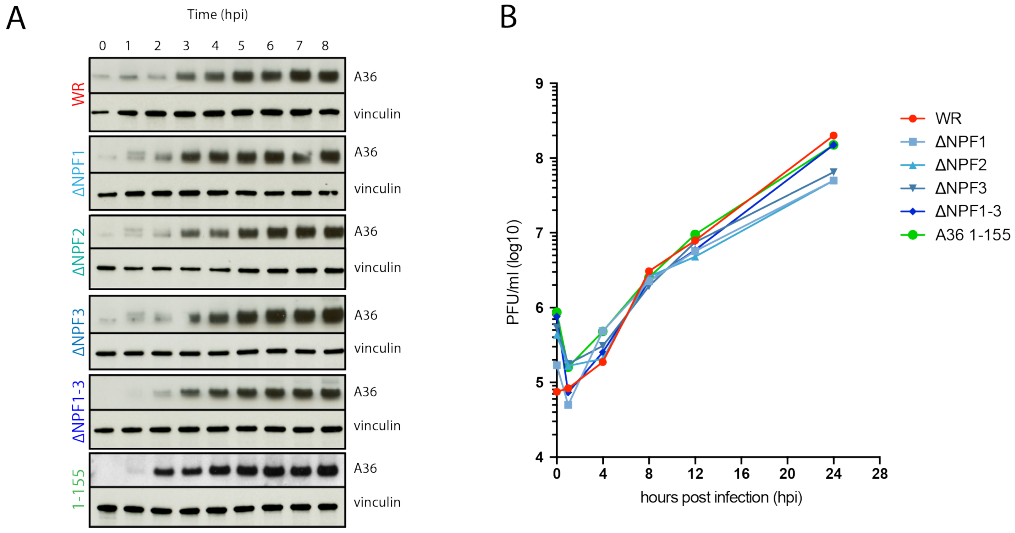

Figure 4.6. Loss of NPF motifs does not impact on A36 expression or virus replication

A Immunoblot analysis of A36 expression every hour post infection with the A36 recombinant viruses. Cells were infected with a MOI=1. Whole-cell lysates were collected at 0-8 hpi. Vinculin is shown as a cellular loading control. **B** Single step growth curves following infection with A36 recombinant viruses compared to WR. BS-C-1 cells were infected with MOI=10 of the indicated viruses. At the indicated times cells were collected and viral titres determined by plaque assay on BS-C-1 cells. This graph shows mean titres from two independent experiments.

4.2.4 The A36 NPF motifs recruit intersectin-1 and Eps15 to Vaccinia virus

In vitro biochemical analysis showed that the loss of all three A36 NPF motifs abolished the interaction of intersectin-1, Eps15, and AP-2 with A36 (Figure 3.4 C). I next sought to address whether this also the case during infection. During infection with WR, N-WASP dependent actin tails propel viral particles away from clathrin and AP-2 at the plasma membrane. Previous data has determined that cells lacking N-WASP (N-WASP -/- MEFs) are unable to form actin tails following WR infection (Donnelly et al., 2013; Snapper et al., 2001; Weisswange et al., 2009). The inability of vaccinia to nucleate an actin tail in N-WASP -/- MEFs, results in an increase of virus particles at the membrane that are still associated with clathrin and AP-2 (Humphries et al., 2012). Following infection of N-WASP +/+ MEFs with WR, only 18% of CEV co-localise with AP-2 (Humphries et al., 2012). Following WR infection of N-WASP -/- MEFs, the level of co-localisation increases to around 30% (Humphries et al., 2012). This increase in AP-2 recruitment was used to our advantage, in order to give a greater dynamic range from which differences in the recruitment of clathrin, AP-2, intersectin-1 and Eps15 could be discerned between the A36 ΔNPF recombinant viruses.

N-WASP -/- MEFs were infected with WR, and the A36 ΔNPF1, 2, 3, A36 ΔNPF1-3, and A36 1-155 viruses for 8 hours before being fixed and processed for immunofluorescence imaging. Co-localisation of clathrin, AP-2, intersectin-1 and Eps15 to CEV was determined using immunofluorescence staining of the respective endogenous proteins (Figure 4.7 A). Co-localisation was quantified manually in an unbiased manner. Following WR infection, the percentage of clathrin, AP-2, intersectin-1, and Eps15 associated with CEV was in the range of 50-65%, consistent with their co-recruitment to viral particles. Depletion of individual A36 NPF motifs (A36 ΔNPF1, 2, 3) did not result in a significant change in the recruitment of clathrin, AP-2, intersectin-1 or Eps15 to CEVs compared to WR infection (Figure 4.7 B). Although the loss of individual NPF motifs abolished binding of AP-2, intersectin-1 and Eps15 from cell lysates *in vitro*, this is not the case during infection (Figure 3.4 C, 4.7 B).

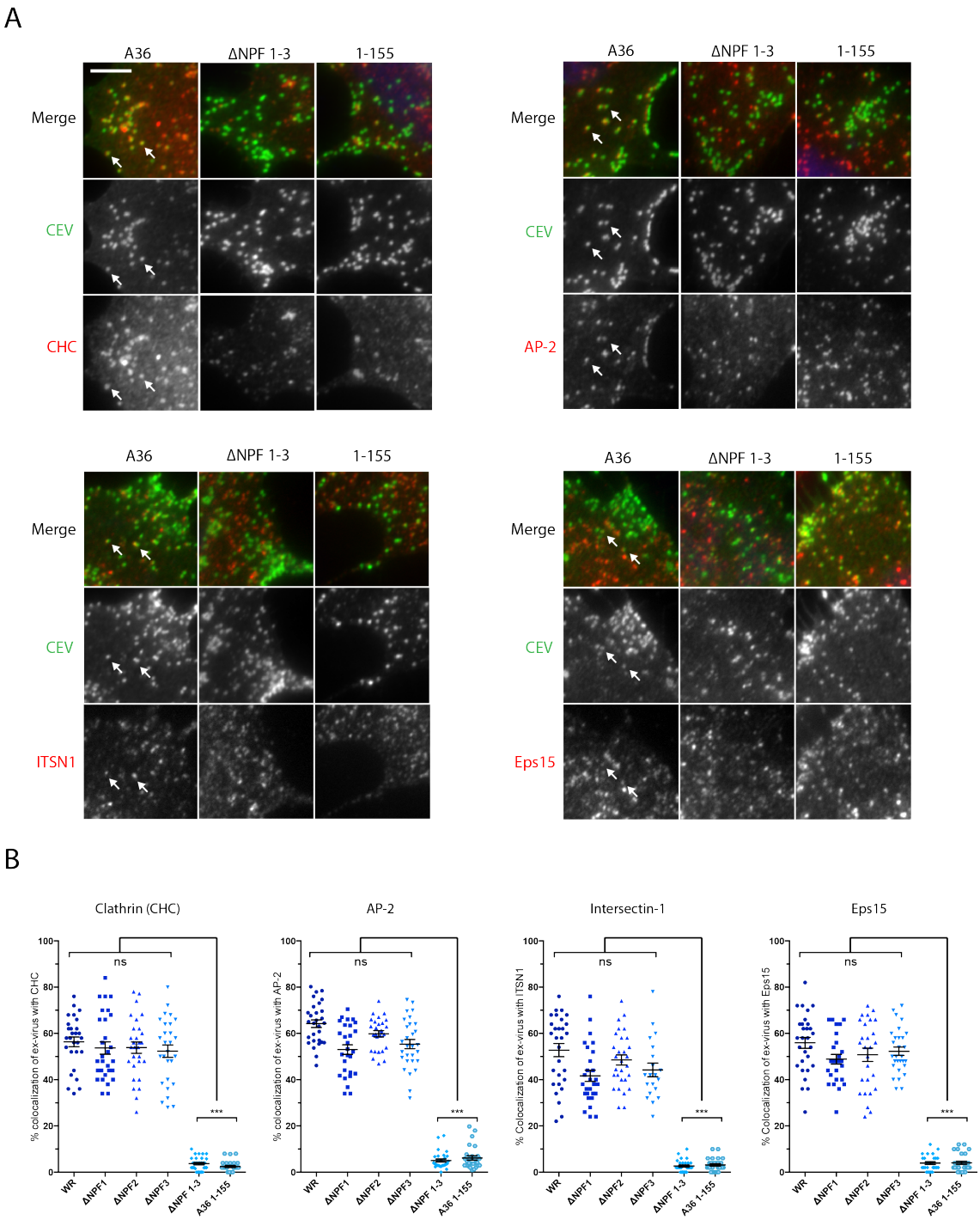

Figure 4.7. Three A36 NPF motifs are required to recruit clathrin, AP-2, intersectin-1, and Eps15 to CEV

A Representative immunofluorescence images of vaccinia infected N-WASP -/- cells fixed at 8 hours post infection. Cells were stained prior to permeabilization with a B5 antibody to detect CEV. Images highlight examples of co-localisation with clathrin, AP-2, intersectin-1 and Eps15 following infection with the indicated viruses (white arrows). **B** Graph shows the percentage co-localisation of CEV with clathrin, AP-2, intersectin-1, and Eps15. Error bars represent SEM from 100 particles counted per cell, in 30 cells, in three independent experiments. A p value of <0.001 is represented by ***. ns indicates a p value > 0.05.

Infection with A36 ΔNPF1-3 and the A36 1-155 truncation mutant lacking all three NPF motifs, however, led to a significant decrease in the recruitment of clathrin, AP-2, intersectin-1, and Eps15 to CEV (Figure 4.7 B). This is in agreement with peptide pull-downs from cell lysates, whereby Eps15 and AP-2 could still be recruited to $A36^{157-196}$ peptides lacking the individual NPF motifs (Δ1, Δ2, Δ3) (Figure 3.6 F). Conversely, following $A36^{157-196}$ peptide pull-down assays with either recombinant or endogenous intersectin-1, intersectin-1 could not bind $A36^{157-196}$ peptides lacking NPF3 (Δ3) (Figure 3.6 E, F). This may indicate that intersectin-1 recruitment to NPF3 during infection is mediated or enhanced by Eps15.

4.2.5 Yaba-like disease virus YL126 is unable to recruit intersectin-1 and Eps15

The significant loss of clathrin, AP-2, intersectin-1 and Eps15 to both the A36 ΔNPF virus and the A36 1-155 virus also suggests that during infection A36 alone is sufficient for recruitment of the endocytic machinery during egress. In order to confirm that A36 was necessary and sufficient to mediate binding of clathrin, AP-2, intersectin-1 and Eps15 during infection, infection with ΔA36R virus was carried out. The inability of ΔA36R to mediate microtubule-based transport to the cell periphery, however, leads to a significant decrease in the number of CEV. As a result of this an alternative approach was used. Previous work in our lab demonstrated that the A36 orthologue in Yaba-like disease virus (YLDV), YL126 was able to recruit both Nck and N-WASP and induce actin tail polymerisation when expressed in the vaccinia A36R gene locus (WR ΔA36R-YLDV126R)(Dodding and Way, 2009). YL126, however, does not contain any NPF motifs (Figure 3.7). N-WASP -/- cells were infected with WR ΔA36R-YLDV126R and processed for immunofluorescence 8 hours post infection. Immunofluorescence analysis revealed that clathrin, AP-2, intersectin-1 and Eps15 are unable to be substantially recruited to the WR ΔA36R-YLDV126R virus (Figure 4.8). YL126 has less than 15% homology with vaccinia A36, and the loss of the NPF motifs in YL126 may contribute to the observed altered actin tail dynamics and decrease in cell-to-cell spread of YLDV compared with that of vaccinia virus (Dodding and Way, 2009). Taken together, co-localisation analysis indicates that the A36 NPF motifs are essential for the recruitment of clathrin, AP-2, intersectin-1, and Eps15 to CEVs during their egress, and that there is functional redundancy between the NPF motifs. The contribution of other IEV proteins

to the recruitment of clathrin, AP-2, intersectin-1, and Eps15 to CEVs if it occurs at all, must be minimal or supportive in its nature.

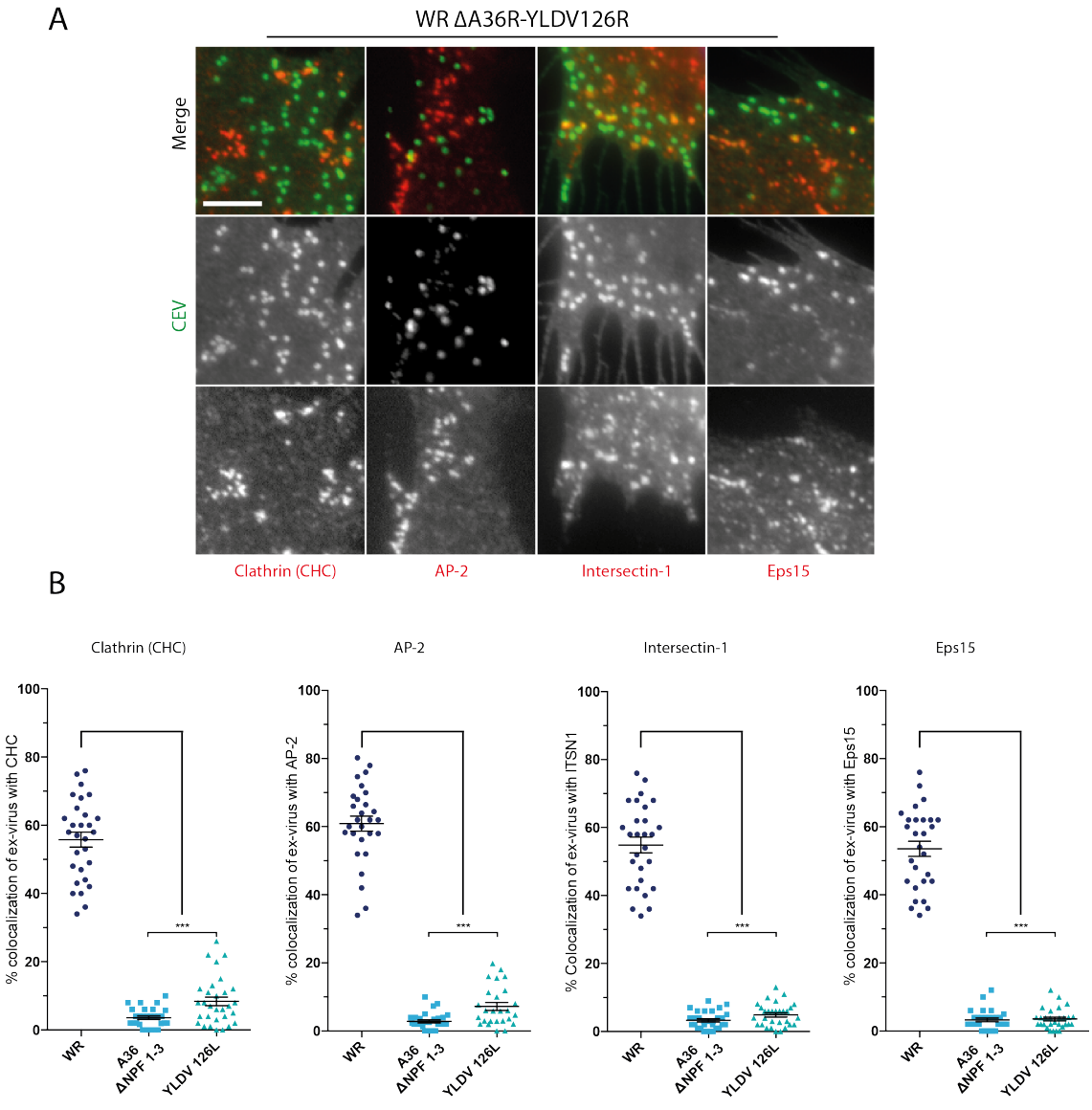

Figure 4.8. YLDV YL126 is unable to recruit endocytic machinery

A Immunofluorescence images of vaccinia infected N-WASP -/- MEFs fixed at 8 hours post infection with the WR ΔA36R-YLDV126R virus. Cells were stained prior to permeabilisation with a B5 antibody to detect CEV, alongside clathrin, AP-2, intersectin-1, and Eps15 post-permeabilisation **B** Graphs show the percentage co-localisation of extracellular viral particles with clathrin, AP-2, intersectin-1, and Eps15. Error bars represent SEM from 50 particles in 30 cells over three independent experiments. A p value of < 0.001 is indicated by ***.

4.2.6 NPF motifs are required for robust actin tail formation

Having determined that the A36 NPF motifs are essential for the recruitment of clathrin, AP-2, intersectin-1 and Eps15, it was next established how their loss impacts on actin tail formation. Transient transfection of the individual A36 ΔNPF mutants during ΔA36R infection resulted in the formation of long actin tails (Figure 4.4). I next sought to determine to what extent actin tail formation and dynamics were altered following infection with individual and triple A36 ΔNPF recombinant viruses. Structured illumination imaging revealed that AP-2 facilitates the polarisation of A36 beneath the CEV, resulting in a robust N-WASP signalling platform (Humphries et al., 2012). RNAi depletion of AP-2 resulted in a more disperse localisation of A36 and N-WASP beneath the virus. In turn this led to fewer, longer, and faster moving actin tails. (Humphries et al., 2012).

Following 8 hours of infection with the A36 ΔNPF recombinant viruses and WR, HeLa cells were fixed and the number of actin tails induced was quantified from immunofluorescence images (Figure 4.9 A). All viruses resulted in the formation of between 51.5 ± 4.0 to 65.9 ± 4.2 actin tails per cell (Figure 4.9 B). In contrast to the RNAi mediated loss of AP-2, this revealed that there was no significant difference in the ability of the A36 ΔNPF viruses to induce actin tails compared to WR. The A36 ΔNPF recombinant viruses (ΔNPF1, 2, 3, and ΔNPF 1-3) and the A36 1-155 virus however did result in the induction of significantly longer actin tails compared to WR (Figure 4.9 A, C). A36 ΔNPF 1-3 and A36 1-155 lead to the greatest increase in actin tail length, both with an average actin tail length of 4.54 ± 0.03 μm compared to WR (2.65 ± 0.02 μm) (Figure 4.9 C). These actin tail lengths were consistent with those measured following transient transfection of the single A36 ΔNPF mutants in ΔA36R virus infected cells (Figure 4.4).

To determine whether the observed increase in actin tail length also resulted in an increase in actin tail velocity, live cell imaging of infected HeLa cells stably expressing LifeAct-Cherry, was carried out. The speed of actin tails induced 8 hours post infection with the A36 ΔNPF mutants and the A36 1-155 virus was measured and compared to WR. The A36 ΔNPF 1-3 and A36 1-155 viruses induced actin tails that moved at an

average speed of 0.29 ± 0.01 μm/s and 0.31 ± 0.01 μm/s respectively, significantly faster than those induced following WR infection (0.20 μm/s ± 0.01 μm/s) (Figure 4.9 D). There was no change in the velocity of actin tails induced by the individual A36 ΔNPF1, 2, or 3 viruses, despite the increase in actin tail length (Figure 4.4, 4.9 C).

Live-cell imaging in phase contrast allows visualisation of the movement of viral particles undergoing both microtubule-based and actin-based transport during infection. The time taken for the WR virus to nucleate an actin tail, was recorded from the point a viral particle becomes stationary at the cell periphery (indicative of viral fusion after microtubule-based transport) until the initiation of the phase dense structure of the actin tail. During viral egress it has been previously reported that the WR virus takes approximately 30 seconds upon arrival at the plasma membrane to nucleate an actin tail (Humphries et al., 2012). Following RNAi depletion of AP-2 this value increases ~ two-fold (Humphries et al., 2012). Previous experiments have additionally determined that fusion of the virus is not affected by the loss of either AP-2 or clathrin (Humphries et al., 2012). Live-cell imaging was carried out in HeLa cells from 8 hours post infection with WR and A36 ΔNPF 1-3 in order to determine actin tail nucleation dynamics. During infection with the A36 ΔNPF 1-3 virus it takes 67.6 ± 3.4 seconds to nucleate an actin tail, over double that of observed during WR infection (29.9 ± 1.0 seconds) (Figure 4.10). The lifetime of actin tails induced by the A36 ΔNPF 1-3 virus was also reduced to 176.8 ± 14.4 seconds compared to those induced by WR (253 ± 9.3 seconds).

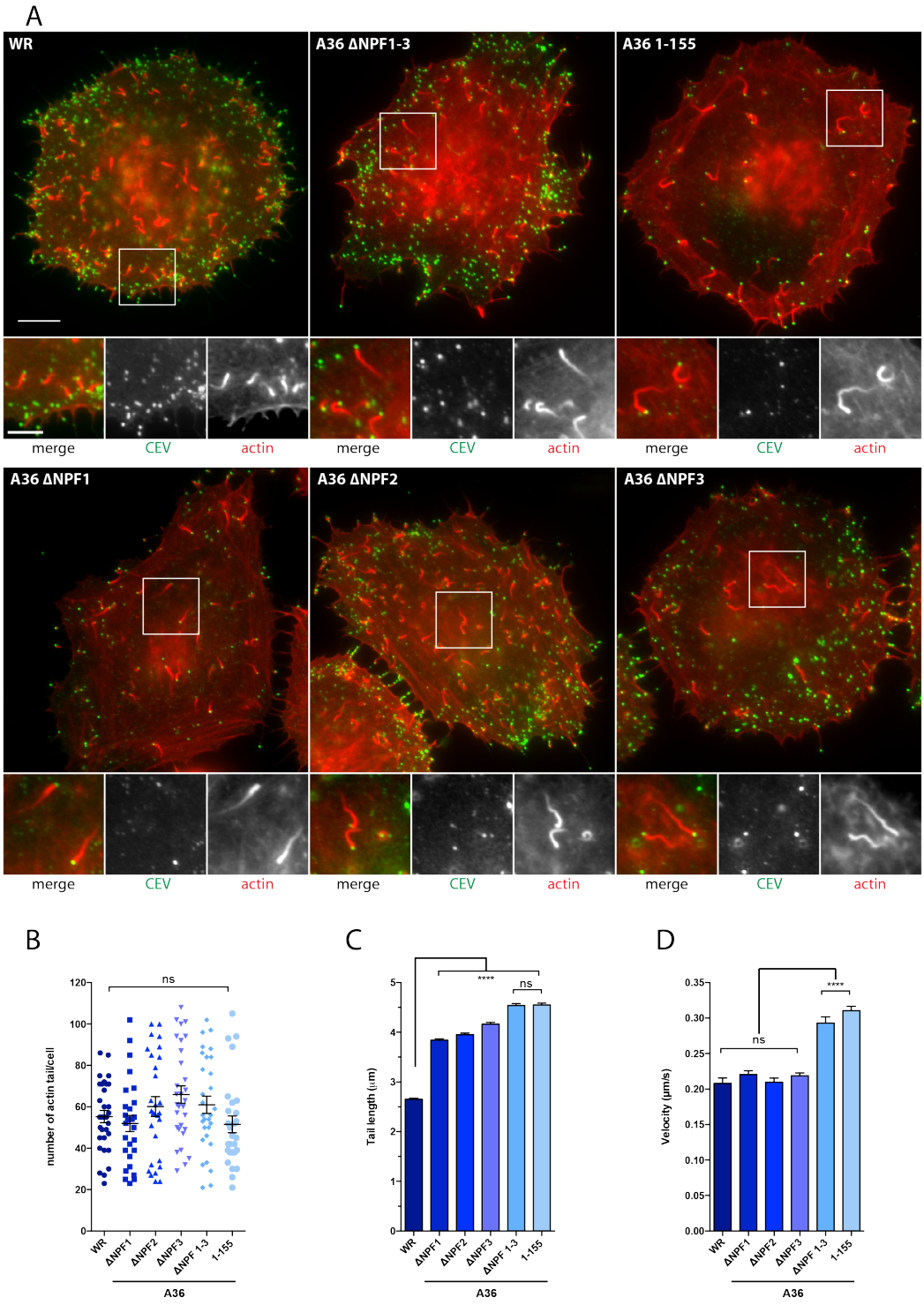

Figure 4.9. Loss of the A36 NPF motifs leads to longer, faster moving actin tails

A Immunofluorescence images of HeLa cells infected with WR, A36 ΔNPF mutant viruses, and A36 1-155 at 8 hpi. Cells were stained with phalloidin and B5 (prior to permeabilization). Scale bar = 10 µm (inset = 5 µm). **B** Quantification of number of actin tails induced per cell. N=30 cells. **C** Quantification of actin tail length. N=400 tails in 60 cells. **D** Quantification of actin tail speed. N=150 tails in 30 cells. Error bars represent SEM over 3 independent experiments in all cases. A p value of <0.0001 is represented by ****. ns indicates a p value > 0.05.

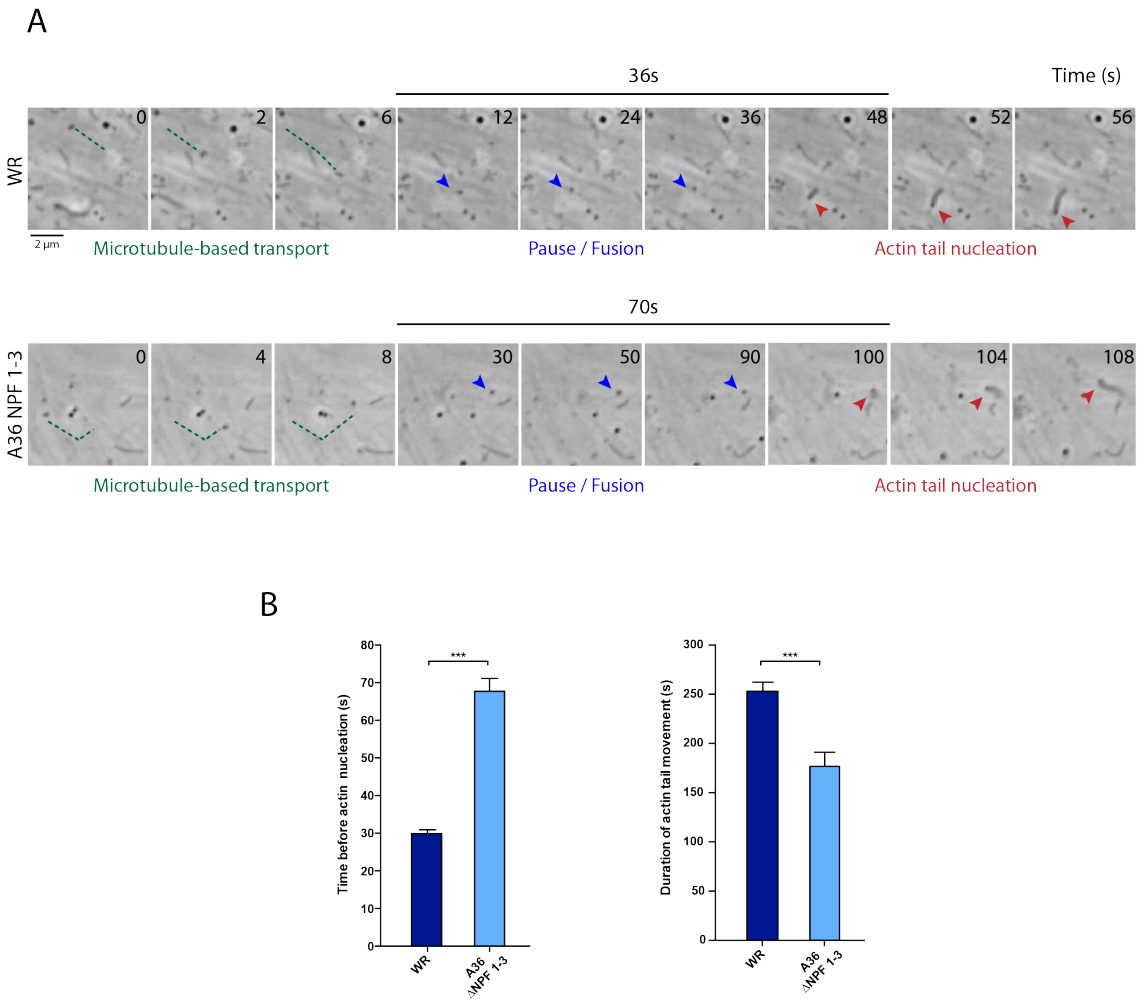

Figure 4.10. Actin tail nucleation is facilitated by the A36 NPF motifs

A Phase contrast images from live-cell imaging of infected cells to visualize the movement of viral particles and subsequent actin tail formation. Microtubule-based motility is detected by a fast linear trajectory (green dashed line). Blue arrows indicate the stationary virus particle. Red arrows show the initiation of actin-based motility. **B** Quantification of the time taken to induce an actin tail once the virus particle becomes stationary in the periphery of the cell (first blue arrow) until the induction of an actin tail (first red arrow). Error bars represent SEM from 60 events in 3 independent experiments in A and B. A p value of < 0.001 is indicated by ***.

4.2.7 Recruitment of N-WASP, WIP, Grb2, and Nck is not NPF dependent

It is clear that the dynamics of the actin tail are significantly altered in vaccinia lacking all three A36 NPF motifs. Previous work has demonstrated the highly dynamic nature of the actin-signalling network beneath the virus (Weisswange et al., 2009). Moreover, this study also highlighted the role that the rate of N-WASP exchange plays in determining the rate of actin tail motility (Weisswange et al., 2009). In order to ascertain whether the changes in actin tail length and speed observed upon infection with A36 ΔNPF 1-3 were as a consequence of an altered recruitment of the actin-signalling complex, recruitment of the core vaccinia actin-signalling complex was investigated in the absence of the A36 NPF motifs. As previously described N-WASP is recruited in complex with WIP, and stabilised beneath the CEV by a network of interactions mediated by Nck and Grb2. Arp2/3 can then be recruited and activated by N-WASP leading to the formation of robust actin tails to promote viral spread. The loss of any one of these components of the vaccinia actin-signalling network results in disruption of the vaccinia actin-signalling network, in the case of Grb2 for example the loss of recruitment results in shorter yet faster moving actin tails (Weisswange et al., 2009).

To determine whether these core components remained present on CEV in the absence of the A36 NPF motifs, HeLa cells were first infected with the A36 ΔNPF 1-3 virus and transfected with GFP-N-WASP, GFP-WIP, GFP-Grb2, and GFP-Nck. Cells were fixed at 8 hours post infection and the ability of vaccinia-induced actin tails to recruit these components was determined via immunofluorescence staining. Interestingly, the localisation of GFP-N-WASP, GFP-WIP, GFP-Grb2, and GFP-Nck to the tips of actin tails was not affected by the loss of the A36 NPF motifs (Figure 4.11). This suggests that it is not the absence of a component of the core actin-signalling network that is responsible for the change in actin tail parameters measured thus far.

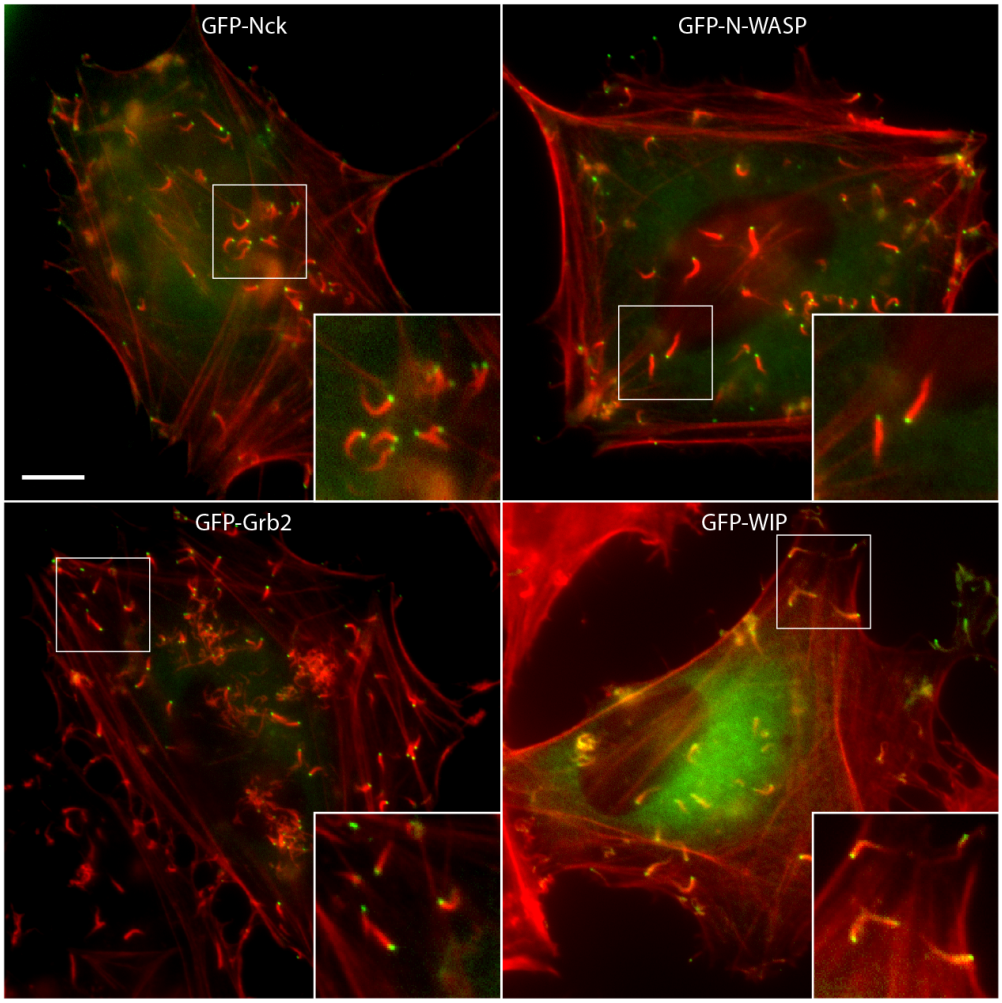

Figure 4.11 A36 ΔNPF 1-3 is able to recruit the core vaccinia actin-signalling network

Representative immunofluorescence images from HeLa cells infected with A36 ΔNPF 1-3 and transfected with GFP-tagged Grb2, Nck, WIP, and N-WASP (green). Nck, N-WASP, Grb2, and WIP can still be recruited to vaccinia induced actin tails in the absence of the A36 NPF motifs. Scale bar = 10 μm.

4.3 Summary

The NPF motifs in vaccinia A36 identified in the previous chapter have a clear functional role during viral egress at the plasma membrane. In this chapter RNAi depletion experiments have shown that the EH domain containing proteins, intersectin-1 and Eps15 act upstream and in the same pathway as AP-2. Depletion of intersectin-1 or Eps15 individually commonly resulted in a decrease in levels of both EH domain containing proteins, in agreement with intersectin-1 constitutively associating with Eps15 to form a complex. The generation of A36 ΔNPF recombinant viruses facilitated closer examination of the significance of the A36 NPF motifs during infection. In contrast to *in vitro* biochemical assays in Chapter 3, during infection all three NPF motifs must be lost to abolish the viral recruitment of clathrin, AP-2, intersectin-1 and Eps15. Intersectin-1 was unable to bind A36 peptides in the absence of NPF3 (Figure 3.6 F). The A36 ΔNPF3 virus is in contrast able to mediate intersectin-1 recruitment during infection (Figure 4.7). This may indicate that Eps15 mediates intersectin-1 binding to A36 ΔNPF3 in this case, or that multiple interactions between all three NPF motifs with both intersectin-1 and Eps15 occur during infection to stabilise recruitment beneath the virus.

Curiously the loss of an individual A36 NPF motif, which remains able to recruit clathrin, AP-2, intersectin-1 and Eps15 to wild type levels in N-WASP -/- cells, resulted in an increase in actin tail length in HeLa cells. It is known that clathrin and AP-2 disassociate from the CEV upon the initiation of actin tails, whereas both intersectin-1 and Eps15 can be recruited to actin tails. (Figure 3.5) (Humphries et al., 2012). The increase in actin tail length induced by the single A36 ΔNPF viruses may suggest that recruitment of intersectin-1 and Eps15 is less stable or abolished following the initiation of actin polymerisation, an avenue that will require future research.

The A36 ΔNPF 1-3 virus lacking all NPF motifs induces longer, faster moving actin tails, that take longer to nucleate and have a shorter lifetime that WR induced actin tails, all in all resulting in a less robust actin tail.

Chapter 5. The role of the A36 NPF motifs during Vaccinia virus spread

5.1 Introduction

A combination of biochemical techniques and a recombinant virus approach has demonstrated that the three NPF motifs in A36 are essential for the recruitment of clathrin, AP-2, Eps15, and intersectin-1 to vaccinia. When these motifs are lost this results in marked defects in N-WASP dependent actin tails. The next key question is how these conserved motifs affect the cell-to-cell spread of vaccinia. Determining the spread of vaccinia through a tissue remains a technical challenge for the virus community. To evaluate viral spread, current research is largely limited to the analysis of viral spread through cultured monolayers. While this allows evaluation of viral plaque size, and is amenable to fixed and live cell imaging, it may not reflect the situation in a tissue. Assessment of the spread of viruses through monolayers, however, remains a useful tool that enables the spatial and temporal analysis of cell-to-cell infection, and has also unveiled novel mechanisms governing how viruses are transmitted from cell-to-cell. The clustering of IEV proteins, actin tail formation, the release of CEVs from the plasma membrane, and the correct entry and fusion of EEVs with neighbouring cells all contribute to efficient viral dissemination (Horsington et al., 2013; Humphries et al., 2012; Payne, 1980; Smith et al., 2003). The loss of any one of these processes results in defective viral spread to some extent.

Deletion of IEV proteins that are required for the both the formation of IEVs and the formation of actin tails universally results in a small plaque phenotype in cell monolayers (Smith and Law, 2004; Smith et al., 2002). The loss of A36 leads to the loss of microtubule-based motility of IEV to the periphery and the induction of actin-tails by CEV. This consequently results in a significant decrease in the size of viral plaques formed in a monolayer of cells and also in a decrease in the release of viral particles (EEV) (Figure 4.5 B) (Parkinson and Smith, 1994; Sanderson et al., 1998; Wolffe et al., 1998). Recent studies have proposed a novel model in which the ability of EEV to induce actin tails on recently infected cells promotes rapid viral spread through a

monolayer (Doceul et al., 2012; Doceul et al., 2010). This super-repulsion of viral particles requires the early expression of A36 and A33 in order to induce actin tails on recently infected cells that are not yet producing infectious viral particles. Actin mediated propulsion of EEVs across these cells is thought to increase the infectious range and plaque size during infection (Doceul et al., 2012; Doceul et al., 2010). Given the importance of A36 in both short and long-range spread of vaccinia EEVs, an interesting question is how the recruitment of AP-2, intersectin-1, and Eps15 via the NPF motifs impacts on viral spread, release, or super-repulsion. RNAi depletion experiments in the previous chapter revealed that the loss of both AP-2 and intersectin-1 resulted in a small plaque phenotype, suggesting that the A36 NPF motifs play a role in viral spread (Figure 4.3).

5.2 Results

5.2.1 A36 NPF motifs promote viral spread

In order to ascertain the affect of the loss of the A36 NPF motifs on viral spread, confluent monolayers of BS-C-1 cells were infected at a low MOI with WR, A36 ΔNPF mutant viruses (ΔNPF1, 2, 3 and ΔNPF1-3) and the truncated A36 1-155 virus. One hour after viral adsorption, media was replaced with a semi-solid carboxy-methyl cellulose overlay in order to limit infection to that mediated by cell-to-cell transmission. Infected monolayers were fixed 48 hours post infection (hpi) and stained with crystal violet to reveal viral plaques (Figure 5.1 A). The diameter of viral plaques was subsequently measured.

Plaques formed by the single A36 ΔNPF mutant viruses had a small but not statistically significant decrease in plaque diameter compared to WR (Figure 5.1 A, B). Infection with the A36 ΔNPF 1-3 and A36 1-155 viruses, however, resulted in a significantly smaller plaque compared to that of WR. On average WR plaques were 1.22 ± 0.04 mm in diameter, whereas plaques formed by A36 ΔNPF 1-3 and A36 1-155 were almost half the size (0.72 ± 0.05 mm and 0.70 ± 0.04 mm respectively) (Figure 5.1). The ΔA36R virus led to the formation of even smaller plaques (0.23 mm ± 0.01 mm). Although ΔA36R can still produce IEV particles, the loss of A36-mediated microtubule

transport to the periphery results in a severe defect in viral spread in agreement with earlier studies (Dodding et al., 2011; Parkinson and Smith, 1994; Rietdorf et al., 2001). This data shows that the loss of all three NPF motifs significantly impacts on viral spread, and that there are no additional factors in the C-terminus of A36 (residues 156-221), that contribute to viral cell-to-cell spread.

A recombinant virus has been previously engineered to express the Yaba-like disease virus YL126 protein in place of A36 in vaccinia virus (Dodding and Way, 2009). The WR-ΔA36R-YL126R virus has been shown to recruit the actin-signalling complex and induce actin tail formation in the absence of A36 (Dodding and Way, 2009). YL126 as indicated earlier in this thesis, does not contain any NPF motifs and is unable to recruit clathrin, AP-2, intersectin-1, or Eps15 to the virus during egress (Figure 3.7, Figure 4.8). I therefore sought to determine how the cell-to-cell spread of WR-ΔA36R-YL126R compared to that of A36 ΔNPF 1-3.

After 48 hours of infection in a confluent monolayer of BS-C-1 cells, WR and the A36 ΔNPF 1-3 virus formed plaques that were 1.43 ± 0.02 mm and 0.88 ± 0.02 mm in diameter respectively, in agreement earlier observations (Figure 5.2 A, B). Plaques formed by WR-ΔA36R-YL126R were even smaller, averaging at 0.52 ± 0.01 mm in diameter (Figure 5.2 A, B). WR-ΔA36R-YL126R however did result in a rescue in plaque size compared that that observed in ΔA36R (Figure 5.1, 5.2). The decrease in WR-ΔA36R-YL126R plaque size is in agreement with the lack of NPF motifs in YL126. Therefore like A36 ΔNPF 1-3, WR-ΔA36R-YL126R results in diminished cell-to-cell spread compared to WR expressing wild type A36. The additional decrease in plaque size observed between vaccinia expressing YLDV126R verses A36 ΔNPF 1-3 is likely to be due to intrinsic differences in the organisation of the YL126 actin-signalling complex. In support of this, previous work has shown that YL126 induced actin tails are less robust and more chaotic in their directionality compared to A36 (Dodding and Way, 2009). Differences between WR-ΔA36R-YL126R and A36 ΔNPF 1-3 may also be due to altered intermolecular interactions between the vaccinia IEV proteins, which may impact on both viral assembly and spread. Although A36 is not directly required for IEV formation, substituting A36 for YL126 may impact on viral assembly due to

altered interactions with other IEV proteins that are required for viral assembly such as A34, B5 or F13 (Rottger et al., 1999). Together these experiments further support the advantage of NPF motifs to promote viral spread. Although not conserved among the *Orthopoxvirus* A36 orthologues as a whole, the NPF motifs may confer a host or cell specific advantage amongst the poxvirus family.

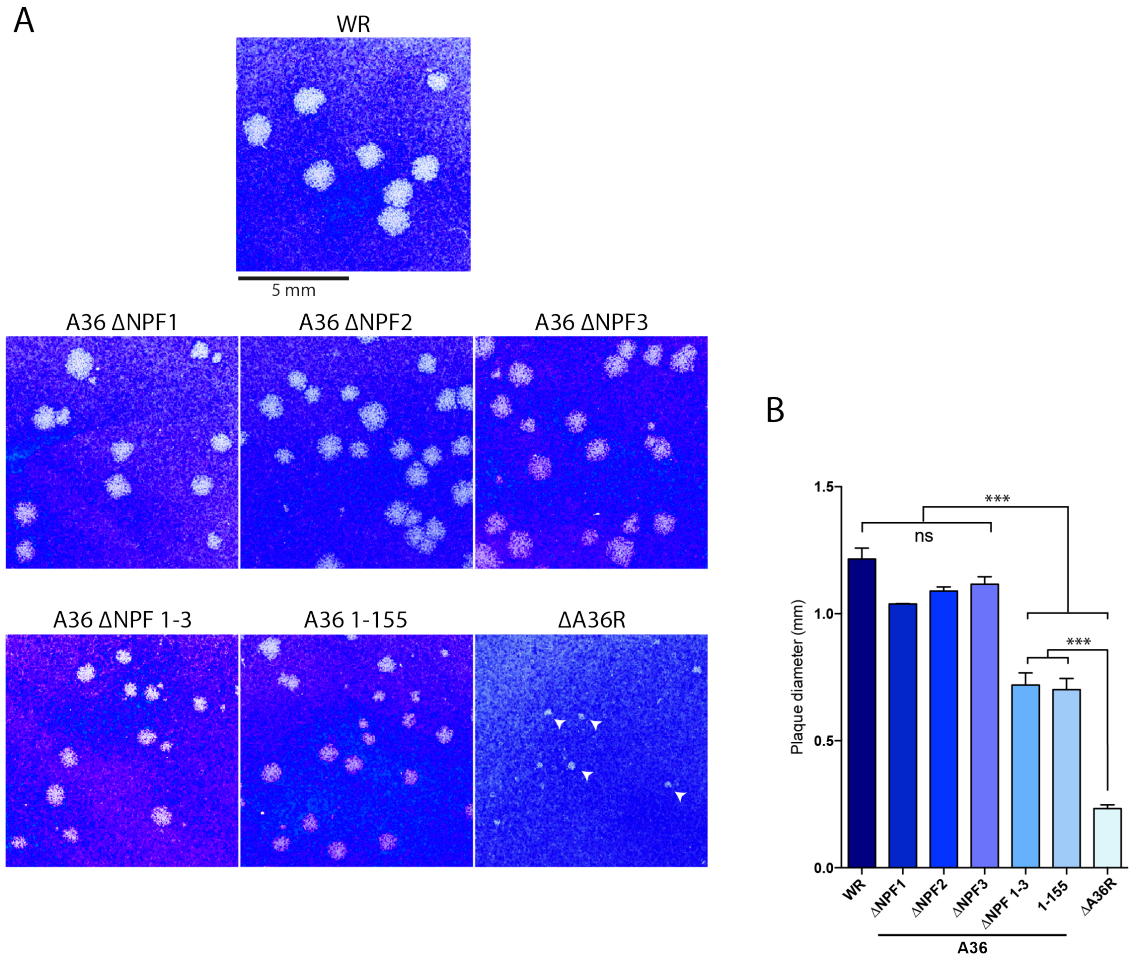

Figure 5.1 The A36 NPF motifs promote viral spread

A Representative images of viral plaques produced by the indicated viruses in confluent BS-C-1 cells revealed by staining with crystal violet 48 hpi. **B** Graph shows quantification of plaque diameters produced by the indicated viruses. Error bars represent SEM from N = 100 plaques in 3 independent experiments. A p value of < 0.001 is indicated by ***. ns indicates a p value > 0.05.

A

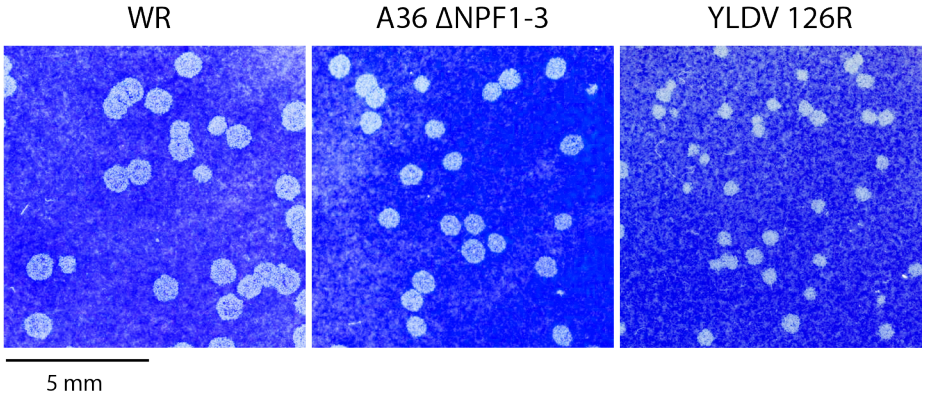

B

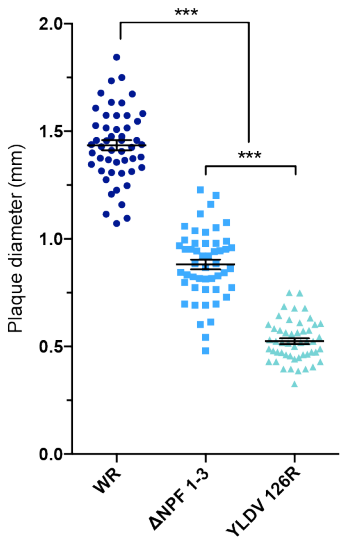

Figure 5.2 The A36 ΔNPF 1-3 and YL126R viruses are deficient in viral spread

A Representative images of viral plaques produced by the indicated viruses in confluent BS-C-1 cells revealed by staining with crystal violet 48 hpi. **B** Graph shows quantification of plaque diameters produced by the indicated viruses. Error bars represent SEM from N = 60 plaques in 3 independent experiments. A p value of < 0.001 is indicated by ***.

5.2.2 A36 NPF motifs promote viral release

A key aspect of viral spread is the ability of EEV to be released from infected cells (Horsington et al., 2013). The amount of EEVs produced from infected cells was therefore quantified in order to determine whether a release defect might contribute to the decrease in plaque size observed following infection with A36 ΔNPF 1-3. Monolayers of BS-C-1 cells were infected with WR and A36 ΔNPF 1-3 at a low multiplicity of infection (MOI = 0.1). In order to quantify EEV numbers, media was collected from infected cells at 16 hpi and infected cells were collected separately to determine the amount of cell-associated virus (IMVs, IEVs, and CEVs) produced. Both EEV fractions and cell-associated virus fractions were quantified by plaque assay titration on monolayers of BS-C-1 cells. Cells were fixed 48 hpi and stained with crystal violet to visualise the number of plaques formed, and therefore determine the number of viral particles produced (pfu/ml). The total cell-associated virus did not differ following infection with WR or A36 ΔNPF 1-3 in agreement with initial growth curves (Figure 4.6 B) (Figure 5.3 A). Both WR and A36 ΔNPF 1-3 led to the production of around 2 x 10^5 infectious particles (IMVs, IEVs, and CEVs) after 16 hours of infection. Infection of BS-C-1 cells with WR lead to the release of 664 EEV/ml. In contrast, A36 ΔNPF 1-3 led to a four-fold decrease in the number of EEV released (149 EEV/ml) (Figure 5.3 B).

A time course of EEV release was carried out in order to assess the dynamics of EEV release between WR and the A36 ΔNPF 1-3 virus. Viral proteins are recycled from the plasma membrane to the TGN in order to facilitate the continuous generation of new IEV and EEV, therefore I sought to determine whether A36 ΔNPF 1-3 EEV were continually released over time, or were stalled due to a recycling defect. As in the previous experiment, confluent BS-C-1 cells were infected with WR and A36 ΔNPF 1-3 at an MOI = 0.1. Supernatants were collected every hour for 16 hours and the numbers of EEVs released were quantified following titration on confluent BS-C-1 monolayers. The amount of EEV released by both viruses increases over time, however, in the case of A36 ΔNPF 1-3 virus this increase is significantly delayed compared to WR (Figure 5.3 C). Taken together this data suggests that the decrease in plaque size observed in the absence of the A36 NPF motifs is due to a significant defect in the release of EEV from the plasma membrane, and is not indicative of a recycling defect.

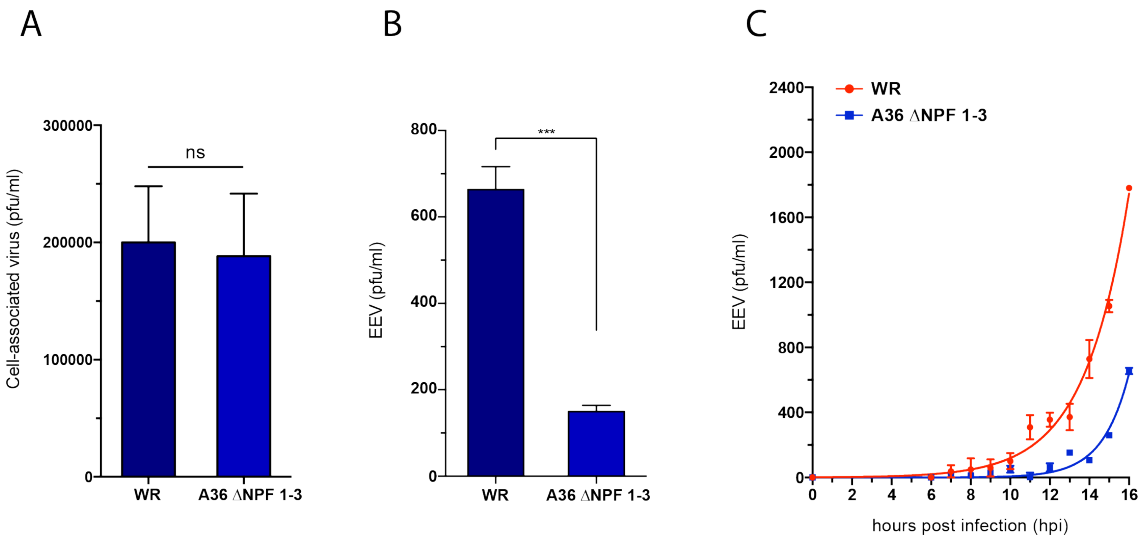

Figure 5.3 The A36 NPF 1-3 virus is deficient in EEV release

A Quantification of the number of cell-associated virus particles at 16 hpi following the infection of BS-C-1 cells with WR or A36 ΔNPF 1-3 viruses. The number of cell-associated virus particles was determined by plaque assay in duplicate on BS-C-1 monolayers. At 48 hpi plaques were fixed, stained with crystal violet, and enumerated. **B** Quantification of the number of EEV released into 1 ml of supernatant at 16 hpi following the infection of BS-C-1 cells with WR or A36 ΔNPF 1-3 viruses. The number of EEVs released was determined by plaque assay as above. **C** Time course of EEV release was determined as above, however, supernatants were collected every hour post infection. Error bars represent SEM over 3 independent experiments. All release assays were carried out in triplicate per experiment. A p value of < 0.001 is indicated by ***. ns indicates a p value > 0.05.

5.2.3 The role of the A36 NPF motifs during vaccinia super-repulsion

Following EEV release viral particles must reach a neighbouring cell in order for infection to progress. Once on the plasma membrane of an adjacent cell the EEV may directly infect this cell. However, if an adjacent cell is already infected, reinfection is inhibited by the presence of the early viral A56-K2 complex present on the plasma membrane, in process termed superinfection exclusion (Laliberte and Moss, 2014; Wagenaar and Moss, 2009). The early expression of the viral proteins A36 and A33 in newly infected cells is however sufficient for EEV to induce an actin tail and be propelled to a non-infected cell (Doceul et al., 2010). This allows vaccinia to spread and infect cells distal from the initial site of infection four-fold faster than would be predicted from the rate of vaccinia virus replication alone (Figure 5.4).

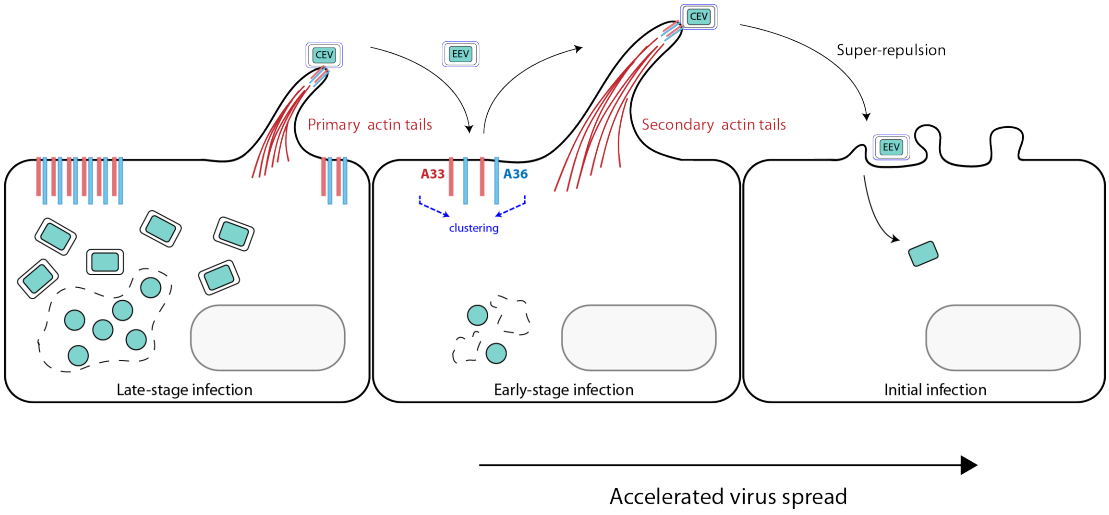

Figure 5.4 Does A36 clustering enhance accelerated viral spread?

A36 and A33 mediate both primary and secondary actin tail formation in order to enhance viral spread via super-repulsion. The role of the A36 NPF motifs to facilitate clustering of viral proteins and mediate super-repulsion in newly infected cells was investigated.

Given the essential role of A36 in actin tail formation, I next investigated the role of the NPF motifs in the formation of actin tails during super-repulsion. In order to do this a similar approach was utilised as in Doceul et al 2010. The natural promoter of the A36R gene induces A36 expression both early and late during infection (Figure 4.6) (Parkinson and Smith, 1994). To separate the early and late expression of A36 during infection, a recombinant virus was generated that expressed A36 solely under a late promoter. Following infection with this virus, recently infected cells are unable to express A36. Therefore upon arrival at the plasma membrane of these cells, EEVs are incapable of inducing secondary actin tails, thus decreasing overall viral spread (Doceul et al., 2010).

In order to generate a virus expressing A36 under a late promoter, WR-ΔA36R was used as the viral backbone. A synthetic late promoter (4b) was synthesised and ligated to the 5' end of the A36R coding region of both wild type and ΔNPF 1-3 A36 (Figure 5.5). This 4b-A36R construct was subcloned into a plasmid containing the right and left arms of homology of the vaccinia thymidine kinase (TK) locus (Chakrabarti et al., 1997). The A36 ΔNPF recombinants generated in the previous chapter were inserted into the endogenous A36R locus, upstream of which contains the endogenous early-late viral promoter. In order to limit A36R expression to late alone, the TK locus was used as an insertion site, as in Doceul et al 2010. Vaccinia thymidine kinase is non-essential, and is expressed during the first 4 hours post infection, after which it is subsequently switched off by a number of viral proteins in a translational repression mechanism (Byrd and Hruby, 2004). Vaccinia strains lacking thymidine kinase have, however, been shown to be less virulent in mice (Buller et al., 1985). The vector consisting of the TK locus homology arms and 4b-A36R (TK_{LA}-4b-A36R-TK_{RA}) was transfected into ΔA36R infected HeLa cells in order to generate recombinants by homologous recombination as described in the previous chapter (Figure 5.5 A). Recombinants were selected by the rescue in plaque size compared to the ΔA36R virus and purified over four rounds of selection (Figure 5.5 B). Viruses expressing A36 wild type or A36 ΔNPF 1-3 under the late 4b promoter will subsequently be referred to as $A36^{late}$ and ΔNPF^{late} respectively.

In order to confirm that expression of A36 was solely under the control of the 4b late promoter a time course was carried out to determine the temporal expression pattern of A36. HeLa cells were infected with an equal MOI of the WR, $A36^{late}$, and ΔNPF^{late} viruses. Lysates were collected every hour post infection and A36 expression assessed by immunoblot analysis. As observed previously, following infection with WR and A36 ΔNPF 1-3, expression of A36 commenced at 1-2 hpi (Figure 4.6 A). In contrast, expression of A36 from $A36^{late}$ and ΔNPF^{late} viruses only began from 7 hpi (Figure 5.6). To confirm late expression of A36, infected cells were also treated with arabinosyl cytosine (AraC). AraC, is a well-characterised inhibitor of DNA synthesis, and during vaccinia infection only permits early gene expression to proceed (Taddie and Traktman, 1993). HeLa cells were treated 1 hour prior to infection with 50 μm/ml of AraC that was maintained throughout infection. HeLa cells were infected with WR, $A36^{late}$ and ΔNPF^{late} viruses in the presence or absence of AraC and cell lysates processed for immunoblot analysis after 12 hpi. A36 is present in WR infected cells with and without AraC treatment, indicating that A36 is expressed both early and late during infection (Figure 5.6). However, following infection with the $A36^{late}$ and ΔNPF^{late} viruses, the presence of AraC prevented expression of A36, indicating that there is no early component of A36 expression, and confirming that expression of A36 in these viruses is solely under the control of a late promoter (Figure 5.6).

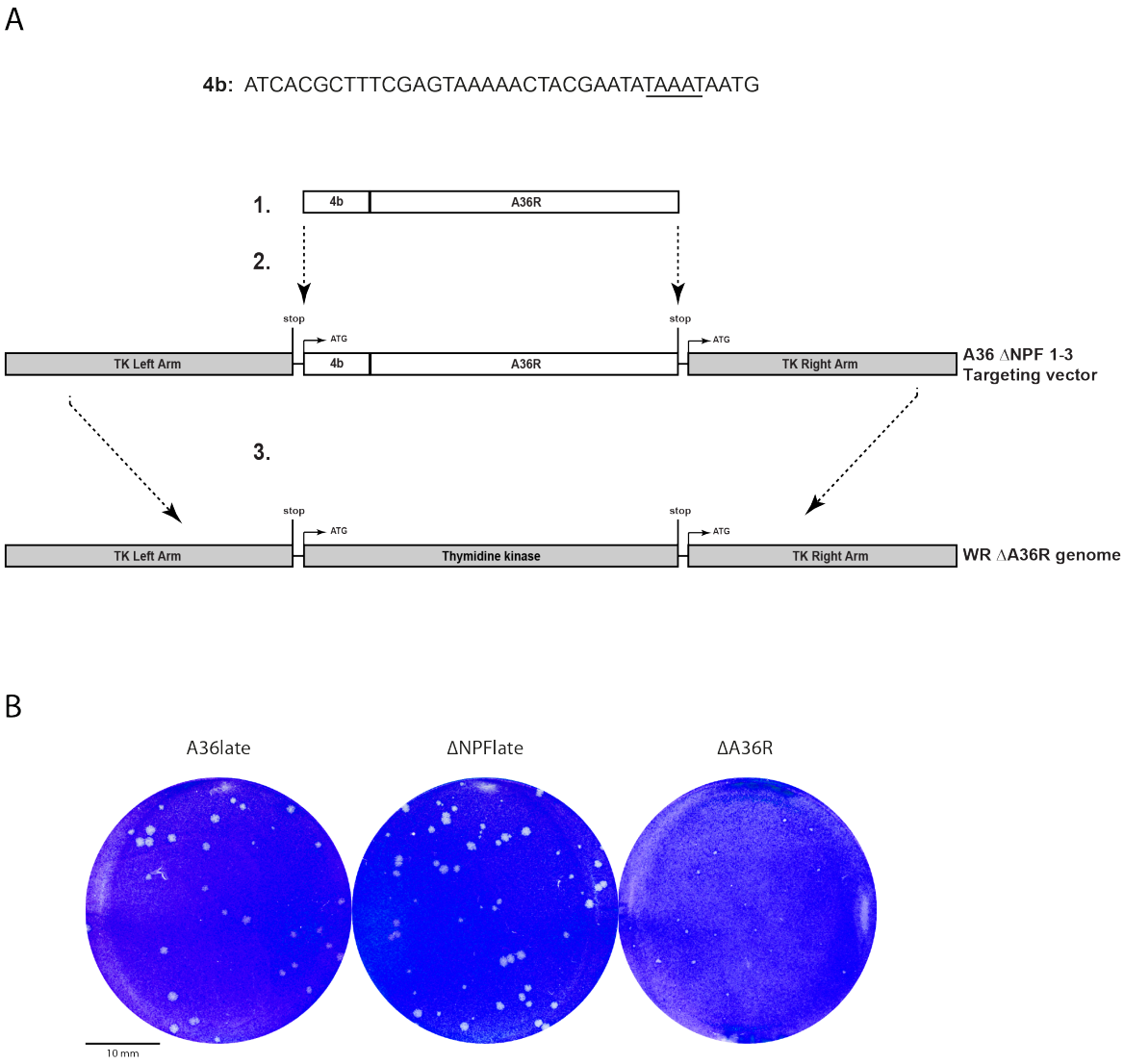

Figure 5.5 Generation of A36 wild type and ΔNPF 1-3 under a late promoter

A The sequence of the 4b promoter used is shown, with the 'late' elements underscored. Schematic detailing the cloning steps taken to generate the late A36 targeting vector. 1. 4b was ligated with full length A36R. 2. 4b-A36R was subcloned into restriction sites flanked by the left and right homology arms of the thymidine kinase gene locus. 3. This was used as the targeting vector in ΔA36R infected HeLa cells. **B** Plaques depicting the rescue in plaque size above that of ΔA36R used to select positive recombinants.

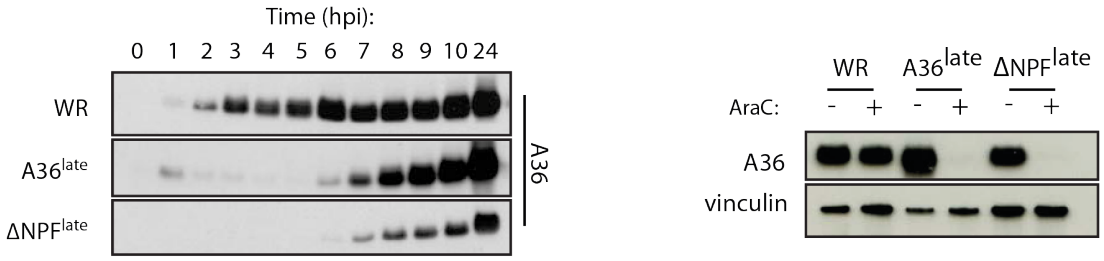

Figure 5.6. Characterisation of the A36^{late} and the ΔNPF^{late} viruses

Immunoblot showing the expression of A36 in cells infected with late A36 viruses compared to WR. AraC treatment of infected HeLa cells blocks expression of late A36 but not A36 expression early during infection. Vinculin is shown as a cellular loading control.

In order to confirm the published defect in viral spread upon late expression of A36, I measured the size of plaques formed in BS-C-1 monolayers following infection with A36^{late} compared to WR at 48 hpi. In agreement with Doceul et al, plaques formed by the A36^{late} virus were significantly smaller than WR (0.61 ± 0.03 mm and 1.21 ± 0.04 mm respectively) (Figure 5.7 A, B). As observed in Chapter 4 expression of A36 ΔNPF 1-3 under the endogenous A36 promoter, led to smaller plaques than those induced by WR (0.71 ± 0.04 mm and 1.21 ± 0.04 mm respectively). Interestingly, there was no significant difference in plaque size between A36 ΔNPF 1-3 under its endogenous promoter compared to wild type A36 expressed under the late promoter (A36^{late}). To determine whether the presence of the A36 NPF motifs contributes to a further decrease in spread when A36 is expressed late during infection, the plaques formed by ΔNPF^{late} viruses were also measured. ΔNPF^{late} also induced smaller plaques than WR, however, these were the same size as both A36 ΔNPF 1-3 and A36^{late} (0.61 ± 0.03 mm) (Figure 5.7 A, B). The loss of the NPF motifs when A36 is expressed late in infection does not result in a further decrease in plaque size, suggesting that the NPF motifs do not contribute to super-repulsion.

A

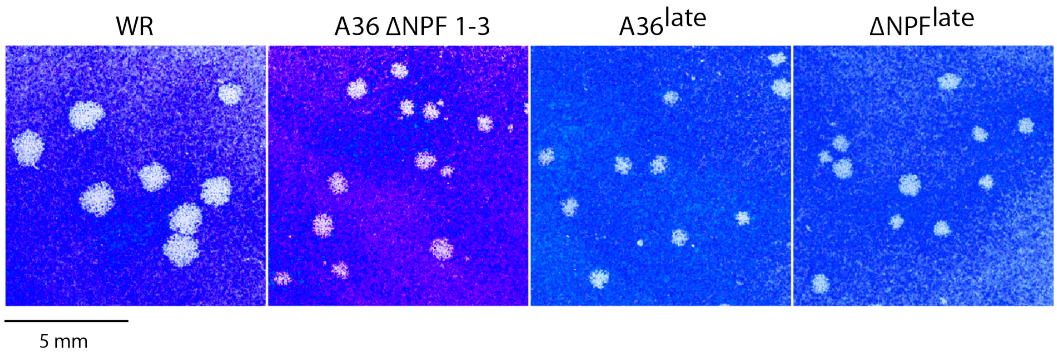

B

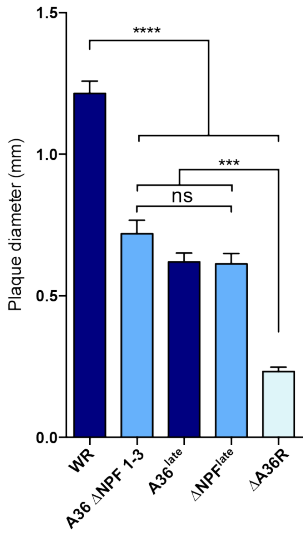

Figure 5.7 The A36^{late} and ΔNPF^{late} viruses are equally deficient in viral spread

A Representative images of viral plaques produced by the indicated viruses in confluent BS-C-1 cells revealed by staining with crystal violet 48 hpi. Scale bar = 5 mm. **B** Graph shows quantification of plaque diameters produced by the indicated viruses. Error bars represent SEM from N = 100 plaques from 3 independent experiments. A p value of < 0.0001 is indicated by ****. A p value of < 0.001 is indicated by ***. ns indicates a p value > 0.05.

I next investigated whether there was a decrease in EEV release at 16 hpi between the A36^{late} and ΔNPF^{late} viruses, as is the case following A36 ΔNPF1-3 infection (Figure 5.3). A36 ΔNPF1-3, A36^{late}, and ΔNPF^{late} all exhibited a significant defect in EEV release, with all three A36 recombinant viruses releasing a quarter of the number of EEVs than WR (Figure 5.8 A). This raises several interesting questions regarding super-repulsion. This data suggests that the plaque size defect observed following infection with the late A36 viruses is largely due to the production of significantly fewer EEVs compared to WR. This implies that while the ability to propel EEV along recently infected cells via early expression of A36 may contribute to viral spread through a monolayer, it may not have as great a contribution as previously suggested.

To examine the process of super-repulsion more closely, I assessed the ability or lack thereof of vaccinia to produce secondary actin tails in cells in the early hours of infection. A time course of infection was carried out in order to determine the optimal time point at which to visualise secondary actin tails by immunofluorescence imaging. Monolayers of BS-C-1 cells fixed at 10-12 hpi resulted in a cluster of 1-2 heavily infected cells surrounded by newly infected cells. The late stage of viral infection was determined based on several criteria such the presence of a large well established viral DNA factory, and a large number of viral particles in the cell periphery. Newly infected cells were classified based on the absence of viral particles, and the lack of a viral DNA factory. In addition plaques were stained for the early viral protein I3, which localises to initial sites of viral replication that precede the formation of the viral factory (Rochester and Traktman, 1998; Welsch et al., 2003). As the number of EEV in contact with neighbouring recently infected cells would directly impact on the ability to induce an actin tail, the ability of viruses to induce secondary actin tails was therefore quantified as a percentage of EEV in contact with neighbouring cells. Although initial quantification suggested a decrease in the ability of A36 ΔNPF 1-3 virus to induce secondary actin tails to the same extent as that of both A36^{late} and ΔNPF^{late}, this was consequently found not to be the case when quantified in a double-blind experiment to eliminate human bias.

The quantification of secondary actin tails proved challenging due to the rarity of such events. The total number of secondary actin tails observed on recently infected cells was extremely low and in the range of 0-10. Analysis of super-repulsion was also complicated by the fact that the morphology of secondary actin tails induced during super-repulsion differed from those produced during primary infection. Secondary actin tails were less uniform, and often punctate or elongated in appearance (Figure 5.8 B). Only actin structures that were distinct from cellular actin staining and resembled an actin tail (albeit long or short) were counted. In addition, it could not always be determined from which cell actin tail-like structures originated, further complicating analysis.

Unbiased experiments which were scored double-blind, were unable to detect a significant difference in the ability of the WR and A36 ΔNPF 1-3 viruses to induce secondary actin tails on recently infected cells (Figure 5.8 B, C). In WR and A36 ΔNPF 1-3 infected BS-C-1 cells approximately 5% of EEVs in contact with recently infected cells were observed to induce an actin tail-like structure. Both $A36^{late}$ and ΔNPF^{late} did exhibit a decrease in the number of secondary actin tails compared to WR and A36 ΔNPF 1-3, although there was no significant difference between the two late A36 viruses (Figure 5.8 C). It is worth noting that on average 1% of both $A36^{late}$ and ΔNPF^{late} EEVs were determined to produce secondary actin tails. As earlier work has shown the requirement of early A36 expression for this process, it can be presumed this 1% represents error in detection of actin tails. This error margin is most likely derived from actin tails counted on the surface of recently infected cells, which are in fact a result of actin tails projecting from the adjacent heavily infected cell. Given the significant challenge in the identification of secondary actin tails, the role of the A36 NPF motifs during this process remains an open question. If correct however, this preliminary analysis would suggest that the A36 NPF motifs do not play an active role in the ability to nucleate actin tails on recently infected cells. Further analysis must be carried out to validate the contribution of this mechanism of spread. Infection with a virus unable to induce the formation of primary actin tails (A36 YdF) would more clearly determine whether the actin structures observed in this analysis were a result of active viral recruitment of the actin-signalling network.

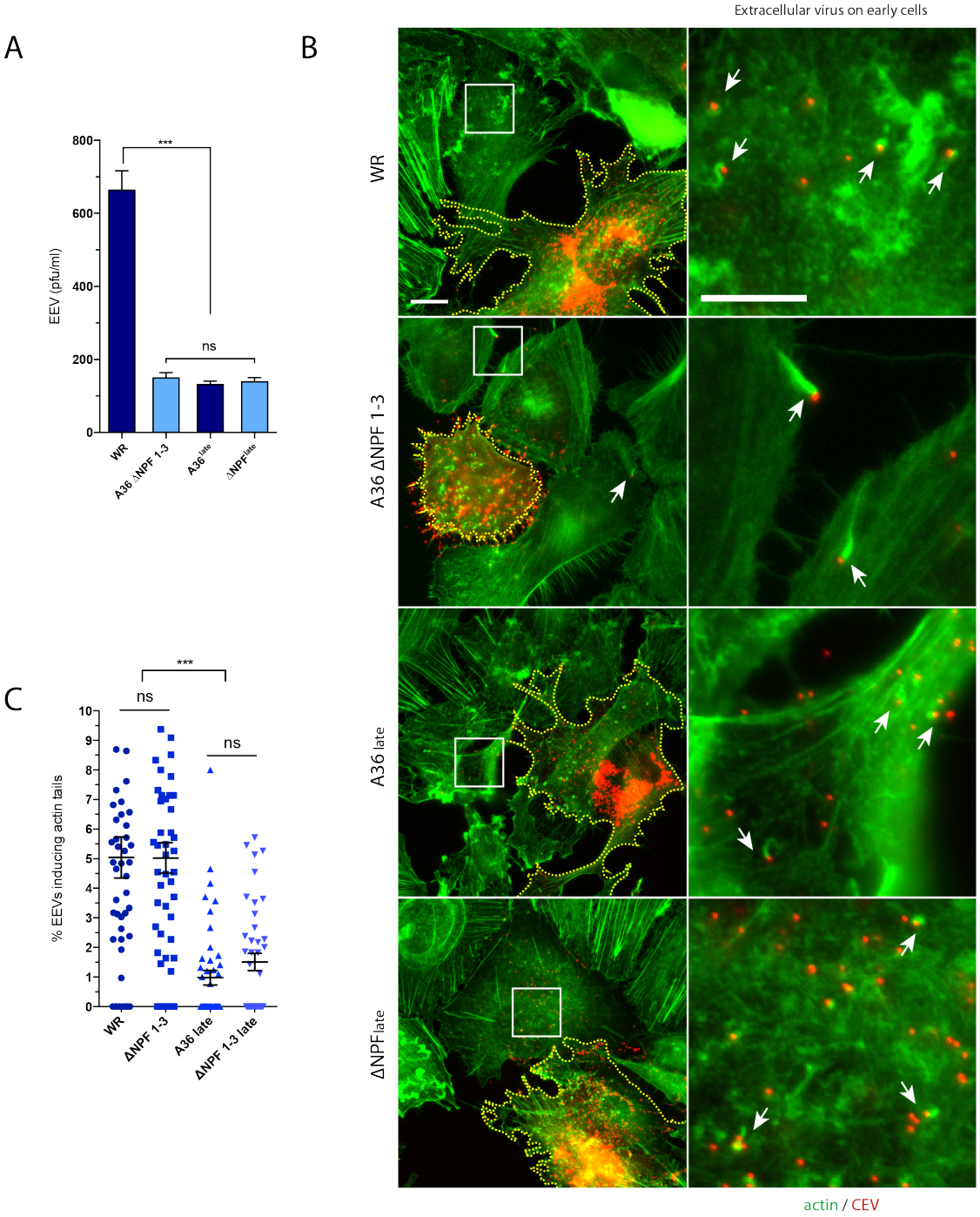

Figure 5.8 Do A36 NPF motifs contribute to super-repulsion?

A The EEV release of late A36 viruses compared to WR and A36 ΔNPF 1-3. EEV were quantified per ml of supernatant at 16 hpi as previously described. Error bars represent SEM over 3 independent experiments. **B** Representative images of monolayers of infected BS-C-1 cells fixed at 12 hpi. Cells were stained with B5 and phalloidin to visualize EEV and actin tails respectively. A dashed yellow line designates heavily infected cells producing EEV. Scale bar = 20 µm. Secondary actin tails on recently infected cells are inset and indicated by white arrows. Scale bar = 10 µm. **C** Quantification of the percentage of EEV inducing secondary actin tails. Error bars represent SEM of N = 60 cells in 3 independent experiments. A p value of < 0.001 is indicated by ***. ns indicates a p value > 0.05.

5.2.4 A36 NPF motifs are required for Cdc42 recruitment

Despite an uncharacterised role during the process of super-repulsion mediated spread, it is clear that the presence of the A36 NPF motifs results in enhanced viral spread through a monolayer of cells, and the ability to release greater numbers of EEV. In Chapters 3 and 4 it was shown that the A36 NPF motifs are required to bind and recruit intersectin-1. In addition RNAi depletion experiments determined that intersectin-1 (along with Eps15) are required to mediate AP-2 recruitment to CEV. Intersectin-1 has been recently shown to promote actin tail formation via its activation of Cdc42 (Humphries et al., 2014). However the mechanism of intersectin-1 and Cdc42 recruitment to vaccinia had not been investigated up to this point. I therefore investigated the role of the A36 NPF motifs during Cdc42 recruitment and whether this facilitates viral spread and release.

To explore whether the recruitment of Cdc42 was dependent on the A36 NPF motifs, HeLa cells were infected with WR or the A36 ΔNPF 1-3 virus, subsequently transfected with GFP-Cdc42, and processed for immunofluorescence at 8 hpi. In contrast to the recruitment of N-WASP observed in Chapter 4, GFP-Cdc42 localises to WR but not the A36 ΔNPF 1-3 virus (Figure 5.9). This confirms that in addition to recruiting AP-2 prior to actin tail formation, intersectin-1 is also required for the localisation of Cdc42 on the virus during egress (Humphries et al., 2014). Intersectin-1 must therefore play a crucial role in both the polarisation of A36 and N-WASP (via AP-2) and N-WASP activation (via Cdc42).

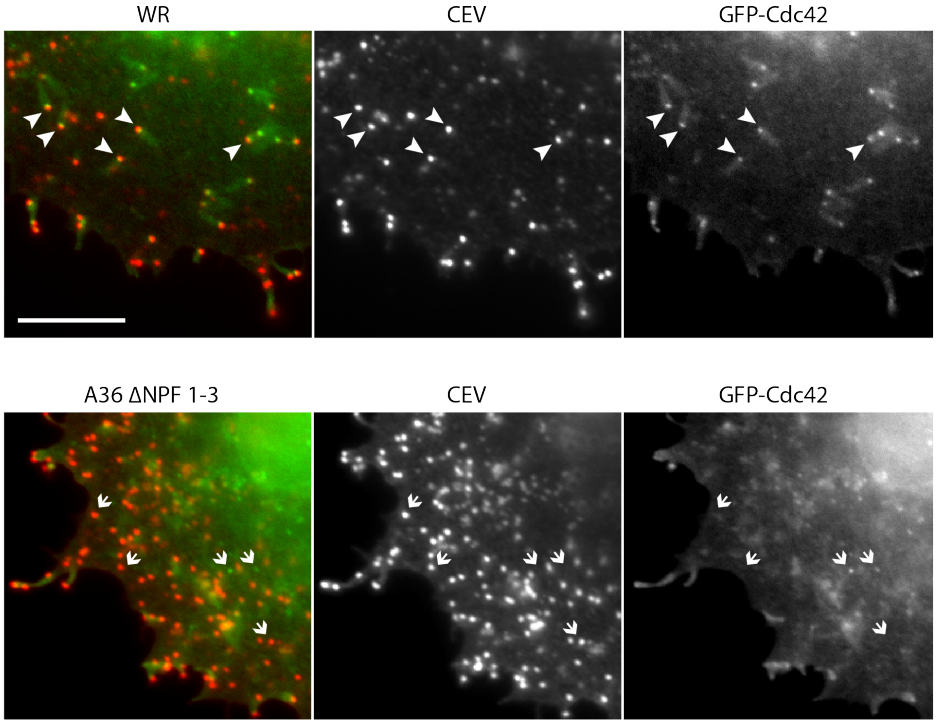

Figure 5.9 A36 NPF motifs are required to recruit Cdc42

Representative immunofluorescence images of HeLa cells expressing GFP-Cdc42 and infected with WR and A36 ΔNPF 1-3 respectively. CEV were stained with B5 antibody prior to permeabilization (white arrows). Scale bars = 10 μm.

To probe the effect of the loss of Cdc42 recruitment to the virus, mouse embryo fibroblasts from N-WASP -/- mice were used that stably express GFP-N-WASP or the GFP-N-WASP H208D mutant that lacks the ability to bind activated Cdc42 (Humphries et al., 2014; Miki et al., 1998; Moreau et al., 2000). The loss of Cdc42 binding to N-WASP H208D was confirmed by GFP-Trap pull-down assays (Figure 5.10). MEFs stably expressing GFP-N-WASP or GFP-N-WASP H208D were transfected with GST-Cdc42 and infected with either WR or A36 ΔNPF 1-3. GFP-Trap pull-downs were carried out from infected cell lysates and analysed by immunoblot. Wild type N-WASP was able to bind GST-Cdc42 and in agreement with published data, the N-WASP H208D mutant was unable to associate with Cdc42 (Figure 5.10) (Humphries et al., 2014; Miki et al., 1998; Moreau et al., 2000). Curiously, while wild type N-WASP could also pull down A36 during infection with WR, the H208D mutant was unable to bind A36. Previous work has established that the N-WASP H208D mutant can still be recruited to CEV at the plasma membrane, although it has an increased turnover rate (Humphries et al., 2014). N-WASP H208D forms a less stable actin-signalling complex

beneath the CEV, which may explain why binding of N-WASP H208D and A36 is not observed in this assay (Humphries et al., 2014). Similarly, A36 ΔNPF 1-3 is unable to associate with either wild type N-WASP or the H208D mutant, despite the fact that N-WASP is detected on virus particles 8 hpi with A36 ΔNPF 1-3 (Figure 4.11). Together this suggests less robust N-WASP recruitment in the absence of the NPF motifs.

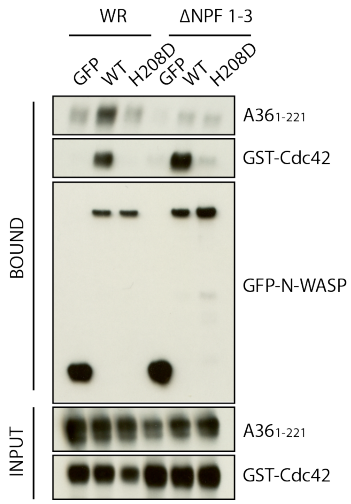

Figure 5.10 N-WASP cannot form a stable complex with A36 ΔNPF 1-3

Immunoblot analysis of GFP-Trap pull-downs performed on N-WASP -/- MEFs infected with WR and A36 ΔNPF 1-3 viruses. MEFs expressing the indicated GFP-N-WASP constructs were transfected with GST-Cdc42. Binding of endogenous A36 or A36 ΔNPF 1-3 expressed during the course of infection is indicated by $A36_{1-221}$.

5.2.5 Distinguishing the duel roles of intersectin-1

Intersectin-1 clearly plays two roles; I therefore sought to address the relative contributions of AP-2 recruitment and N-WASP activation during viral spread and release. The role that the A36 NPF motifs play in viral spread was examined in the absence of Cdc42-mediated activation of N-WASP by taking advantage of N-WASP -/- MEFs expressing GFP-N-WASP-H208D (hereon referred to as NW-H208D). The diameter of WR and A36 ΔNPF 1-3 plaques in confluent monolayers of N-WASP wild type (NW-WT), H208D (NW-H208D), and null (-/-) cell lines were measured. Plaques were visualized by staining with anti-B5 antibody (Figure 5.11 A). In agreement with plaque assays carried out in BS-C-1 cells, infection of NW-WT cells with A36 ΔNPF 1-3, resulted in a significant decrease in plaque diameter at 48 hpi compared to WR

infection (0.92 ± 0.02 mm and 1.18 ± 0.02 mm respectively) (Figure 5.11 B). Infection of WR in NW-H208D cells also results in significantly smaller plaques than in NW-WT cells (0.95 ± 0.02 mm and 1.18 ± 0.02 mm respectively) (Figure 5.11 B). Infection of NW-H208D cells with the A36 ΔNPF 1-3 virus led to an addition decrease, with viral plaques averaging 0.78 ± 0.01 mm in diameter.

During infection with WR, the decrease in plaque size between NW-WT and NW-H208D cells results due to the loss of the ability Cdc42 to bind and locally activate N-WASP H208D beneath the virus (Figure 5.11 D) (Humphries et al., 2014). Plaques induced by WR in NW-H208D cells and those induced by A36 ΔNPF 1-3 in NW-WT cell lines have an equivalent decrease in plaque size. This confirms that intersectin-1 recruitment (via the A36 NPF motifs) is required to recruit and locally activate Cdc42 (Figure 5.11 D). This in turn results in N-WASP activation and enhanced Arp2/3-mediated actin polymerisation. Infection of NW-H208D cells with A36 ΔNPF 1-3 did however result in an additional decrease in plaque size. This suggests that the NPF motifs play an additional role independent of Cdc42. This additive plaque defect is likely to represent the contribution of AP-2 mediated clustering at the plasma membrane.

In order to determine whether the defect in viral spread is mirrored by a reduction in viral release, the extent of EEV released during infection of N-WASP MEFs was determined as previously described (Figure 5.11 C). Following infection with WR, NW-WT cells produced on average 660 EEVs/ml after 16 hours of infection, comparable to WR EEV release from BS-C-1 cells (Figure 5.3). In NW-H208D cells WR EEV release decreased by half to 338 EEVs/ml (Figure 5.11 C). Loss of the A36 NPF motifs led to a significant defect in EEV release in both the WT and H208D N-WASP cell lines. Following infection with A36 ΔNPF 1-3, NW-WT cells produced on average 311 EEV/ml, in N-WASP H208D cells this further decreased to an average of 197 EEV/ml. Taken together this data supports a role for intersectin-1 upstream of Cdc42 and N-WASP to enhance both viral spread and release. This role is dependent on the presence of the A36 NPF motifs, which also mediate AP-2 and clathrin recruitment.

In order to obtain further evidence for this model I used a selective small molecular inhibitor (ZCL278) that disrupts Cdc42-intersectin-1 binding (Friesland et al., 2013). This inhibitor results in the disruption of a number of Cdc42-intersectin-1 specific functions such as golgi organisation, cell motility and grown cone dynamics (Friesland et al., 2013). The size of plaques were measured following infection with WR or A36 ΔNPF 1-3 viruses in N-WASP WT or H208D cell lines in the presence of ZCL278. Plaque assays in the presence of DMSO were used as controls (Figure 5.11 A). In all cases plaques formed on NW-WT and NW-H208D cells were significantly decreased in size compared to controls (Figure 5.11 A, Figure 5.12 A). In contrast, plaques formed in N-WASP -/- cells were the same size with or without drug treatment (Figure 5.11 A, Figure 5.12 A). This implies that ZCL278 treatment does not have any N-WASP independent off target effects during vaccinia infection.

NW-WT and NW-H208D cells were infected with WR or A36 ΔNPF 1-3 in the presence of ZCL278. After 48 hours plaques were fixed, permeabilized, stained with B5 antibody, and measured as previously described. In the presence of ZCL278 WR plaques in NW-WT and NW-H208D cells were equal in size (0.68 ± 0.02 mm and 0.69 ± 0.01 mm respectively), confirming that drug treatment was successful in blocking Cdc42 activity in a viral context (Figure 5.12 A, B, C). Following ZCL278 treatment of A36 ΔNPF 1-3 infected NW-WT cells, there was no additional decrease in plaque size (0.64 ± 0.01 mm). A36 ΔNPF 1-3 infection of NW-H208D cells, however, once again led to a further decrease in plaque size to 0.55 mm ± 0.01 in the presence of ZCL278 (Figure 5.12 A, B).

Taken as a whole, this data supports the crucial role that intersectin-1 plays in mediating N-WASP activation via Cdc42. This data also confirms that the NPF motifs are primarily responsible for recruitment of intersectin-1 to the virus, which is essential for Cdc42 mediated activation of N-WASP. WR infection of NW-H208D cells and A36 ΔNPF 1-3 infection of NW-WT cells both led to an equivalent decrease in spread and release compared to WR infection of NW-WT cells. This decrease results due to the loss of Cdc42 mediated activation of N-WASP in both cases (Figure 5.11 D). In NW-

H208D cells, Cdc42 is unable to bind N-WASP, and during A36 ΔNPF 1-3 infection Cdc42 is not recruited to CEV.

The additional contribution of the NPF motifs to mediate AP-2 recruitment and clustering of the actin signalling complex was revealed following A36 ΔNPF 1-3 infection of NW-H208D cells compared to WT-NW cells. Infection of NW-H208D cells with the A36 ΔNPF 1-3 exhibited an additional decrease in plaque size and release, however plaques did not diminish to those formed in N-WASP -/- cells. This highlights a Cdc42-independent, N-WASP dependent role of intersectin-1, and is indicative of the requirement of intersectin-1 to recruit AP-2. Moreover this suggests that clathrin mediated clustering of A36 and its actin-polymerisation machinery is primarily to facilitate the formation of a dense N-WASP signalling network, and does not provide any additional force to extrude the virus from the membrane or release IEV tethering to the membrane. Consistent with this, plaques in N-WASP -/- MEFs are equivalent following infection with WR or A36 ΔNPF 1-3, confirming the A36 NPF motifs do not play a role in viral spread independent of N-WASP.

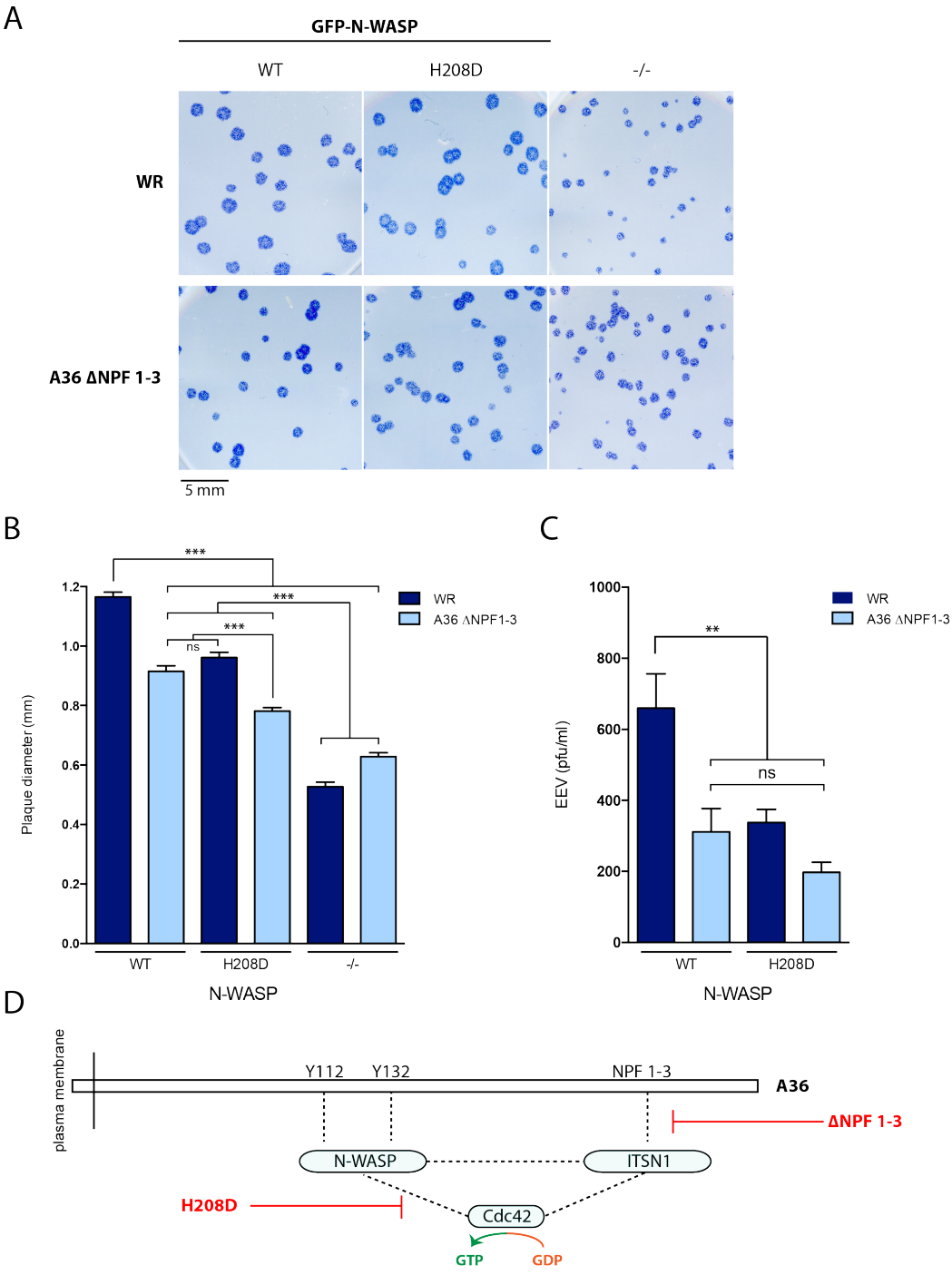

Figure 5.11 Loss of N-WASP-Cdc42 interaction mimics the loss of the A36 NPF motifs

A Representative images of WR and A36 ΔNPF 1-3 plaques formed in N-WASP -/- MEFs expressing GFP-N-WASP or GFP-N-WASP-H208D and stained with anti-B5 antibody. **B** Quantification of plaque diameter at 48 hpi. Error bars represent SEM of N=100-150 plaques in three independent experiments. **C** Quantification of EEV release at 16 hpi from GFP-N-WASP cell lines infected with WR or A36 ΔNPF 1-3. Error bars represent SEM over 3 independent experiments. A p value of < 0.001 is indicated by ***. A p value of < 0.01 is indicated by **. ns indicates a p value > 0.05. **D** Schematic illustrating the intersectin-1-Cdc42-N-WASP signalling network mediated by A36.

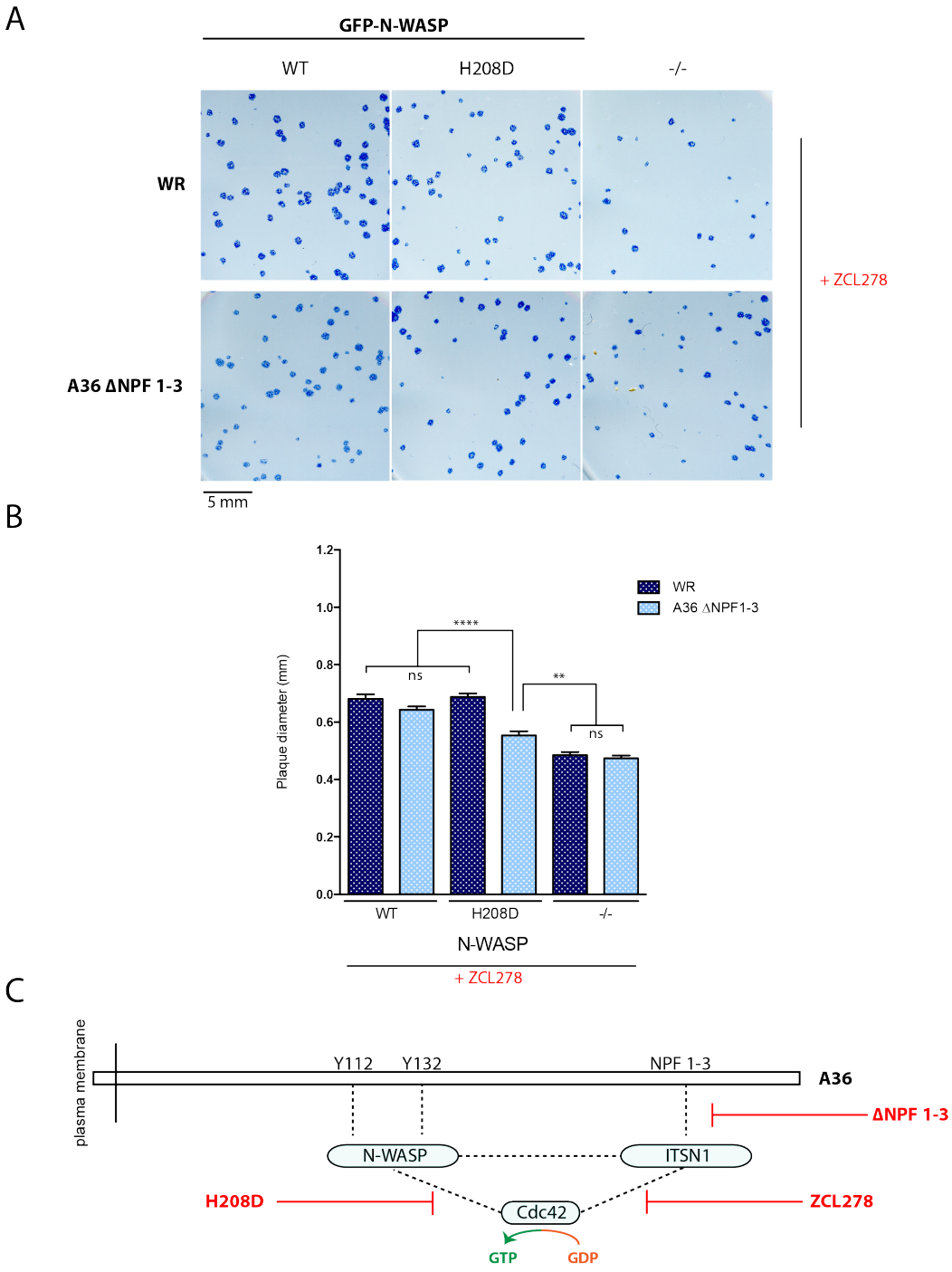

Figure 5.12 ZCL278 treatment of GFP-N-WASP cell lines confirms the requirement of the NPF motifs for viral spread

A Representative images of WR and A36 ΔNPF 1-3 plaques formed in N-WASP -/- MEFs expressing GFP-N-WASP or GFP-N-WASP-H208D and stained with anti-B5 antibody. Cells were maintained in 50 µM ZCL278 during the course of infection. **B** Quantification of plaque diameter at 48 hpi. Error bars represent SEM of N=100-150 plaques in three independent experiments. A p value of < 0.0001 is indicated by ****. A p value of < 0.01 is indicated by **. ns indicates a p value > 0.05. **C** Schematic illustrating the additional effect of ZCL278 treatment in the vaccinia actin-signalling network.

5.2.6 Viral release mediated by the A36 NPF motifs is actin-dependent

Given the marked defect in viral release upon loss of the A36 NPF motifs, I sought to more closely investigate the mechanism governing release of CEV from the plasma membrane. My data suggest that the primary role of the A36 NPF motifs is to recruit intersectin-1 and mediate Cdc42 dependent N-WASP activation. The A36 YdF mutant contains two phenylalanine substitutions in place of A36 tyrosine 112 and 132 (Rietdorf et al., 2001). This A36 mutant cannot be phosphorylated and therefore cannot recruit the vaccinia actin-polymerisation machinery (Moreau et al., 2000; Rietdorf et al., 2001). A36 YdF can, however, associate with AP-2 via the three NPF motifs (Figure 5.13 A). It has been previously established that infection with a virus expressing A36 YdF results in a small plaque phenotype and is defective in its ability to release EEV (Horsington et al., 2013). It has been suggested that without actin polymerisation as a driving force, the A36 YdF virus remains trapped in invaginated pits at the plasma membrane, this in turn inhibits EEV release (Horsington et al., 2013). A36 ΔNPF1-3 despite releasing fewer EEV can make still make actin tails. Given the reduced EEV release of both A36 YdF and A36 ΔNPF1-3 viruses, I sought to determine the contribution of the actin driving force for viral release.

In order to address this question, I combined the YdF and ΔNPF 1-3 mutations in a single A36 recombinant virus. The A36 YdF-ΔNPF recombinant virus was created via homologous recombination into the A36R locus in cells infected WR-ΔA36R as previously described (see Figure 4.5). The temporal expression of A36 following infection with A36 YdF and A36 YdF-ΔNPF viruses in HeLa cells was unchanged from that of WR (Figure 5.13 B & Figure 4.6). In order to determine how the spread of vaccinia is affected in the absence of both actin polymerisation and AP-2 recruitment, I initially measured the size of plaques induced by A36 YdF-ΔNPF compared to the A36 YdF and A36 ΔNPF 1-3 viruses. Infection with A36 YdF and A36 YdF-ΔNPF resulted in plaques that were both on average 0.61 ± 0.02 mm in diameter, significantly smaller that those observed following infection with both WR and A36 ΔNPF 1-3 (1.4 ± 0.01 mm and 0.93 ± 0.02 mm respectively) (Figure 5.13 C).

Next I sought to determine whether the combination of the loss actin tails (YdF) and clathrin recruitment (ΔNPF) lead to an additive decrease in EEV release at 16 hpi. Curiously, both A36-YdF and A36-YdF-ΔNPF viruses were found to release an equivalent number of EEVs as each other, as well as, that of the A36 ΔNPF 1-3 virus (on average 200 EEVs/ml) (Figure 5.13 D). Although A36 ΔNPF 1-3 induces significantly larger plaques than either of the A36-YdF or A36-YdF-ΔNPF viruses, EEV release was equally low in all viruses compared to WR (Figure 5.13 C, D).

As there is no additive defect in either plaque size or EEV release between the A36-YdF and A36-YdF-ΔNPF viruses, this confirms that clathrin alone in the absence of actin polymerisation is not sufficient to aid CEV release from the plasma membrane. This supports the notion that an actin-dependent step is required to promote viral release from the plasma membrane. The increase in plaque size of A36 ΔNPF 1-3 compared to both the A36-YdF and A36-YdF-ΔNPF viruses may be indicative of differences in the extent of viral presentation on the plasma membrane. A36 ΔNPF 1-3 although defective in viral release, would however be predicted to be extruded from the plasma membrane in the membrane in an actin-dependent manner, and therefore able to mediate direct cell-to-cell spread to some extent. In contrast, both A36-YdF and A36-YdF-ΔNPF viruses are predicted to be trapped within membrane in the absence of actin polymerisation, and thus unable to contact neighbouring cells, and limiting their spread.

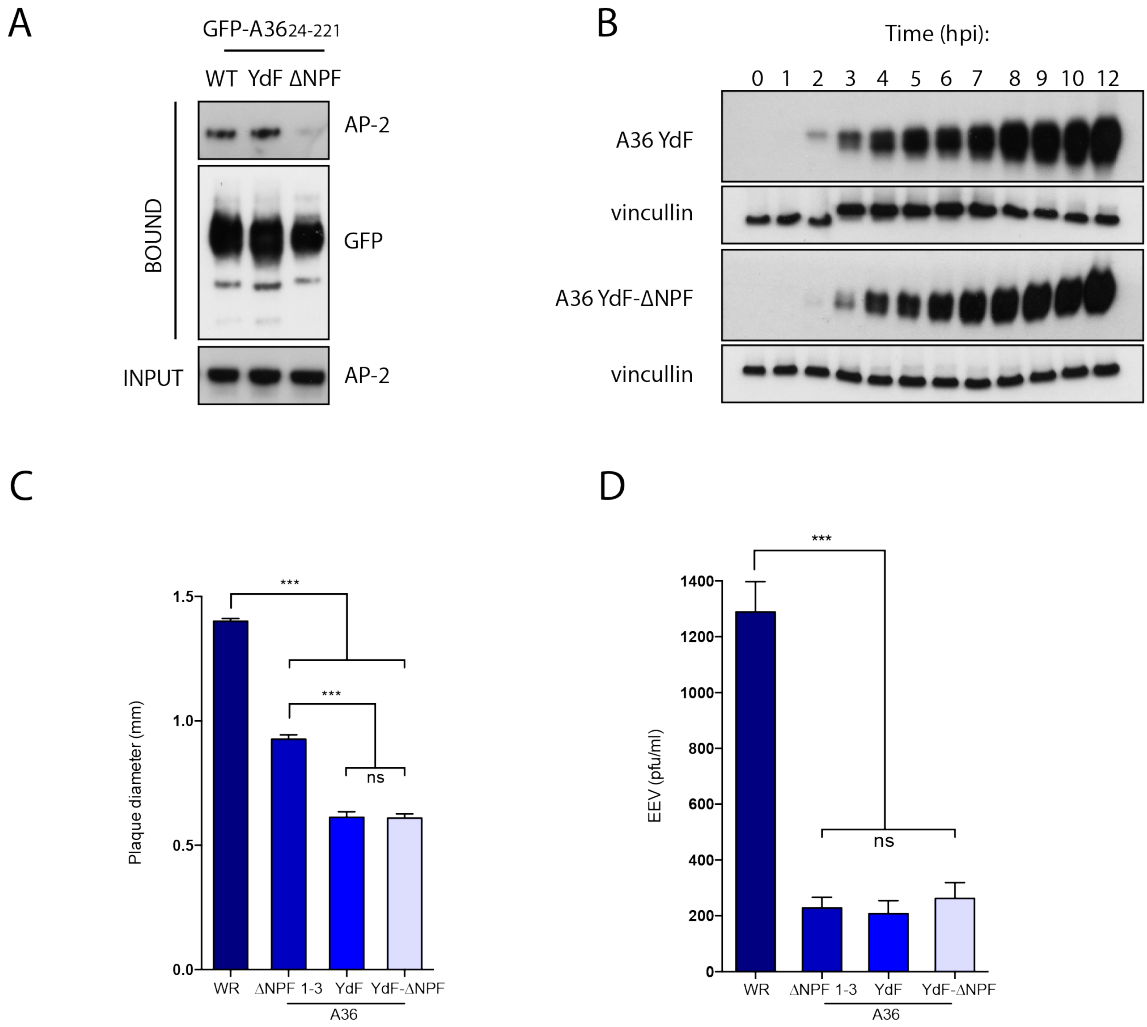

Figure 5.13 Loss of NPF motifs does not impact viral spread in the absence of actin polymerisation

A GFP-Trap pull-down assay on GFP-A36 1-221 WT, YdF and ΔNPF 1-3 mutants. The YdF mutant does not prevent AP-2 recruitment. **B** Immunoblot showing a time course of A36 expression. HeLa cells were infected with YdF and YdF-ΔNPF viruses respectively and samples collected every hour for 12 hpi. **C** Quantification of WR, A36-ΔNPF 1-3, YdF, and YdF-ΔNPF plaque diameter in BS-C-1 cells. Cells were fixed and stained with crystal violet 48 hpi to visualise plaques. N=100. **D** The number of EEV released/ml following infection of BS-C-1 cells with WR, A36-ΔNPF 1-3, YdF, and YdF-ΔNPF viruses. Supernatants were collected at 16 hpi and EEV numbers quantified by plaque assay after 48 hpi. Error bars represent SEM over 3 independent experiments. A p value of < 0.001 is indicated by ***. ns indicates a p value > 0.05.

5.3 Summary

In this chapter I have investigated the role of the endocytic NPF motifs during viral release and spread. The loss of the NPF motifs reduces cell-to-cell spread of the virus, and this is as a direct consequence of reduced viral release from primary infected cells. To investigate a possible role for the A36 NPF motifs during super-repulsion of viral particles, EEV release of the late viruses was quantified. Interestingly the ability of vaccinia to release EEV when A36 (wild type or ΔNPF) was solely under a late promoter was diminished by a quarter, as was the case with the A36 ΔNPF 1-3 virus. No evidence, however, could be found to link the role of NPF motifs to the ability to induce actin tails during super-repulsion. It is highly likely, however, that the dynamics of actin tail formation induced by EEVs (secondary actin tails) would differ from those induced from cell derived IEVs (primary actin tails).

The A36 NPF motifs are however required to recruit Cdc42 via intersectin-1, and thus to promote N-WASP activation beneath the virion. Loss of the NPF motifs in the absence of Cdc42 activity indicated that the ability of the virus to recruit AP-2 and clathrin machinery to enhance viral spread was also dependent on N-WASP mediated actin-polymerisation. Generation of the A36 YdF-ΔNPF virus allowed the closer investigation of the role of the NPF motifs independent of tyrosine phosphorylation. This confirmed that clathrin is unable to facilitate CEV release in the absence of the actin-polymerisation complex.

Chapter 6. Discussion

The functional characterisation of the vaccinia IEV protein A36 has revealed an intricate and highly complex signalling network that enables and promotes viral egress. N-WASP is recruited together with WIP, and is stabilised beneath the virus via a network of interactions with Nck, Grb2, and Cdc42 (Donnelly et al., 2013; Humphries et al., 2014; Weisswange et al., 2009). Prior to actin polymerisation, AP-2 and clathrin are recruited to cluster the actin-signalling network, resulting in highly efficient actin tail formation (Humphries et al., 2012). In this thesis, I aimed to characterise the mechanism governing AP-2 and clathrin recruitment, and have revealed that A36 utilises host like NPF motifs to recruit the EH domain containing proteins intersectin-1 and Eps15. I showed that intersectin-1 and Eps15 are required to mediate AP-2 recruitment via A36, and also that the NPF motifs of A36 are necessary and sufficient for recruitment of the endocytic machinery. Furthermore, intersectin-1 appears to act as a key modulator, regulating both AP-2 and actin dependent processes in order to enhance viral spread and release.

6.1 The first characterised viral NPF motifs

During the course of this study, I aimed to characterise the molecular mechanism governing the recruitment of AP-2 and clathrin to vaccinia during viral egress. I identified and characterised three Asn-Pro-Phe (NPF) motifs in A36 that are highly conserved among the *Orthopoxviruses* and essential for the recruitment of AP-2 and clathrin (Figure 3.7, 4.7). These NPF motifs were shown to mediate binding of AP-2 and clathrin via the EH domain containing proteins, intersectin-1 and Eps15 (Figure 3.6). Eps15 is a key component of clathrin-coated pits, and acts to facilitate recruitment of AP-2 to early endocytic sites (Benmerah et al., 1998; Benmerah et al., 2000; Tebar et al., 1996). Intersectin-1 plays a role in the regulation of actin dynamics, and has also been linked to exocytic events at the plasma membrane (Hussain et al., 2001; Yamabhai et al., 1998). Intersectin-1 and Eps15 both bind NPF motifs in a range of host factors, however no NPF motifs have been identified or characterised in a viral context up to this point.

Multiple pathogens utilise short host-like motifs to promote all stages of infection. Short linear peptide motifs are extremely advantageous as they can be easily packaged into viral genomes, and enable single viral proteins, such as A36, to mediate many different processes (Davey et al., 2012; Dinkel et al., 2014; Hagai et al., 2014; Handa et al., 2013). A36 alone facilitates binding to kinesin-1 via the WE/WD motifs, Nck and Grb2 via phosphotyrosine 112 and 132, and has in this thesis been shown to recruit intersectin-1 and Eps15 via conserved NPF motifs (Figure 3.7, 4.7) (Dodding et al., 2011; Frischknecht et al., 1999a; Scaplehorn et al., 2002; Weisswange et al., 2009). Closer analysis of the primary sequence of A36 also reveals the presence of the endocytic internalization motif, NPxY at residues 155-158 as well as a predicted PDZ-binding motif at its C-terminus (216-221: SVVSLV) (Figure 6.1) (Chen et al., 1990; Davey et al., 2012). NPxY motifs are found in receptor tyrosine kinases and typically mediate binding to Dab-2 PTB domains and have also been shown to bind to FERM-like domains in sorting nexins (Ghai and Collins, 2011; Keyel et al., 2006; Morris and Cooper, 2001; Smith et al., 2006).

A36 >

42 62
MMLVPLITVTVVAGTILVCYILYICRKKIRTVYNDNKIIMTKLKKIKSSNSSKSSKSTDSESDWEDHCSAMEQNNDVDNISRNE

134 150 155
ILDDDSFAGSLIWDNESNVMAPSTEHIYDSVAGSTLLINNDRNEQTIYQNTTVVINETETVEVLNEDTKQNPNYSSNPFVNY

221
NKTSICSKSNPFITELNNKFSENNPFRRAHSDDYLNKQEQDHEHDDIESSVVSLV

Figure 6.1 A36 contains two low complexity regions (LCRs), a NPxY motif, and a PDZ-binding motif

Primary sequence of A36. The characterised NPF, phosphotyrosine motifs, and kinesin-1 binding WE/WD motifs are highlighted in red. Additional motifs included NPxY Dab2 binding motif and a predicted PDZ binding motif (both highlighted in blue). Predicted low complexity regions (LCRs) are underscored. Transmembrane domain is shown in green.

These predicted motifs, however, do not yet have a clear functional role during vaccinia infection. The truncated A36 1-155 virus was initially generated to ascertain the role of C-terminal tyrosines Y158, Y166, Y200. Early studies showed, that loss of these residues did not affect the tyrosine phosphorylation levels of A36 (Frischknecht et al., 1999a; Weisswange, 2008). The A36 1-155 virus lacks all three NPF motifs, the predicted PDZ motif and also disrupts the NPxY motif. Multiple assays presented in this thesis have shown that A36 ΔNPF 1-3 and A36 1-155 viruses exhibit identical phenotypes. Both recombinant viruses induced longer, faster actin tails than those induced by WR (Figure 4.9). Neither virus could recruit clathrin, AP-2, intersectin-1 or Eps15, leading to equally defective cell-to-cell spread (Figure 4.7, 5.1). Further investigation of the NPxY and PDZ-binding motifs in isolation, would shed light as to whether these potential motifs have a functional role during earlier stages of infection.

The residues flanking the NPF motifs have been previously implicated in the specificity and binding to EH domains (de Beer et al., 2000; Enmon et al., 2000; Rumpf et al., 2008; Salcini et al., 1997; Wong et al., 1995). Analysis of intersectin-1 EH1 binding to a panel of NPF peptides concluded that intersectin-1 EH1 preferentially binds NPF motifs at the C terminus, and is prevented from binding internal NPF motifs (Yamabhai et al., 1998). Neither of the A36 NPF motifs are located in close proximity to the C-terminus, this may explain the observation that intersectin-1 EH1 binds A36 NPF motifs with lower affinity compared to intersectin-1 EH2 (Figure 3.6 D). Similarly, the high prevalence of S/T residues at positions -1 and -2 respective to the NPF motif in host endocytic proteins, suggests that an additional level of regulation mediating EH domain binding may be conferred via S/T phosphorylation (Paoluzi et al., 1998; Salcini et al., 1997; Yamabhai et al., 1998). In accordance with this, A36 NPF1 contains a serine at -1 and -2, and NPF2 contains a serine residue at position -1. Previous work has shown that A36 is heavily phosphorylated on serine residues, which may be therefore be required to mediate NPF to EH domain binding specificity (Wolffe et al., 2001). Comparison of peptide pull-downs with recombinant Eps15 EH domains 1-3 varied from those carried out in the presence of endogenous Eps15 from cell extracts. While endogenous Eps15 was able to bind NPF2 in isolation, recombinant GST-Eps15 showed clearly reduced

binding to NPF2 (Figure 3.6 E, F). This difference may be a direct result of phosphorylation of the serine preceding NPF2 to enhance binding to Eps15.

While peptide pull down assays determined that the C-terminus of A36 can directly bind both Eps15 and intersectin-1 via their respective EH domains, future *in vitro* ITC measurements may reveal specificity of certain EH domains to particular NPF motifs (Fig 3.6). Together with live cell imaging during infection, this approach would assist in uncovering both the stoichiometry and hierarchy of A36-mediated recruitment at the plasma membrane. It remains unknown whether A36 preferentially binds intersectin-1 or Eps15, or whether binding of one is sufficient, which in turn localises the other to A36 via hetero-oligomerization of their respective coiled-coil domains *in vivo* (Cupers et al., 1997; Wong et al., 2012). Interestingly, imaging during infection showed only a small subset of viral particles recruited both simultaneously (Figure 3.5 C).

Knowledge of the preferred binding of A36 to particular EH domains and EH domain containing proteins will lead to greater insight into the complex regulation of the endocytic machinery during viral egress. A fascinating property of many viral proteins is the ability to coordinate multiple signalling networks. How A36 is spatially regulated during kinesin-based transport of IEV, after fusion with the plasma membrane, and during recruitment of endocytic and actin components, remains to be elucidated. Structural analysis of A36 binding to the EH domains of intersectin-1 or Eps15 could lead us some way towards understanding the conformation of A36 at a distinct stage of viral egress, and how binding of distinct cellular machinery is coordinated in three-dimensional space.

6.2 Interactions and organisation of A36

During the generation of the C- and N-terminal truncations of A36 described in chapter 3, it was observed that the full-length cytoplasmic domain could biochemically interact with itself (Figure 6.2). How A36 is trafficked to the TGN prior to wrapping, how A36 is specifically localised to the outer IEV membrane and how A36 is subsequently retrieved from the plasma membrane after viral egress, remain key open questions at this time.

We now understand the roles that AP-2 and clathrin play in clustering of A36 beneath the virus (Humphries et al., 2012). In addition, it would be interesting to determine whether the intra- and intermolecular interactions of A36 with other IEV proteins and itself plays a part in the maintenance of a tightly clustered IEV scaffold after clathrin dissociates from the viral particle, maintaining a robust actin-signalling network (Humphries et al., 2012). The self-interaction of A36 may provide an additional layer of regulation during egress at the plasma membrane, and perhaps even earlier during viral morphogenesis.

As it stands, the minimal region of A36 that can self-interact consists of residues 120-155, which is able to associate with the N-terminal of A36 spanning residues 55-120 (Figure 6.2). One attractive hypothesis may be that a central hub of residues in A36 may act as a hinge in order to shift the conformation state of the protein from closed to open conformation. This may additionally be dependent on the phosphorylation state of A36.

The cytoplasmic region of A36 is predicted to be largely disordered, and SMART sequence analysis of A36 identified two low complexity regions (LCRs) spanning residues 42-62 and 134-150 (underlined in Figure 6.1, 6.2 B) (Letunic et al., 2015; Schultz et al., 1998). Both of these regions of low complexity lie within the regions of self-interaction identified experimentally and therefore may act as sticky patches, mediating open and closed conformations of A36 in vivo and/or be responsible to facilitate clustering of the actin-signalling network beneath the CEV during egress.

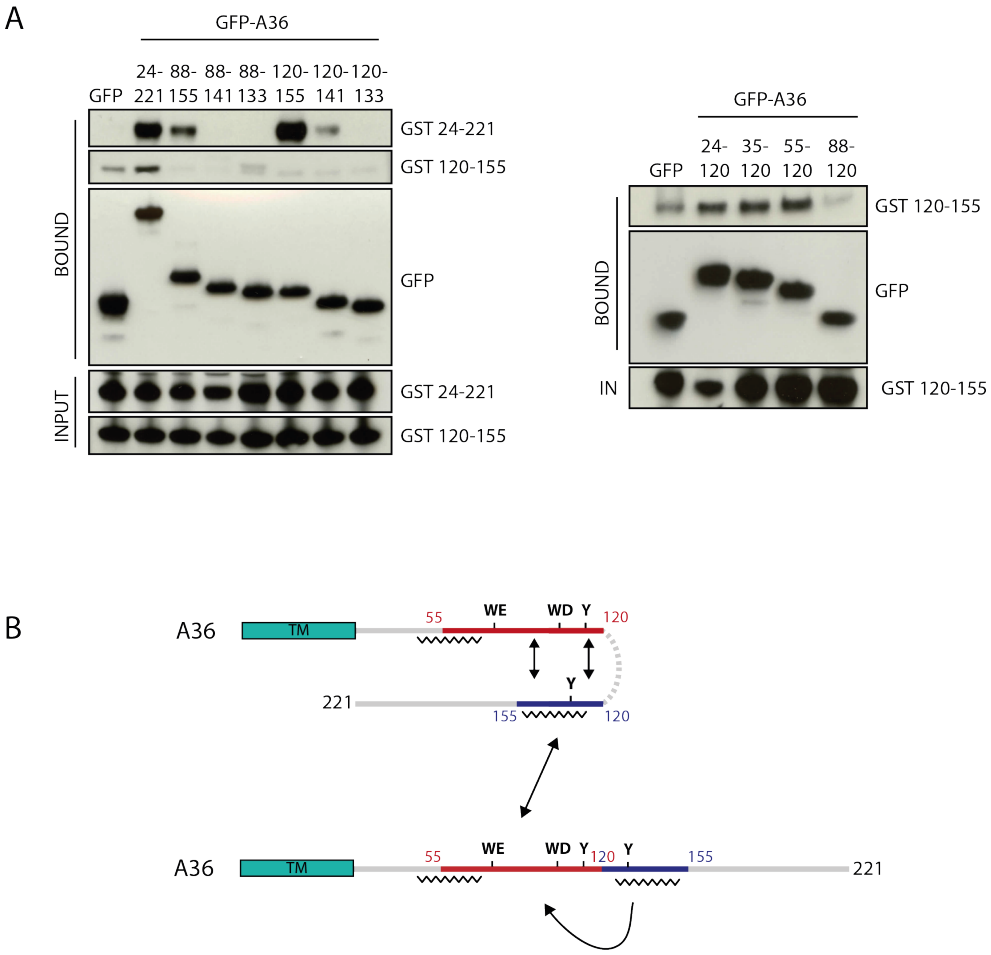

Figure 6.2 Mechanisms of A36 self-organisation

A Immunoblot following GFP-Trap pull-downs on truncations of GFP-A36 with GST-A36$^{24\text{-}221}$ or GST-A36$^{120\text{-}155}$. In both cases GST-A36$^{120\text{-}155}$ can mediate binding to A36$^{24\text{-}221}$ and vice versa. In addition GST-A36$^{120\text{-}155}$ can specifically bind the N-terminal A36$^{55\text{-}120}$. **B** Model of the potential inter- and intra-molecular organisation of A36. Pull-down assays have identified residues 55-120 (red) and 120-155 (blue) as regions mediating self-interaction. Tyrosine motifs (112 and 132), and kinesin-1 binding WE/WD motifs (64/97) are highlighted in bold. The two low complexity regions (LCRs) (residues 42-62 and 134-150) are underscored.

6.3 Interplay between clathrin machinery and actin dynamics

6.3.1 Recruitment and activation of intersectin-1

The discovery and characterisation of the A36 NPF motifs described in this thesis uncovers the role of the EH domain containing protein, intersectin-1, to enhance viral spread and release (Figure 4.3). Intersectin-1 has been shown to act as a Cdc42 GEF, activating Cdc42 via direct binding to its C-terminal DH domain (Hussain et al., 2001; Kintscher et al., 2010). In addition, intersectin-1 can directly bind the central proline-rich region of N-WASP via multiple interactions with its SH3 domains; this upregulates intersectin-1 GEF activity and enhances binding of intersectin-1 to Cdc42 (Hussain et al., 2001; Rohatgi et al., 1999; Zamanian and Kelly, 2003). This in turn activates a feed-forward loop, which enhances activation of N-WASP via Cdc42, thus promoting Arp2/3-dependent actin polymerisation (Humphries et al., 2014; Hussain et al., 2001). It is now clear that this canonical signalling pathway is activated by vaccinia during actin tail formation as well as EEV release (Figure 5.11, 5.12) (Humphries et al., 2014). Interestingly, recent work has also implicated intersectin-1 (and its homologue, intersectin-2) in the formation of actin-rich invadopodia, via direct binding to WIP (Gryaznova et al., 2015). WIP binding is directly mediated via the SH3A, C, E domains of intersectin-1/2, and was shown to occur independently of N-WASP.

As N-WASP and WIP are recruited to A36 in complex with one another, it could be predicted that intersectin-1 recruitment to vaccinia occurs directly via the WIP, N-WASP, Cdc42 signalling network (Donnelly et al., 2013; Weisswange et al., 2009). I have determined that although A36 ΔNPF 1-3, can recruit WIP and N-WASP, it is unable to recruit either intersectin-1 or Cdc42 to the virus, thus neither WIP nor N-WASP are sufficient to recruit intersectin-1 to vaccinia in the absence of the A36 NPF motifs (Figure 4.11, 4.7, 5.9). Furthermore, co-localisation analysis determined that approximately 60% of CEV could recruit intersectin-1 in N-WASP -/- cells, confirming that intersectin-1 is recruited to vaccinia independently of N-WASP (Figure 4.7). Analysis of cell-to-cell spread and EEV release demonstrated that WR infection of a N-WASP mutant that is unable to bind Cdc42 (N-WASP H208D) resulted in decreased viral spread and release to the same extent as that of N-WASP wild type cells infected

with A36 ΔNPF 1-3 (Figure 5.11). Overall, this strongly suggests that the A36 NPF motifs are required to mediate Cdc42 activation of N-WASP.

Following its recruitment via the A36 NPF motifs, intersectin-1 must then itself be activated. Intersectin-1 is regulated by an autoinhibition mechanism, mediated by a conserved tryptophan (W1221) within the short linker region between the fifth SH3 domain (SH3E) and the DH domain (Ahmad and Lim, 2010; Kintscher et al., 2010). Although N-WASP is still able to bind the intersectin-1 SH3 domains in its autoinhibited state, N-WASP binding is unable to relieve this autoinhibition (Hussain et al., 2001; Kintscher et al., 2010; Zamanian and Kelly, 2003). This demonstrates that N-WASP binding alone is not sufficient to reveal the catalytically active DH-PH domains of intersectin-1, and therefore cannot stimulate its GEF activity (Kintscher et al., 2010). How autoinhibition of intersectin-1 is relieved is at present unknown. One possibility is that binding of the N-terminal EH domains to the A36 NPF motifs mediates a conformation change to release binding. While an alternative hypothesis is that direct AP-2 binding to the SH3A-B linker via the WADF motif (residues 843-846) releases the autoinhibited conformation of intersectin-1 (Pechstein et al., 2010). Following release of autoinhibition, intersectin-1 can then bind and activate Cdc42, and in turn activate N-WASP (Hussain et al., 2001; Kintscher et al., 2010; Zamanian and Kelly, 2003). The relative proximity of the tryptophan (W1221) responsible for maintaining autoinhibition of intersectin-1 with the AP-2 binding site (residues 843-846) suggests this may be a likely scenario (Figure 6.3). Following activation of intersectin-1, enhanced binding of activated N-WASP via multiple interactions with the SH3 domains of intersectin-1 could subsequently disrupt AP-2 binding. This hypothetical model may explain the mechanism governing the temporal dissociation of AP-2 and the clathrin coat upon actin tail formation (Humphries et al., 2012). Future studies involving the disruption of the intersectin-1 AP-2 binding site would give valuable insight regarding both the release of intersectin-1 autoinhibition, and also as to whether the dissociation of AP-2 and clathrin is dependent on N-WASP binding to intersectin-1.

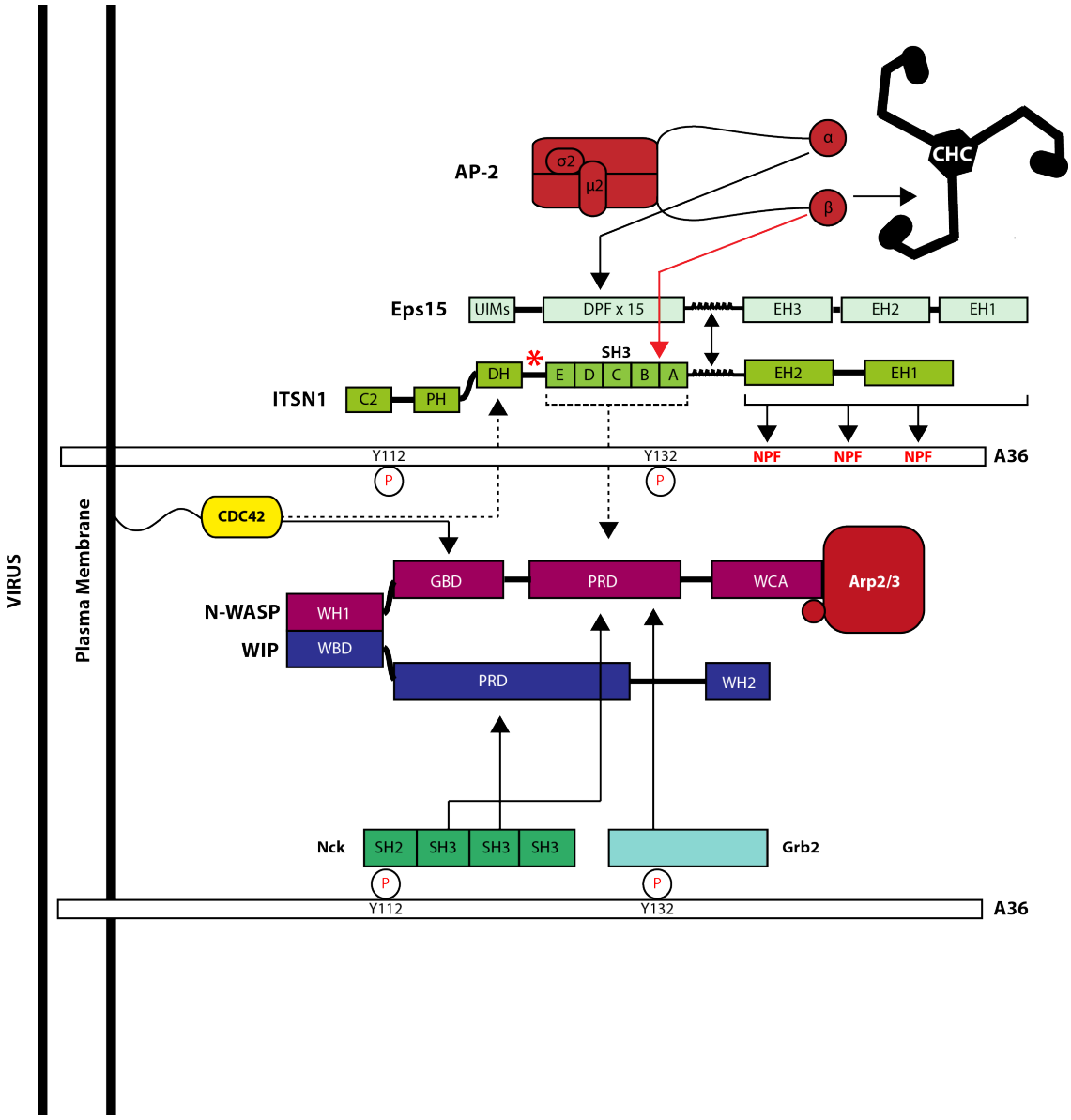

Figure 6.3 Updated model of the A36 vaccinia actin and clathrin signaling network

The multiple interactions that form between the various components of the actin-signaling network. The A36 NPF motifs directly recruit intersectin-1 and Eps15 which in turn mediate binding of AP-2 and clathrin. Recruitment of intersectin-1 mediates binding of Cdc42 and N-WASP, stabilizing the actin-signaling network. Intersectin-1 has also been shown to recruit AP-2 via the WADF motif within SH3A-SH3B linker region (843-846). Red asterisk indicates SH3E-DH linker region that mediates autoinhibition of intersectin-1 via a conserved tryptophan (W1221).

6.3.2 Atypical EH domain containing proteins

N-WASP plays an essential role in promoting Arp2/3 activation, which in turn facilitates the formation of actin tails to enhance viral egress and spread. Numerous studies have found that N-WASP utilises multiple cellular inputs to enhance its activation and to provide tight regulation of its actin nucleation activity. Aside from the known vaccinia mediated signalling pathways mentioned thus far, Grb2 can function alongside Cdc42 to enhance N-WASP activation, while Nck and $PI(4,5)P_2$ are also able to act together to activate N-WASP in a Cdc42-independent manner (Carlier et al., 2000; Rohatgi et al., 2001). In addition, $PI(4,5)P_2$ can promote the activation of N-WASP in a Cdc42-dependent manner in the presence of WIP (Bu et al., 2010; Ho et al., 2006; Martinez-Quiles et al., 2001; Takano et al., 2008).

The precise role and function of $PI(4,5)P_2$ at the vaccinia plasma membrane interface is currently unknown. It has been suggested that $PI(4,5)P_2$ can facilitate the activation of Cdc42, prior to N-WASP activation (Rohatgi et al., 2000; Rohatgi et al., 1999; Rohatgi et al., 2001). In addition, the recruitment of clathrin during endocytic events occurs at $PI(4,5)P_2$-rich membranes, acting as a hub to link the clathrin machinery and actin-dependent events during clathrin-mediated endocytosis (Cocucci et al., 2012). In the context of vaccinia infection, $PI(4,5)P_2$-rich membranes may play a similar role to coordinate the temporal and spatial events at the membrane during viral egress.

A unique family of EH domain containing proteins, EHD1-4, are atypical in containing a single C terminal EH domain (Grant and Caplan, 2008; Kieken et al., 2010; Salcini et al., 1997). EHDs localize to distinct membrane compartments and have been implicated in endosomal recycling and sorting, and more recently in direct lipid binding (Caplan et al., 2002; Naslavsky et al., 2009; Naslavsky et al., 2006). EHD2 specifically localize to the plasma membrane, and has been shown to directly interact with $PI(4,5)P_2$ (Blume et al., 2007; Daumke et al., 2007; Naslavsky et al., 2009; Simone et al., 2013). EHD2 has also been observed to associate with multiple actin rich structures such as filopodia, microspikes, and actin-rich ruffles at the plasma membrane (George et al., 2007; Guilherme et al., 2004). Curiously, evidence of a link between EHD2 and the actin cytoskeleton comes in the form of a conserved cluster of acidic residues directly

preceding the C terminal EH domain (Guilherme et al., 2004). This acidic cluster has been postulated to mimic the acidic cluster found in the WCA domain of N-WASP, thus actively promoting Arp2/3-dependent actin polymerization (Guilherme et al., 2004; Simone et al., 2014).

I have shown that the loss of the A36 NPF motifs inhibits viral spread and release, and more specifically that this is dependent on Cdc42 activation (Figure 5.11, 5.12). While it is presumed that intersectin-1 is the crucial link between the NPF motifs and Cdc42, it cannot be ruled out that another EH domain containing protein additionally promotes Cdc42 activation. For example, the recruitment of EHD2 could facilitate localization of IEVs to PI(4,5)P_2-rich membranes, promoting Cdc42 activation in a PI(4,5)P_2 dependent manner, thus enhancing viral spread and release. The role of EHDs in a viral context are yet to be examined, however, they may act as a crucial link between PI(4,5)P_2 -rich sites at the plasma membrane and the actin-polymerization machinery.

6.4 The super-repulsion hypothesis

Vaccinia is able to enhance the rate and spread of infection in an A36 dependent manner, via the induction of actin tails. The A36 NPF motifs support actin polymerisation in two ways. Firstly, they facilitate clustering of the A36 and N-WASP signalling complex that supports actin tail formation (Figure 4.7) (Humphries et al., 2012). Secondly, the A36 NPF motifs recruit intersectin-1 and Cdc42 to facilitate N-WASP activation and enhance actin polymerisation beneath the virus (Figure 4.7, 5.9). I initially sought to determine whether the decrease in viral spread observed upon infection with A36 ΔNPF 1-3 could be due to a loss or decrease in the ability of this virus to induce secondary actin tails during super-repulsion of EEV.

The mechanisms governing actin tail formation must differ between actin tails generated by CEVs during egress from heavily infected cells (primary actin tails), and actin tails induced on recently infected cells by released EEV (secondary actin tails). During fusion of CEV with the plasma membrane, A36 is delivered to the membrane pre-clustered beneath the virion. In addition CEV-induced actin tails at the plasma

membrane during egress are supported by luminal interactions of the IEV proteins, B5 and A34, tightly localised beneath the virus. In contrast during the formation of secondary actin tails during super-repulsion, only A36 and A33, expressed early during infection, are present at the surface of recently infected cells. The delivery of early A36 and A33 to the plasma membrane via endosomal trafficking, would instead result in a more disperse localisation of A36 and A33 at the membrane. Therefore, I would predict that the A36 NPF motifs play an even more important role by mediating AP-2 recruitment at the membrane. Thereby, inducing clustering of A36 in a clathrin-dependent manner, to zip up the actin-polymerisation machinery beneath the incoming EEV, analogous to clathrin pit formation.

Preliminary identification of secondary actin tails was challenging, due to the rarity of capturing such events in fixed cells and difficulty of capturing actin tails in early infected highly motile cells, during live cell imaging. However, my analysis could not detect a significant change in the number of superinfecting actin tails between WR and the A36 ΔNPF 1-3 virus (Figure 5.8). This data agrees with the fact that the loss of the A36 NPF motifs does not impact on the number of primary actin tails induces by CEV (Figure 4.9). This also implies that neither A36 clustering nor Cdc42 recruitment are essential for the induction of secondary actin tails formed during super-repulsion.

My data however, impacts on the current interpretation of the importance of super-repulsion to enhance viral spread. While EEV are typically released from cells 6-8 hours following initial infection, the decrease in plaque size observed following infection with A36$_{late}$ compared to that of wild type A36 may be largely due to the defect or delay in EEV release observed (Figure 5.7, 5.8) (Payne and Kristenson, 1979). A36 is crucial for both microtubule-mediated transport to the cell periphery and nucleation of actin tails in order to enhance viral spread. In the absence of microtubule-mediated transport, IEV are estimated to diffuse through the cytosol to the cell periphery, at a rate of 5.7 hours / 10μm of cytoplasm (Smith et al., 2003; Sodeik, 2000). The loss of A36 expression during the early hours of infection is therefore hugely detrimental to virus spread and release. The late A36 recombinant viruses generated in chapter 5, commenced A36 expression at 7 hpi, compared to 1-2 hpi when expressed

under the endogenous A36 promoter (Figure 5.6). When EEV release was determined at 16 hpi, the late A36 viruses would have been undergoing extremely limited ΔA36-like diffusion through the cytosol for 7 hours prior to A36 expression. In contrast, during endogenous A36 expression, infected cells have been actively releasing EEV for approximately 10 hours. While a decrease in super-repulsion may play an additional role, I would argue that the ability of the virus to release large numbers of EEV would heavily outweigh the affect of super-repulsion in this case.

6.5 What governs viral release?

In Chapter 5, I demonstrated that the interaction between the EH domain containing proteins, via A36 NPF motifs, is required for efficient viral dissemination. Despite this, little is known about mechanisms of virus release, *in vivo*. Evidence suggests that EEV mediated release, rather than IMVs released following cell lysis, is primarily responsible for dissemination of the virus through tissue (Payne, 1980). Unlike IMV particles, EEVs have greater resistance to antibody-mediated neutralization and complement-mediated viral lysis (Benhnia et al., 2009; Cohen et al., 2011; Ichihashi, 1996; Wolffe et al., 1998).

The loss of the A36 NPF motifs resulted in a significant decrease in the ability of the virus to release EEV (Figure 5.3). Interestingly, this defect was to the same extent as that of the A36 YdF virus, which cannot induce actin tails (Figure 5.13, 6.4). This, however, raises the question as to how both impact EEV release to such a great extent. Actin polymerisation beneath the virus has been shown to enhance clustering of A36 and provide the driving force to push the virion out of invaginations in the membrane (Horsington et al., 2013). A36 YdF cannot recruit Nck or Grb2 and therefore lacks the ability to induce actin tails (Rietdorf et al., 2001; Scaplehorn et al., 2002; Ward and Moss, 2001). The loss of actin polymerisation is thought to trap A36 YdF virions in invaginated pits at the plasma membrane, thus inhibiting both the release of EEV and the extent of viral presentation on the cell surface. This additionally limits contact with neighbouring cells, and disrupts CEV mediated cell-to-cell spread (Figure 6.4).

In the absence of Cdc42, intersectin-1, AP-2 and clathrin, A36 ΔNPF 1-3 still recruits the core components of the actin-signalling complex, and is able to induce actin tails, though they are less robust (Figure 4.10, 4.11, 6.4). This extent of actin polymerisation clearly enhances cell-to-cell spread through a plaque, as A36 YdF forms significantly smaller plaques than A36 ΔNPF 1-3 (Figure 5.13). Both A36 YdF and A36 ΔNPF 1-3, however, led to a similar reduction in EEV release (Figure 5.13). This calls into question the importance of actin polymerisation in the final step of EEV release as a driving force to release tethering of EEV from the plasma membrane during virus release. If actin polymerisation were an essential process for the physical release of EEV, one would expect to see a far greater decrease in EEV release in A36 YdF compared to A36 ΔNPF 1-3.

Interestingly, infection with the A36 YdF-ΔNPF virus did not result in additive defects in either plaque size or EEV release compared to A36 YdF alone (Figure 5.13 C, D). This confirms that the role of clathrin during viral egress is primarily to enhance actin polymerisation, as without the capacity to induce actin tails the ability of clathrin to cluster A36 is redundant. In order to determine whether viral presentation on the plasma membrane varied amongst the A36 recombinant viruses, preliminary EM imaging was carried out, however further analysis is required in order to fully appreciate how differences in virion presentation at the plasma membrane affects both the release and spread of EEV.

These findings provide interesting insight for the design of oncolytic poxviruses, as the increase in viral spread mediated by the NPF motifs, could be harnessed to increase oncolytic potential. To date four poxviruses have been investigated as an oncolytic viral backbone: vaccinia virus, myxoma virus, racoonpox virus, and yaba-like disease virus (Chan et al., 2013; Evgin et al., 2010; Hu et al., 2001; Kochneva et al., 2012). Several strategies have been utilised in order to enhance EEV release in these viruses. Examples include the generation of a recombinant virus that encoded matrix metallopeptidase 9 (MMP9) to enhance the spread of EEV (Schafer et al., 2012). Similarly the introduction of mutations in vaccinia A34 that are known to disrupt tethering of the CEV to the host cell and promote EEV release, results in recombinant strains with enhanced EEV spread

through tumours and greater anti-tumour effects (Thirunavukarasu et al., 2013). The presence of the NPF motifs to promote viral spread can now be considered advantageous in the rational choice and design of future oncolytic viruses, as viral strains lacking these motifs, including both yaba-like disease virus and mxyoma virus, may need to be additionally modified to further enhance EEV spread. This has been carried out to great effect in myxoma virus, whereby insertion of vaccinia F11 resulted in enhance viral spread (Irwin and Evans, 2012). It is worth noting in the future that any combination therapy which disrupts the conserved intersectin-1:Cdc42:N-WASP signalling pathway, may also hinder the spread of oncolytic poxviruses through tissue.

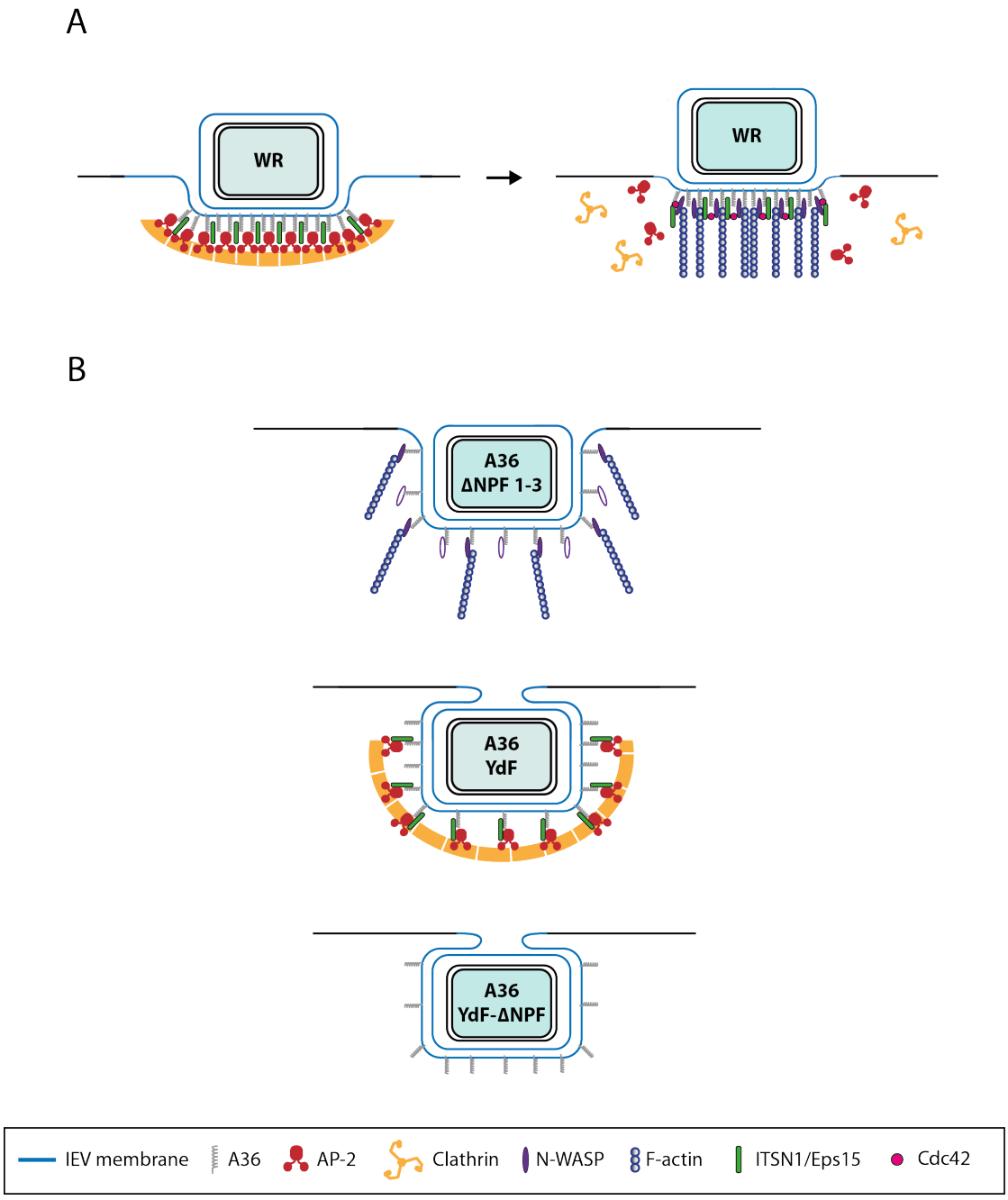

Figure 6.4 Models of actin-mediated vaccinia egress

A WR is able to recruit clathrin to cluster the vaccinia-signalling network and promote actin-mediated release from the plasma membrane. **B** All three recombinant viruses (A36 ΔNPF 1-3, A36 YdF, and A36 YdF-ΔNPF) result in defective EEV release to the same extent, despite differences in recruitment of the clathrin and actin signalling networks, and proposed differences in the extent of viral presentation on the plasma membrane (Figure 5.13).

6.6 NPF motifs as a conserved pathogen signalling scaffold

Multiple viral and bacterial pathogens hijack clathrin in order to enhance their entry and spread, and EPEC and vaccinia also appear to use similar clathrin adaptors proteins to do so. Vaccinia virus hijacks AP-2, Eps15 and intersectin-1 to facilitate clathrin recruitment; similarly EPEC recruits Eps15, and epsin-1 alongside the clathrin adaptor, Dab2 (Bonazzi et al., 2011; Humphries and Way, 2013; Lin et al., 2011). Given these similarities it would be interesting to determine whether epsin-1 and Dab2 are also recruited during A36 dependent actin polymerisation. Although EPEC Tir protein does not contain NPF or NPxY motifs, A36 contains an NPxY internalisation motif, discussed earlier that may play a role in mediating Dab2 recruitment.

Yaba-like disease virus encodes a functional A36 orthologue, 126R that has been shown to rescue actin-based motility during ΔA36R infection. YLDV-126R, does not contain NPF motifs and consequently was unable to restore recruitment of clathrin, AP-2, intersectin-1 or Eps15, when expressed in place of vaccinia A36 (Figure 4.8). Subsequent bioinformatic analysis of the YLDV proteome reveals, however, that the protein encoded by the YLDV 150R gene contains two NPF motifs. The functional role of YLDV-150R is yet to be determined. YLDV-150R encodes a 100 aa protein, containing a predicted transmembrane domain at its N-terminus as well as two NPF motifs at residues 52-54 and 72-74 (Figure 6.5). This as of yet uncharacterised protein is highly conserved amongst multiple genera of the *Chordopoxvirus* family. The Tanapox (Yatapoxvirus), Swinepox (Suipoxvirus), Lumpy skin disease virus (Capripoxvirus), and Myxoma virus (Leporipoxvirus) homologues of YL150R each contain two conserved NPF motifs.

These NPF motifs may be predicted to play a functional role during viral spread and act to compensate for the lack of NPF motifs in the YLDV A36 homologue. It could be predicted in these viruses' 150R and the A36 orthologue, 126R acts together in trans to couple recruitment of the endocytic machinery with that of actin polymerisation. This avenue will require further investigation in order to ascertain the broader functional relevance of the NPF motifs during viral pathogenesis.

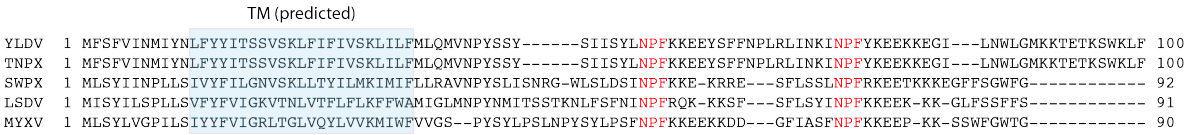

Figure 6.5 Yaba-like disease virus 150R reveals conserved NPF motifs

Clustal omega alignment of YLDV (Yaba-like disease virus) – 150R (Q9DHG3), TNPX (Tanapox virus) – 150R (A7XCU1), SWPX (Swinepox virus Kasza) – C2L (VC02), LSDV (Lumpy skin disease virus) – LD153 (Q77GF7), and MYXV (Myxoma virus Lausanne) – MT4A (Q9YQ06). UniProtKD ID is shown in parenthesis. NPF motifs are highlighted in red, and predicted transmembrane domain in blue.

6.7 Future Perspectives

The discovery of functional NPF motifs in vaccinia A36 uncovers an additional layer of regulation during viral egress at the plasma membrane. This thesis has concentrated on the two best characterised EH domain containing proteins, intersectin-1 and Eps15. The ability of intersectin-1 and Eps15 to act as multi-protein scaffolds during endocytic events and actin polymerisation makes them ideal candidates for hijacking by vaccinia, and other viruses. The closer analysis of the role of intersectin-2 and Eps15R, alongside other EH domain containing proteins such as the EHD (Eps15 Homology Domain) proteins must now be investigated further. It is clear from the conservation of the NPF motifs among the *Chordopoxvirus* family that EH domain containing proteins are a key strategy to promote viral infection.

Crucially, the stoichiometry of the vaccinia actin-signalling complex remains unknown, and would reveal precisely how co-ordination of multiple signalling inputs are integrated in order to promote actin-polymerisation. Additionally, little is known about the regulation and stoichiometry of the EH domain containing proteins during canonical clathrin mediated endocytosis *in vivo*. Although i*n vitro* assays have highlighted the ability of intersectin-1/2 and Eps15/15R to hetero- and homo-oligomerise, how different complexes of EH domains assemble, and whether they mediate distinct functions remains to be understood. Vaccinia A36R will in future provide a useful tool to determine how intersectin-1 along with Eps15 together coordinate N-WASP, Cdc42,

AP-2 at the plasma membrane. Furthermore, while clathrin is only present at the virus during egress briefly prior to actin tail formation, intersectin-1 and Eps15 remain on the actin tail following initiation of actin polymerisation. How vaccinia is able to dissociate from the vast clathrin cage remains to be determined. Whether actin is required to disassemble the clathrin cage or clathrin disassembly must first occur prior to actin tail formation remains unknown at present. Release of intersectin-1 autoinhibition may reveal vital clues to the coordination of clathrin disassembly via competing N-WASP and AP-2 interactions.

Vaccinia A36 once again proves to be a crucial multifunctional protein, and the analysis of how the vast cellular endocytic and actin components are regulated and coordinated by intersectin-1 and other EH domain containing proteins, will no doubt uncover further levels of complexity and enhance our understanding of both viral egress and the interface of actin and clathrin dynamics *in vivo*.

References

Aghamohammadzadeh, S., and Ayscough, K.R. (2009). Differential requirements for actin during yeast and mammalian endocytosis. Nat Cell Biol *11*, 1039-1042.

Agwunobi, J.O. (2007). Should the US and Russia destroy their stocks of smallpox virus? Bmj *334*, 775.

Ahle, S., Mann, A., Eichelsbacher, U., and Ungewickell, E. (1988). Structural relationships between clathrin assembly proteins from the Golgi and the plasma membrane. The EMBO journal *7*, 919-929.

Ahmad, K.F., and Lim, W.A. (2010). The minimal autoinhibited unit of the guanine nucleotide exchange factor intersectin. PloS one *5*, e11291.

Albelda, S.M., and Thorne, S.H. (2014). Giving oncolytic vaccinia virus more BiTE. Mol Ther *22*, 6-8.

Amann, K.J., and Pollard, T.D. (2001). The Arp2/3 complex nucleates actin filament branches from the sides of pre-existing filaments. Nat Cell Biol *3*, 306-310.

Anitei, M., and Hoflack, B. (2012). Bridging membrane and cytoskeleton dynamics in the secretory and endocytic pathways. Nat Cell Biol *14*, 11-19.

Anton, I.M., Jones, G.E., Wandosell, F., Geha, R., and Ramesh, N. (2007). WASP-interacting protein (WIP): working in polymerisation and much more. Trends in cell biology *17*, 555-562.

Antonescu, C.N., Aguet, F., Danuser, G., and Schmid, S.L. (2011). Phosphatidylinositol-(4,5)-bisphosphate regulates clathrin-coated pit initiation, stabilization, and size. Mol Biol Cell *22*, 2588-2600.

Arakawa, Y., Cordeiro, J.V., Schleich, S., Newsome, T.P., and Way, M. (2007). The release of vaccinia virus from infected cells requires RhoA-mDia modulation of cortical actin. Cell host & microbe *1*, 227-240.

Araki, Y., Kawano, T., Taru, H., Saito, Y., Wada, S., Miyamoto, K., Kobayashi, H., Ishikawa, H.O., Ohsugi, Y., Yamamoto, T.*, et al.* (2007). The novel cargo Alcadein induces vesicle association of kinesin-1 motor components and activates axonal transport. The EMBO journal *26*, 1475-1486.

Assarsson, E., Greenbaum, J.A., Sundstrom, M., Schaffer, L., Hammond, J.A., Pasquetto, V., Oseroff, C., Hendrickson, R.C., Lefkowitz, E.J., Tscharke, D.C.*, et al.* (2008). Kinetic analysis of a complete poxvirus transcriptome reveals an immediate-early class of genes. Proceedings of the National Academy of Sciences of the United States of America *105*, 2140-2145.

Ayscough, K.R. (2000). Endocytosis and the development of cell polarity in yeast require a dynamic F-actin cytoskeleton. Curr Biol *10*, 1587-1590.

Baba, T., Damke, H., Hinshaw, J.E., Ikeda, K., Schmid, S.L., and Warnock, D.E. (1995). Role of dynamin in clathrin-coated vesicle formation. Cold Spring Harb Symp Quant Biol *60*, 235-242.

Bailly, M., Ichetovkin, I., Grant, W., Zebda, N., Machesky, L.M., Segall, J.E., and Condeelis, J. (2001). The F-actin side binding activity of the Arp2/3 complex is essential for actin nucleation and lamellipod extension. Curr Biol *11*, 620-625.

Baroudy, B.M., and Moss, B. (1982). Sequence homologies of diverse length tandem repetitions near ends of vaccinia virus genome suggest unequal crossing over. Nucleic Acids Res *10*, 5673-5679.

Batchelder, E.M., and Yarar, D. (2010). Differential requirements for clathrin-dependent endocytosis at sites of cell-substrate adhesion. Mol Biol Cell *21*, 3070-3079.

Batonick, M., Favre, M., Boge, M., Spearman, P., Honing, S., and Thali, M. (2005). Interaction of HIV-1 Gag with the clathrin-associated adaptor AP-2. Virology *342*, 190-200.

Benedetti, H., Raths, S., Crausaz, F., and Riezman, H. (1994). The END3 gene encodes a protein that is required for the internalization step of endocytosis and for actin cytoskeleton organization in yeast. Mol Biol Cell *5*, 1023-1037.

Benesch, S., Polo, S., Lai, F.P., Anderson, K.I., Stradal, T.E., Wehland, J., and Rottner, K. (2005). N-WASP deficiency impairs EGF internalization and actin assembly at clathrin-coated pits. Journal of cell science *118*, 3103-3115.

Benhnia, M.R., McCausland, M.M., Moyron, J., Laudenslager, J., Granger, S., Rickert, S., Koriazova, L., Kubo, R., Kato, S., and Crotty, S. (2009). Vaccinia virus extracellular enveloped virion neutralization in vitro and protection in vivo depend on complement. Journal of virology *83*, 1201-1215.

Benmerah, A., Begue, B., Dautry-Varsat, A., and Cerf-Bensussan, N. (1996). The ear of alpha-adaptin interacts with the COOH-terminal domain of the Eps 15 protein. The Journal of biological chemistry *271*, 12111-12116.

Benmerah, A., Gagnon, J., Begue, B., Megarbane, B., Dautry-Varsat, A., and Cerf-Bensussan, N. (1995). The tyrosine kinase substrate eps15 is constitutively associated with the plasma membrane adaptor AP-2. The Journal of cell biology *131*, 1831-1838.

Benmerah, A., Lamaze, C., Begue, B., Schmid, S.L., Dautry-Varsat, A., and Cerf-Bensussan, N. (1998). AP-2/Eps15 interaction is required for receptor-mediated endocytosis. The Journal of cell biology *140*, 1055-1062.

Benmerah, A., Poupon, V., Cerf-Bensussan, N., and Dautry-Varsat, A. (2000). Mapping of Eps15 domains involved in its targeting to clathrin-coated pits. The Journal of biological chemistry *275*, 3288-3295.

Bernardini, M.L., Mounier, J., d'Hauteville, H., Coquis-Rondon, M., and Sansonetti, P.J. (1989). Identification of icsA, a plasmid locus of Shigella flexneri that governs bacterial intra- and intercellular spread through interaction with F-actin. Proceedings of the National Academy of Sciences of the United States of America *86*, 3867-3871.

Bernheim-Groswasser, A., Wiesner, S., Golsteyn, R.M., Carlier, M.F., and Sykes, C. (2002). The dynamics of actin-based motility depend on surface parameters. Nature *417*, 308-311.

Blanchoin, L., Amann, K.J., Higgs, H.N., Marchand, J.B., Kaiser, D.A., and Pollard, T.D. (2000). Direct observation of dendritic actin filament networks nucleated by Arp2/3 complex and WASP/Scar proteins. Nature *404*, 1007-1011.

Blanchoin, L., and Pollard, T.D. (2002). Hydrolysis of ATP by polymerized actin depends on the bound divalent cation but not profilin. Biochemistry *41*, 597-602.

Blasco, R., and Moss, B. (1992). Role of cell-associated enveloped vaccinia virus in cell-to-cell spread. Journal of virology *66*, 4170-4179.

Blasco, R., Sisler, J.R., and Moss, B. (1993). Dissociation of progeny vaccinia virus from the cell membrane is regulated by a viral envelope glycoprotein: effect of a point mutation in the lectin homology domain of the A34R gene. Journal of virology *67*, 3319-3325.

Blume, J.J., Halbach, A., Behrendt, D., Paulsson, M., and Plomann, M. (2007). EHD proteins are associated with tubular and vesicular compartments and interact with specific phospholipids. Experimental cell research *313*, 219-231.

Boettner, D.R., Friesen, H., Andrews, B., and Lemmon, S.K. (2011). Clathrin light chain directs endocytosis by influencing the binding of the yeast Hip1R homologue, Sla2, to F-actin. Mol Biol Cell *22*, 3699-3714.

Bonazzi, M., Vasudevan, L., Mallet, A., Sachse, M., Sartori, A., Prevost, M.C., Roberts, A., Taner, S.B., Wilbur, J.D., Brodsky, F.M.*, et al.* (2011). Clathrin phosphorylation is required for actin recruitment at sites of bacterial adhesion and internalization. The Journal of cell biology *195*, 525-536.

Bonder, E.M., Fishkind, D.J., and Mooseker, M.S. (1983). Direct measurement of critical concentrations and assembly rate constants at the two ends of an actin filament. Cell *34*, 491-501.

Boone, R.F., and Moss, B. (1978). Sequence complexity and relative abundance of vaccinia virus mRNA's synthesized in vivo and in vitro. Journal of virology *26*, 554-569.

Boulant, S., Kural, C., Zeeh, J.C., Ubelmann, F., and Kirchhausen, T. (2011). Actin dynamics counteract membrane tension during clathrin-mediated endocytosis. Nat Cell Biol *13*, 1124-1131.

Boulter, E., and Garcia-Mata, R. (2012). Analysis of the role of RhoGDI1 and isoprenylation in the degradation of RhoGTPases. Methods in molecular biology *827*, 97-105.

Boulter, E.A., and Appleyard, G. (1973). Differences between extracellular and intracellular forms of poxvirus and their implications. Progress in medical virology Fortschritte der medizinischen Virusforschung Progres en virologie medicale *16*, 86-108.

Brett, T.J., Legendre-Guillemin, V., McPherson, P.S., and Fremont, D.H. (2006). Structural definition of the F-actin-binding THATCH domain from HIP1R. Nature structural & molecular biology *13*, 121-130.

Brodsky, F.M. (2012). Diversity of clathrin function: new tricks for an old protein. Annu Rev Cell Dev Biol *28*, 309-336.

Brodsky, F.M., Chen, C.Y., Knuehl, C., Towler, M.C., and Wakeham, D.E. (2001). Biological basket weaving: formation and function of clathrin-coated vesicles. Annu Rev Cell Dev Biol *17*, 517-568.

Broyles, S.S. (2003). Vaccinia virus transcription. The Journal of general virology *84*, 2293-2303.

Bu, W., Lim, K.B., Yu, Y.H., Chou, A.M., Sudhaharan, T., and Ahmed, S. (2010). Cdc42 interaction with N-WASP and Toca-1 regulates membrane tubulation, vesicle formation and vesicle motility: implications for endocytosis. PloS one *5*, e12153.

Buller, R.M., Smith, G.L., Cremer, K., Notkins, A.L., and Moss, B. (1985). Decreased virulence of recombinant vaccinia virus expression vectors is associated with a thymidine kinase-negative phenotype. Nature *317*, 813-815.

Byrd, C.M., and Hruby, D.E. (2004). Construction of recombinant vaccinia virus: cloning into the thymidine kinase locus. Methods in molecular biology *269*, 31-40.

Cameron, L.A., Footer, M.J., van Oudenaarden, A., and Theriot, J.A. (1999). Motility of ActA protein-coated microspheres driven by actin polymerization. Proceedings of the National Academy of Sciences of the United States of America *96*, 4908-4913.

Campellone, K.G., and Welch, M.D. (2010). A nucleator arms race: cellular control of actin assembly. Nat Rev Mol Cell Biol *11*, 237-251.

Camus, G., Segura-Morales, C., Molle, D., Lopez-Verges, S., Begon-Pescia, C., Cazevieille, C., Schu, P., Bertrand, E., Berlioz-Torrent, C., and Basyuk, E. (2007). The clathrin adaptor complex AP-1 binds HIV-1 and MLV Gag and facilitates their budding. Mol Biol Cell *18*, 3193-3203.

Caplan, S., Naslavsky, N., Hartnell, L.M., Lodge, R., Polishchuk, R.S., Donaldson, J.G., and Bonifacino, J.S. (2002). A tubular EHD1-containing compartment involved in the recycling of major histocompatibility complex class I molecules to the plasma membrane. The EMBO journal *21*, 2557-2567.

Carbone, R., Fre, S., Iannolo, G., Belleudi, F., Mancini, P., Pelicci, P.G., Torrisi, M.R., and Di Fiore, P.P. (1997). eps15 and eps15R are essential components of the endocytic pathway. Cancer research *57*, 5498-5504.

Carlier, M.F., Nioche, P., Broutin-L'Hermite, I., Boujemaa, R., Le Clainche, C., Egile, C., Garbay, C., Ducruix, A., Sansonetti, P., and Pantaloni, D. (2000). GRB2 links signaling to actin assembly by enhancing interaction of neural Wiskott-Aldrich syndrome protein (N-WASp) with actin-related protein (ARP2/3) complex. The Journal of biological chemistry *275*, 21946-21952.

Carpentier, D.C., Gao, W.N., Ewles, H., Morgan, G.W., and Smith, G.L. (2015). Vaccinia virus protein complex F12/E2 interacts with kinesin light chain isoform 2 to engage the kinesin-1 motor complex. PLoS Pathog *11*, e1004723.

Carroll, S.Y., Stirling, P.C., Stimpson, H.E., Giesselmann, E., Schmitt, M.J., and Drubin, D.G. (2009). A yeast killer toxin screen provides insights into a/b toxin entry, trafficking, and killing mechanisms. Developmental cell *17*, 552-560.

Carter, G.C., Rodger, G., Murphy, B.J., Law, M., Krauss, O., Hollinshead, M., and Smith, G.L. (2003). Vaccinia virus cores are transported on microtubules. The Journal of general virology *84*, 2443-2458.

Chakrabarti, S., Sisler, J.R., and Moss, B. (1997). Compact, synthetic, vaccinia virus early/late promoter for protein expression. BioTechniques *23*, 1094-1097.

Chan, W.M., Rahman, M.M., and McFadden, G. (2013). Oncolytic myxoma virus: the path to clinic. Vaccine *31*, 4252-4258.

Chang, S.J., Chang, Y.X., Izmailyan, R., Tang, Y.L., and Chang, W. (2010). Vaccinia virus A25 and A26 proteins are fusion suppressors for mature virions and determine strain-specific virus entry pathways into HeLa, CHO-K1, and L cells. Journal of virology *84*, 8422-8432.

Chen, H., Fre, S., Slepnev, V.I., Capua, M.R., Takei, K., Butler, M.H., Di Fiore, P.P., and De Camilli, P. (1998). Epsin is an EH-domain-binding protein implicated in clathrin-mediated endocytosis. Nature *394*, 793-797.

Chen, W.J., Goldstein, J.L., and Brown, M.S. (1990). NPXY, a sequence often found in cytoplasmic tails, is required for coated pit-mediated internalization of the low density lipoprotein receptor. The Journal of biological chemistry *265*, 3116-3123.

Chen, X.J., Squarr, A.J., Stephan, R., Chen, B., Higgins, T.E., Barry, D.J., Martin, M.C., Rosen, M.K., Bogdan, S., and Way, M. (2014). Ena/VASP proteins cooperate with the WAVE complex to regulate the actin cytoskeleton. Developmental cell *30*, 569-584.

Chereau, D., Kerff, F., Graceffa, P., Grabarek, Z., Langsetmo, K., and Dominguez, R. (2005). Actin-bound structures of Wiskott-Aldrich syndrome protein (WASP)-homology domain 2 and the implications for filament assembly. Proceedings of the National Academy of Sciences of the United States of America *102*, 16644-16649.

Chiu, W.L., Lin, C.L., Yang, M.H., Tzou, D.L., and Chang, W. (2007). Vaccinia virus 4c (A26L) protein on intracellular mature virus binds to the extracellular cellular matrix laminin. Journal of virology *81*, 2149-2157.

Chung, C.S., Hsiao, J.C., Chang, Y.S., and Chang, W. (1998). A27L protein mediates vaccinia virus interaction with cell surface heparan sulfate. Journal of virology *72*, 1577-1585.

Cocucci, E., Aguet, F., Boulant, S., and Kirchhausen, T. (2012). The first five seconds in the life of a clathrin-coated pit. Cell *150*, 495-507.

Coda, L., Salcini, A.E., Confalonieri, S., Pelicci, G., Sorkina, T., Sorkin, A., Pelicci, P.G., and Di Fiore, P.P. (1998). Eps15R is a tyrosine kinase substrate with characteristics of a docking protein possibly involved in coated pits-mediated internalization. The Journal of biological chemistry *273*, 3003-3012.

Cohen, M.E., Xiao, Y., Eisenberg, R.J., Cohen, G.H., and Isaacs, S.N. (2011). Antibody against extracellular vaccinia virus (EV) protects mice through complement and Fc receptors. PloS one *6*, e20597.

Collins, B.M., McCoy, A.J., Kent, H.M., Evans, P.R., and Owen, D.J. (2002). Molecular architecture and functional model of the endocytic AP2 complex. Cell *109*, 523-535.

Condit, R.C. (2010). Surf and turf: mechanism of enhanced virus spread during poxvirus infection. Viruses *2*, 1050-1054.

Condit, R.C., Motyczka, A., and Spizz, G. (1983). Isolation, characterization, and physical mapping of temperature-sensitive mutants of vaccinia virus. Virology *128*, 429-443.

Condit, R.C., Moussatche, N., and Traktman, P. (2006). In a nutshell: structure and assembly of the vaccinia virion. Adv Virus Res *66*, 31-124.

Condit, R.C., and Niles, E.G. (2002). Regulation of viral transcription elongation and termination during vaccinia virus infection. Biochim Biophys Acta *1577*, 325-336.

Confalonieri, S., Salcini, A.E., Puri, C., Tacchetti, C., and Di Fiore, P.P. (2000). Tyrosine phosphorylation of Eps15 is required for ligand-regulated, but not constitutive, endocytosis. The Journal of cell biology *150*, 905-912.

Cossart, P., and Sansonetti, P.J. (2004). Bacterial invasion: the paradigms of enteroinvasive pathogens. Science *304*, 242-248.

Cossart, P., and Veiga, E. (2008). Non-classical use of clathrin during bacterial infections. J Microsc *231*, 524-528.

Cudmore, S., Cossart, P., Griffiths, G., and Way, M. (1995). Actin-based motility of vaccinia virus. Nature *378*, 636-638.

Cupers, P., Jadhav, A.P., and Kirchhausen, T. (1998). Assembly of clathrin coats disrupts the association between Eps15 and AP-2 adaptors. The Journal of biological chemistry *273*, 1847-1850.

Cupers, P., ter Haar, E., Boll, W., and Kirchhausen, T. (1997). Parallel dimers and anti-parallel tetramers formed by epidermal growth factor receptor pathway substrate clone 15. The Journal of biological chemistry *272*, 33430-33434.

Cureton, D.K., Massol, R.H., Saffarian, S., Kirchhausen, T.L., and Whelan, S.P. (2009). Vesicular stomatitis virus enters cells through vesicles incompletely coated with clathrin that depend upon actin for internalization. PLoS Pathog *5*, e1000394.

Cureton, D.K., Massol, R.H., Whelan, S.P., and Kirchhausen, T. (2010). The length of vesicular stomatitis virus particles dictates a need for actin assembly during clathrin-dependent endocytosis. PLoS Pathog *6*, e1001127.

Cyrklaff, M., Risco, C., Fernandez, J.J., Jimenez, M.V., Esteban, M., Baumeister, W., and Carrascosa, J.L. (2005). Cryo-electron tomography of vaccinia virus. Proceedings of the National Academy of Sciences of the United States of America *102*, 2772-2777.

Dahl, R., and Kates, J.R. (1970). Intracellular structures containing vaccinia DNA: isolation and characterization. Virology *42*, 453-462.

Dales, S., and Mosbach, E.H. (1968). Vaccinia as a model for membrane biogenesis. Virology *35*, 564-583.

Danino, D., and Hinshaw, J.E. (2001). Dynamin family of mechanoenzymes. Curr Opin Cell Biol *13*, 454-460.

Dannhauser, P.N., and Ungewickell, E.J. (2012). Reconstitution of clathrin-coated bud and vesicle formation with minimal components. Nat Cell Biol *14*, 634-639.

Dart, A.E., Donnelly, S.K., Holden, D.W., Way, M., and Caron, E. (2012). Nck and Cdc42 co-operate to recruit N-WASP to promote FcgammaR-mediated phagocytosis. Journal of cell science *125*, 2825-2830.

Daumke, O., Lundmark, R., Vallis, Y., Martens, S., Butler, P.J., and McMahon, H.T. (2007). Architectural and mechanistic insights into an EHD ATPase involved in membrane remodelling. Nature *449*, 923-927.

Davey, N.E., Van Roey, K., Weatheritt, R.J., Toedt, G., Uyar, B., Altenberg, B., Budd, A., Diella, F., Dinkel, H., and Gibson, T.J. (2012). Attributes of short linear motifs. Mol Biosyst *8*, 268-281.

de Beer, T., Carter, R.E., Lobel-Rice, K.E., Sorkin, A., and Overduin, M. (1998). Structure and Asn-Pro-Phe binding pocket of the Eps15 homology domain. Science *281*, 1357-1360.

de Beer, T., Hoofnagle, A.N., Enmon, J.L., Bowers, R.C., Yamabhai, M., Kay, B.K., and Overduin, M. (2000). Molecular mechanism of NPF recognition by EH domains. Nature structural biology *7*, 1018-1022.

DeFilippes, F.M. (1982). Restriction enzyme mapping of vaccinia virus DNA. Journal of virology *43*, 136-149.

Delatour, V., Helfer, E., Didry, D., Le, K.H., Gaucher, J.F., Carlier, M.F., and Romet-Lemonne, G. (2008). Arp2/3 controls the motile behavior of N-WASP-functionalized GUVs and modulates N-WASP surface distribution by mediating transient links with actin filaments. Biophys J *94*, 4890-4905.

Dell'Angelica, E.C., Klumperman, J., Stoorvogel, W., and Bonifacino, J.S. (1998). Association of the AP-3 adaptor complex with clathrin. Science *280*, 431-434.

Delom, F., and Fessart, D. (2011). Role of Phosphorylation in the Control of Clathrin-Mediated Internalization of GPCR. Int J Cell Biol *2011*, 246954.

Di Pietro, S.M., Cascio, D., Feliciano, D., Bowie, J.U., and Payne, G.S. (2010). Regulation of clathrin adaptor function in endocytosis: novel role for the SAM domain. The EMBO journal *29*, 1033-1044.

Dinkel, H., Van Roey, K., Michael, S., Davey, N.E., Weatheritt, R.J., Born, D., Speck, T., Kruger, D., Grebnev, G., Kuban, M.*, et al.* (2014). The eukaryotic linear motif resource ELM: 10 years and counting. Nucleic Acids Res *42*, D259-266.

Ditlev, J.A., Michalski, P.J., Huber, G., Rivera, G.M., Mohler, W.A., Loew, L.M., and Mayer, B.J. (2012). Stoichiometry of Nck-dependent actin polymerization in living cells. The Journal of cell biology *197*, 643-658.

Doceul, V., Hollinshead, M., Breiman, A., Laval, K., and Smith, G.L. (2012). Protein B5 is required on extracellular enveloped vaccinia virus for repulsion of superinfecting virions. The Journal of general virology *93*, 1876-1886.

Doceul, V., Hollinshead, M., van der Linden, L., and Smith, G.L. (2010). Repulsion of superinfecting virions: a mechanism for rapid virus spread. Science *327*, 873-876.

Dodding, M.P., Mitter, R., Humphries, A.C., and Way, M. (2011). A kinesin-1 binding motif in vaccinia virus that is widespread throughout the human genome. The EMBO journal *30*, 4523-4538.

Dodding, M.P., Newsome, T.P., Collinson, L.M., Edwards, C., and Way, M. (2009). An E2-F12 complex is required for intracellular enveloped virus morphogenesis during vaccinia infection. Cell Microbiol *11*, 808-824.

Dodding, M.P., and Way, M. (2009). Nck- and N-WASP-dependent actin-based motility is conserved in divergent vertebrate poxviruses. Cell host & microbe *6*, 536-550.

Domann, E., Wehland, J., Rohde, M., Pistor, S., Hartl, M., Goebel, W., Leimeister-Wachter, M., Wuenscher, M., and Chakraborty, T. (1992). A novel bacterial virulence gene in Listeria monocytogenes required for host cell microfilament interaction with homology to the proline-rich region of vinculin. The EMBO journal *11*, 1981-1990.

Domi, A., and Beaud, G. (2000). The punctate sites of accumulation of vaccinia virus early proteins are precursors of sites of viral DNA synthesis. The Journal of general virology *81*, 1231-1235.

Donnelly, S.K., Weisswange, I., Zettl, M., and Way, M. (2013). WIP Provides an Essential Link between Nck and N-WASP during Arp2/3-Dependent Actin Polymerization. Curr Biol *23*, 999-1006.

Doray, B., Lee, I., Knisely, J., Bu, G., and Kornfeld, S. (2007). The gamma/sigma1 and alpha/sigma2 hemicomplexes of clathrin adaptors AP-1 and AP-2 harbor the dileucine recognition site. Mol Biol Cell *18*, 1887-1896.

Doria, M., Salcini, A.E., Colombo, E., Parslow, T.G., Pelicci, P.G., and Di Fiore, P.P. (1999). The eps15 homology (EH) domain-based interaction between eps15 and hrb connects the molecular machinery of endocytosis to that of nucleocytosolic transport. The Journal of cell biology *147*, 1379-1384.

Drake, M.T., Downs, M.A., and Traub, L.M. (2000). Epsin binds to clathrin by associating directly with the clathrin-terminal domain. Evidence for cooperative binding through two discrete sites. The Journal of biological chemistry *275*, 6479-6489.

Drozdetskiy, A., Cole, C., Procter, J., and Barton, G.J. (2015). JPred4: a protein secondary structure prediction server. Nucleic Acids Res *43*, W389-394.

Dubochet, J., Adrian, M., Richter, K., Garces, J., and Wittek, R. (1994). Structure of intracellular mature vaccinia virus observed by cryoelectron microscopy. Journal of virology *68*, 1935-1941.

Duncan, M.C., Cope, M.J., Goode, B.L., Wendland, B., and Drubin, D.G. (2001). Yeast Eps15-like endocytic protein, Pan1p, activates the Arp2/3 complex. Nat Cell Biol *3*, 687-690.

Duncan, S.A., and Smith, G.L. (1992). Identification and characterization of an extracellular envelope glycoprotein affecting vaccinia virus egress. Journal of virology *66*, 1610-1621.

Earley, A.K., Chan, W.M., and Ward, B.M. (2008). The vaccinia virus B5 protein requires A34 for efficient intracellular trafficking from the endoplasmic reticulum to the site of wrapping and incorporation into progeny virions. Journal of virology *82*, 2161-2169.

Egile, C., Loisel, T.P., Laurent, V., Li, R., Pantaloni, D., Sansonetti, P.J., and Carlier, M.F. (1999). Activation of the CDC42 effector N-WASP by the Shigella flexneri IcsA protein promotes actin nucleation by Arp2/3 complex and bacterial actin-based motility. The Journal of cell biology *146*, 1319-1332.

Ehrlich, M., Boll, W., Van Oijen, A., Hariharan, R., Chandran, K., Nibert, M.L., and Kirchhausen, T. (2004). Endocytosis by random initiation and stabilization of clathrin-coated pits. Cell *118*, 591-605.

Engqvist-Goldstein, A.E., and Drubin, D.G. (2003). Actin assembly and endocytosis: from yeast to mammals. Annu Rev Cell Dev Biol *19*, 287-332.

Engqvist-Goldstein, A.E., Kessels, M.M., Chopra, V.S., Hayden, M.R., and Drubin, D.G. (1999). An actin-binding protein of the Sla2/Huntingtin interacting protein 1 family is a novel component of clathrin-coated pits and vesicles. The Journal of cell biology *147*, 1503-1518.

Engqvist-Goldstein, A.E., Warren, R.A., Kessels, M.M., Keen, J.H., Heuser, J., and Drubin, D.G. (2001). The actin-binding protein Hip1R associates with clathrin during early stages of endocytosis and promotes clathrin assembly in vitro. The Journal of cell biology *154*, 1209-1223.

Engqvist-Goldstein, A.E., Zhang, C.X., Carreno, S., Barroso, C., Heuser, J.E., and Drubin, D.G. (2004). RNAi-mediated Hip1R silencing results in stable association between the endocytic machinery and the actin assembly machinery. Mol Biol Cell *15*, 1666-1679.

Enmon, J.L., de Beer, T., and Overduin, M. (2000). Solution structure of Eps15's third EH domain reveals coincident Phe-Trp and Asn-Pro-Phe binding sites. Biochemistry *39*, 4309-4319.

Erickson, H.P. (2007). Evolution of the cytoskeleton. BioEssays : news and reviews in molecular, cellular and developmental biology *29*, 668-677.

Esteban, D.J., and Buller, R.M. (2005). Ectromelia virus: the causative agent of mousepox. The Journal of general virology *86*, 2645-2659.

Evgin, L., Vaha-Koskela, M., Rintoul, J., Falls, T., Le Boeuf, F., Barrett, J.W., Bell, J.C., and Stanford, M.M. (2010). Potent oncolytic activity of raccoonpox virus in the absence of natural pathogenicity. Mol Ther *18*, 896-902.

Fazioli, F., Minichiello, L., Matoskova, B., Wong, W.T., and Di Fiore, P.P. (1993). eps15, a novel tyrosine kinase substrate, exhibits transforming activity. Molecular and cellular biology *13*, 5814-5828.

Fernandez-Chacon, R., Achiriloaie, M., Janz, R., Albanesi, J.P., and Sudhof, T.C. (2000). SCAMP1 function in endocytosis. The Journal of biological chemistry *275*, 12752-12756.

Fingerhut, A., von Figura, K., and Honing, S. (2001). Binding of AP2 to sorting signals is modulated by AP2 phosphorylation. The Journal of biological chemistry *276*, 5476-5482.

Firat-Karalar, E.N., and Welch, M.D. (2011). New mechanisms and functions of actin nucleation. Curr Opin Cell Biol *23*, 4-13.

Fotin, A., Cheng, Y., Sliz, P., Grigorieff, N., Harrison, S.C., Kirchhausen, T., and Walz, T. (2004). Molecular model for a complete clathrin lattice from electron cryomicroscopy. Nature *432*, 573-579.

Friesland, A., Zhao, Y., Chen, Y.H., Wang, L., Zhou, H., and Lu, Q. (2013). Small molecule targeting Cdc42-intersectin interaction disrupts Golgi organization and suppresses cell motility. Proceedings of the National Academy of Sciences of the United States of America *110*, 1261-1266.

Frischknecht, F., Cudmore, S., Moreau, V., Reckmann, I., Rottger, S., and Way, M. (1999a). Tyrosine phosphorylation is required for actin-based motility of vaccinia but not Listeria or Shigella. Curr Biol *9*, 89-92.

Frischknecht, F., Moreau, V., Rottger, S., Gonfloni, S., Reckmann, I., Superti-Furga, G., and Way, M. (1999b). Actin-based motility of vaccinia virus mimics receptor tyrosine kinase signalling. Nature *401*, 926-929.

Fujimoto, L.M., Roth, R., Heuser, J.E., and Schmid, S.L. (2000). Actin assembly plays a variable, but not obligatory role in receptor-mediated endocytosis in mammalian cells. Traffic *1*, 161-171.

Gallusser, A., and Kirchhausen, T. (1993). The beta 1 and beta 2 subunits of the AP complexes are the clathrin coat assembly components. The EMBO journal *12*, 5237-5244.

Garcia, E., Jones, G.E., Machesky, L.M., and Anton, I.M. (2012). WIP: WASP-interacting proteins at invadopodia and podosomes. European journal of cell biology *91*, 869-877.

Garcia, E., Machesky, L.M., Jones, G.E., and Anton, I.M. (2014). WIP is necessary for matrix invasion by breast cancer cells. European journal of cell biology *93*, 413-423.

Gasman, S., Chasserot-Golaz, S., Malacombe, M., Way, M., and Bader, M.F. (2004). Regulated exocytosis in neuroendocrine cells: a role for subplasmalemmal Cdc42/N-WASP-induced actin filaments. Mol Biol Cell *15*, 520-531.

Geada, M.M., Galindo, I., Lorenzo, M.M., Perdiguero, B., and Blasco, R. (2001). Movements of vaccinia virus intracellular enveloped virions with GFP tagged to the F13L envelope protein. The Journal of general virology *82*, 2747-2760.

Geli, M.I., and Riezman, H. (1998). Endocytic internalization in yeast and animal cells: similar and different. Journal of cell science *111 (Pt 8)*, 1031-1037.

George, M., Ying, G., Rainey, M.A., Solomon, A., Parikh, P.T., Gao, Q., Band, V., and Band, H. (2007). Shared as well as distinct roles of EHD proteins revealed by biochemical and functional comparisons in mammalian cells and C. elegans. BMC Cell Biol *8*, 3.

Ghai, R., and Collins, B.M. (2011). PX-FERM proteins: A link between endosomal trafficking and signaling? Small GTPases *2*, 259-263.

Gilbert, H.R., and Frieden, C. (1983). Preparation, purification and properties of a crosslinked trimer of G-actin. Biochemical and biophysical research communications *111*, 404-408.

Goebel, S.J., Johnson, G.P., Perkus, M.E., Davis, S.W., Winslow, J.P., and Paoletti, E. (1990). The complete DNA sequence of vaccinia virus. Virology *179*, 247-266, 517-263.

Goldberg, M.B., and Theriot, J.A. (1995). Shigella flexneri surface protein IcsA is sufficient to direct actin-based motility. Proceedings of the National Academy of Sciences of the United States of America *92*, 6572-6576.

Goley, E.D., and Welch, M.D. (2006). The ARP2/3 complex: an actin nucleator comes of age. Nat Rev Mol Cell Biol *7*, 713-726.

Goode, B.L., Rodal, A.A., Barnes, G., and Drubin, D.G. (2001). Activation of the Arp2/3 complex by the actin filament binding protein Abp1p. The Journal of cell biology *153*, 627-634.

Gottlieb, T.A., Ivanov, I.E., Adesnik, M., and Sabatini, D.D. (1993). Actin microfilaments play a critical role in endocytosis at the apical but not the basolateral surface of polarized epithelial cells. The Journal of cell biology *120*, 695-710.

Grant, B.D., and Caplan, S. (2008). Mechanisms of EHD/RME-1 protein function in endocytic transport. Traffic *9*, 2043-2052.

Grassart, A., Cheng, A.T., Hong, S.H., Zhang, F., Zenzer, N., Feng, Y., Briner, D.M., Davis, G.D., Malkov, D., and Drubin, D.G. (2014). Actin and dynamin2 dynamics and interplay during clathrin-mediated endocytosis. The Journal of cell biology *205*, 721-735.

Grove, J., and Marsh, M. (2011). The cell biology of receptor-mediated virus entry. The Journal of cell biology *195*, 1071-1082.

Gruenberg, J. (2009). Viruses and endosome membrane dynamics. Curr Opin Cell Biol *21*, 582-588.

Gruenheid, S., DeVinney, R., Bladt, F., Goosney, D., Gelkop, S., Gish, G.D., Pawson, T., and Finlay, B.B. (2001). Enteropathogenic E. coli Tir binds Nck to initiate actin pedestal formation in host cells. Nat Cell Biol *3*, 856-859.

Gryaznova, T., Kropyvko, S., Burdyniuk, M., Gubar, O., Kryklyva, V., Tsyba, L., and Rynditch, A. (2015). Intersectin adaptor proteins are associated with actin-regulating protein WIP in invadopodia. Cellular signalling *27*, 1499-1508.

Gubser, C., Hue, S., Kellam, P., and Smith, G.L. (2004). Poxvirus genomes: a phylogenetic analysis. Journal of General Virology *85*, 105-117.

Guilherme, A., Soriano, N.A., Bose, S., Holik, J., Bose, A., Pomerleau, D.P., Furcinitti, P., Leszyk, J., Corvera, S., and Czech, M.P. (2004). EHD2 and the novel EH domain

binding protein EHBP1 couple endocytosis to the actin cytoskeleton. The Journal of biological chemistry *279*, 10593-10605.

Guipponi, M., Scott, H.S., Chen, H., Schebesta, A., Rossier, C., and Antonarakis, S.E. (1998). Two isoforms of a human intersectin (ITSN) protein are produced by brain-specific alternative splicing in a stop codon. Genomics *53*, 369-376.

Haffner, C., Di Paolo, G., Rosenthal, J.A., and de Camilli, P. (2000). Direct interaction of the 170 kDa isoform of synaptojanin 1 with clathrin and with the clathrin adaptor AP-2. Curr Biol *10*, 471-474.

Haffner, C., Takei, K., Chen, H., Ringstad, N., Hudson, A., Butler, M.H., Salcini, A.E., Di Fiore, P.P., and De Camilli, P. (1997). Synaptojanin 1: localization on coated endocytic intermediates in nerve terminals and interaction of its 170 kDa isoform with Eps15. FEBS letters *419*, 175-180.

Hagai, T., Azia, A., Babu, M.M., and Andino, R. (2014). Use of host-like peptide motifs in viral proteins is a prevalent strategy in host-virus interactions. Cell Rep *7*, 1729-1739.

Hall, A. (2012). Rho family GTPases. Biochemical Society transactions *40*, 1378-1382.

Hammond, E. (2007). Should the US and Russia destroy their stocks of smallpox virus? Brit Med J *334*, 776-776.

Handa, Y., Durkin, C.H., Dodding, M.P., and Way, M. (2013). Vaccinia virus F11 promotes viral spread by acting as a PDZ-containing scaffolding protein to bind myosin-9A and inhibit RhoA signaling. Cell host & microbe *14*, 51-62.

Heinzen, R.A., Hayes, S.F., Peacock, M.G., and Hackstadt, T. (1993). Directional actin polymerization associated with spotted fever group Rickettsia infection of Vero cells. Infection and immunity *61*, 1926-1935.

Heizmann, C.W., and Hunziker, W. (1991). Intracellular calcium-binding proteins: more sites than insights. Trends in biochemical sciences *16*, 98-103.

Henne, W.M., Boucrot, E., Meinecke, M., Evergren, E., Vallis, Y., Mittal, R., and McMahon, H.T. (2010). FCHo proteins are nucleators of clathrin-mediated endocytosis. Science *328*, 1281-1284.

Higgs, H.N., and Pollard, T.D. (2000). Activation by Cdc42 and PIP(2) of Wiskott-Aldrich syndrome protein (WASp) stimulates actin nucleation by Arp2/3 complex. The Journal of cell biology *150*, 1311-1320.

Hinrichsen, L., Harborth, J., Andrees, L., Weber, K., and Ungewickell, E.J. (2003). Effect of clathrin heavy chain- and alpha-adaptin-specific small inhibitory RNAs on endocytic accessory proteins and receptor trafficking in HeLa cells. The Journal of biological chemistry *278*, 45160-45170.

Hinshaw, J.E. (2000). Dynamin and its role in membrane fission. Annu Rev Cell Dev Biol *16*, 483-519.

Hirst, J., Barlow, L.D., Francisco, G.C., Sahlender, D.A., Seaman, M.N., Dacks, J.B., and Robinson, M.S. (2011). The fifth adaptor protein complex. PLoS Biol *9*, e1001170.

Hirst, J., Irving, C., and Borner, G.H. (2013). Adaptor protein complexes AP-4 and AP-5: new players in endosomal trafficking and progressive spastic paraplegia. Traffic *14*, 153-164.

Ho, H.Y., Rohatgi, R., Lebensohn, A.M., and Kirschner, M.W. (2006). In vitro reconstitution of cdc42-mediated actin assembly using purified components. Methods in enzymology *406*, 174-190.

Ho, H.Y., Rohatgi, R., Lebensohn, A.M., Le, M., Li, J., Gygi, S.P., and Kirschner, M.W. (2004). Toca-1 mediates Cdc42-dependent actin nucleation by activating the N-WASP-WIP complex. Cell *118*, 203-216.

Hoffmann, P.R., deCathelineau, A.M., Ogden, C.A., Leverrier, Y., Bratton, D.L., Daleke, D.L., Ridley, A.J., Fadok, V.A., and Henson, P.M. (2001). Phosphatidylserine (PS) induces PS receptor-mediated macropinocytosis and promotes clearance of apoptotic cells. The Journal of cell biology *155*, 649-659.

Hollinshead, M., Vanderplasschen, A., Smith, G.L., and Vaux, D.J. (1999). Vaccinia virus intracellular mature virions contain only one lipid membrane. Journal of virology *73*, 1503-1517.

Honing, S., Ricotta, D., Krauss, M., Spate, K., Spolaore, B., Motley, A., Robinson, M., Robinson, C., Haucke, V., and Owen, D.J. (2005). Phosphatidylinositol-(4,5)-bisphosphate regulates sorting signal recognition by the clathrin-associated adaptor complex AP2. Molecular cell *18*, 519-531.

Hood, F.E., and Royle, S.J. (2009). Functional equivalence of the clathrin heavy chains CHC17 and CHC22 in endocytosis and mitosis. Journal of cell science *122*, 2185-2190.

Horsington, J., Lynn, H., Turnbull, L., Cheng, D., Braet, F., Diefenbach, R.J., Whitchurch, C.B., Karupiah, G., and Newsome, T.P. (2013). A36-dependent Actin Filament Nucleation Promotes Release of Vaccinia Virus. PLoS Pathog *9*, e1003239.

Hruby, D.E., Guarino, L.A., and Kates, J.R. (1979). Vaccinia virus replication. I. Requirement for the host-cell nucleus. Journal of virology *29*, 705-715.

Hsiao, J.C., Chung, C.S., and Chang, W. (1999). Vaccinia virus envelope D8L protein binds to cell surface chondroitin sulfate and mediates the adsorption of intracellular mature virions to cells. Journal of virology *73*, 8750-8761.

Hu, Y., Lee, J., McCart, J.A., Xu, H., Moss, B., Alexander, H.R., and Bartlett, D.L. (2001). Yaba-like disease virus: an alternative replicating poxvirus vector for cancer gene therapy. Journal of virology *75*, 10300-10308.

Huang, J.H., Liu, Z.Q., Liu, S., Jiang, S., and Chen, Y.H. (2006). Identification of the HIV-1 gp41 core-binding motif--HXXNPF. FEBS letters *580*, 4807-4814.

Huang, J.H., Qi, Z., Wu, F., Kotula, L., Jiang, S., and Chen, Y.H. (2008). Interaction of HIV-1 gp41 core with NPF motif in Epsin: implication in endocytosis of HIV. The Journal of biological chemistry *283*, 14994-15002.

Huang, K.M., D'Hondt, K., Riezman, H., and Lemmon, S.K. (1999). Clathrin functions in the absence of heterotetrameric adaptors and AP180-related proteins in yeast. The EMBO journal *18*, 3897-3908.

Humphries, A.C., Dodding, M.P., Barry, D.J., Collinson, L.M., Durkin, C.H., and Way, M. (2012). Clathrin potentiates vaccinia-induced actin polymerization to facilitate viral spread. Cell host & microbe *12*, 346-359.

Humphries, A.C., Donnelly, S.K., and Way, M. (2014). Cdc42 and the Rho GEF intersectin-1 collaborate with Nck to promote N-WASP-dependent actin polymerisation. Journal of cell science *127*, 673-685.

Humphries, A.C., and Way, M. (2013). The non-canonical roles of clathrin and actin in pathogen internalization, egress and spread. Nature reviews Microbiology *11*, 551-560.

Husain, M., and Moss, B. (2003). Intracellular trafficking of a palmitoylated membrane-associated protein component of enveloped vaccinia virus. Journal of virology *77*, 9008-9019.

Husain, M., Weisberg, A.S., and Moss, B. (2006). Existence of an operative pathway from the endoplasmic reticulum to the immature poxvirus membrane. Proceedings of the National Academy of Sciences of the United States of America *103*, 19506-19511.

Husain, M., Weisberg, A.S., and Moss, B. (2007). Sequence-independent targeting of transmembrane proteins synthesized within vaccinia virus factories to nascent viral membranes. Journal of virology *81*, 2646-2655.

Hussain, N.K., Jenna, S., Glogauer, M., Quinn, C.C., Wasiak, S., Guipponi, M., Antonarakis, S.E., Kay, B.K., Stossel, T.P., Lamarche-Vane, N.*, et al.* (2001). Endocytic protein intersectin-l regulates actin assembly via Cdc42 and N-WASP. Nat Cell Biol *3*, 927-932.

Hussain, N.K., Yamabhai, M., Ramjaun, A.R., Guy, A.M., Baranes, D., O'Bryan, J.P., Der, C.J., Kay, B.K., and McPherson, P.S. (1999). Splice variants of intersectin are components of the endocytic machinery in neurons and nonneuronal cells. The Journal of biological chemistry *274*, 15671-15677.

Huxley, H.E. (1963). Electron Microscope Studies on the Structure of Natural and Synthetic Protein Filaments from Striated Muscle. Journal of molecular biology *7*, 281-308.

Hyun, T.S., Rao, D.S., Saint-Dic, D., Michael, L.E., Kumar, P.D., Bradley, S.V., Mizukami, I.F., Oravecz-Wilson, K.I., and Ross, T.S. (2004). HIP1 and HIP1r stabilize

receptor tyrosine kinases and bind 3-phosphoinositides via epsin N-terminal homology domains. The Journal of biological chemistry *279*, 14294-14306.

Iannolo, G., Salcini, A.E., Gaidarov, I., Goodman, O.B., Jr., Baulida, J., Carpenter, G., Pelicci, P.G., Di Fiore, P.P., and Keen, J.H. (1997). Mapping of the molecular determinants involved in the interaction between eps15 and AP-2. Cancer research *57*, 240-245.

Ichihashi, Y. (1996). Extracellular enveloped vaccinia virus escapes neutralization. Virology *217*, 478-485.

Innocenti, M., Gerboth, S., Rottner, K., Lai, F.P., Hertzog, M., Stradal, T.E., Frittoli, E., Didry, D., Polo, S., Disanza, A.*, et al.* (2005). Abi1 regulates the activity of N-WASP and WAVE in distinct actin-based processes. Nat Cell Biol *7*, 969-976.

Irwin, C.R., and Evans, D.H. (2012). Modulation of the myxoma virus plaque phenotype by vaccinia virus protein F11. Journal of virology *86*, 7167-7179.

Isaacs, S.N., Wolffe, E.J., Payne, L.G., and Moss, B. (1992). Characterization of a vaccinia virus-encoded 42-kilodalton class I membrane glycoprotein component of the extracellular virus envelope. Journal of virology *66*, 7217-7224.

Jackson, A.P., Seow, H.F., Holmes, N., Drickamer, K., and Parham, P. (1987). Clathrin light chains contain brain-specific insertion sequences and a region of homology with intermediate filaments. Nature *326*, 154-159.

Jackson, L.P., Kelly, B.T., McCoy, A.J., Gaffry, T., James, L.C., Collins, B.M., Honing, S., Evans, P.R., and Owen, D.J. (2010). A large-scale conformational change couples membrane recruitment to cargo binding in the AP2 clathrin adaptor complex. Cell *141*, 1220-1229.

Jenner, E. (1798). An Inquiry into the Causes and Effects of Variolae Vaccinae, a Disease Discovered in Some Western Counties of England.

Johannsdottir, H.K., Mancini, R., Kartenbeck, J., Amato, L., and Helenius, A. (2009). Host cell factors and functions involved in vesicular stomatitis virus entry. Journal of virology *83*, 440-453.

Johnston, S.C., and Ward, B.M. (2009). Vaccinia virus protein F12 associates with intracellular enveloped virions through an interaction with A36. Journal of virology *83*, 1708-1717.

Joklik, W.K., and Becker, Y. (1964). The Replication and Coating of Vaccinia DNA. Journal of molecular biology *10*, 452-474.

Kaksonen, M., Peng, H.B., and Rauvala, H. (2000). Association of cortactin with dynamic actin in lamellipodia and on endosomal vesicles. Journal of cell science *113 Pt 24*, 4421-4426.

Kaksonen, M., Toret, C.P., and Drubin, D.G. (2006). Harnessing actin dynamics for clathrin-mediated endocytosis. Nat Rev Mol Cell Biol *7*, 404-414.

Kalthoff, C., Alves, J., Urbanke, C., Knorr, R., and Ungewickell, E.J. (2002). Unusual structural organization of the endocytic proteins AP180 and epsin 1. The Journal of biological chemistry *277*, 8209-8216.

Katz, E., Ward, B.M., Weisberg, A.S., and Moss, B. (2003). Mutations in the vaccinia virus A33R and B5R envelope proteins that enhance release of extracellular virions and eliminate formation of actin-containing microvilli without preventing tyrosine phosphorylation of the A36R protein. Journal of virology *77*, 12266-12275.

Katz, E., Wolffe, E., and Moss, B. (2002). Identification of second-site mutations that enhance release and spread of vaccinia virus. Journal of virology *76*, 11637-11644.

Kay, B.K., Scholle, M.D., and Stevens, F.J. (2004). EH Domains and Their Ligands, in Modular Protein Domains (Weinheim, FRG: Wiley-VCH Verlag GmbH & Co).

Keen, J.H., Chestnut, M.H., and Beck, K.A. (1987). The clathrin coat assembly polypeptide complex. Autophosphorylation and assembly activities. The Journal of biological chemistry *262*, 3864-3871.

Keen, J.H., Willingham, M.C., and Pastan, I.H. (1979). Clathrin-coated vesicles: isolation, dissociation and factor-dependent reassociation of clathrin baskets. Cell *16*, 303-312.

Kelleher, J.F., Atkinson, S.J., and Pollard, T.D. (1995). Sequences, structural models, and cellular localization of the actin-related proteins Arp2 and Arp3 from Acanthamoeba. The Journal of cell biology *131*, 385-397.

Kelly, B.T., Graham, S.C., Liska, N., Dannhauser, P.N., Honing, S., Ungewickell, E.J., and Owen, D.J. (2014). Clathrin adaptors. AP2 controls clathrin polymerization with a membrane-activated switch. Science *345*, 459-463.

Kelly, B.T., McCoy, A.J., Spate, K., Miller, S.E., Evans, P.R., Honing, S., and Owen, D.J. (2008). A structural explanation for the binding of endocytic dileucine motifs by the AP2 complex. Nature *456*, 976-979.

Kelly, B.T., and Owen, D.J. (2011). Endocytic sorting of transmembrane protein cargo. Curr Opin Cell Biol *23*, 404-412.

Kenny, B. (1999). Phosphorylation of tyrosine 474 of the enteropathogenic Escherichia coli (EPEC) Tir receptor molecule is essential for actin nucleating activity and is preceded by additional host modifications. Molecular microbiology *31*, 1229-1241.

Kenny, B., DeVinney, R., Stein, M., Reinscheid, D.J., Frey, E.A., and Finlay, B.B. (1997). Enteropathogenic E. coli (EPEC) transfers its receptor for intimate adherence into mammalian cells. Cell *91*, 511-520.

Kessels, M.M., and Qualmann, B. (2004). The syndapin protein family: linking membrane trafficking with the cytoskeleton. Journal of cell science *117*, 3077-3086.

Keyel, P.A., Mishra, S.K., Roth, R., Heuser, J.E., Watkins, S.C., and Traub, L.M. (2006). A single common portal for clathrin-mediated endocytosis of distinct cargo governed by cargo-selective adaptors. Mol Biol Cell *17*, 4300-4317.

Kieken, F., Sharma, M., Jovic, M., Giridharan, S.S., Naslavsky, N., Caplan, S., and Sorgen, P.L. (2010). Mechanism for the selective interaction of C-terminal Eps15 homology domain proteins with specific Asn-Pro-Phe-containing partners. The Journal of biological chemistry *285*, 8687-8694.

Kim, A.S., Kakalis, L.T., Abdul-Manan, N., Liu, G.A., and Rosen, M.K. (2000). Autoinhibition and activation mechanisms of the Wiskott-Aldrich syndrome protein. Nature *404*, 151-158.

Kintscher, C., Wuertenberger, S., Eylenstein, R., Uhlendorf, T., and Groemping, Y. (2010). Autoinhibition of GEF activity in Intersectin 1 is mediated by the short SH3-DH domain linker. Protein science : a publication of the Protein Society *19*, 2164-2174.

Kirchhausen, T. (1999). Adaptors for clathrin-mediated traffic. Annu Rev Cell Dev Biol *15*, 705-732.

Kirchhausen, T., Bonifacino, J.S., and Riezman, H. (1997). Linking cargo to vesicle formation: receptor tail interactions with coat proteins. Curr Opin Cell Biol *9*, 488-495.

Kirchhausen, T., and Harrison, S.C. (1981). Protein organization in clathrin trimers. Cell *23*, 755-761.

Kirchhausen, T., Harrison, S.C., Chow, E.P., Mattaliano, R.J., Ramachandran, K.L., Smart, J., and Brosius, J. (1987). Clathrin heavy chain: molecular cloning and complete primary structure. Proceedings of the National Academy of Sciences of the United States of America *84*, 8805-8809.

Kirchhausen, T., Owen, D., and Harrison, S.C. (2014). Molecular structure, function, and dynamics of clathrin-mediated membrane traffic. Cold Spring Harbor perspectives in biology *6*, a016725.

Klumperman, J., Hille, A., Veenendaal, T., Oorschot, V., Stoorvogel, W., von Figura, K., and Geuze, H.J. (1993). Differences in the endosomal distributions of the two mannose 6-phosphate receptors. The Journal of cell biology *121*, 997-1010.

Kochneva, G.V., Sivolobova, G.F., Iudina, K.V., Babkin, I.V., Chumakov, P.M., and Netesov, S.V. (2012). [Oncolytic poxviruses]. Mol Gen Mikrobiol Virusol, 8-15.

Kocks, C., Gouin, E., Tabouret, M., Berche, P., Ohayon, H., and Cossart, P. (1992). L. monocytogenes-induced actin assembly requires the actA gene product, a surface protein. Cell *68*, 521-531.

Kocks, C., Marchand, J.B., Gouin, E., d'Hauteville, H., Sansonetti, P.J., Carlier, M.F., and Cossart, P. (1995). The unrelated surface proteins ActA of Listeria monocytogenes and IcsA of Shigella flexneri are sufficient to confer actin-based motility on Listeria innocua and Escherichia coli respectively. Molecular microbiology *18*, 413-423.

Koh, T.W., Verstreken, P., and Bellen, H.J. (2004). Dap160/intersectin acts as a stabilizing scaffold required for synaptic development and vesicle endocytosis. Neuron *43*, 193-205.

Konecna, A., Frischknecht, R., Kinter, J., Ludwig, A., Steuble, M., Meskenaite, V., Indermuhle, M., Engel, M., Cen, C., Mateos, J.M.*, et al.* (2006). Calsyntenin-1 docks vesicular cargo to kinesin-1. Mol Biol Cell *17*, 3651-3663.

Kosaka, T., and Ikeda, K. (1983). Reversible blockage of membrane retrieval and endocytosis in the garland cell of the temperature-sensitive mutant of Drosophila melanogaster, shibirets1. The Journal of cell biology *97*, 499-507.

Lakadamyali, M., Rust, M.J., and Zhuang, X. (2006). Ligands for clathrin-mediated endocytosis are differentially sorted into distinct populations of early endosomes. Cell *124*, 997-1009.

Laliberte, J.P., and Moss, B. (2009). Appraising the apoptotic mimicry model and the role of phospholipids for poxvirus entry. Proceedings of the National Academy of Sciences of the United States of America *106*, 17517-17521.

Laliberte, J.P., and Moss, B. (2014). A novel mode of poxvirus superinfection exclusion that prevents fusion of the lipid bilayers of viral and cellular membranes. Journal of virology *88*, 9751-9768.

Laliberte, J.P., Weisberg, A.S., and Moss, B. (2011). The membrane fusion step of vaccinia virus entry is cooperatively mediated by multiple viral proteins and host cell components. PLoS Pathog *7*, e1002446.

Lamaze, C., Fujimoto, L.M., Yin, H.L., and Schmid, S.L. (1997). The actin cytoskeleton is required for receptor-mediated endocytosis in mammalian cells. The Journal of biological chemistry *272*, 20332-20335.

Law, M., Carter, G.C., Roberts, K.L., Hollinshead, M., and Smith, G.L. (2006). Ligand-induced and nonfusogenic dissolution of a viral membrane. Proceedings of the National Academy of Sciences of the United States of America *103*, 5989-5994.

Law, M., Hollinshead, R., and Smith, G.L. (2002). Antibody-sensitive and antibody-resistant cell-to-cell spread by vaccinia virus: role of the A33R protein in antibody-resistant spread. The Journal of general virology *83*, 209-222.

Law, M., and Smith, G.L. (2001). Antibody neutralization of the extracellular enveloped form of vaccinia virus. Virology *280*, 132-142.

Le Clainche, C., and Carlier, M.F. (2008). Regulation of actin assembly associated with protrusion and adhesion in cell migration. Physiol Rev *88*, 489-513.

Le Clainche, C., Pauly, B.S., Zhang, C.X., Engqvist-Goldstein, A.E., Cunningham, K., and Drubin, D.G. (2007). A Hip1R-cortactin complex negatively regulates actin assembly associated with endocytosis. The EMBO journal *26*, 1199-1210.

Lee, E., and De Camilli, P. (2002). Dynamin at actin tails. Proceedings of the National Academy of Sciences of the United States of America *99*, 161-166.

Legendre-Guillemin, V., Metzler, M., Lemaire, J.F., Philie, J., Gan, L., Hayden, M.R., and McPherson, P.S. (2005). Huntingtin interacting protein 1 (HIP1) regulates clathrin assembly through direct binding to the regulatory region of the clathrin light chain. The Journal of biological chemistry *280*, 6101-6108.

Leite, F., and Way, M. (2015). The role of signalling and the cytoskeleton during Vaccinia Virus egress. Virus research.

Letunic, I., Doerks, T., and Bork, P. (2015). SMART: recent updates, new developments and status in 2015. Nucleic Acids Res *43*, D257-260.

Lewit-Bentley, A., and Rety, S. (2000). EF-hand calcium-binding proteins. Curr Opin Struct Biol *10*, 637-643.

Lin, A.E., Benmerah, A., and Guttman, J.A. (2011). Eps15 and Epsin1 are crucial for enteropathogenic Escherichia coli pedestal formation despite the absence of adaptor protein 2. The Journal of infectious diseases *204*, 695-703.

Lin, C.L., Chung, C.S., Heine, H.G., and Chang, W. (2000). Vaccinia virus envelope H3L protein binds to cell surface heparan sulfate and is important for intracellular mature virion morphogenesis and virus infection in vitro and in vivo. Journal of virology *74*, 3353-3365.

Liu, A.P., Loerke, D., Schmid, S.L., and Danuser, G. (2009). Global and local regulation of clathrin-coated pit dynamics detected on patterned substrates. Biophys J *97*, 1038-1047.

Liu, S.H., Towler, M.C., Chen, E., Chen, C.Y., Song, W., Apodaca, G., and Brodsky, F.M. (2001). A novel clathrin homolog that co-distributes with cytoskeletal components functions in the trans-Golgi network. The EMBO journal *20*, 272-284.

Liu, S.H., Wong, M.L., Craik, C.S., and Brodsky, F.M. (1995). Regulation of clathrin assembly and trimerization defined using recombinant triskelion hubs. Cell *83*, 257-267.

Locker, J.K., Kuehn, A., Schleich, S., Rutter, G., Hohenberg, H., Wepf, R., and Griffiths, G. (2000). Entry of the two infectious forms of vaccinia virus at the plasma membane is signaling-dependent for the IMV but not the EEV. Mol Biol Cell *11*, 2497-2511.

Loerke, D., Mettlen, M., Yarar, D., Jaqaman, K., Jaqaman, H., Danuser, G., and Schmid, S.L. (2009). Cargo and dynamin regulate clathrin-coated pit maturation. PLoS Biol *7*, e57.

Loisel, T.P., Boujemaa, R., Pantaloni, D., and Carlier, M.F. (1999). Reconstitution of actin-based motility of Listeria and Shigella using pure proteins. Nature *401*, 613-616.

Lynn, H., Horsington, J., Ter, L.K., Han, S., Chew, Y.L., Diefenbach, R.J., Way, M., Chaudhri, G., Karupiah, G., and Newsome, T.P. (2012). Loss of cytoskeletal transport during egress critically attenuates ectromelia virus infection in vivo. Journal of virology *86*, 7427-7443.

Ma, L., Cantley, L.C., Janmey, P.A., and Kirschner, M.W. (1998). Corequirement of specific phosphoinositides and small GTP-binding protein Cdc42 in inducing actin assembly in Xenopus egg extracts. The Journal of cell biology *140*, 1125-1136.

Machesky, L.M., Atkinson, S.J., Ampe, C., Vandekerckhove, J., and Pollard, T.D. (1994). Purification of a cortical complex containing two unconventional actins from Acanthamoeba by affinity chromatography on profilin-agarose. The Journal of cell biology *127*, 107-115.

Machesky, L.M., Mullins, R.D., Higgs, H.N., Kaiser, D.A., Blanchoin, L., May, R.C., Hall, M.E., and Pollard, T.D. (1999). Scar, a WASp-related protein, activates nucleation of actin filaments by the Arp2/3 complex. Proceedings of the National Academy of Sciences of the United States of America *96*, 3739-3744.

Marchand, J.B., Kaiser, D.A., Pollard, T.D., and Higgs, H.N. (2001). Interaction of WASP/Scar proteins with actin and vertebrate Arp2/3 complex. Nat Cell Biol *3*, 76-82.

Marie, B., Sweeney, S.T., Poskanzer, K.E., Roos, J., Kelly, R.B., and Davis, G.W. (2004). Dap160/intersectin scaffolds the periactive zone to achieve high-fidelity endocytosis and normal synaptic growth. Neuron *43*, 207-219.

Maritzen, T., Schmidt, M.R., Kukhtina, V., Higman, V.A., Strauss, H., Volkmer, R., Oschkinat, H., Dotti, C.G., and Haucke, V. (2010). A novel subtype of AP-1-binding motif within the palmitoylated trans-Golgi network/endosomal accessory protein Gadkin/gamma-BAR. The Journal of biological chemistry *285*, 4074-4086.

Marsh, M., and Helenius, A. (2006). Virus entry: open sesame. Cell *124*, 729-740.

Martina, J.A., Bonangelino, C.J., Aguilar, R.C., and Bonifacino, J.S. (2001). Stonin 2: an adaptor-like protein that interacts with components of the endocytic machinery. The Journal of cell biology *153*, 1111-1120.

Martinez-Quiles, N., Rohatgi, R., Anton, I.M., Medina, M., Saville, S.P., Miki, H., Yamaguchi, H., Takenawa, T., Hartwig, J.H., Geha, R.S.*, et al.* (2001). WIP regulates N-WASP-mediated actin polymerization and filopodium formation. Nat Cell Biol *3*, 484-491.

Massol, R.H., Boll, W., Griffin, A.M., and Kirchhausen, T. (2006). A burst of auxilin recruitment determines the onset of clathrin-coated vesicle uncoating. Proceedings of the National Academy of Sciences of the United States of America *103*, 10265-10270.

Matsui, Y., Kikuchi, A., Araki, S., Hata, Y., Kondo, J., Teranishi, Y., and Takai, Y. (1990). Molecular cloning and characterization of a novel type of regulatory protein (GDI) for smg p25A, a ras p21-like GTP-binding protein. Molecular and cellular biology *10*, 4116-4122.

Maurer, M.E., and Cooper, J.A. (2006). The adaptor protein Dab2 sorts LDL receptors into coated pits independently of AP-2 and ARH. Journal of cell science *119*, 4235-4246.

Mayr, A. (2003). Smallpox vaccination and bioterrorism with pox viruses. Comp Immunol Microbiol Infect Dis *26*, 423-430.

McCann, R.O., and Craig, S.W. (1997). The I/LWEQ module: a conserved sequence that signifies F-actin binding in functionally diverse proteins from yeast to mammals. Proceedings of the National Academy of Sciences of the United States of America *94*, 5679-5684.

McFadden, G. (2005). Poxvirus tropism. Nature reviews Microbiology *3*, 201-213.

McGavin, M.K., Badour, K., Hardy, L.A., Kubiseski, T.J., Zhang, J., and Siminovitch, K.A. (2001). The intersectin 2 adaptor links Wiskott Aldrich Syndrome protein (WASp)-mediated actin polymerization to T cell antigen receptor endocytosis. The Journal of experimental medicine *194*, 1777-1787.

McMahon, H.T. (1999). Endocytosis: an assembly protein for clathrin cages. Curr Biol *9*, R332-335.

McMahon, H.T., and Boucrot, E. (2011). Molecular mechanism and physiological functions of clathrin-mediated endocytosis. Nat Rev Mol Cell Biol *12*, 517-533.

McNiven, M.A., Kim, L., Krueger, E.W., Orth, J.D., Cao, H., and Wong, T.W. (2000). Regulated interactions between dynamin and the actin-binding protein cortactin modulate cell shape. The Journal of cell biology *151*, 187-198.

Mercer, J., and Helenius, A. (2008). Vaccinia virus uses macropinocytosis and apoptotic mimicry to enter host cells. Science *320*, 531-535.

Mercer, J., and Helenius, A. (2009). Virus entry by macropinocytosis. Nat Cell Biol *11*, 510-520.

Mercer, J., Schelhaas, M., and Helenius, A. (2010). Virus entry by endocytosis. Annu Rev Biochem *79*, 803-833.

Merrifield, C.J. (2004). Seeing is believing: imaging actin dynamics at single sites of endocytosis. Trends in cell biology *14*, 352-358.

Merrifield, C.J., Feldman, M.E., Wan, L., and Almers, W. (2002). Imaging actin and dynamin recruitment during invagination of single clathrin-coated pits. Nat Cell Biol *4*, 691-698.

Merrifield, C.J., and Kaksonen, M. (2014). Endocytic accessory factors and regulation of clathrin-mediated endocytosis. Cold Spring Harbor perspectives in biology *6*, a016733.

Merrifield, C.J., Moss, S.E., Ballestrem, C., Imhof, B.A., Giese, G., Wunderlich, I., and Almers, W. (1999). Endocytic vesicles move at the tips of actin tails in cultured mast cells. Nat Cell Biol *1*, 72-74.

Messa, M., Fernandez-Busnadiego, R., Sun, E.W., Chen, H., Czapla, H., Wrasman, K., Wu, Y., Ko, G., Ross, T., Wendland, B*., et al.* (2014). Epsin deficiency impairs endocytosis by stalling the actin-dependent invagination of endocytic clathrin-coated pits. Elife *3*, e03311.

Mettlen, M., Stoeber, M., Loerke, D., Antonescu, C.N., Danuser, G., and Schmid, S.L. (2009). Endocytic accessory proteins are functionally distinguished by their differential effects on the maturation of clathrin-coated pits. Mol Biol Cell *20*, 3251-3260.

Meyer, C., Zizioli, D., Lausmann, S., Eskelinen, E.L., Hamann, J., Saftig, P., von Figura, K., and Schu, P. (2000). mu1A-adaptin-deficient mice: lethality, loss of AP-1 binding and rerouting of mannose 6-phosphate receptors. The EMBO journal *19*, 2193-2203.

Miele, A.E., Watson, P.J., Evans, P.R., Traub, L.M., and Owen, D.J. (2004). Two distinct interaction motifs in amphiphysin bind two independent sites on the clathrin terminal domain beta-propeller. Nature structural & molecular biology *11*, 242-248.

Miki, H., Miura, K., and Takenawa, T. (1996). N-WASP, a novel actin-depolymerizing protein, regulates the cortical cytoskeletal rearrangement in a PIP2-dependent manner downstream of tyrosine kinases. The EMBO journal *15*, 5326-5335.

Miki, H., Sasaki, T., Takai, Y., and Takenawa, T. (1998). Induction of filopodium formation by a WASP-related actin-depolymerizing protein N-WASP. Nature *391*, 93-96.

Mitsunari, T., Nakatsu, F., Shioda, N., Love, P.E., Grinberg, A., Bonifacino, J.S., and Ohno, H. (2005). Clathrin adaptor AP-2 is essential for early embryonal development. Molecular and cellular biology *25*, 9318-9323.

Mooren, O.L., Galletta, B.J., and Cooper, J.A. (2012). Roles for actin assembly in endocytosis. Annu Rev Biochem *81*, 661-686.

Moreau, V., Frischknecht, F., Reckmann, I., Vincentelli, R., Rabut, G., Stewart, D., and Way, M. (2000). A complex of N-WASP and WIP integrates signalling cascades that lead to actin polymerization. Nat Cell Biol *2*, 441-448.

Morgan, G.W., Hollinshead, M., Ferguson, B.J., Murphy, B.J., Carpentier, D.C., and Smith, G.L. (2010). Vaccinia protein F12 has structural similarity to kinesin light chain and contains a motor binding motif required for virion export. PLoS Pathog *6*, e1000785.

Morgan, J.R., Prasad, K., Jin, S., Augustine, G.J., and Lafer, E.M. (2003). Eps15 homology domain-NPF motif interactions regulate clathrin coat assembly during synaptic vesicle recycling. The Journal of biological chemistry *278*, 33583-33592.

Morris, S.M., and Cooper, J.A. (2001). Disabled-2 colocalizes with the LDLR in clathrin-coated pits and interacts with AP-2. Traffic *2*, 111-123.

Moss, B. (1990). Regulation of vaccinia virus transcription. Annu Rev Biochem *59*, 661-688.

Moss, B., and Ward, B.M. (2001). High-speed mass transit for poxviruses on microtubules. Nat Cell Biol *3*, E245-246.

Motley, A., Bright, N.A., Seaman, M.N., and Robinson, M.S. (2003). Clathrin-mediated endocytosis in AP-2-depleted cells. The Journal of cell biology *162*, 909-918.

Mullins, R.D., Heuser, J.A., and Pollard, T.D. (1998). The interaction of Arp2/3 complex with actin: nucleation, high affinity pointed end capping, and formation of branching networks of filaments. Proceedings of the National Academy of Sciences of the United States of America *95*, 6181-6186.

Nakashima, S., Morinaka, K., Koyama, S., Ikeda, M., Kishida, M., Okawa, K., Iwamatsu, A., Kishida, S., and Kikuchi, A. (1999). Small G protein Ral and its downstream molecules regulate endocytosis of EGF and insulin receptors. The EMBO journal *18*, 3629-3642.

Naslavsky, N., McKenzie, J., Altan-Bonnet, N., Sheff, D., and Caplan, S. (2009). EHD3 regulates early-endosome-to-Golgi transport and preserves Golgi morphology. Journal of cell science *122*, 389-400.

Naslavsky, N., Rahajeng, J., Sharma, M., Jovic, M., and Caplan, S. (2006). Interactions between EHD proteins and Rab11-FIP2: a role for EHD3 in early endosomal transport. Mol Biol Cell *17*, 163-177.

Newmark, P. (1980). Smallpox: gone for good? Nature *285*, 62.

Newsome, T.P., Scaplehorn, N., and Way, M. (2004). SRC mediates a switch from microtubule- to actin-based motility of vaccinia virus. Science *306*, 124-129.

Newsome, T.P., Weisswange, I., Frischknecht, F., and Way, M. (2006). Abl collaborates with Src family kinases to stimulate actin-based motility of vaccinia virus. Cell Microbiol *8*, 233-241.

Nishida, E., and Sakai, H. (1983). Kinetic analysis of actin polymerization. Journal of biochemistry *93*, 1011-1020.

Norbury, C.C. (2006). Drinking a lot is good for dendritic cells. Immunology *117*, 443-451.

Offenhauser, N., Santolini, E., Simeone, A., and Di Fiore, P.P. (2000). Differential patterns of expression of Eps15 and Eps15R during mouse embryogenesis. Mech Dev *95*, 309-312.

Ohno, H. (2006). Clathrin-associated adaptor protein complexes. Journal of cell science *119*, 3719-3721.

Ohno, H., Stewart, J., Fournier, M.C., Bosshart, H., Rhee, I., Miyatake, S., Saito, T., Gallusser, A., Kirchhausen, T., and Bonifacino, J.S. (1995). Interaction of tyrosine-based sorting signals with clathrin-associated proteins. Science *269*, 1872-1875.

Okamoto, M., Schoch, S., and Sudhof, T.C. (1999). EHSH1/intersectin, a protein that contains EH and SH3 domains and binds to dynamin and SNAP-25. A protein connection between exocytosis and endocytosis? The Journal of biological chemistry *274*, 18446-18454.

Oldstone, M. (1998). Viruses, Plagues, and History (Oxford University Press).

Orth, J.D., Krueger, E.W., Cao, H., and McNiven, M.A. (2002). The large GTPase dynamin regulates actin comet formation and movement in living cells. Proceedings of the National Academy of Sciences of the United States of America *99*, 167-172.

Otsuki, M., Itoh, T., and Takenawa, T. (2003). Neural Wiskott-Aldrich syndrome protein is recruited to rafts and associates with endophilin A in response to epidermal growth factor. The Journal of biological chemistry *278*, 6461-6469.

Owen, D.J., Collins, B.M., and Evans, P.R. (2004). Adaptors for clathrin coats: structure and function. Annu Rev Cell Dev Biol *20*, 153-191.

Owen, D.J., and Evans, P.R. (1998). A structural explanation for the recognition of tyrosine-based endocytotic signals. Science *282*, 1327-1332.

Padrick, S.B., Cheng, H.C., Ismail, A.M., Panchal, S.C., Doolittle, L.K., Kim, S., Skehan, B.M., Umetani, J., Brautigam, C.A., Leong, J.M*., et al.* (2008). Hierarchical regulation of WASP/WAVE proteins. Molecular cell *32*, 426-438.

Padrick, S.B., Doolittle, L.K., Brautigam, C.A., King, D.S., and Rosen, M.K. (2011). Arp2/3 complex is bound and activated by two WASP proteins. Proceedings of the National Academy of Sciences of the United States of America *108*, E472-479.

Page, L.J., and Robinson, M.S. (1995). Targeting signals and subunit interactions in coated vesicle adaptor complexes. The Journal of cell biology *131*, 619-630.

Panchal, S.C., Kaiser, D.A., Torres, E., Pollard, T.D., and Rosen, M.K. (2003). A conserved amphipathic helix in WASP/Scar proteins is essential for activation of Arp2/3 complex. Nature structural biology *10*, 591-598.

Panner, B.J., and Honig, C.R. (1967). Filament ultrastructure and organization in vertebrate smooth muscle. Contraction hypothesis based on localization of actin and myosin. The Journal of cell biology *35*, 303-321.

Paoletti, E., and Grady, L.J. (1977). Transcriptional complexity of vaccinia virus in vivo and in vitro. Journal of virology *23*, 608-615.

Paoluzi, S., Castagnoli, L., Lauro, I., Salcini, A.E., Coda, L., Fre, S., Confalonieri, S., Pelicci, P.G., Di Fiore, P.P., and Cesareni, G. (1998). Recognition specificity of individual EH domains of mammals and yeast. The EMBO journal *17*, 6541-6550.

Parkinson, J.E., and Smith, G.L. (1994). Vaccinia virus gene A36R encodes a M(r) 43-50 K protein on the surface of extracellular enveloped virus. Virology *204*, 376-390.

Payne, L.G. (1980). Significance of extracellular enveloped virus in the in vitro and in vivo dissemination of vaccinia. The Journal of general virology *50*, 89-100.

Payne, L.G., and Kristenson, K. (1979). Mechanism of vaccinia virus release and its specific inhibition by N1-isonicotinoyl-N2-3-methyl-4-chlorobenzoylhydrazine. Journal of virology *32*, 614-622.

Pearse, B.M. (1976). Clathrin: a unique protein associated with intracellular transfer of membrane by coated vesicles. Proceedings of the National Academy of Sciences of the United States of America *73*, 1255-1259.

Pearse, B.M., and Bretscher, M.S. (1981). Membrane recycling by coated vesicles. Annu Rev Biochem *50*, 85-101.

Pearse, B.M., and Robinson, M.S. (1984). Purification and properties of 100-kd proteins from coated vesicles and their reconstitution with clathrin. The EMBO journal *3*, 1951-1957.

Pechstein, A., Bacetic, J., Vahedi-Faridi, A., Gromova, K., Sundborger, A., Tomlin, N., Krainer, G., Vorontsova, O., Schafer, J.G., Owe, S.G.*, et al.* (2010). Regulation of synaptic vesicle recycling by complex formation between intersectin 1 and the clathrin adaptor complex AP2. Proceedings of the National Academy of Sciences of the United States of America *107*, 4206-4211.

Peden, A.A., Rudge, R.E., Lui, W.W., and Robinson, M.S. (2002). Assembly and function of AP-3 complexes in cells expressing mutant subunits. The Journal of cell biology *156*, 327-336.

Pelkmans, L., and Helenius, A. (2003). Insider information: what viruses tell us about endocytosis. Curr Opin Cell Biol *15*, 414-422.

Pennington, T.H. (1974). Vaccinia virus polypeptide synthesis: sequential appearance and stability of pre- and post-replicative polypeptides. The Journal of general virology *25*, 433-444.

Phillips, N., Hayward, R.D., and Koronakis, V. (2004). Phosphorylation of the enteropathogenic E. coli receptor by the Src-family kinase c-Fyn triggers actin pedestal formation. Nat Cell Biol *6*, 618-625.

Pizarro-Cerda, J., Bonazzi, M., and Cossart, P. (2010). Clathrin-mediated endocytosis: what works for small, also works for big. BioEssays : news and reviews in molecular, cellular and developmental biology *32*, 496-504.

Ploubidou, A., Moreau, V., Ashman, K., Reckmann, I., Gonzalez, C., and Way, M. (2000). Vaccinia virus infection disrupts microtubule organization and centrosome function. The EMBO journal *19*, 3932-3944.

Pollard, T.D. (2007). Regulation of actin filament assembly by Arp2/3 complex and formins. Annu Rev Biophys Biomol Struct *36*, 451-477.

Pollard, T.D., and Borisy, G.G. (2003). Cellular motility driven by assembly and disassembly of actin filaments. Cell *112*, 453-465.

Pollard, T.D., and Cooper, J.A. (1986). Actin and actin-binding proteins. A critical evaluation of mechanisms and functions. Annu Rev Biochem *55*, 987-1035.

Pollard, T.D., and Weeds, A.G. (1984). The rate constant for ATP hydrolysis by polymerized actin. FEBS letters *170*, 94-98.

Pond, L., Kuhn, L.A., Teyton, L., Schutze, M.P., Tainer, J.A., Jackson, M.R., and Peterson, P.A. (1995). A role for acidic residues in di-leucine motif-based targeting to the endocytic pathway. The Journal of biological chemistry *270*, 19989-19997.

Postigo, A., Cross, J.R., Downward, J., and Way, M. (2006). Interaction of F1L with the BH3 domain of Bak is responsible for inhibiting vaccinia-induced apoptosis. Cell Death Differ *13*, 1651-1662.

Postigo, A., and Ferrer, P.E. (2009). Viral inhibitors reveal overlapping themes in regulation of cell death and innate immunity. Microbes Infect *11*, 1071-1078.

Poupon, V., Polo, S., Vecchi, M., Martin, G., Dautry-Varsat, A., Cerf-Bensussan, N., Di Fiore, P.P., and Benmerah, A. (2002). Differential nucleocytoplasmic trafficking between the related endocytic proteins Eps15 and Eps15R. The Journal of biological chemistry *277*, 8941-8948.

Prehoda, K.E., Scott, J.A., Mullins, R.D., and Lim, W.A. (2000). Integration of multiple signals through cooperative regulation of the N-WASP-Arp2/3 complex. Science *290*, 801-806.

Prescott, D.M., Kates, J., and Kirkpatrick, J.B. (1971). Replication of vaccinia virus DNA in enucleated L-cells. Journal of molecular biology *59*, 505-508.

Pucharcos, C., Estivill, X., and de la Luna, S. (2000). Intersectin 2, a new multimodular protein involved in clathrin-mediated endocytosis. FEBS letters *478*, 43-51.

Qualmann, B., and Kelly, R.B. (2000). Syndapin isoforms participate in receptor-mediated endocytosis and actin organization. The Journal of cell biology *148*, 1047-1062.

Qualmann, B., Kessels, M.M., and Kelly, R.B. (2000). Molecular links between endocytosis and the actin cytoskeleton. The Journal of cell biology *150*, F111-116.

Rapoport, I., Miyazaki, M., Boll, W., Duckworth, B., Cantley, L.C., Shoelson, S., and Kirchhausen, T. (1997). Regulatory interactions in the recognition of endocytic sorting signals by AP-2 complexes. The EMBO journal *16*, 2240-2250.

Raths, S., Rohrer, J., Crausaz, F., and Riezman, H. (1993). end3 and end4: two mutants defective in receptor-mediated and fluid-phase endocytosis in Saccharomyces cerevisiae. The Journal of cell biology *120*, 55-65.

Reider, A., Barker, S.L., Mishra, S.K., Im, Y.J., Maldonado-Baez, L., Hurley, J.H., Traub, L.M., and Wendland, B. (2009). Syp1 is a conserved endocytic adaptor that contains domains involved in cargo selection and membrane tubulation. The EMBO journal *28*, 3103-3116.

Reider, A., and Wendland, B. (2011). Endocytic adaptors--social networking at the plasma membrane. Journal of cell science *124*, 1613-1622.

Ricotta, D., Conner, S.D., Schmid, S.L., von Figura, K., and Honing, S. (2002). Phosphorylation of the AP2 mu subunit by AAK1 mediates high affinity binding to membrane protein sorting signals. The Journal of cell biology *156*, 791-795.

Ridley, A.J. (2011). Life at the leading edge. Cell *145*, 1012-1022.

Rietdorf, J., Ploubidou, A., Reckmann, I., Holmstrom, A., Frischknecht, F., Zettl, M., Zimmermann, T., and Way, M. (2001). Kinesin-dependent movement on microtubules precedes actin-based motility of vaccinia virus. Nat Cell Biol *3*, 992-1000.

Risco, C., Rodriguez, J.R., Lopez-Iglesias, C., Carrascosa, J.L., Esteban, M., and Rodriguez, D. (2002). Endoplasmic reticulum-Golgi intermediate compartment membranes and vimentin filaments participate in vaccinia virus assembly. Journal of virology *76*, 1839-1855.

Roberts, K.L., and Smith, G.L. (2008). Vaccinia virus morphogenesis and dissemination. Trends in microbiology *16*, 472-479.

Robinson, M.S. (1987). 100-kD coated vesicle proteins: molecular heterogeneity and intracellular distribution studied with monoclonal antibodies. The Journal of cell biology *104*, 887-895.

Robinson, M.S. (2004). Adaptable adaptors for coated vesicles. Trends in cell biology *14*, 167-174.

Robinson, M.S., and Bonifacino, J.S. (2001). Adaptor-related proteins. Curr Opin Cell Biol *13*, 444-453.

Robinson, R.C., Turbedsky, K., Kaiser, D.A., Marchand, J.B., Higgs, H.N., Choe, S., and Pollard, T.D. (2001). Crystal structure of Arp2/3 complex. Science *294*, 1679-1684.

Rochester, S.C., and Traktman, P. (1998). Characterization of the single-stranded DNA binding protein encoded by the vaccinia virus I3 gene. Journal of virology *72*, 2917-2926.

Rodal, A.A., Sokolova, O., Robins, D.B., Daugherty, K.M., Hippenmeyer, S., Riezman, H., Grigorieff, N., and Goode, B.L. (2005). Conformational changes in the Arp2/3 complex leading to actin nucleation. Nature structural & molecular biology *12*, 26-31.

Rodriguez, J.F., Janeczko, R., and Esteban, M. (1985). Isolation and characterization of neutralizing monoclonal antibodies to vaccinia virus. Journal of virology *56*, 482-488.

Rodriguez, J.F., and Smith, G.L. (1990). IPTG-dependent vaccinia virus: identification of a virus protein enabling virion envelopment by Golgi membrane and egress. Nucleic Acids Res *18*, 5347-5351.

Rohatgi, R., Ho, H.Y., and Kirschner, M.W. (2000). Mechanism of N-WASP activation by CDC42 and phosphatidylinositol 4, 5-bisphosphate. The Journal of cell biology *150*, 1299-1310.

Rohatgi, R., Ma, L., Miki, H., Lopez, M., Kirchhausen, T., Takenawa, T., and Kirschner, M.W. (1999). The interaction between N-WASP and the Arp2/3 complex links Cdc42-dependent signals to actin assembly. Cell *97*, 221-231.

Rohatgi, R., Nollau, P., Ho, H.Y., Kirschner, M.W., and Mayer, B.J. (2001). Nck and phosphatidylinositol 4,5-bisphosphate synergistically activate actin polymerization through the N-WASP-Arp2/3 pathway. The Journal of biological chemistry *276*, 26448-26452.

Roos, J., and Kelly, R.B. (1998). Dap160, a neural-specific Eps15 homology and multiple SH3 domain-containing protein that interacts with Drosophila dynamin. The Journal of biological chemistry *273*, 19108-19119.

Roos, N., Cyrklaff, M., Cudmore, S., Blasco, R., Krijnse-Locker, J., and Griffiths, G. (1996). A novel immunogold cryoelectron microscopic approach to investigate the structure of the intracellular and extracellular forms of vaccinia virus. The EMBO journal *15*, 2343-2355.

Roper, R.L., Payne, L.G., and Moss, B. (1996). Extracellular vaccinia virus envelope glycoprotein encoded by the A33R gene. Journal of virology *70*, 3753-3762.

Rosel, J., and Moss, B. (1985). Transcriptional and translational mapping and nucleotide sequence analysis of a vaccinia virus gene encoding the precursor of the major core polypeptide 4b. Journal of virology *56*, 830-838.

Roth, T.F., and Porter, K.R. (1964). Yolk Protein Uptake in the Oocyte of the Mosquito Aedes Aegypti. L. The Journal of cell biology *20*, 313-332.

Rottger, S., Frischknecht, F., Reckmann, I., Smith, G.L., and Way, M. (1999). Interactions between vaccinia virus IEV membrane proteins and their roles in IEV assembly and actin tail formation. Journal of virology *73*, 2863-2875.

Rozelle, A.L., Machesky, L.M., Yamamoto, M., Driessens, M.H., Insall, R.H., Roth, M.G., Luby-Phelps, K., Marriott, G., Hall, A., and Yin, H.L. (2000). Phosphatidylinositol 4,5-bisphosphate induces actin-based movement of raft-enriched vesicles through WASP-Arp2/3. Curr Biol *10*, 311-320.

Rumpf, J., Simon, B., Jung, N., Maritzen, T., Haucke, V., Sattler, M., and Groemping, Y. (2008). Structure of the Eps15-stonin2 complex provides a molecular explanation for EH-domain ligand specificity. The EMBO journal *27*, 558-569.

Saffarian, S., Cocucci, E., and Kirchhausen, T. (2009). Distinct dynamics of endocytic clathrin-coated pits and coated plaques. PLoS Biol *7*, e1000191.

Salcini, A.E., Confalonieri, S., Doria, M., Santolini, E., Tassi, E., Minenkova, O., Cesareni, G., Pelicci, P.G., and Di Fiore, P.P. (1997). Binding specificity and in vivo targets of the EH domain, a novel protein-protein interaction module. Genes Dev *11*, 2239-2249.

Sanderson, C.M., Frischknecht, F., Way, M., Hollinshead, M., and Smith, G.L. (1998). Roles of vaccinia virus EEV-specific proteins in intracellular actin tail formation and low pH-induced cell-cell fusion. The Journal of general virology *79 (Pt 6)*, 1415-1425.

Sanderson, C.M., Hollinshead, M., and Smith, G.L. (2000). The vaccinia virus A27L protein is needed for the microtubule-dependent transport of intracellular mature virus particles. The Journal of general virology *81*, 47-58.

Sandgren, K.J., Wilkinson, J., Miranda-Saksena, M., McInerney, G.M., Byth-Wilson, K., Robinson, P.J., and Cunningham, A.L. (2010). A differential role for macropinocytosis in mediating entry of the two forms of vaccinia virus into dendritic cells. PLoS Pathog *6*, e1000866.

Scaplehorn, N., Holmstrom, A., Moreau, V., Frischknecht, F., Reckmann, I., and Way, M. (2002). Grb2 and Nck act cooperatively to promote actin-based motility of vaccinia virus. Curr Biol *12*, 740-745.

Schafer, S., Weibel, S., Donat, U., Zhang, Q., Aguilar, R.J., Chen, N.G., and Szalay, A.A. (2012). Vaccinia virus-mediated intra-tumoral expression of matrix metalloproteinase 9 enhances oncolysis of PC-3 xenograft tumors. BMC Cancer *12*, 366.

Scheele, U., Kalthoff, C., and Ungewickell, E. (2001). Multiple interactions of auxilin 1 with clathrin and the AP-2 adaptor complex. The Journal of biological chemistry *276*, 36131-36138.

Schelhaas, M. (2010). Come in and take your coat off - how host cells provide endocytosis for virus entry. Cell Microbiol *12*, 1378-1388.

Schepis, A., Schramm, B., de Haan, C.A., and Locker, J.K. (2006). Vaccinia virus-induced microtubule-dependent cellular rearrangements. Traffic *7*, 308-323.

Schlossman, D.M., Schmid, S.L., Braell, W.A., and Rothman, J.E. (1984). An enzyme that removes clathrin coats: purification of an uncoating ATPase. The Journal of cell biology *99*, 723-733.

Schmelz, M., Sodeik, B., Ericsson, M., Wolffe, E.J., Shida, H., Hiller, G., and Griffiths, G. (1994). Assembly of vaccinia virus: the second wrapping cisterna is derived from the trans Golgi network. Journal of virology *68*, 130-147.

Schmidt, F.I., Bleck, C.K., Helenius, A., and Mercer, J. (2011). Vaccinia extracellular virions enter cells by macropinocytosis and acid-activated membrane rupture. The EMBO journal *30*, 3647-3661.

Schmidt, F.I., Bleck, C.K., Reh, L., Novy, K., Wollscheid, B., Helenius, A., Stahlberg, H., and Mercer, J. (2013). Vaccinia virus entry is followed by core activation and proteasome-mediated release of the immunomodulatory effector VH1 from lateral bodies. Cell Rep *4*, 464-476.

Schmidt, F.I., and Mercer, J. (2012). Vaccinia virus egress: actin OUT with clathrin. Cell host & microbe *12*, 263-265.

Schmidt, M.R., Maritzen, T., Kukhtina, V., Higman, V.A., Doglio, L., Barak, N.N., Strauss, H., Oschkinat, H., Dotti, C.G., and Haucke, V. (2009). Regulation of endosomal membrane traffic by a Gadkin/AP-1/kinesin KIF5 complex. Proceedings of the National Academy of Sciences of the United States of America *106*, 15344-15349.

Schramm, B., de Haan, C.A., Young, J., Doglio, L., Schleich, S., Reese, C., Popov, A.V., Steffen, W., Schroer, T., and Locker, J.K. (2006). Vaccinia-virus-induced cellular contractility facilitates the subcellular localization of the viral replication sites. Traffic *7*, 1352-1367.

Schultz, J., Milpetz, F., Bork, P., and Ponting, C.P. (1998). SMART, a simple modular architecture research tool: identification of signaling domains. Proceedings of the National Academy of Sciences of the United States of America *95*, 5857-5864.

Sengar, A.S., Wang, W., Bishay, J., Cohen, S., and Egan, S.E. (1999). The EH and SH3 domain Ese proteins regulate endocytosis by linking to dynamin and Eps15. The EMBO journal *18*, 1159-1171.

Senkevich, T.G., Ward, B.M., and Moss, B. (2004). Vaccinia virus entry into cells is dependent on a virion surface protein encoded by the A28L gene. Journal of virology *78*, 2357-2366.

Simone, L.C., Caplan, S., and Naslavsky, N. (2013). Role of phosphatidylinositol 4,5-bisphosphate in regulating EHD2 plasma membrane localization. PloS one *8*, e74519.

Simone, L.C., Naslavsky, N., and Caplan, S. (2014). Scratching the surface: actin' and other roles for the C-terminal Eps15 homology domain protein, EHD2. Histol Histopathol *29*, 285-292.

Smith, C.A., Dho, S.E., Donaldson, J., Tepass, U., and McGlade, C.J. (2004). The cell fate determinant numb interacts with EHD/Rme-1 family proteins and has a role in endocytic recycling. Mol Biol Cell *15*, 3698-3708.

Smith, C.J., and Pearse, B.M. (1999). Clathrin: anatomy of a coat protein. Trends in cell biology *9*, 335-338.

Smith, G.A., Portnoy, D.A., and Theriot, J.A. (1995). Asymmetric distribution of the Listeria monocytogenes ActA protein is required and sufficient to direct actin-based motility. Molecular microbiology *17*, 945-951.

Smith, G.L., and Law, M. (2004). The exit of vaccinia virus from infected cells. Virus research *106*, 189-197.

Smith, G.L., Murphy, B.J., and Law, M. (2003). Vaccinia virus motility. Annu Rev Microbiol *57*, 323-342.

Smith, G.L., Vanderplasschen, A., and Law, M. (2002). The formation and function of extracellular enveloped vaccinia virus. The Journal of general virology *83*, 2915-2931.

Smith, M.J., Hardy, W.R., Murphy, J.M., Jones, N., and Pawson, T. (2006). Screening for PTB domain binding partners and ligand specificity using proteome-derived NPXY peptide arrays. Molecular and cellular biology *26*, 8461-8474.

Snapper, S.B., Takeshima, F., Anton, I., Liu, C.H., Thomas, S.M., Nguyen, D., Dudley, D., Fraser, H., Purich, D., Lopez-Ilasaca, M.*, et al.* (2001). N-WASP deficiency reveals distinct pathways for cell surface projections and microbial actin-based motility. Nat Cell Biol *3*, 897-904.

Sodeik, B. (2000). Mechanisms of viral transport in the cytoplasm. Trends in microbiology *8*, 465-472.

Sodeik, B., Doms, R.W., Ericsson, M., Hiller, G., Machamer, C.E., van 't Hof, W., van Meer, G., Moss, B., and Griffiths, G. (1993). Assembly of vaccinia virus: role of the intermediate compartment between the endoplasmic reticulum and the Golgi stacks. The Journal of cell biology *121*, 521-541.

Sodeik, B., and Krijnse-Locker, J. (2002). Assembly of vaccinia virus revisited: de novo membrane synthesis or acquisition from the host? Trends in microbiology *10*, 15-24.

Sorkin, A. (2004). Cargo recognition during clathrin-mediated endocytosis: a team effort. Curr Opin Cell Biol *16*, 392-399.

Stimpson, H.E., Toret, C.P., Cheng, A.T., Pauly, B.S., and Drubin, D.G. (2009). Early-arriving Syp1p and Ede1p function in endocytic site placement and formation in budding yeast. Mol Biol Cell *20*, 4640-4651.

Stokes, G.V. (1976). High-voltage electron microscope study of the release of vaccinia virus from whole cells. Journal of virology *18*, 636-643.

Strynadka, N.C., and James, M.N. (1989). Crystal structures of the helix-loop-helix calcium-binding proteins. Annu Rev Biochem *58*, 951-998.

Suzuki, R., Toshima, J.Y., and Toshima, J. (2012). Regulation of clathrin coat assembly by Eps15 homology domain-mediated interactions during endocytosis. Mol Biol Cell *23*, 687-700.

Swimm, A., Bommarius, B., Reeves, P., Sherman, M., and Kalman, D. (2004). Complex kinase requirements for EPEC pedestal formation. Nat Cell Biol *6*, 795; author reply 795-796.

Taddie, J.A., and Traktman, P. (1993). Genetic characterization of the vaccinia virus DNA polymerase: cytosine arabinoside resistance requires a variable lesion conferring phosphonoacetate resistance in conjunction with an invariant mutation localized to the 3'-5' exonuclease domain. Journal of virology *67*, 4323-4336.

Takano, K., Toyooka, K., and Suetsugu, S. (2008). EFC/F-BAR proteins and the N-WASP-WIP complex induce membrane curvature-dependent actin polymerization. The EMBO journal *27*, 2817-2828.

Tang, H.Y., Munn, A., and Cai, M. (1997). EH domain proteins Pan1p and End3p are components of a complex that plays a dual role in organization of the cortical actin cytoskeleton and endocytosis in Saccharomyces cerevisiae. Molecular and cellular biology *17*, 4294-4304.

Taunton, J. (2001). Actin filament nucleation by endosomes, lysosomes and secretory vesicles. Curr Opin Cell Biol *13*, 85-91.

Taylor, M.J., Perrais, D., and Merrifield, C.J. (2011). A high precision survey of the molecular dynamics of mammalian clathrin-mediated endocytosis. PLoS Biol *9*, e1000604.

Tebar, F., Confalonieri, S., Carter, R.E., Di Fiore, P.P., and Sorkin, A. (1997). Eps15 is constitutively oligomerized due to homophilic interaction of its coiled-coil region. The Journal of biological chemistry *272*, 15413-15418.

Tebar, F., Sorkina, T., Sorkin, A., Ericsson, M., and Kirchhausen, T. (1996). Eps15 is a component of clathrin-coated pits and vesicles and is located at the rim of coated pits. The Journal of biological chemistry *271*, 28727-28730.

ter Haar, E., Harrison, S.C., and Kirchhausen, T. (2000). Peptide-in-groove interactions link target proteins to the beta-propeller of clathrin. Proceedings of the National Academy of Sciences of the United States of America *97*, 1096-1100.

ter Haar, E., Musacchio, A., Harrison, S.C., and Kirchhausen, T. (1998). Atomic structure of clathrin: a beta propeller terminal domain joins an alpha zigzag linker. Cell *95*, 563-573.

Thirunavukarasu, P., Sathaiah, M., Gorry, M.C., O'Malley, M.E., Ravindranathan, R., Austin, F., Thorne, S.H., Guo, Z.S., and Bartlett, D.L. (2013). A rationally designed

A34R mutant oncolytic poxvirus: improved efficacy in peritoneal carcinomatosis. Mol Ther *21*, 1024-1033.

Thorne, S.H. (2008). Oncolytic vaccinia virus: From bedside to benchtop and back. Curr Opin Mol Ther *10*, 387-392.

Ti, S.C., and Pollard, T.D. (2011). Purification of actin from fission yeast Schizosaccharomyces pombe and characterization of functional differences from muscle actin. The Journal of biological chemistry *286*, 5784-5792.

Tilney, L.G., and Portnoy, D.A. (1989). Actin filaments and the growth, movement, and spread of the intracellular bacterial parasite, Listeria monocytogenes. The Journal of cell biology *109*, 1597-1608.

Tolonen, N., Doglio, L., Schleich, S., and Krijnse Locker, J. (2001). Vaccinia virus DNA replication occurs in endoplasmic reticulum-enclosed cytoplasmic mini-nuclei. Mol Biol Cell *12*, 2031-2046.

Tooze, J., Hollinshead, M., Reis, B., Radsak, K., and Kern, H. (1993). Progeny vaccinia and human cytomegalovirus particles utilize early endosomal cisternae for their envelopes. European journal of cell biology *60*, 163-178.

Toret, C.P., and Drubin, D.G. (2006). The budding yeast endocytic pathway. Journal of cell science *119*, 4585-4587.

Torres, E., and Rosen, M.K. (2006). Protein-tyrosine kinase and GTPase signals cooperate to phosphorylate and activate Wiskott-Aldrich syndrome protein (WASP)/neuronal WASP. The Journal of biological chemistry *281*, 3513-3520.

Toshima, J., Toshima, J.Y., Duncan, M.C., Cope, M.J., Sun, Y., Martin, A.C., Anderson, S., Yates, J.R., 3rd, Mizuno, K., and Drubin, D.G. (2007). Negative regulation of yeast Eps15-like Arp2/3 complex activator, Pan1p, by the Hip1R-related protein, Sla2p, during endocytosis. Mol Biol Cell *18*, 658-668.

Townsley, A.C., and Moss, B. (2007). Two distinct low-pH steps promote entry of vaccinia virus. Journal of virology *81*, 8613-8620.

Townsley, A.C., Weisberg, A.S., Wagenaar, T.R., and Moss, B. (2006). Vaccinia virus entry into cells via a low-pH-dependent endosomal pathway. Journal of virology *80*, 8899-8908.

Traub, L.M. (2009). Tickets to ride: selecting cargo for clathrin-regulated internalization. Nat Rev Mol Cell Biol *10*, 583-596.

Traub, L.M., and Bonifacino, J.S. (2013). Cargo recognition in clathrin-mediated endocytosis. Cold Spring Harbor perspectives in biology *5*, a016790.

Tsutsui, K. (1983). Release of vaccinia virus from FL cells infected with the IHD-W strain. J Electron Microsc (Tokyo) *32*, 125-140.

Tsutsui, K., Uno, F., Akatsuka, K., and Nii, S. (1983). Electron microscopic study on vaccinia virus release. Arch Virol *75*, 213-218.

Turner, P.C., and Moyer, R.W. (2008). The vaccinia virus fusion inhibitor proteins SPI-3 (K2) and HA (A56) expressed by infected cells reduce the entry of superinfecting virus. Virology *380*, 226-233.

Ungewickell, E., and Branton, D. (1981). Assembly units of clathrin coats. Nature *289*, 420-422.

Ungewickell, E., Ungewickell, H., Holstein, S.E., Lindner, R., Prasad, K., Barouch, W., Martin, B., Greene, L.E., and Eisenberg, E. (1995). Role of auxilin in uncoating clathrin-coated vesicles. Nature *378*, 632-635.

Upton, C., Slack, S., Hunter, A.L., Ehlers, A., and Roper, R.L. (2003). Poxvirus orthologous clusters: toward defining the minimum essential poxvirus genome. Journal of virology *77*, 7590-7600.

Uruno, T., Liu, J., Zhang, P., Fan, Y., Egile, C., Li, R., Mueller, S.C., and Zhan, X. (2001). Activation of Arp2/3 complex-mediated actin polymerization by cortactin. Nat Cell Biol *3*, 259-266.

van Eijl, H., Hollinshead, M., Rodger, G., Zhang, W.H., and Smith, G.L. (2002). The vaccinia virus F12L protein is associated with intracellular enveloped virus particles and is required for their egress to the cell surface. The Journal of general virology *83*, 195-207.

van Eijl, H., Hollinshead, M., and Smith, G.L. (2000). The vaccinia virus A36R protein is a type Ib membrane protein present on intracellular but not extracellular enveloped virus particles. Virology *271*, 26-36.

Vanderplasschen, A., Mathew, E., Hollinshead, M., Sim, R.B., and Smith, G.L. (1998). Extracellular enveloped vaccinia virus is resistant to complement because of incorporation of host complement control proteins into its envelope. Proceedings of the National Academy of Sciences of the United States of America *95*, 7544-7549.

Vassilopoulos, S., Esk, C., Hoshino, S., Funke, B.H., Chen, C.Y., Plocik, A.M., Wright, W.E., Kucherlapati, R., and Brodsky, F.M. (2009). A role for the CHC22 clathrin heavy-chain isoform in human glucose metabolism. Science *324*, 1192-1196.

Veiga, E., and Cossart, P. (2005). Listeria hijacks the clathrin-dependent endocytic machinery to invade mammalian cells. Nat Cell Biol *7*, 894-900.

Wagenaar, T.R., and Moss, B. (2007). Association of vaccinia virus fusion regulatory proteins with the multicomponent entry/fusion complex. Journal of virology *81*, 6286-6293.

Wagenaar, T.R., and Moss, B. (2009). Expression of the A56 and K2 proteins is sufficient to inhibit vaccinia virus entry and cell fusion. Journal of virology *83*, 1546-1554.

Wagenaar, T.R., Ojeda, S., and Moss, B. (2008). Vaccinia virus A56/K2 fusion regulatory protein interacts with the A16 and G9 subunits of the entry fusion complex. Journal of virology *82*, 5153-5160.

Wakeham, D.E., Abi-Rached, L., Towler, M.C., Wilbur, J.D., Parham, P., and Brodsky, F.M. (2005). Clathrin heavy and light chain isoforms originated by independent mechanisms of gene duplication during chordate evolution. Proceedings of the National Academy of Sciences of the United States of America *102*, 7209-7214.

Wang, C., Yan, X., Chen, Q., Jiang, N., Fu, W., Ma, B., Liu, J., Li, C., Bednarek, S.Y., and Pan, J. (2013). Clathrin light chains regulate clathrin-mediated trafficking, auxin signaling, and development in Arabidopsis. Plant Cell *25*, 499-516.

Wang, Y.L. (1985). Exchange of actin subunits at the leading edge of living fibroblasts: possible role of treadmilling. The Journal of cell biology *101*, 597-602.

Ward, B.M., and Moss, B. (2001). Vaccinia virus intracellular movement is associated with microtubules and independent of actin tails. Journal of virology *75*, 11651-11663.

Ward, B.M., and Moss, B. (2004). Vaccinia virus A36R membrane protein provides a direct link between intracellular enveloped virions and the microtubule motor kinesin. Journal of virology *78*, 2486-2493.

Warner, A.K., Keen, J.H., and Wang, Y.L. (2006). Dynamics of membrane clathrin-coated structures during cytokinesis. Traffic *7*, 205-215.

Way, M., Pope, B., Gooch, J., Hawkins, M., and Weeds, A.G. (1990). Identification of a region in segment 1 of gelsolin critical for actin binding. The EMBO journal *9*, 4103-4109.

Weaver, A.M., Heuser, J.E., Karginov, A.V., Lee, W.L., Parsons, J.T., and Cooper, J.A. (2002). Interaction of cortactin and N-WASp with Arp2/3 complex. Curr Biol *12*, 1270-1278.

Weaver, A.M., Karginov, A.V., Kinley, A.W., Weed, S.A., Li, Y., Parsons, J.T., and Cooper, J.A. (2001). Cortactin promotes and stabilizes Arp2/3-induced actin filament network formation. Curr Biol *11*, 370-374.

Weisswange, I. (2008). Analysis of Vaccinia virus actin tail nucleating complex dynamics. In London Research Institute (University College London).

Weisswange, I., Newsome, T.P., Schleich, S., and Way, M. (2009). The rate of N-WASP exchange limits the extent of ARP2/3-complex-dependent actin-based motility. Nature *458*, 87-91.

Welch, M.D., Iwamatsu, A., and Mitchison, T.J. (1997). Actin polymerization is induced by Arp2/3 protein complex at the surface of Listeria monocytogenes. Nature *385*, 265-269.

Welch, M.D., Rosenblatt, J., Skoble, J., Portnoy, D.A., and Mitchison, T.J. (1998). Interaction of human Arp2/3 complex and the Listeria monocytogenes ActA protein in actin filament nucleation. Science *281*, 105-108.

Welch, M.D., and Way, M. (2013). Arp2/3-mediated actin-based motility: a tail of pathogen abuse. Cell host & microbe *14*, 242-255.

Welsch, S., Doglio, L., Schleich, S., and Krijnse Locker, J. (2003). The vaccinia virus I3L gene product is localized to a complex endoplasmic reticulum-associated structure that contains the viral parental DNA. Journal of virology *77*, 6014-6028.

Wendland, B., Emr, S.D., and Riezman, H. (1998). Protein traffic in the yeast endocytic and vacuolar protein sorting pathways. Curr Opin Cell Biol *10*, 513-522.

WHO (1972). WHO Expert Committee on Smallpox Eradication. Second report. World Health Organ Tech Rep Ser *493*, 1-64.

Wiesner, S., Helfer, E., Didry, D., Ducouret, G., Lafuma, F., Carlier, M.F., and Pantaloni, D. (2003). A biomimetic motility assay provides insight into the mechanism of actin-based motility. The Journal of cell biology *160*, 387-398.

Wilbur, J.D., Chen, C.Y., Manalo, V., Hwang, P.K., Fletterick, R.J., and Brodsky, F.M. (2008). Actin binding by Hip1 (huntingtin-interacting protein 1) and Hip1R (Hip1-related protein) is regulated by clathrin light chain. The Journal of biological chemistry *283*, 32870-32879.

Wilbur, J.D., Hwang, P.K., Ybe, J.A., Lane, M., Sellers, B.D., Jacobson, M.P., Fletterick, R.J., and Brodsky, F.M. (2010). Conformation switching of clathrin light chain regulates clathrin lattice assembly. Developmental cell *18*, 841-848.

Winter, D., Lechler, T., and Li, R. (1999). Activation of the yeast Arp2/3 complex by Bee1p, a WASP-family protein. Curr Biol *9*, 501-504.

Wolffe, E.J., Weisberg, A.S., and Moss, B. (1998). Role for the vaccinia virus A36R outer envelope protein in the formation of virus-tipped actin-containing microvilli and cell-to-cell virus spread. Virology *244*, 20-26.

Wolffe, E.J., Weisberg, A.S., and Moss, B. (2001). The vaccinia virus A33R protein provides a chaperone function for viral membrane localization and tyrosine phosphorylation of the A36R protein. Journal of virology *75*, 303-310.

Wong, K.A., Wilson, J., Russo, A., Wang, L., Okur, M.N., Wang, X., Martin, N.P., Scappini, E., Carnegie, G.K., and O'Bryan, J.P. (2012). Intersectin (ITSN) family of scaffolds function as molecular hubs in protein interaction networks. PloS one *7*, e36023.

Wong, W.T., Kraus, M.H., Carlomagno, F., Zelano, A., Druck, T., Croce, C.M., Huebner, K., and Di Fiore, P.P. (1994). The human eps15 gene, encoding a tyrosine kinase substrate, is conserved in evolution and maps to 1p31-p32. Oncogene *9*, 1591-1597.

Wong, W.T., Schumacher, C., Salcini, A.E., Romano, A., Castagnino, P., Pelicci, P.G., and Di Fiore, P.P. (1995). A protein-binding domain, EH, identified in the receptor tyrosine kinase substrate Eps15 and conserved in evolution. Proceedings of the National Academy of Sciences of the United States of America *92*, 9530-9534.

Woodrum, D.T., Rich, S.A., and Pollard, T.D. (1975). Evidence for biased bidirectional polymerization of actin filaments using heavy meromyosin prepared by an improved method. The Journal of cell biology *67*, 231-237.

Yamabhai, M., Hoffman, N.G., Hardison, N.L., McPherson, P.S., Castagnoli, L., Cesareni, G., and Kay, B.K. (1998). Intersectin, a novel adaptor protein with two Eps15 homology and five Src homology 3 domains. The Journal of biological chemistry *273*, 31401-31407.

Yamaguchi, H., Lorenz, M., Kempiak, S., Sarmiento, C., Coniglio, S., Symons, M., Segall, J., Eddy, R., Miki, H., Takenawa, T.*, et al.* (2005). Molecular mechanisms of invadopodium formation: the role of the N-WASP-Arp2/3 complex pathway and cofilin. The Journal of cell biology *168*, 441-452.

Yamauchi, A., Kim, C., Li, S., Marchal, C.C., Towe, J., Atkinson, S.J., and Dinauer, M.C. (2004). Rac2-deficient murine macrophages have selective defects in superoxide production and phagocytosis of opsonized particles. Journal of immunology *173*, 5971-5979.

Yang, Z., and Moss, B. (2009). Interaction of the vaccinia virus RNA polymerase-associated 94-kilodalton protein with the early transcription factor. Journal of virology *83*, 12018-12026.

Yarar, D., To, W., Abo, A., and Welch, M.D. (1999). The Wiskott-Aldrich syndrome protein directs actin-based motility by stimulating actin nucleation with the Arp2/3 complex. Curr Biol *9*, 555-558.

Yarar, D., Waterman-Storer, C.M., and Schmid, S.L. (2005). A dynamic actin cytoskeleton functions at multiple stages of clathrin-mediated endocytosis. Mol Biol Cell *16*, 964-975.

Ybe, J.A., Greene, B., Liu, S.H., Pley, U., Parham, P., and Brodsky, F.M. (1998). Clathrin self-assembly is regulated by three light-chain residues controlling the formation of critical salt bridges. The EMBO journal *17*, 1297-1303.

Yeung, T., Barlowe, C., and Schekman, R. (1995). Uncoupled packaging of targeting and cargo molecules during transport vesicle budding from the endoplasmic reticulum. The Journal of biological chemistry *270*, 30567-30570.

Zalevsky, J., Lempert, L., Kranitz, H., and Mullins, R.D. (2001). Different WASP family proteins stimulate different Arp2/3 complex-dependent actin-nucleating activities. Curr Biol *11*, 1903-1913.

Zamanian, J.L., and Kelly, R.B. (2003). Intersectin 1L guanine nucleotide exchange activity is regulated by adjacent src homology 3 domains that are also involved in endocytosis. Mol Biol Cell *14*, 1624-1637.

Zettl, M., and Way, M. (2002). The WH1 and EVH1 domains of WASP and Ena/VASP family members bind distinct sequence motifs. Curr Biol *12*, 1617-1622.

Zhang, J., Shehabeldin, A., da Cruz, L.A., Butler, J., Somani, A.K., McGavin, M., Kozieradzki, I., dos Santos, A.O., Nagy, A., Grinstein, S.*, et al.* (1999). Antigen receptor-induced activation and cytoskeletal rearrangement are impaired in Wiskott-Aldrich syndrome protein-deficient lymphocytes. The Journal of experimental medicine *190*, 1329-1342.

Zhang, W.H., Wilcock, D., and Smith, G.L. (2000). Vaccinia virus F12L protein is required for actin tail formation, normal plaque size, and virulence. Journal of virology *74*, 11654-11662.

Zhang, Y., and Moss, B. (1992). Immature viral envelope formation is interrupted at the same stage by lac operator-mediated repression of the vaccinia virus D13L gene and by the drug rifampicin. Virology *187*, 643-653.

Zizioli, D., Meyer, C., Guhde, G., Saftig, P., von Figura, K., and Schu, P. (1999). Early embryonic death of mice deficient in gamma-adaptin. The Journal of biological chemistry *274*, 5385-5390.

So long and thanks for all the fish…